

A New Method for Controlling the Interfacial Stresses in Beams Strengthened with Prestressed CFRP Laminate

Master's Thesis in the International Master's programme Structural Engineering

ARSHAD ABOSH

AMJAD HUSSAIN MOHAMMED

Department of Civil and Environmental Engineering

Division of Structural Engineering

Steel and Timber Structures

CHALMERS UNIVERSITY OF TECHNOLOGY

Göteborg, Sweden 2007

Master's Thesis 2007:79

MASTER'S THESIS 2007:79

A New Method for Controlling the Interfacial Stresses in Beams Strengthened with Prestressed CFRP Laminate

Master's Thesis in the *International Master's programme Structural Engineering*

ARSHAD ABOSH

AMJAD HUSSAIN MOHAMMED

Department of Civil and Environmental Engineering
Division of Structural Engineering
Steel and Timber Structures
CHALMERS UNIVERSITY OF TECHNOLOGY
Göteborg, Sweden 2007

A New Method for Controlling the Interfacial Stresses in Beams Strengthened with Prestressed CFRP Laminate

Master's Thesis in the *International Master's programme Structural Engineering*

ARSHAD ABOSH

AMJAD HUSSAIN MOHAMMED

© Arshad abosh

Amjad hussain mohammed, 2007

Master's Thesis 2007:79

Department of Civil and Environmental Engineering

Division of Structural Engineering

Steel and Timber *Structures*

Chalmers University of Technology

SE-412 96 Göteborg

Sweden

Telephone: + 46 (0)31-772 1000

Cover:

Shear stress distribution in the adhesive layer due to loading, Section 7.1; Shear stress distribution in the adhesive layer after modification, Section 7.6.

Chalmers repro services / Department of Civil and Environmental Engineering
Göteborg, Sweden 2007

A New Method for Controlling the Interfacial Stresses in Beams Strengthened with Prestressed CFRP Laminate

Master's Thesis in the *International Master's programme Structural Engineering*

ARSHAD ABOSH

AMJAD HUSSAIN MOHAMMED

Department of Civil and Environmental Engineering

Division of Structural Engineering

Steel and Timber *Structures*

Chalmers University of Technology

ABSTRACT

The use of CFRP (Carbon Fibre Reinforced Polymers) laminates in strengthening and repair work have gone through a big development during last years. Composite materials are becoming increasingly popular in the construction industry for strengthening purposes. These materials, particularly CFRP, offer several advantages such as resistance to corrosion, a high strength to weight ratio, and unlimited delivery length (in sheet form), thus eliminating the need for joints. By prestressing the laminate, the ultra high tensile strength of the composite material can be utilized and more advantages are brought to the strengthening technique.

The advantages of the CFRP laminates have been proved, but the behaviour of members strengthened with prestressed CFRP laminates has to be clarified. Prestressed CFRP laminate bonded to a steel beam generate high interfacial stresses at the laminate ends which usually exceed the strength of the adhesive materials used in bonding. Different mechanical anchorages have been used to solve the problem of high interfacial stresses. The mechanical anchorages are however too complicated to handle. Hence a new technique is developed to control the interfacial stresses. In this method the stiffness of the adhesive is modified by applying the heat to the adhesive. By doing this the high shear stress value is reduced and distributed over a larger area. In this thesis the new technique to control these interfacial stresses is investigated using finite element analysis.

A composite plate was modelled in the finite element program ABAQUS. The model consists of plain-stress elements to represent the steel plate, adhesive and CFRP laminate. The model is verified by comparing the results from the FE-analysis with that from a simplified analytical solution. Different parameters like location of heat source, time of heating and length of heat source is studied in details to understand the heating effect on the composite plate. Parametric study of the materials was performed to understand the effect of material properties on the magnitude of interfacial stresses.

In conclusion, the results from the FE analysis show that the new technique developed is promising to reduce the interfacial shear stresses. Further study is needed to clarify the effect of temperature on the development of interfacial stresses

Key words: FE analysis, CFRP, prestressing system, shear stress, peeling stress, normal stress, thermal analysis, mechanical analysis, thermal boundary condition, mechanical boundary condition, conduction, convection, radiation.

En ny Teknik för Kontrollering Skjuvspänningar i en Balk Förstärkt med Förspänd CFRP Laminatet

Examensarbete inom Civilingenjörs Programmet Väg- och vatten byggnad

ARSHAD ABOSH

AMJAD HUSSAIN MOHAMMED

Institutionen för bygg- och miljöteknik

Avdelningen för konstruktionsteknik

Stål- och träbyggnad

Chalmers tekniska högskola

SAMMANFATTNING

Användningen av komposita material för förstärkning och reparation har genomgått en stor utveckling under de sista åren. Av denna komposit material har CFRP (Carbone Fibre Reinforced Polymers) varit mycket populära i konstruktionsindustrin för förstärknings- och reparationssyfte. CFRP erbjuder många fördelar så som motstånd till korrosion, lågvikt och höghållfasthet. Om CFRP laminat dessutom förspänns innan applicering kan den högre draghållfastheten som kompositen har utnyttjas effektivare. Fördelarna med CFRP förstärkning har bevisats, men beteendet hos konstruktionselement som är förstärkta med förspända CFRP laminat behöver studeras och undersökas. Förstärkningen med förspänd CFRP laminat resulterar i regel i höga spänningar i limfogen vid laminatets ändar. Skjuvspänning som uppträder vid laminatets ändar kan t.ex. överskrida många gånger skjuvhållfastheten hos epoxilimmet som används för att binda CFRP-laminatet till stålbalken.

Olika mekaniska förankringar har använts för att ta hand om de höga spänningarna i limskiktet. Mekaniska förankringar är dock ganska dyra att tillverka och installera och de medför i många fall vissa förändringar i den förstärkta konstruktionen som är komplicerade att behandla i praktiken. En ny teknik har därför utvecklats och studerats för att kontrollera de höga spänningarna i epoxilimskikt. Den nya tekniken går ut på att modifiera limmets styvhet i områden med höga spänningar genom att lokalt värma upp limskiktet vid laminatändan. Uppvärmningen av limmet medför en minskning av limmets styvhet lokalt och medför därmed att spänningarna i limskiktet omfördelas över ett större område. Detta medför i sin tur en minskning av toppvärdena hos dessa spänningar. Tekniken har undersökts i denna rapport med finita element analyser av en stålplåt med ett pålimmat CFRP-laminat. Programmet ABAQUS har använts i modelleringen. Modellen består av skalelement som representera stålplattan, limskiktet och CFRP laminatet. Sedan har modellen verifierats genom att jämföra FE- analysen med en analytisk lösning. Olika parameter som kan påverka beteendet hos det komposita elementet såsom storleken hos det uppvärmda området och uppvärmningstiden har utstuderat i detalj för att få förståelse för hur en komposit platta påverkas av värme. En parameterstudie har också utförts för att studera hur olika materialegenskaper inverkar på fördelningen av spänningarna i limfogen. Resultaten från FE-analysen visar att den nya tekniken kan medföra en stor minskning av skjuv- och normalspänningen i limfogen.

Nyckelord: Förstärkning, CFRP-stål komposit, skjuvspänningar, normalspänningar, förspänning, termisk analys, mekanisk analys, termiska randvillkorar, mekaniska randvillkor, värme konduktion, värme konvektion, värme utstrålning

Contents

ABSTRACT	V
SAMMANFATTNING	VI
CONTENTS	VII
PREFACE	XI
NOTATIONS	XII
1 INTRODUCTION	1
1.1 Problem definition	1
1.2 Aim and objectives	2
1.3 Limitations	2
1.4 Background	2
1.5 Properties of CFRP composite materials	5
1.5.1 Carbon fibre- reinforced polymers	5
1.5.2 Adhesive resins proprieties	7
1.5.3 Adhesive curing	7
2 ANALYTICAL SOLUTION FOR THE INTERFACIAL SHEAR STRESSES IN BEAM STRENGTHENED WITH PRESTRESSED CFRP	11
2.1 Interfacial stresses in composite beams	11
2.2 Analysis of the interfacial shear stress in the beam strengthened with prestressed CFRP:	11
3 BEAM STRENGTHENED WITH PRESTRESSED CFRP LAMINATE-LITERATURE REVIEW	13
3.1 Prestressing for strengthening and repair of the existing structure	13
3.2 External Prestressing (CFRP) Techniques	15
3.2.1 Cambered beam system	15
3.2.2 Tensioning against external reaction frame	16
3.2.3 Tensioning against the strengthened beam itself	16
3.2.4 Problems with prestressing CFRP laminate	17
3.3 Mechanical Anchorage	18
3.3.1 Experimental application of prestressed CFRP on concrete members	18
3.3.2 Concrete surface preparation	18
3.3.3 Prestressing system developed by University of Missouri- Rolla	18
3.3.4 Prestressing system developed by University of Missouri- Rolla	21
3.3.5 Flexural Strengthening of RC slab by Prestressed CFRP System Enhanced with the Presence of GFRP Anchor Spikes	24
3.3.6 The LEOBA prestressed CFRP tendon system	26
3.4 Practical on-site Application for Strengthening and Repair of Concrete Structures with Prestressed CFRP	29

3.4.1	Field Applications	29
3.5	Strengthening and repair of steel structures	34
3.5.1	The Hythe Bridge project-ROBUST	34
3.6	Fast heat-induced curing for prestressed strengthened system	35
3.7	Discussion	37
4	PRINCIPLE OF CONTROLLING INTERFACIAL STRESSES	39
4.1	Principle	39
4.2	Consequences due to heating	43
5	HEAT TRANSFERS ESSENTIALS	45
5.1	Definition of heat parameters	45
5.1.1	Heat transfers	45
5.1.2	Conduction Heat Transfer	45
5.1.3	Convection Heat Transfer	47
5.1.4	Radiation Heat Transfer	48
5.1.5	Heat Capacity	50
5.1.6	Steady state analysis	50
5.1.7	Transient Analysis	50
5.1.8	Coupled Thermal Analysis	51
5.1.9	Uncoupled Thermal Analysis	51
5.1.10	Thermal Boundary Condition	51
5.2	Mathematical Modelling	52
5.2.1	Solid mechanics	52
5.2.2	Linear Elasticity	58
5.2.3	Initial strain	59
5.3	Thermal Analysis	60
5.3.1	Heat Transfer	60
5.3.2	One-dimensional heat flow	60
5.3.3	Solid Mechanics + Thermal analysis	63
6	FINITE ELEMENT MODELLING	65
6.1	Problem Description	65
6.2	Finite Element Modelling	67
6.3	Thermal analysis	68
6.3.1	Material Properties	68
6.3.2	Thermal Boundary Conditions and load application	71
6.3.3	Transient thermal analysis	74
6.3.4	Meshing	76
6.4	Stress analysis (Mechanical analysis)	79
6.4.1	Mechanical Boundary Conditions and load application	80
6.4.2	Meshing	80
7	RESULTS & DISCUSSION	81

7.1	Mechanical Analysis/ Development of shear and peeling stresses	81
7.2	Convergence Study	86
7.3	Validation of the Model	89
7.4	Thermal Analysis	90
7.5	Thermal stress analysis	101
7.6	Stress analysis due to combined effect of heating and tensioning	103
7.7	Parametric Study	110
8	SUMMARY AND CONCLUSIONS	115
8.1	Temperature distribution and interfacial stresses	115
8.2	Further studies	116
9	REFERENCES	119
10	APPENDIX	123

Preface

This master thesis is a part of an experimental research on composite member that is being carried out at the Division of Structural Engineering, Steel and Timber Structures at the Department of Civil and Environmental Engineering at Chalmers University of Technology, Göteborg, Sweden.

We would like to express our gratitude to our supervisor Dr. Mohammed Al-Emrani for his valuable guidance and unlimited support. We always learned something new whenever we had a chance to discuss with him. We are also thankful to PhD student Reza Haghani, M.Sc for his utmost contribution in correcting the errors in results.

Of-course we need to extend our thanks to Per Kettil in the mechanical department at Chalmers University of Technology for helping us with the modeling in ABAQUS software. We also thank Björn Mattsson from the building physics department for his valuable advices regarding the thermal analysis.

We would like to take this opportunity to thank our opponent group Anna Björklund, Joakim Höglind and all our friends at Chalmers, who helped us throughout our work.

Arshad Abosh wants to devote all his work to the soul of his mother Najiba. He also wants to thank his brothers and sisters for supporting him. They are all miles away but each of them in their own way has made this work possible. He is also grateful to his wife Walat for her support.

Amjad Hussain Mohammed wants to dedicate all his work to his mother Zaheda Firdose Khanam and father Mohammed Hussain. He also wants to thank his elder brothers and sister for their continuous support and encouragements, who were the source for his inspiration.

Furthermore, we would like to thank all the people that made it possible to study here in Sweden and made the last eighteen months the most beautiful days of our life.

Göteborg, February 2007

Arshad Abosh

Amjad Hussain Mohammed

تم بعون الله تعالى انهاء العمل في مشروع التخرج للحصول على درجة الماجستير في تحليل و تصميم المنشآت من جامعة
جالمرز اهدى كل عملي الي العالمة امي العزيزة نجيبه لتعبها و سهرها طيلة حياتي الدراسية فلولها و بركتها لما وصلت
الي هدفي. كذلك اهدى رسالة الماجستير الي زوجتي العزيزة المهندسة ولات على وقوفها بجاني و تحملها لي في دراستي
للماجستير. وكذلك اعبر عن شكري الي اخواني و خالي و حماتي على دعمهم المعنوي لي خلال دراستي

ارشد عبوش

Notations

Abbreviations

FRP	Fibre reinforced polymer
CFRP	Carbon fibre reinforced polymer
GFRP	Glass fibre reinforced polymer
2D	Two dimension
3D	Three dimensions

Roman upper case letters

A_s	Area of the steel
A_l	Area of the CFRP laminate
D	Constitutive matrix
E_s	Modulus of elasticity for steel
E_l	Modulus of elasticity for CFRP laminates.
G	Shear modulus of elasticity
P_0	Prestressing force
P_s	Prestressing force in steel
P_l	prestressing force in laminate
S	Stress tensor
τ	Shear stress
T_s	Surface temperature

Roman lower case letters

α	Coefficient of thermal expansion
α_r	Radiation coefficient
e	emissivity
h_c	Convection coefficient
k	Conduction coefficient.
t	traction vector
u	Displacement vector
ω	Constant include geometrical and material parameters of the composite Plate

1 Introduction

1.1 Problem definition

Engineers have always searched for methods which are cooperative economically and practically for developing and enhancing existing structures as an alternative of replacing and demolishing the structural elements. In some type of structures, it is not always feasible to make replacement and it is not always the best solution. In Europe a large numbers of Railway and Highway Bridges are classified to be older than 50 years. An effective way to improve the load carrying capacity of these bridges and increase allowable axel load and truck weight without exerting disruption of the traffic flow on the bridges, and without adding more self weight to the strengthened structures, is to employ strengthening using composite materials such as carbon fibre-reinforced polymer (CFRP).

Due to their high durability and fatigue resistance and their superior strength-to-weight ratio, CFRP composites have captured wide application areas in the field of strengthening recently. These materials have been successfully used in strengthening of existing concrete, masonry and timber structures. In the field of steel structures, there is a raising interest for the possible application of the CFRP due to their:

- Resistance to corrosion.
- Light weight and excellent mechanical properties (i.e., their strength and stiffness).
- Efficiencies in enhancing the load carrying capacity of the strengthened members.

In order to improve the efficiency of strengthening technique using CFRP, and to exploit the full strength of CFRP laminates, the laminates can be prestressed. Prestressed CFRP have been used as an efficient way for strengthening damaged concrete structures.

In general there is one critical area which requires special attention when using prestressed composite materials. Due to prestressing of the laminates high stress concentrations are present at the anchorage zone. The high interfacial stresses in the anchorage zone are in general above the capacity of conventional adhesive used to bond the composite laminate and will accordingly limit the level of prestressing that can be applied to the laminate.

In this thesis, a new innovative technique is examined where the development of interfacial stresses at the ends of the prestressed laminate is controlled through local heat treatment of the adhesive.

1.2 Aim and objectives

Previous research studies on strengthening steel structures using CFRP laminate have illustrated that in order to utilize the maximum strength of the laminate, the laminate should be prestressed. The aim of this thesis is to study a new technique which can be employed to control the development of the interfacial stresses at the end of the prestressed laminate so as to avoid the use of the mechanical anchorage device. As a criterion, the prestressing system must be simple, affective and applicable in practice. On the other hand the system has to introduce lower shear and peeling stresses at the ends of the laminate after the release of prestressing force.

1.3 Limitations

This study will only explain the development of the interfacial stresses at the ends of the laminate due to tensioning of the steel plate and the way of reducing these stresses. The load carrying capacity of the strengthened plate has not been included. Neither the failure modes of the strengthened system nor the non-linearity behaviour of the whole composite plate is taken into consideration. Material properties of adhesive and CFRP laminate are gathered from some previous tests, internet and literature references, because the temperature dependent material properties were not available during the time of performing the analysis.

1.4 Background

FRP products were used first to strengthen concrete structures in the 1950's [34]. During the next two decades, the quality of the FRP materials improved considerably, manufacturing methods became more automated and material costs decreased. The use of these materials for external reinforcement of concrete bridge structure's started in the 1980s, first as an alternative to steel plate bonding and then as a substitute for steel confinement shells for bridge columns.

The technology for external retrofitting was developed primarily in Japan (sheet wrapping) and Europe (laminate bonding) [35]. The principles behind externally bonding FRP plates or wraps to concrete structures are very similar to the principles used in application of bonded steel plates. In general, the member's flexural, shear, or axial strength is increased or better mobilized by the external application of high tensile strength material.

Strengthening and retrofitting of steel structures is done today by adding steel plates to the existing members bolting or welding the plates to the weakened parts of the structures. This method is simple and the structures can be in use during the strengthening works partially. The shortcomings of using this method are represented

by the risk of corrosion, fatigue cracking of welded connections and high stress concentration near the bolts. There are difficulties in transporting, handling and installing the heavy steel plates. Other disadvantages are that the steel plates exist in limited lengths, which make the process more labour demanding and time intense. Old steel types are not weld able, which further limits the available strengthening methods. Furthermore welding cranes to the cover of the steel girder for transporting purpose decrease the fatigue strength.

The motivations for using CFRP laminate as an attractive solution for post strengthening are turned to low material costs, low weight and comparably simpler installation, unlimited material length availability, and resistance to corrosion with excellent mechanical properties. CFRP are used in concrete structures to improve the functionality of different structural elements such as laminate attached to the concrete beams for increasing the flexural and shear capacity, or sheets warped to concrete column to add confinement and flexural capacity to the columns. Through research it has been found that the plate bonding results in an increase in the stiffness and ultimate capacity of the strengthened member, reduce tensile strain in the concrete and delay in the appearance of the first visual cracks.

In case of externally strengthened concrete elements the common failure mode is the debonding between CFRP plate ends and the concrete or concrete cover separation due to high stress concentration as in Figure 1.1.



Figure 1.1 Debonding failure in concrete beam [22], [23]

In case of steel structure, the most common failure modes are as follow:

1. Tensile rupture of the composite material.
2. Yielding of the steel and the excessive deformation.
3. Adhesion failures between the adhesive and the steel substrate, between the adhesive and the laminate, at the end of the laminate.
4. Interlaminar failure within the laminate itself.
5. Failure of the adhesive itself.

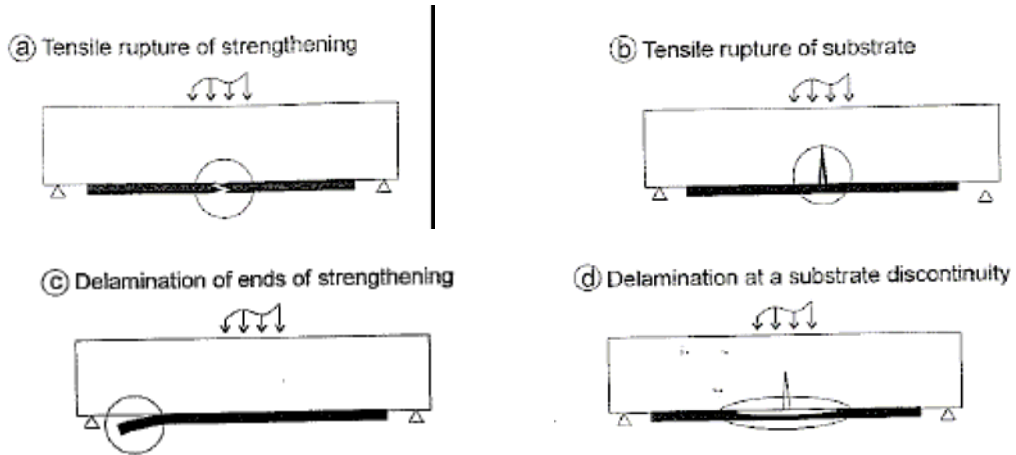


Figure 1.2 Failures in Steel beam strengthened with CFRP [9]

Previous researches have shown that the plate end debonding can be prevented by using additional anchors such as CFRP U-jackets or nails and bolts at the CFRP plate ends as in Figure 1.3.

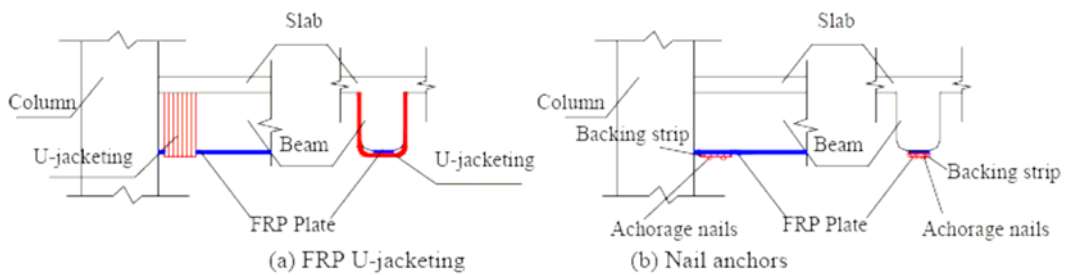


Figure 1.3 Different mechanical anchorage systems [27]

One technique that reduces the stresses at the plate ends without the use of external anchorage system is to taper the CFRP laminate at the ends, and increase the adhesive thickness correspondently as seen in Figure 1.4. The stress concentration is reduced as the length of the taper increases to some extent.

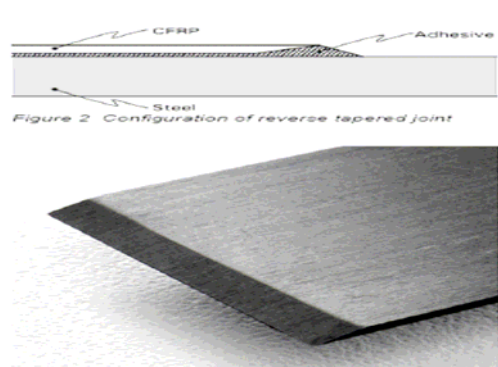


Figure 1.4 CFRP strip with taper at the end [24]

Another technique that provide the greatest anchorage force possible and reduce stresses concentration at the ends of the laminate can be decreased without using any type of mechanical anchorages is to continue the bonded laminate under the supports of the beam as illustrated in Figure.1.5.

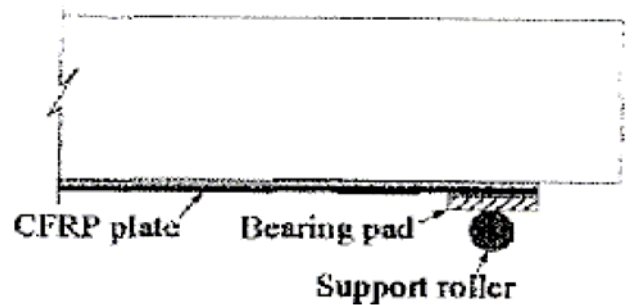


Figure 1.5 Clamped anchorage system [8]

1.5 Properties of CFRP composite materials

1.5.1 Carbon fibre- reinforced polymers

Composite materials can generally be defined as a combination of two or more materials (constituent), with properties derived from the individual constituents. The properties of the resulted material may have the combined characteristics of the constituent or different. Hence carbon fibre-reinforced polymer CFRP is a kind of composite. Therefore, the definition of a carbon fibre-reinforced polymer CFRP composite CFRP is an assembly of two materials or more of different nature. In general one material is discontinuous and called the *reinforcement*, the other is less stiff and weaker. It is continuous and is called the *matrix*.

The reinforcement can be described as fibrous or particulate. The fibres are continuous (long fibre) or discontinuous (short fibre). The arrangement and the orientation of these fibres determine the mechanical properties of the composite. [4].The principle fibres used in CFRP strengthening materials are *carbon* as in Figure 1.6. Carbon fibres are characterized by both high strength and stiffness, relatively low coefficient of thermal expansion and high electrical conductivity.

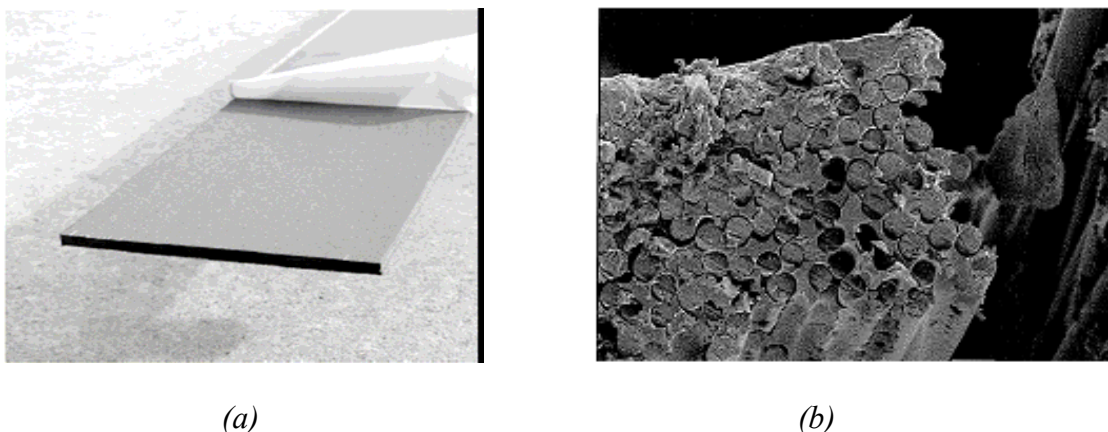


Figure 1.6 (a) CFRP Sheet [24] (b) Arrangement of fibres in CFRP

Carbon fibers might be available in different grades according to the fibre content in the laminate. They can be in,

- High-strength (HS).
- High-modulus (HM).
- Ultra-high-modulus (UHM)

The following table shows the properties of some type of reinforcing fibres

Table 1.1 Properties of reinforcing fibres [9]

Property	Carbon fibre			Aramid fibre	E-glass fibre
	HS	HM	UHM		
Modulus of elasticity (GPa)	230-240	295-390	440-640	125-130	70-85
Strength (MPa)	4300-4900	2740-5940	2600-4020	3200-3600	2460-2580
Strain to failure %	1.9-2.1	0.7-1.9	0.4-0.8	2.4	3.5
Density (kg/m ³)	1800	1730-1810	1910-2120	1390-14700	2600
Coefficient of thermal expansion (parallel to fibre) (10 ⁶ /°C)	-0.38	-0.83	-1.1	2.1	4.9

The matrix is defined as a polymer matrix resins, such as polyester, isopolyester, vinyl ester, epoxy, phenolic in addition to fillers and additive. The function of the polymer (resin) is to “glue” and holds the composite together and influences the physical properties of the end product. In addition, the durability properties of the composite depend upon the matrix material such as determining the heat, fire and chemical resistance of the composite. The matrix transfers force to the fibres by interfacial shear and protects the delicate fibres against violent environments.

Table 1.2 Properties of matrix materials [9]

Property	Epoxy	Polyester	Phenolic	Polyurethane
Modulus of elasticity (GPa)	2.6-3.8	3.1-4.6	3.0-4.0	0.5
Tensile strength (MPa)	60-85	50-75	60-80	15-25
Strain to failure %	1.5-8.0	1.0-2.5	1.0-1.8	10
Poisson's ratio	0.3-0.4	0.35-0.38	Not available	0.4
Coefficient of thermal expansion (parallel to fibre) (10 ⁶ /°C)	30-70	30-70	80	40
Density (kg/m ³)	1110-1200	1110-1250	1000-1250	1150-1200

The fibres in the composite sheets can be arranged to provide a quasi-isotropic or an anisotropic composite material. If the arrangements of the fibres are done with equal proportion in multiple directions, for instance 0° , 30° , 60° , 90° in this case the composite demonstrate quasi-isotropic properties. While in the case if fibres arrangements are predominate in a single direction, the composite is expressed as unidirectional.

CFRP composites used are anisotropic, whereas steel is relatively isotropic (uniform properties in all directions, independent of applied load). Therefore, CFRP composite properties are uni-directional; it means that the best mechanical properties are in the direction of the fibre.

Summarizing, CFRP composites are composed of resins, reinforcements, fillers, and additives. Each of these ingredients plays an important role in the manufacturing process and final performance of the end product (combination result). The type and quantity of materials selected in addition to the combination process to manufacture the product, will affect the mechanical properties and performance.

1.5.2 Adhesive resins proprieties

Epoxy adhesives are chemical compounds for joining components. They require clean surfaces compatible with the adhesive. Epoxy resins exhibit high strength, low shrinkage during cure and good dimensional stability. Epoxy adhesives are widely used for their toughness and resistance to chemical and environmental damage. While most epoxies are two-part adhesives cured at room temperature, some thermally cured or thermoset one-part epoxies systems are available. Depending on the formulation, epoxy resins are used as potting agents, resin binders in fibre construction, electrical conductors and various structural bonding applications.

Epoxy adhesives are available in a wide range of chemical compositions, which allow for a number of different setting styles. These setting styles include single component setting, dual-component setting, thermosetting, and radiation curing, which include UV and visible light curing. Single component epoxy adhesives consist of one resin that hardens by reaction with surface moisture, a surface applied activator-primer, or through the application of heat. Dual or multi-component adhesive or sealant systems consist of two or more resins or a resin and a hardener, cross-linker, activator or catalyst that when combined react and cure into a polymerized compound or bond. Two component epoxy adhesive systems are mixed and then applied. Thermoset epoxy adhesives are cross-linked polymeric resins cured using heat or heat and pressure. Cured thermoset resins do not melt and flow when heated, but they may soften

1.5.3 Adhesive curing

Temperature has a significant influence on the mechanical properties of the adhesive. Figure 1.7a shows that curing of adhesive at rather higher temperature may speed up the development of the flexural strength of the adhesive. For already cured adhesive,

however the stiffness of the adhesive is reduced as T_g (Glass Transition Temperature) is approached as shown in the Figure 1.7b. Therefore the properties of adhesive which is used depend on the environmental condition, type of members which has to be strengthened and type of strengthening (prestress or not).

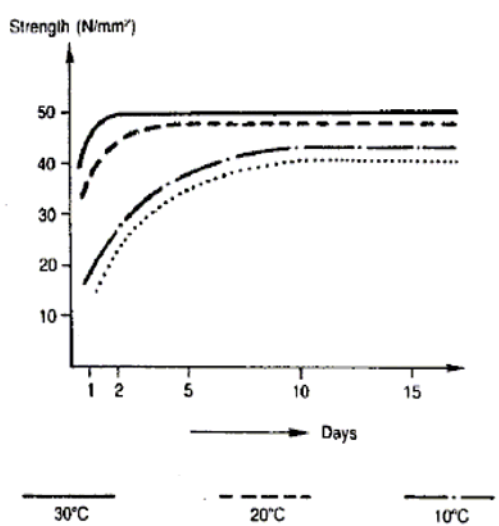


Figure 1.7a Effect of formulation and curing temperature on the development of flexural strength of two-part adhesive [15]

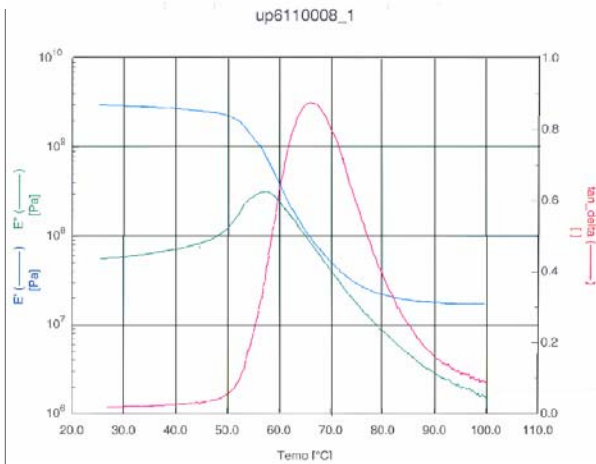


Figure 1.7b Temperature effects on the adhesive stiffness [15]

Much research has been done in order to investigate the mechanical properties of adhesive at different service temperature. Figure 1.8 shows two types of adhesive (A & B) with different properties tested at different service temperatures. The stiffness and strength of the adhesive were reduced by increasing the temperature.

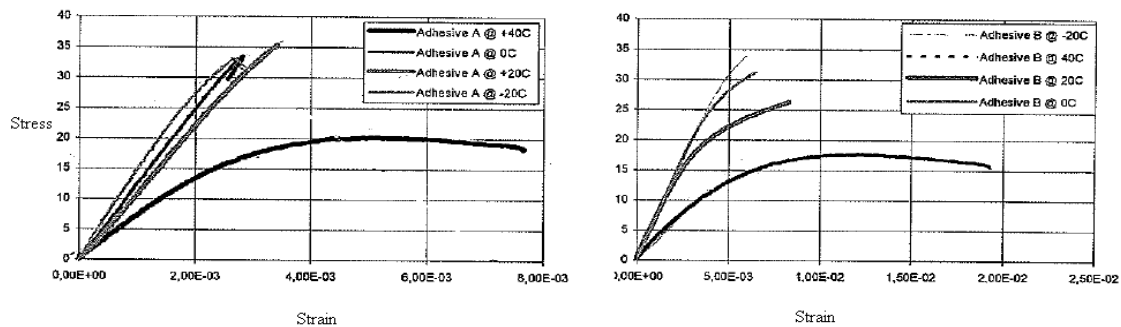
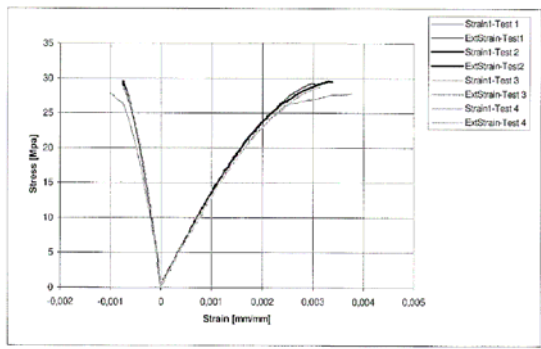


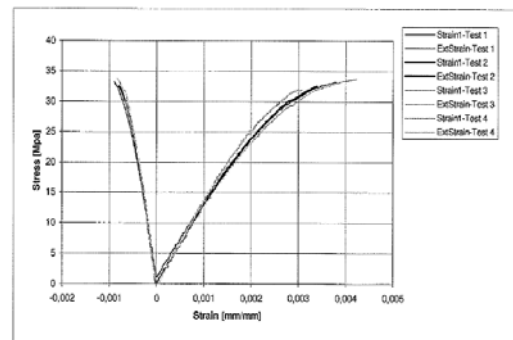
Figure 1.8 Effect of temperature on different adhesive [15]

The strength of the adhesive which is used in bonding at room temperature increases with curing time as in Figure 1.9. However, long time curing might not be practical and competitive in the some civil engineering problems. Therefore the curing time of the adhesive used for bonding the composite material to the original member can be reduced by increasing the temperature to certain level (below T_g). Reducing the curing

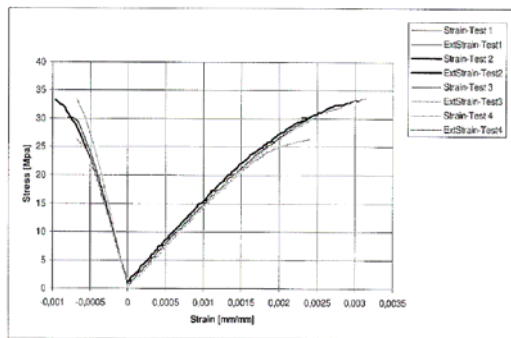
time is important factors in case were disturbance of the function of the structure during the strengthening work should be minimized, like strengthening work in bridge



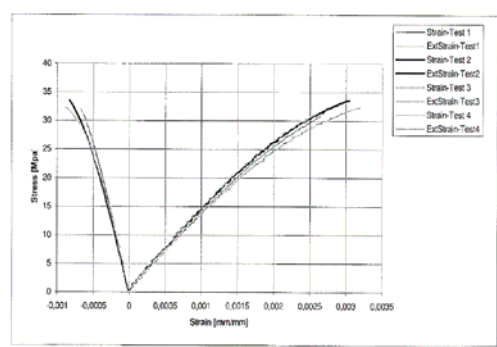
Stress & strain curves with adhesive A
(1 day curing)



Stress & strain curves with A
(3 day curing)



Stress & strain curves with adhesive A
(5 day curing)



Stress & strain curves with A
(7 day curing)

Figure 1.9 Stress and strain for adhesive A at different curing time [15]

2 Analytical Solution for the Interfacial Shear Stresses in Beam Strengthened With Prestressed CFRP

2.1 Interfacial stresses in composite beams

Metallic beams strengthened with CFRP laminate commonly fail by rupture of the strengthened material or debonding of the laminate because of the high shear stress at the end of the laminates. The Prestressing force carried by the laminate is transferred to the steel beam by the adhesive layer. Because of free ends of the laminate and high prestressing force at the end, stress-concentration in the adhesive layer, in the interface between steel-adhesive or laminate-adhesive, might cause debonding of the strengthened beam.

2.2 Analysis of the interfacial shear stress in the beam strengthened with prestressed CFRP:

Prestressing of the CFRP laminates results in higher shear stress at the end of the laminates which causes failure in the adhesive or laminate. Recently calculation models have been developed to predict the magnitude of maximum shear stress at the end of the laminate [2]. The analysis was based on establishing the compatibility and equilibrium conditions for a steel beam strengthened with a prestressed laminate bonded to the beam lower flange. The derivation of the interfacial shear stress was made for a steel beam with typical I-section, and it is applicable to any beam with arbitrary cross-section and material properties, see Appendix [A]. The following differential equation was obtained.

$$\frac{d^2}{dx^2}(\tau(x)) = \omega^2 \cdot \tau(x)$$

In which $\tau(x)$ is the shear stress along the adhesive layer and ω is a constant which includes the material and geometrical parameters of the composite beam.

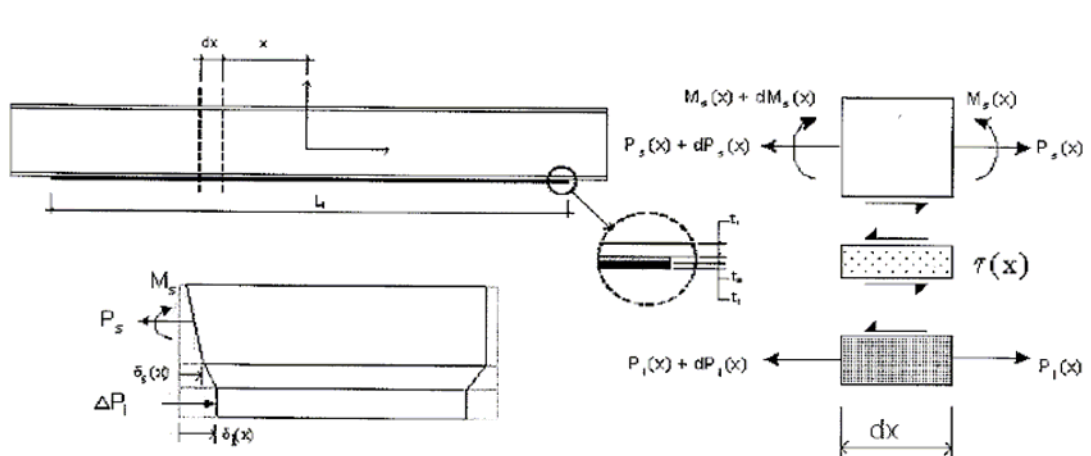


Figure 2.1 Equilibrium forces and deformation compatibility for a segment in a steel beam strengthened with prestressed CFRP [2]

When the boundary conditions are applied, the expression for the interfacial shear stress is obtained as below.

$$\tau(x) = \frac{G.P_0}{t_0.A_l.E_l} \cdot \frac{\sinh(\omega.x)}{\omega.\cosh\left(\frac{\omega.L}{2}\right)}$$

Where, P_0 is the initial prestressing force.

The residual axial force in the laminate after loses due to instantaneous deformation in the composite member is:

$$P_l(x) = \frac{P_0}{A_l.E_l} \left(1 - \frac{\cosh(\omega.x)}{\cosh\left(\omega.\frac{L}{2}\right)} \right) \cdot \frac{1}{\left(\frac{1}{A_l.E_l} + \frac{1}{A_s.E_s} + \frac{h^2}{4.E_s.I_s} \right)}$$

The distribution of the uplifting (negative) bending moment along the length of the strengthened beam is obtained as:

$$M_s(x) = -P_0 \cdot \frac{h}{2} \cdot \frac{\left(1 - \frac{\cosh(\omega.x)}{\cosh\left(\omega.\frac{L}{2}\right)} \right)}{\left(1 + \frac{A_l.E_l}{A_s.E_s} + \frac{A_l.E_l.h^2}{4.E_s.I_s} \right)}$$

The material and geometrical properties of the CFRP laminate and adhesive has a significant effect on the interfacial shear stress when investigated using the analytical solutions. In order to decrease the shear stress at the ends of the laminate, the adhesive must be flexible and for that the stiffness of the adhesive should be less and the thickness of the adhesive should be higher in order to distribute the shear stresses. The laminate should be stiff enough so that the initial strain from the applied pre-stressing force which affects the shear stress is limited. The stiffness of the laminate is increased either by increasing the modulus of elasticity of the laminate or by increasing the cross-sectional area i.e. the thickness and the width of the laminate. The properties have been studied by implementing in an example in the Appendix [A], in order to optimize the parameters to decrease the interfacial shear stress.

3 Beam Strengthened with Prestressed CFRP Laminate - Literature Review

3.1 Prestressing for strengthening and repair of the existing structure

The use of external prestressing in strengthening and repair is gaining popularity in bridge constructions because of it include the possibility of monitoring and replacing tendons. External prestressing is defined as prestress introduced by high strength cable, plate or sheet, which is placed outside the cross section and attached to the beam by different concepts. The methodology of prestressing is expressed and employed in different ways during different times. The first application of that was made as early as 2700 B.C. on the Egyptians sailing ships and afterward on Roman arch bridges. The real “father” of prestressing is the Frenchman Eugène Freyssinet, who in 1928 defined prestressing as a technique which consists of subjecting a material, in this case (reinforced concrete), to loads which produce stresses opposed to those generated in operation, through the use of cables. The technique of prestressing has later on evolved to reach the field of steel structures about four decades ago. The technique for realizing prestressed steel was then achieved through external cables as seen in Figure 3.1 [34].

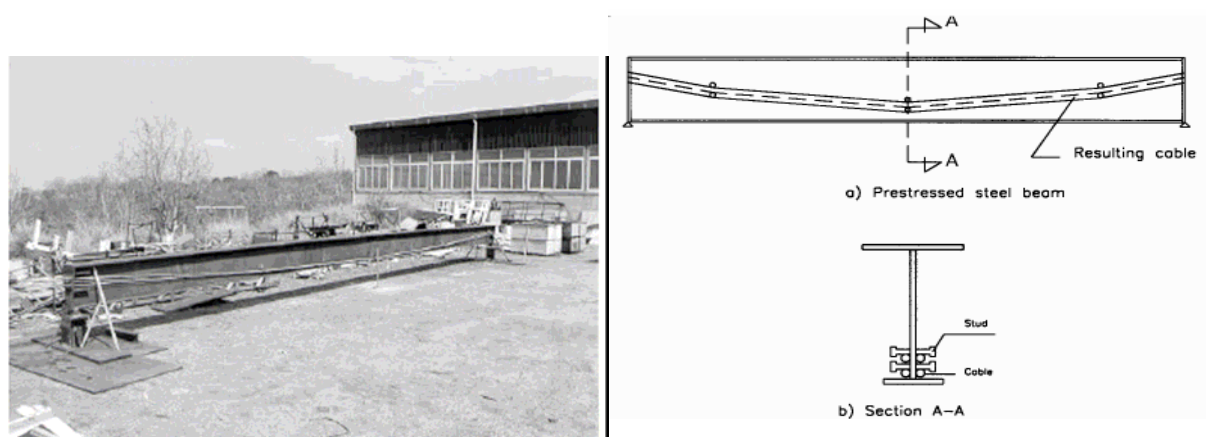


Figure 3.1 Steel beam prestressed externally by cables [36]

The concept of prestressing in structural engineering is basically the application of compressive stresses to the structure internally or externally in order to counteract the internal forces generated in the structure by the external actions. The application of the prestressing force with a certain eccentricity introduces a moment along the member, which will camber the member in the opposite direction and reduce the deformation induced by loading the member, see Figure 3.2 [26].

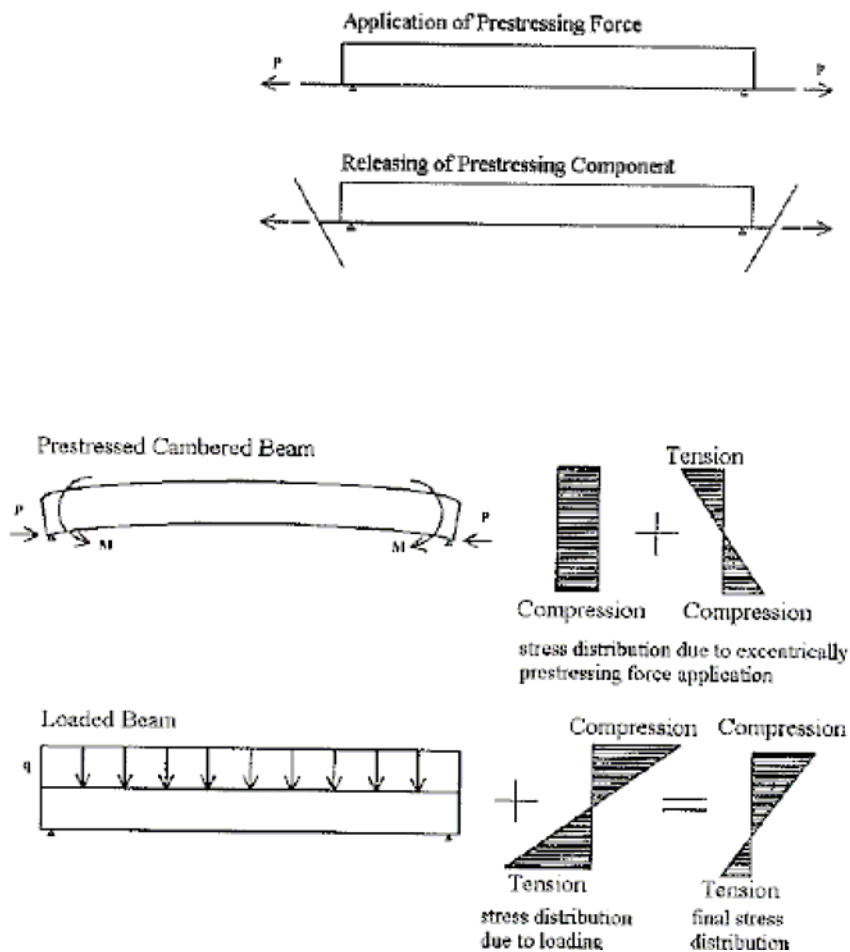


Figure 3.2 Effect of Prestressing [29]

Many advantages can be attained by using prestressing; some of them are briefly listed below [29]:

1. Prestressing minimizes the effect of cracks in concrete elements by holding the concrete in compression.
2. Lighter elements permit the use of longer spanning members with a high strength to weight characteristic.
3. The ability to control deflections in prestressed beams and slabs permits longer spans to be achieved.
4. Prestressing permits a more efficient usage of reinforcing steel and enables the economic use of high tensile steels and high strength concrete.
5. Prestressing allows a reduction of beam depths to be achieved for equivalent design strengths.
6. Fatigue failure is resisted by inducing the compressive stress.

3.2 External Prestressing (CFRP) Techniques

The previous chapter gives some basic principles of enhancing the structural members by means of prestressing. The (CFRP) sheets can be prestressed by exploiting and following the same concepts and principles, in order to restore and increase the capacity of the different types of structural members. This has been done by developing several systems, which introduce a prestress in the laminate. These systems generally fall into three categories:

- a) Cambered beam system.
- b) Tensioning against external reaction frame.
- c) Tensioning against the strengthened beam itself.

3.2.1 Cambered beam system

This kind of prestressing system is very simple. It can be done by cambering the beam upward using hydraulic jacks at mid-span, bonding of the CFRP laminate to the tensile face of the beam, or welding a plate of the same material to the web. The jacks are removed after the epoxy is completely cured.

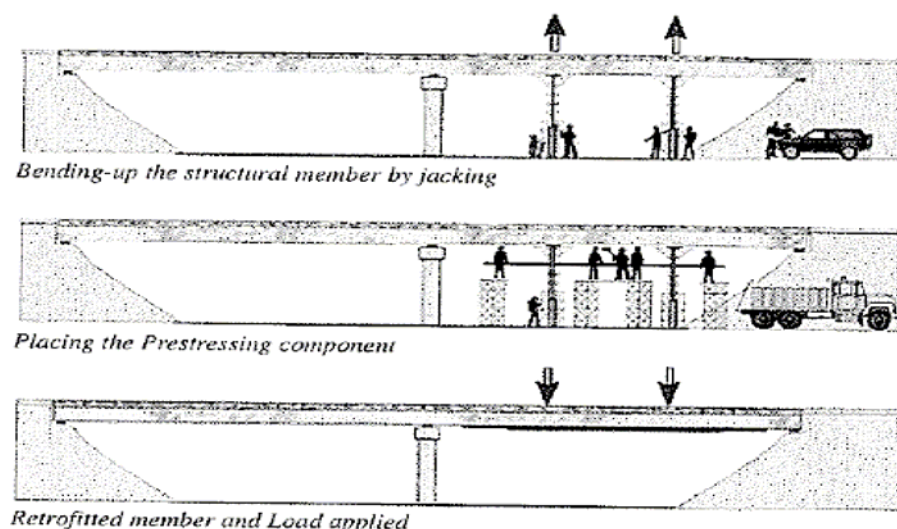


Figure 3.3 Procedure of cambered beam system [8]

The shortcoming of this system is only a low level of prestressing is induced into the sheets upon releasing of the hydraulic jacks. It has been seen that this method is not very practical and it can not be applied in all situations, for instance in case of bridge girder over water, floating structure is needed in this case. It means that the efforts required to camber the beam is extensive in relative to the low prestressing induced in the CFRP sheets.

3.2.2 Tensioning against external reaction frame

In this system the prestressing is induced in the CFRP by tensioning the laminate against an independent device which is called prestressing bed or prestressing device. The CFRP laminate is tensioned by prestressing bed, and bonded to the lower face of the beam by epoxy adhesive. Once the adhesive is cured totally, the prestressing system is released gradually. The tensioning laminate will introduce compression stress in the structural member, which decreases the tension stress in the member due to applied loads.

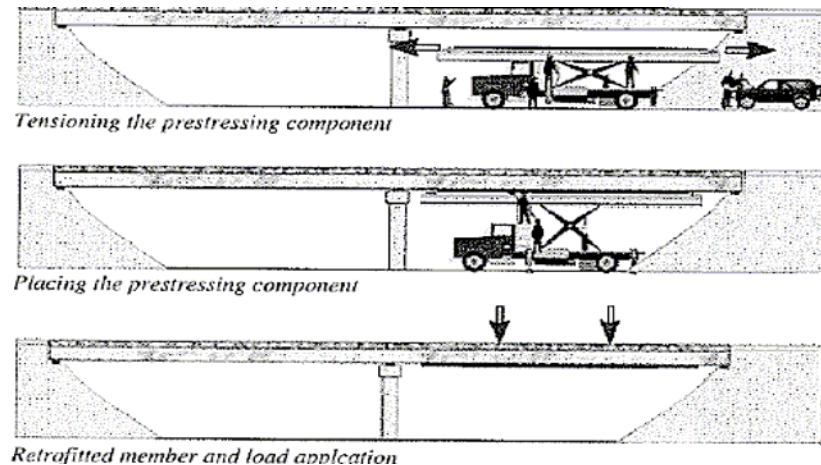


Figure 3.4 Procedure of external prestressing system [8]

High prestressing level can be achieved from this system which results in an increase in flexural strength to about 80%. This system is applicable for beams up to 4.5m long, which narrows down the appropriateness of the method.

3.2.3 Tensioning against the strengthened beam itself

This system of prestressing required less effort and less equipment to perform the prestressing. Since all arrangements are made in the structural element without any external device. The prestressed CFRP laminate is tensioned by hydraulic jacks mounted at one or both ends. In this way the tension forces introduced to the prestressing component exert compressive stress in the structural element. The simplicity of this method do not limit the application of it, concerning to the length of the structural member. The prestressing level can be controlled and the profile of the prestressing component customized. It was noticed that the flexural strengthen could be increased effectively, and the mode of failure was by shearing in the anchorage zone.

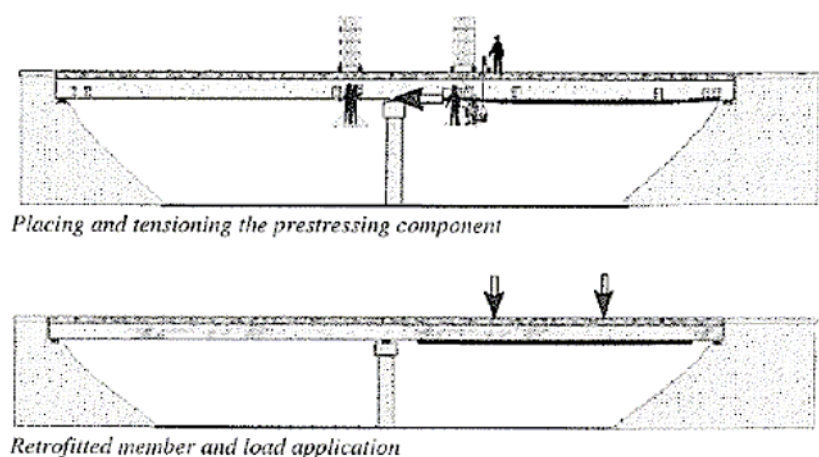


Figure 3.5 Procedure of self- prestressing device [8]

3.2.4 Problems with prestressing CFRP laminate

The release of the prestressing force in the CFRP introduces high shear and peeling stress at the ends of the Laminate, which in turn might results in an immediate delaminating of the sheets in case of concrete member. All failure modes are possible in concrete and steel beams; often in concrete failure is by the concrete cover itself. In the steel, all failure modes are possible depending up on the adhesive strength, the bond between adherents and the laminate strength. The failure can occur in adhesive or laminate itself. The methods which have been suggested to decrease the peak value of the interfacial stress are the following systems

- a) Mechanical anchorage system.
- b) Curing technique by heating the adhesive.

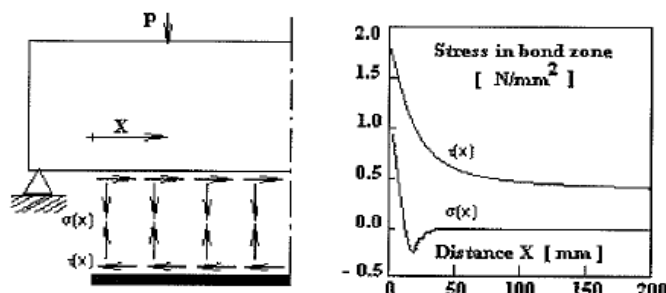


Figure 3.6 Shear & peeling stress at the end of the member [10]

3.3 Mechanical Anchorage

Anchorage of post-tensioning kits needs to be designed so that the full strength of the tendon or sheet can be developed and the failure of the sheet at braking load occurs outside the anchorage. The mechanical anchorage can be made using a suitable kind of mechanical device, which provides a smooth transfer of force from the CFRP sheet to the anchors as well as from the anchors to the structure. This process leads to the distribution of the shear stress over a large area which reduces the peak value. Some experimental applications for prestressing of CFRP, anchored at the ends by mechanical anchorage system are described below.

3.3.1 Experimental application of prestressed CFRP on concrete members

Many experimental works have been done to investigate the efficiency of the structural elements strengthened with (CFRP) as apart of research programs in Universities or Institutes. The tests have been done under controlled conditions regarding temperature; moisture and other sever conditions in order to obtain practical results analogous with theoretical analysis. Many of these works have no real performance in the site; therefore more investigations have to be done in this field.

3.3.2 Concrete surface preparation

The first stage before performing strengthening with CFRP, concrete surface should be prepared. Repairing and smoothing a concrete surface is very important for effective development of bond between a laminate and the concrete surface. The areas with visible cracking should be prepared by removing loose concrete and replacing it with patching concrete and small cracks should be filled with cement based grout material. Sandblasting has to be used to smooth the surface prior to bond it with CFRP. The aggregate should be uncovered to increase the bond between adhesive and concrete, and the corroded steel should be replaced and the concrete behind it should be checked to avoid future corrosion. Grease, dust or any other contaminate agent can be removed by sweeping and vacuum cleaning. It is recommended to apply a primer to the surface to assure the maximum adherent between the concrete surface and adhesive.

3.3.3 Prestressing system developed by University of Missouri-Rolla

Test description:

This test might be classified as a Category B , in which an external prestressing device is used. The prestressing is introduced in the CFRP sheet in transverse direction instead of longitudinal. The mechanical device consists of a steel beam, the CFRP

sheet which is anchored to anchorage device at the ends of the beam and then an uplift displacement is applied at two points close to the anchorage regions. The concept of uplift displacement decreases the force required to impose the initial prestressing on the CFRP by about 100 times.



Figure 3.7 Prestressing technique [22]

The anchorage system consists of one removable steel plate at each end to anchor the CFRP sheets and the other fixed plate attached to steel beam. The plates are bolted against each other with the sheets placed (bonded) in between them. The loading region is made of steel strip to support the prestressed CFRP, two threaded rods rounded by steel nuts, which are tightened against the steel beam to prestress CFRP manually. The rods and nuts are placed symmetrically to the centre line of the cross-section. The friction between steel strip and nuts are decreased by using two thrust bearing, which are placed symmetrically to the same line [22].

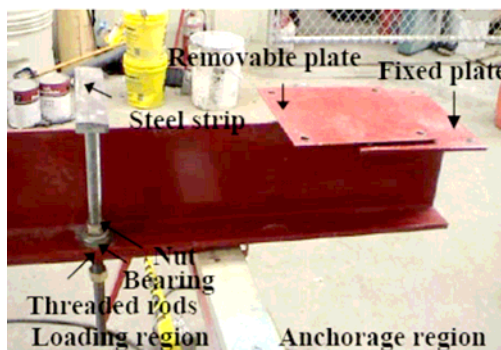


Figure 3.8 Main component

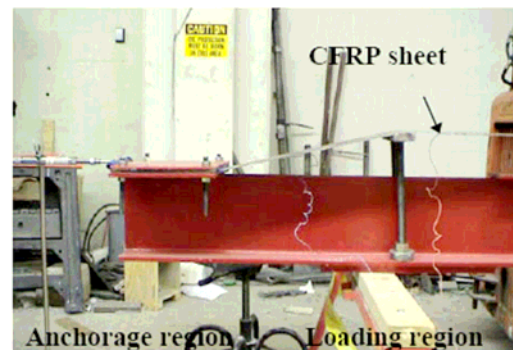


Figure 3.9 Prestressing of the CFRP sheet [22]

Procedure:

The CFRP sheet is bonded to the removable plates, which is fastened to the fixed plates by bolts. High pressure is applied to the CFRP sheets through the steel plates and bolts, to prevent slipping of the CFRP which results in the loss of prestressing

force. Hence further tests showed that the friction resulting from the high pressure applied by the bolts was sufficient to anchor the sheets during prestressing.

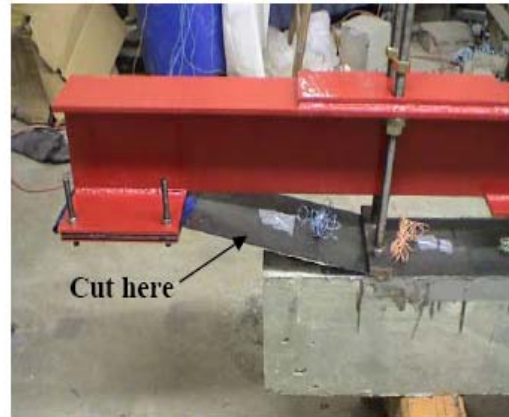


Figure 3.10 Application of CFRP [22] Figure 3.11 Removing of mechanical device

The next stage is to prestress the CFRP sheet by tightening the nuts manually, by doing so the threaded rods and steel strips move upwards and start to prestress the CFRP sheet until 15% of its ultimate strength. After prestressing of the CFRP sheet is done it is applied to the RC beam as in Figure 3.10. In this case the adhesive is spread on the concrete member and the sheet is bonded to the concrete beam. The prestressing device is kept in place until the adhesive is cured properly as seen in Figures 3.10 and 3.11.

Test result

The loss of prestress was recorded to be about 6% which occurred when the prestress was released, after cutting the CFRP sheet near the ends of the RC beam. Three RC beams were tested. The first one was used as a control beam. The second one was with un-prestressed CFRP sheet and the third beam was with prestressed CFRP sheet. These three beams were tested to ultimate condition under a four-point loading test setup. The results obtained after testing the specimens are shown in the table 3.1[22].

Table 3.1 Comparison of results [22]

Beam	No. of CFRP Sheets	CFRP Sheet Prestress (% f_{fu})	CFRP Sheet Area $\text{mm}^2 (\text{in}^2)$	CFRP U-Wrap widths $\text{mm}(\text{in})$
A	--	--	--	--
B	1 ⁽¹⁾⁽²⁾	--	31.6 (0.049)	--
C	1 ⁽¹⁾⁽²⁾	15	31.6 (0.049)	127 (5)

3.3.4 Prestressing system developed by University of Missouri-Rolla

In the experimental work performed by Raafat El-Hacha, R. Gordon Wight, and Mark F. Green a new anchorage system has been discussed to decrease stress concentrations at the ends of the laminate [11].

Test description

The test is classified under category C, where no external frames are required to perform the prestressing in the laminate. The work consist of testing of CFRP sheets using different anchoring system and then applying the most effective technique to large scale post-tensioned concrete T-beam. Types of anchors which are studied were round bar, Figure 3.12.a, elliptical bar, Figure 3.12.b, and flat plate, Figure 3.12.c assembled with single, double and triple layers of CFRP.

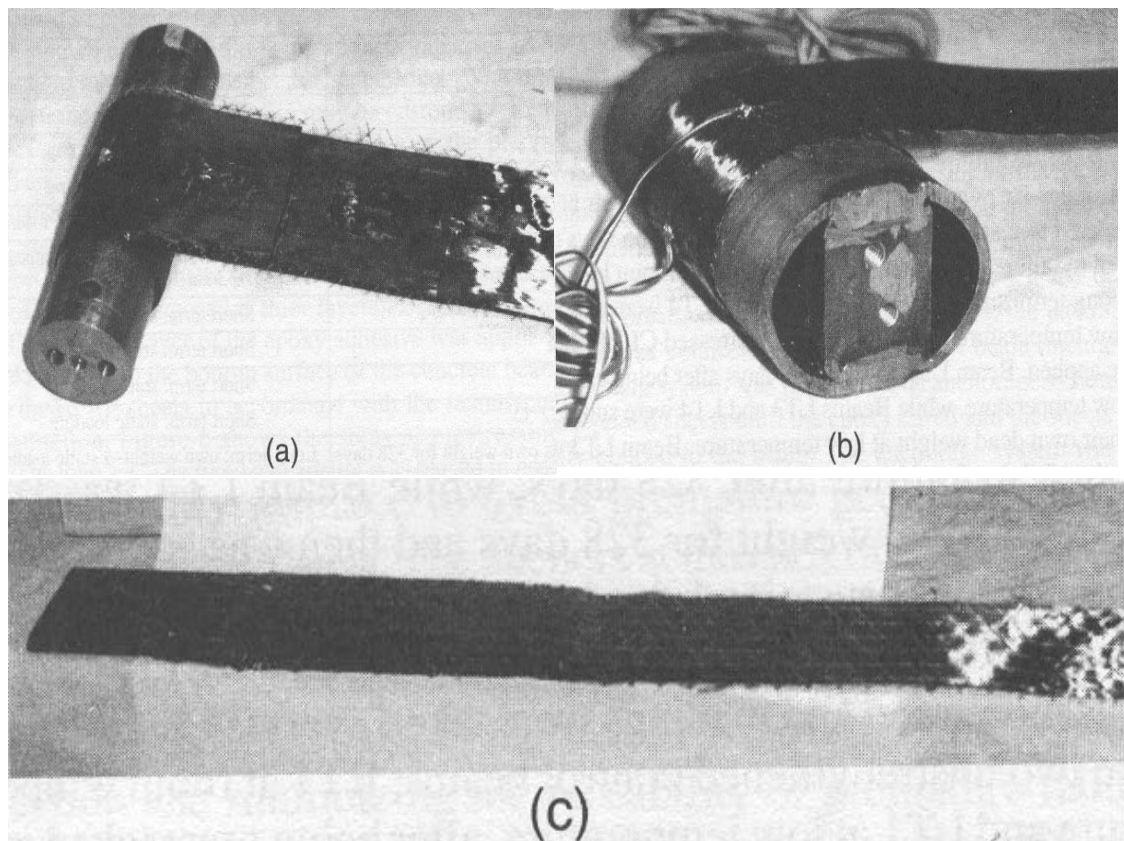


Figure 3.12 Different anchors; (a) round bars, (b) elliptical bars and (c) flat plates [13]

Tension test for the different anchoring systems showed above, the flat plate is more appropriate system and higher stress can be attained. This system is based on fixing one end of the CFRP sheet while tensioning the other end to the required prestressing level by means of hydraulic jacks and finally bonding it to the structural members. A maximum tensile stress of about 1300Mpa was employed to represent the ultimate tensile strength of the CFRP sheets. The main components in the test system consist of the anchoring elements and hydraulic jacks which can be seen in Figure 3.13.

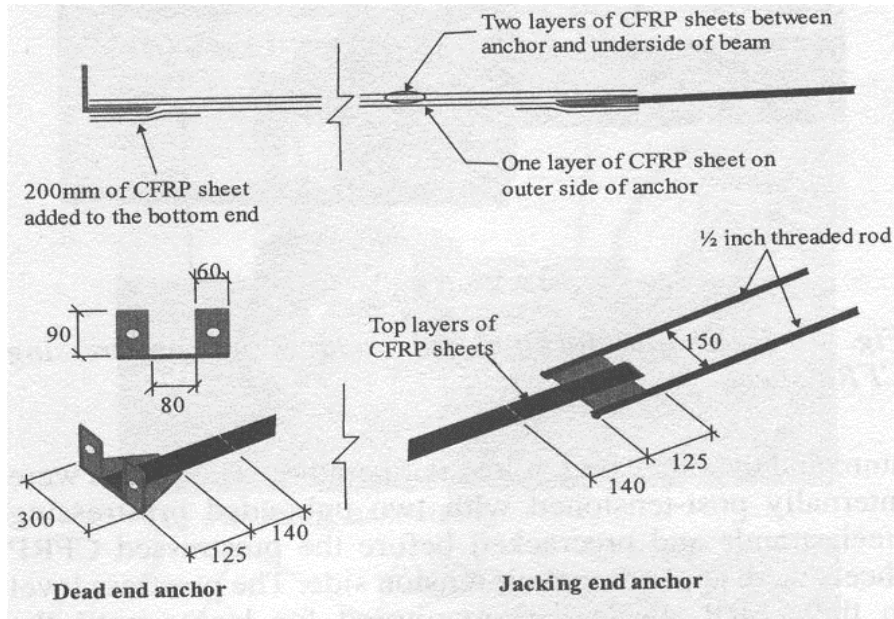


Figure 3.13 Details of fixed and tensioning ends [13]

Procedure:

The behavior of the 4.5m long, pre-cracked post-tensioned T-beam strengthened with the prestressed CFRP using the developed anchorage system in different temperature (room (22°C) and low temperature (-28°C)) was studied and also the estimated prestress loss in the prestressed CFRP sheets with the time and temperatures being noted.

The bottom surface of the pre-cracked T-beam was strengthened over a length of 3m and 2m using two sets of CFRP sheets to increase the capacity of the structural member, stressed individually to about 50% of the sheet's ultimate tensile strength. Before performing the prestressing, a thin layer of the epoxy adhesive was applied by knife to the bottom surface of the concrete beam and the CFRP sheets in accordance with the manufacturing instruction. After the described level of prestressing was achieved and after curing of the epoxy, the jacking ends anchor was connected to the permanent beam anchors in order to avoid premature peeling failure at the ends of the sheets. The procedure can be seen in Figure 3.14[13]

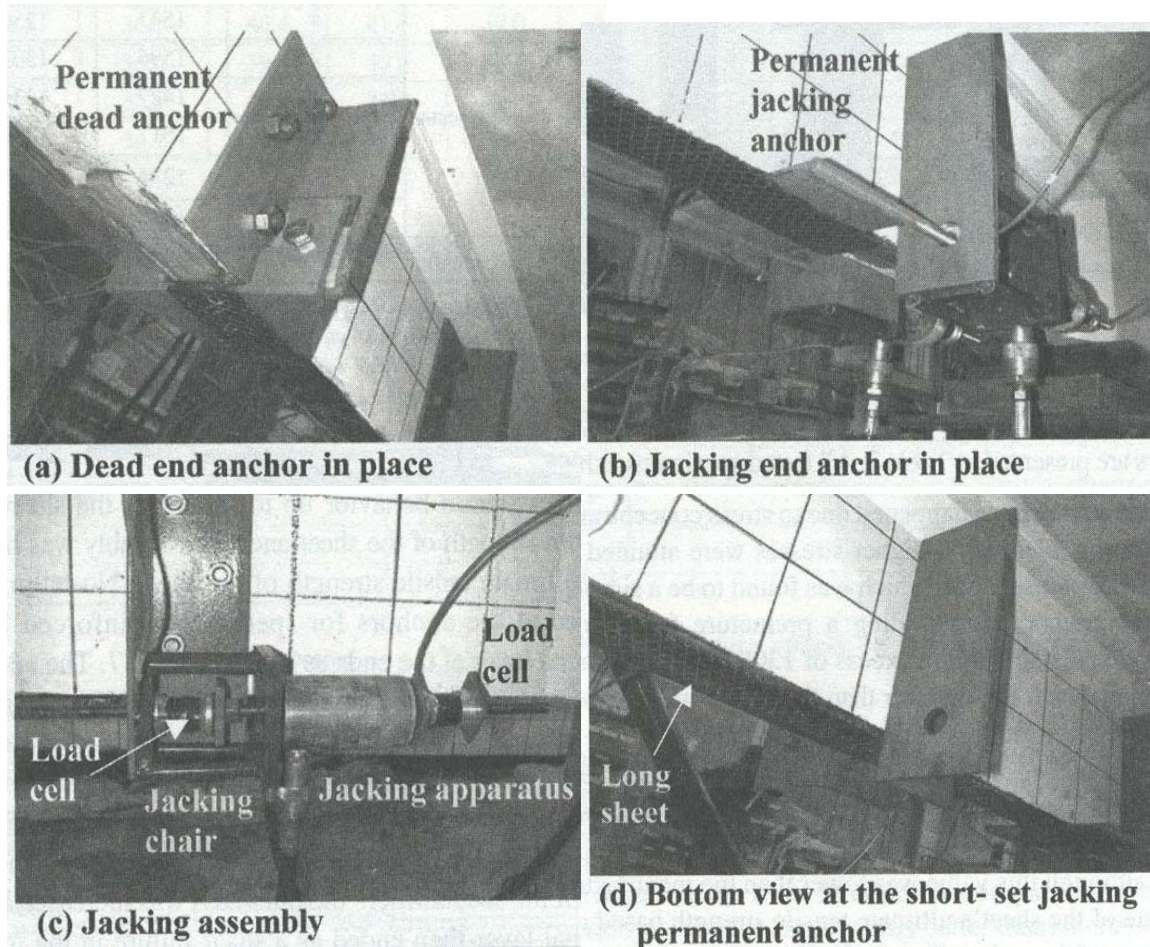


Figure 3.14 Prestressing schemes [13]

Results:

Tension test for the developed anchorage system exhibited linear stress-strain behavior up to the failure of the sheets and no failure was observed at the anchors reinforced by additional layers at the ends. The reason was that the extra layers at the ends shifted the failure away from the sheet-anchor connection to the location where the thickness of the CFRP increased. Failure occurred due to rupture of the sheets at the location where the thickness was increased. The average breaking stress values in the laminate ranged between 1029-1412 MPa.

The average short term time dependent loss including anchor set at room temperature was found to be approximately 16% of the sheet's ultimate tensile strength. Moreover prestress losses due to long-term were not observed and just a 4% variation in the prestress level was found due to temperature change (decreased to -28°C). The average long term prestress loss after 1 year was around 11% at the normal temperature and 4.5% due to low temperature [13].

3.3.5 Flexural Strengthening of RC slab by Prestressed CFRP System Enhanced with the Presence of GFRP Anchor Spikes

Test description:

This test might be classified as a Category C, in which no external prestressing device is used. The system was investigated under a four-point static load test setup at the University of Missouri Rolla (UMR). The mechanical device which was used in the prestressing process consists of steel cables, anchors at the ends made of steel angles, hydraulic jacks, CFRP sheets, and GFRP spikes as seen in Figure 3.15 and Figure 3.17. Prestressing of the CFRP sheets was achieved by imposing a camber profile on the concrete slab such that upon release of the prestressing system initial stresses would develop in these CFRP sheets. The spikes were used to anchor CFRP sheets to the RC slab, to prevent debonding of the CFRP sheets due to the initial stresses after releasing of prestressing system.

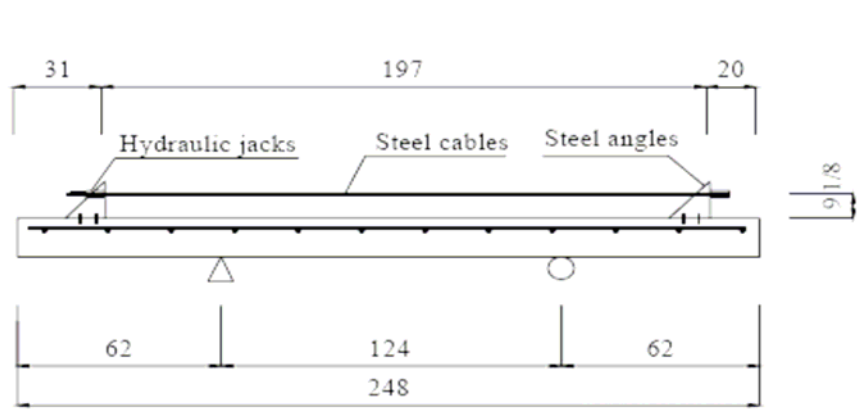


Figure 3.15 Mechanical device components [21]

Procedure:

Slab of dimension 1000 x 220 x 6300 mm was fabricated under normal laboratory condition. Detail of the slab reinforcement is given in Figure 3.16. Special kinds of the spikes were manufactured of GFRP material and consist of two parts. The first one is pre-cured part which was inserted in the drilled holes in concrete slab and the other part include dry fibers, which was used for bonding purpose as seen in Figure 3.17.

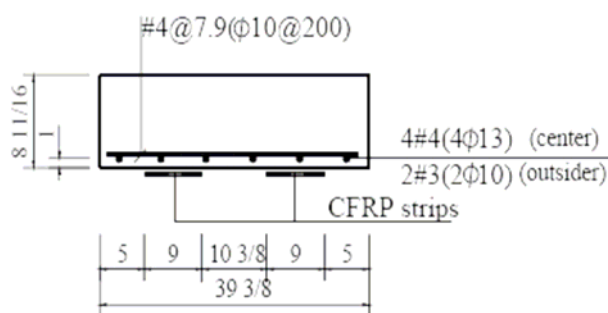


Figure 3.16 Slab details

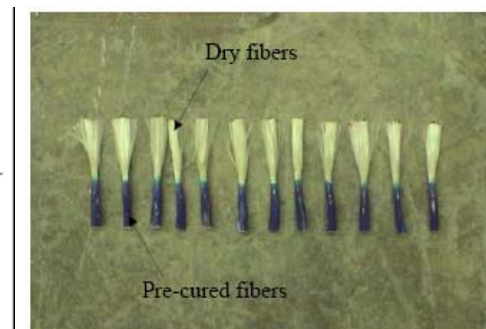


Figure 3.17 CFRP Anchor spikes [21]

Strengthening of the slab by using the developed prestressing CFRP system with presence of the GFRP anchor spikes include the following steps

Step 1: Installing of the prestressing and the anchoring device on the RC slab. Two steel cables are stressed to a desired prestressing level by means of hydraulic jacks. The details can be seen in Figure 3.18.



Figure 3.18 Concrete slab under Prestressing [21]

Step 2: Bonding of CFRP sheets to the concrete surface with an epoxy-based adhesive. It should be noted that the concrete surface has been cleaned and sandblasted before spreading of epoxy. Thereafter twelve holes with 90 mm depth and 12.7 mm diameter were drilled and cleaned by an air vacuum for installation of the GFRP anchor spikes. The spikes were inserted to the pre-drilled holes by embedding the pre-cured part of the spikes to the holes and distributing of the dry part equally and bonding it to the outer surface of the sheets, Figure 3.19.

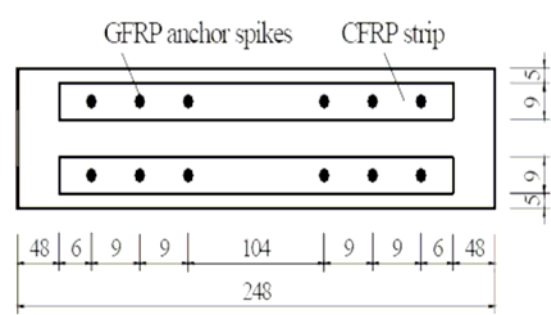


Figure 3.19 Inserting of spikes

Figure 3.20 Locations of the spikes [21]

Step 3: In this stage the steel cable from step 1 were released after curing of the CFRP sheets and spikes and the temporary anchors (steel angel) were removed. The load was applied in order to check the capacity of the slab and the efficiency of the anchoring system. It should be observed that one control slab with the same reinforcement and a dimension without strengthening was tested under the same load condition.

Results:

These strengthened and un-strengthened slabs were tested to the ultimate strength and subjected to a simply supported 4-point concentrated static loading test setup. Test results indicate that both the serviceability and flexural capacity were significantly increased due to the presence of the prestressed CFRP sheets. The strengthened slab failed due to rupture of the CFRP sheets at mid-span and no debonding at ends of the CFRP sheets was observed, as can be seen in Figure 3.21. Furthermore, bond stress profiles along the length of the CFRP sheets were computed from strain gauge data and indicate that the GFRP anchor spikes were effective in preventing debonding of the CFRP sheets and stress concentration was less than that in the un-strengthened slab.

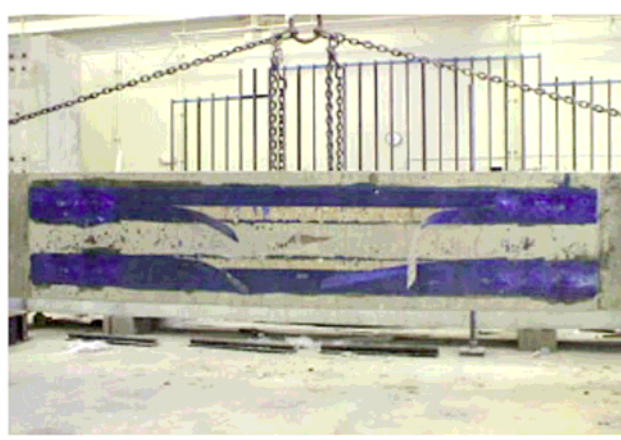


Figure 3.21 Rupture of the CFRP at mid span [21]

The ultimate load and moment capacity based on the assumption that each of the strips break completely were 17.21 kN and 85.30 kNm respectively, while the theoretical analyses results were 22.27 kN and 103.6 kNm. This is due to the fact that loss was induced in the prestressing system during releasing of cables. For the case of un-strengthened slab the ultimate load which was recorded was about 5.6 kN.

The deflection at mid-span was 141 mm, compared with 100 mm for the control slab. The calculated ultimate theoretical deflection was 170 mm, which was based on a moment-curvature analysis and computed according to the conjugate beam theory.

3.3.6 The LEOBA prestressed CFRP tendon system

In this research the high shear stress in the adhesive at the ends of the laminate has been treated by using a developed mechanical anchorage system. The system consist of a temporary friction anchors and permanent double-lapped anchorage system, which provide a smooth transfers of prestressed force from the laminates to the anchors as well as from the anchors to the structural member.

Principle of Reducing Shear Stress

The lamina is stressed using friction anchors, which can be used as temporary anchors for the stressing operation to reach the defined stress level and hold CFRP strips until final, bonded anchorages are installed and cured (permanent anchor). Then these temporary anchors can be removed and used for the next stressing operation.

The permanent anchorage of CFRP strips is formed by a double-lapped adhered connection in between bolted steel plates as shown in Figure 3.22 [5].

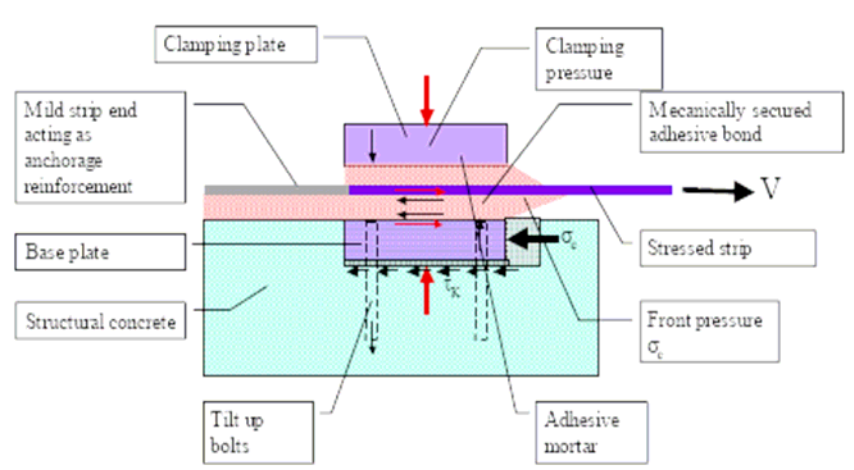


Figure 3.22 Transfer of prestressing force from the double-lapped permanent anchor to the concrete [9]

After stressing of the CFRP lamina and installing of the permanent anchors, the final permanent anchors are loaded from the rear during removing of the temporary anchors. This case of loading produce shear stress distribution of a bonded CFRP lamina in thin adhesive layers, which characterized by high shear stress at the mid-end side of the anchor and steep decrease of the shear stress along the bonded length of the stressed-end side. For further loading and by increasing strains and stresses beyond the prestressing level, the anchorage system is then loaded from its front, on the contrary of the first case as in Figure 3.23. At the ultimate stage (at breaking load of the CFRP lamina) the adding both shear force distribution cases a uniform shear stress distribution can be obtained, which provide the required high anchorage efficiency.

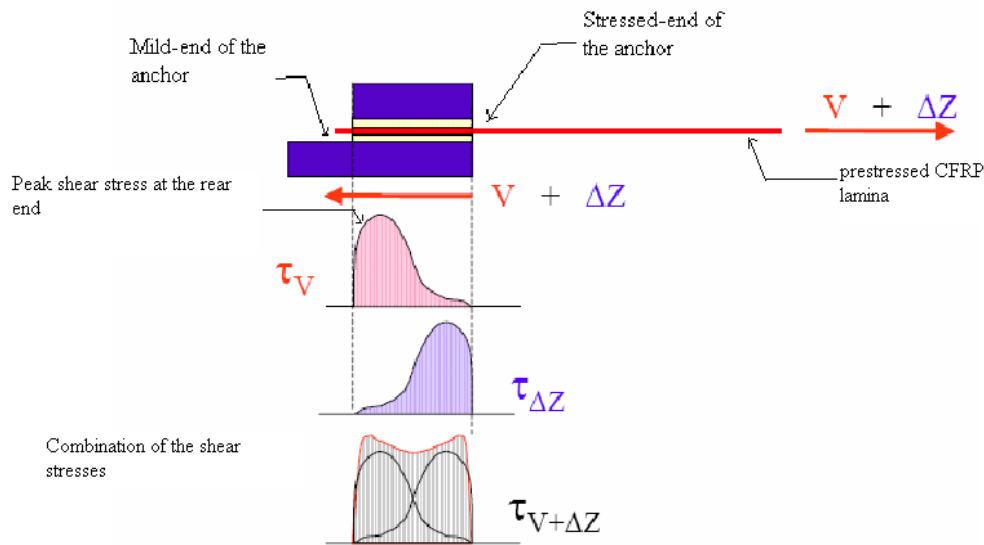


Figure 3.23 Shear stress distribution inside the final anchorage induced by rear-loading of prestressing force V (τ_V), front-loading of additional forces ΔZ ($\tau_{\Delta Z}$) and its super position ($\tau_{V+\Delta Z}$) [9]

Experimental part of the Double lapped anchorage system

The efficiency of the developed system has been checked in static load test as shown in Figure 3.24. The test device consists of two concrete blocks connected by an intermediate jack which introduces the tensile stress in the CFRP strips. A steel base plate of the permanent anchors formed the lower part and inserted into the recess of the concrete blocks to insure the effective transfers of the force into the concrete. The clamping part formed the upper part for the permanent anchorage system and coated the lower part with CFRP strips surrounded by adhesive bed in between. The CFRP strips were clamped between a two part frictional anchorage by high tensile bolts, to increase the adhesive strength and the interlaminar shear strength. The temporary stressing anchors were fixed to steel cross girders at the ends of the concrete blocks. The prestressing in the CFRP strips has been introduced by pushing the jacks away from each other to get the described prestressing level as shown in Figure 3.24.

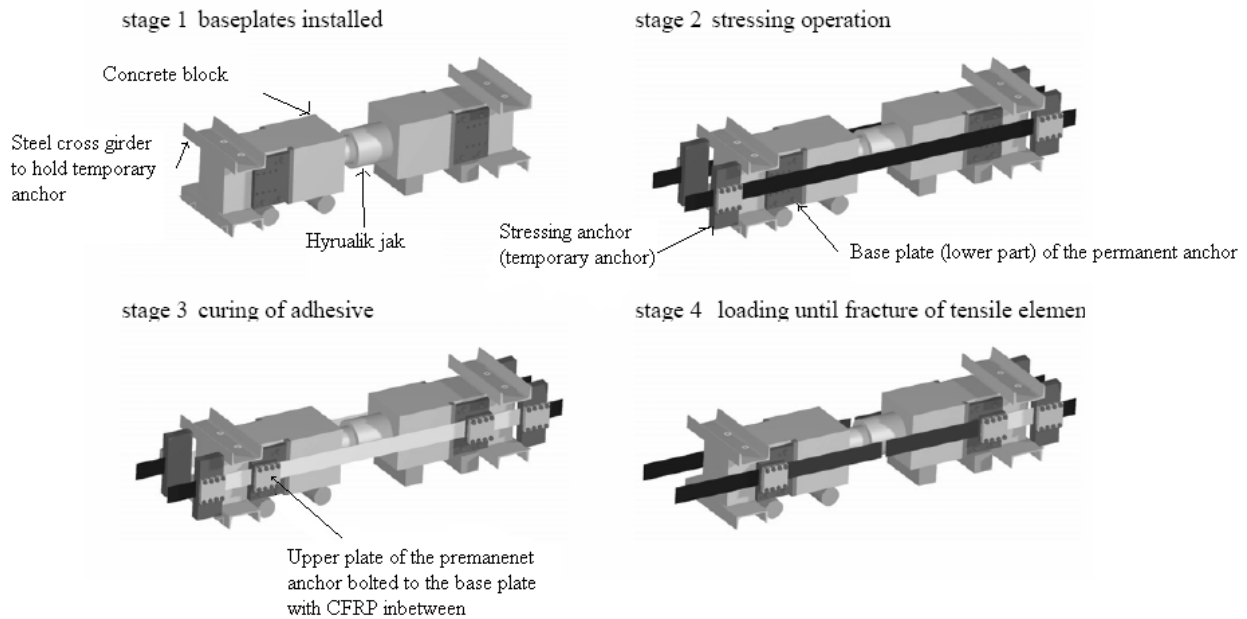


Figure 3.24 Test arrangement and test stages of static load test, “push-apart test” [9]

Results:

The laminates failed at load corresponding to 13% and 15% above their design strength. Therefore the minimum capacity of about 13-15% over the design failure force has considered being good enough.

3.4 Practical on-site Application for Strengthening and Repair of Concrete Structures with Prestressed CFRP

In this section the systems that have been applied or tested on existing structures are studied. In this manner, the ultimate load-carrying capacities of these systems are often not documented and the possible fracture modes are not established.

3.4.1 Field Applications

- The rehabilitation of a post-tensioned 4-span plate girder bridge with cracks at the bottom of the beams near the supports due to inadequate tendon profile was done in 1998. In the first generation the monostrip tendons of CFRP consisting of 50mm x 1.2mm Sika Carbodur strips which were stressed to 60 kN was used.



Figure 3.25 Staggered anchorages of the Gomadingen Rehabilitation in 1998 [5]



Figure 3.26 Working stages: above: Stressing, below: curing, Sparkasse [5]

In further development, the size of the strips and the prestressing force was subsequently increased. A 90mm x 1.4mm strip with 165 kN prestressing force was applied in Oct. 2001 at the Koerschtal Bridge near Stuttgart, Germany. (Figure 3.27 and 3.28)



Figure 3.27 Four-lane Koerschtal Bridge near Stuttgart strengthened by 20 CFRP Mono-strip Tendons Oct 2001



Figure 3.28 Strengthened web at Koerschtal Bridge, five stressed 90x1.4 mm² strips, unbonded mild anchorage strips at the ends [6]

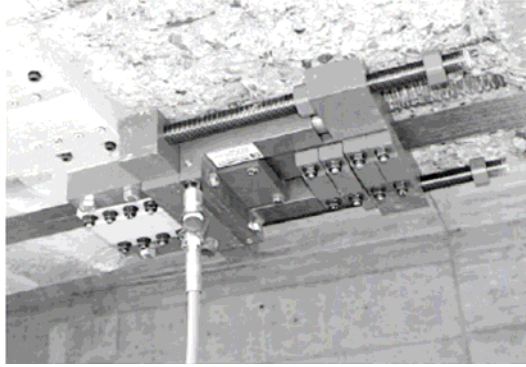


Figure 3.29 225 kN stressing jack with temporary anchor and permanent anchor in place, stressing 2nd generation



Figure 3.30 Stressed 90 x 1,4 mm² strips at Koerschtal Bridge near Stuttgart, Germany Oct.2001, unbonded mild anchorages strips at the ends [5]

- A concrete bridge in Ravenna, Italy was strengthened by four CFRP Monostrip tendons, each 30m long in Oct. 2003. Due to a truck collision two of the four internal tendons of the one of the prestressed concrete girders were cut and repair and strengthening works were necessary. By applying 4 external CFRP tendons, each stressed to 165kN, the girder got back to its load bearing capacity. The strengthening operation was supervised by onsite deflection measurements and a final insitu load test proved the effectiveness of the strengthening work.



Figure 3.31 Side view of Ravenna Bridge and leoba-CarboDur arrangement with four CFRP tendons [5]

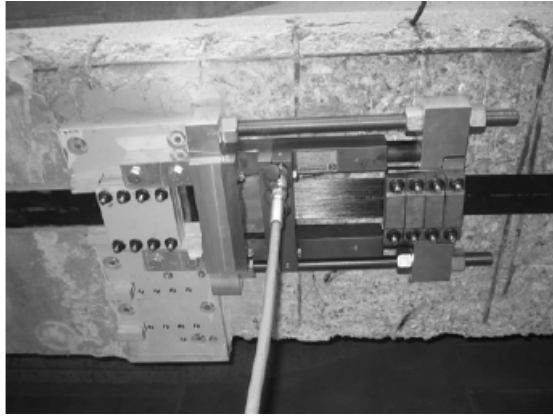


Figure 3.32 Stressing operation, total stressing length 27cm

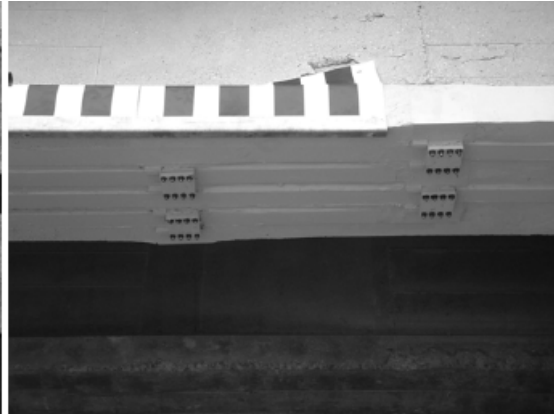


Figure 3.33 Final stage of staggered anchorages [5]

- The bridge for the Neckar valley Highway Overpass near Heilbronn Germany which was built in 1965-67 with a span of 585m had to be repaired, strengthened and refurbished. The bridge consists of two parallel superstructures with 15 spans of 39m length each and was post-tensioned in longitudinal and transversal direction with 32mm diameter bars. The cross-sections are double T beams with 3m depth and have originally built without diaphragms. Steel pipe diaphragms have been added at the supports to reduce support rotations. The bridge has 14 coupling joints per superstructure where all 42 bars were coupled. All coupling joints were cracked at the time of repair which resulted in an unacceptable cyclic stress range in the bar couplers. Prestressing forces are needed in the coupling vicinity to reduce the live load band width of stress range in the bar couplers.

The CFRP tendons were selected for the repair because of the economy. The bending moment was calculated assuming 70% residual prestressing force, 12K temperature gradient and alternative live loads with almost 50% traffic load which causes a maximum stress of 27600kNm and a minimum stress of 20483kNm.

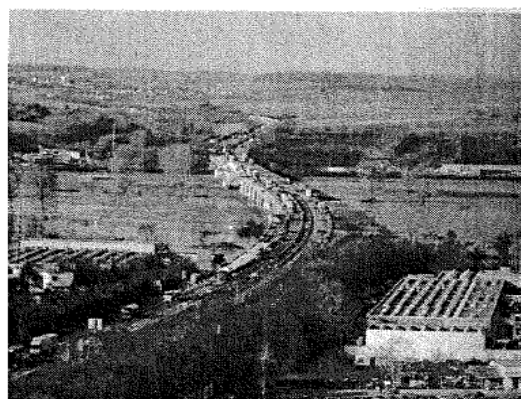


Figure 4.34 Six-lane Highway Bridge across river Neckar near Heilbronn, Germany strengthened by 252 CFRP Mono-strip Tendon [6]

The steel stress band width in the couplers was reduced by 33% bringing the stress below the fatigue limit of the couplers after the use of 9 additional CFRP tendons with 90mm x 1.4mm cross-section and 150kN prestressing force, the bending moment – steel stress diagram was also shifted as shown in the Figure 3.35.

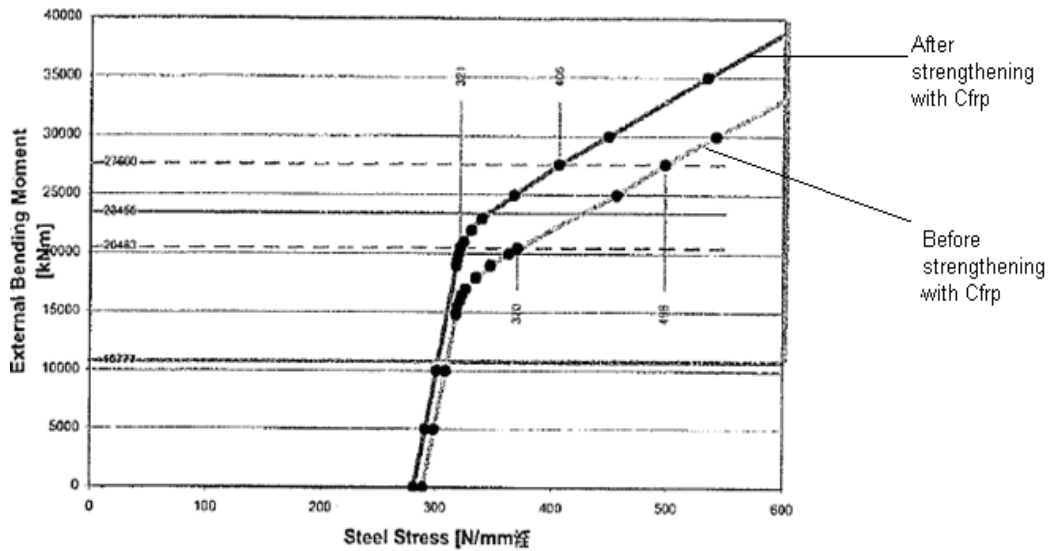


Figure 3.35 Bending Moment – Steel Stress Diagram, Neckar Valley Approach Bridge [6]

The stressing sequence and the arrangement of 7 tendons underneath and 2 along the faces of the webs are shown in the Figures 3.36.

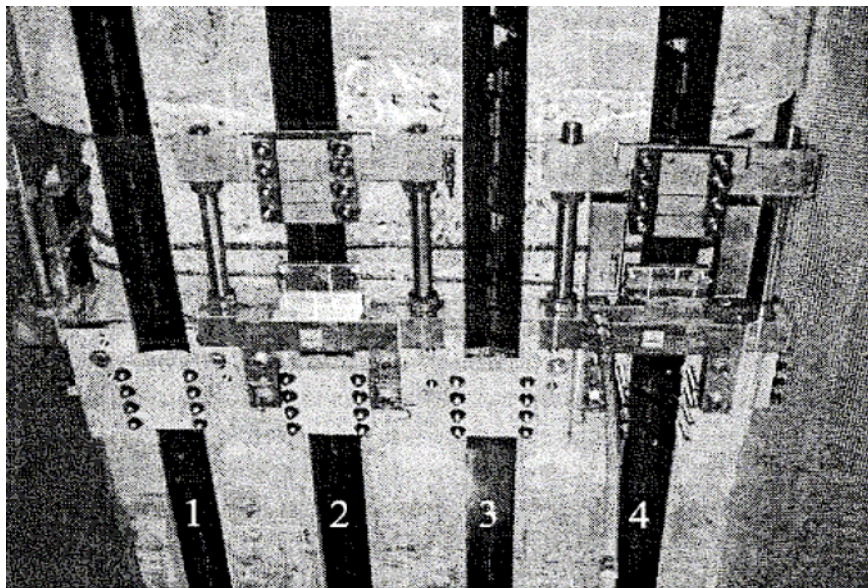


Figure 3.36 Stressed CFRP tendons underneath the web: Nr.1 dead end, Nr. 3 dead end, Nr. 4 during stressing with horse shoe jack

3.5 Strengthening and repair of steel structures

This section includes one application of prestressed CFRP on metallic beam, in order to increase the load carrying capacity of the members. As mentioned before in concrete structures, steel members have to be prepared to ensure the desirable performance of the strengthening system. The steel surface should be sandblasted and roughened by sandpaper to remove paint and corrosion. Both the steel and laminate have to be cleaned with acetone to remove dust and any other contaminate agent. In order to avoid galvanized corrosion induced by a galvanic reaction of the steel with the carbon fibres, a thin layer of prime should be applied on the steel surface.

3.5.1 The Hythe Bridge project-ROBUST

The Hythe Bridge in Oxford, UK was constructed in 1874 and consist of two square clear spans of 7.8m. The bridge decks made of 8 inverted T-section cast iron beams and brick jack arches between the beam flanges. The view and typical section of the bridge is shown in Figures 3.37 [12].

The bridge had load carrying capacity of about 7.5 tonnes, and according to new EU regulation, the bridge capacity should not be less than 40 tonnes. The inspection works showed that the bridge was weak with respect to moment capacity, but able to support the full 40 tonnes of the load in shear. Therefore in 1997 the weakened beams of the bridge have strengthened using prestressed CFRP, in order to increase the capacity from 7.5 tonnes to 40. The prestressed was designed to remove all tensile stresses from the cast iron beams under the full loading condition. Therefore each beam was stressed with four CFRP plates, and each CFRP stressed to a total of 18 tonnes.

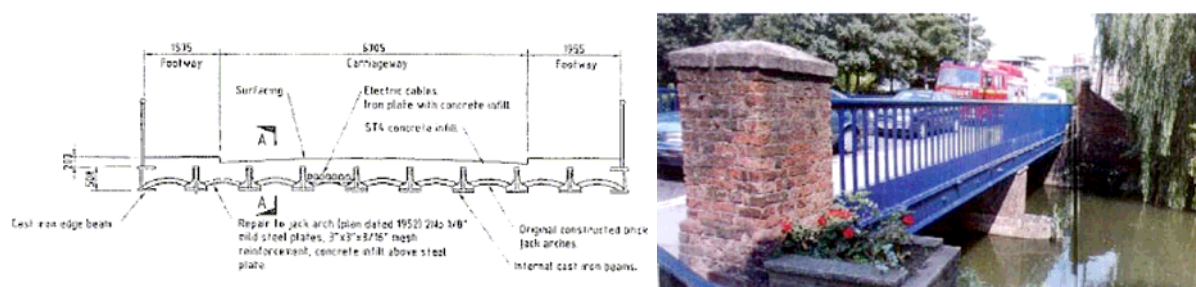


Figure 3.37 View and typical Cross-section of the bridge [14]

The CFRP ends bonded to steel plates to provide means of attaching jacking equipment. The final anchorage systems were attached to the weakened beams, consist of several plates bonded and bolted to the beam. Hydraulic jacks were used to prestress the CFRP. The end plates of the laminates were inserted into the anchorage

system, and the stressed plate is secured after extension by a shear pin that transfers load from the end-tab to the anchorage.

This method provides a practical solution for strengthening of the bridge, since the work could be carried through without closing the bridge for traffic.

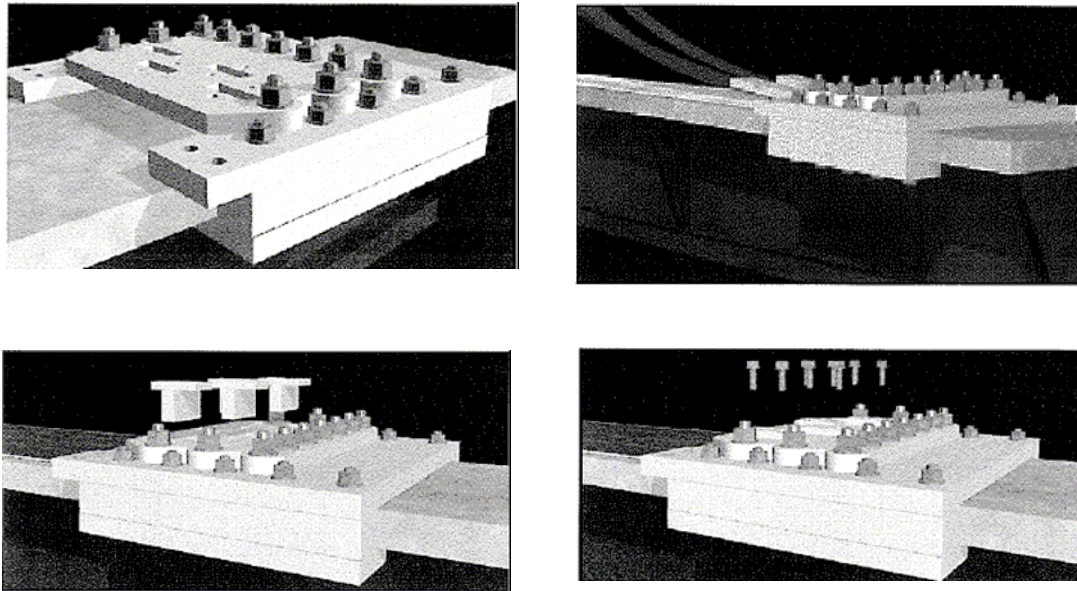


Figure 3.38 Prestressing and anchorage system [16]

3.6 Fast heat-induced curing for prestressed strengthened system

The concept of curing adhesive by heating has been recently implemented in a system of strengthening structural members with prestressed CFRP, in order to reduce the level of Prestressing in the laminate. Meier [15] has recently developed a new tensioning device which allows variation of the prestress in the laminate. This variation facilitates application of the laminate with a gradual reduction of a prestress to zero at the end, and then reducing the effect of shearing at the end of the concrete members. A heating system is used to speed up the curing of the adhesive in the bonded sections and allow bonding of the subsequent sections within the working life of the adhesive.

Procedure

The Prestressing device consist of two tensioning unites (rollers) connected to each other by means of a beam. The laminate is rounded over the rollers and clamped at the ends. The laminate may be tensioned by turning one of the rollers, as shown in Figure 3.43 and Figure 3.44. The fully pretensioned section in the centre of the laminate is bonded to the member by adhesive. After curing of that part by means of heating system the tensioning force is slightly reduced and another section bonded at either side. This process is repeated until the required prestress gradient in the laminate is achieved.

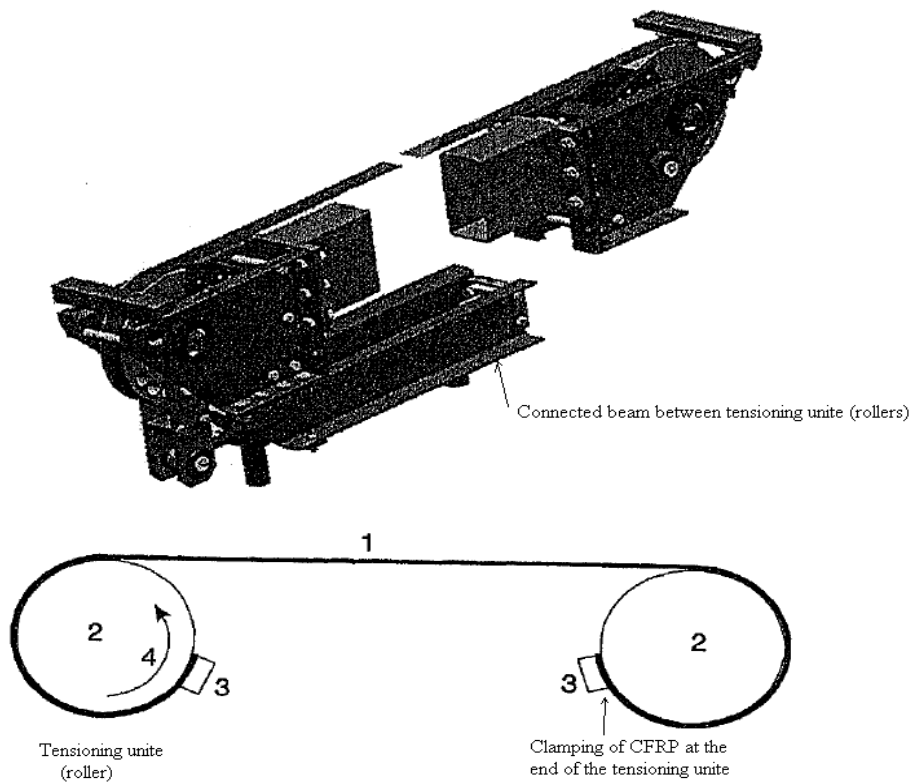


Figure 3.43 System of Prestressing of the laminate [17]

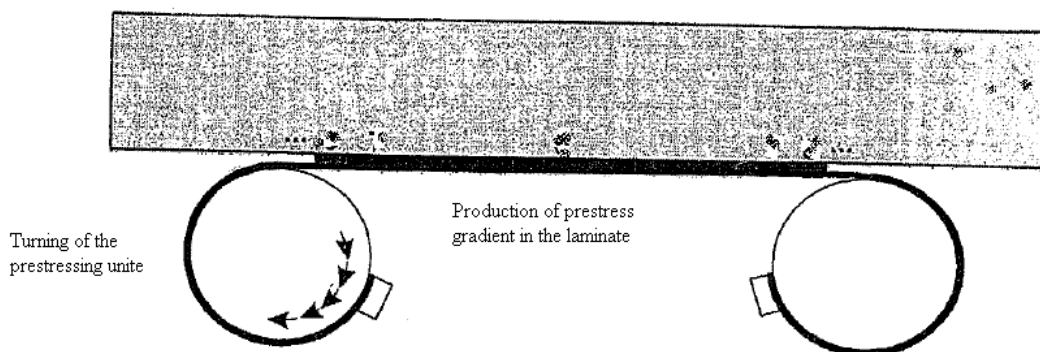


Figure 3.44 Production of prestress gradient in the laminate [17]

Results

The concept of gradual releasing has been tested under laboratory condition and the strain results are illustrated in Figure 3.45. It is apparent from the diagram that the strain along the member is reduced toward the ends, since this method results in high prestress force at the middle which is decreased gradually toward the ends of the laminate. The shear stress at the ends of the laminate is also reduced without using mechanical anchorage system.

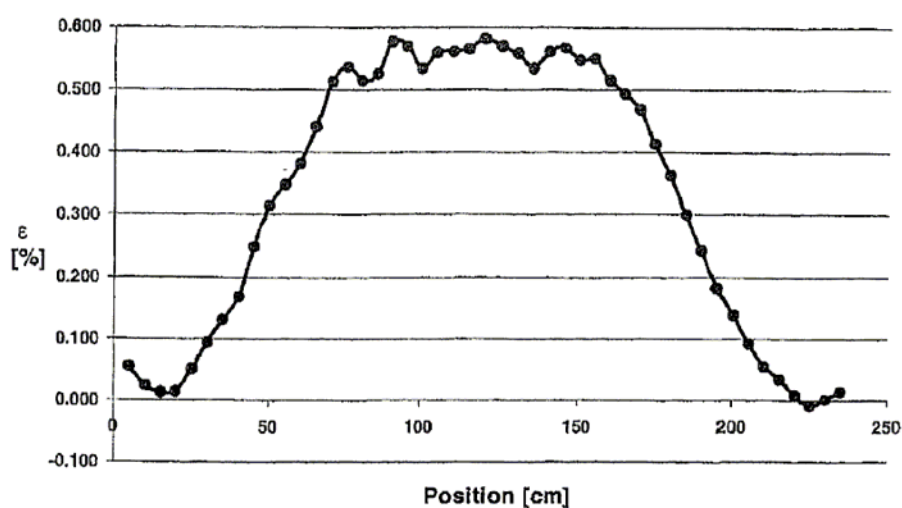


Figure 3.45 Strain over length of 1 mm thick, 50mm wide CFRP laminate bonded to the concrete with prestress gradient [17]

3.7 Discussion

Application of CFRP laminates to reinforce structures is an evolving field which has been under investigation for many decades. Some progress has been achieved concerning laboratory studies but there is no unified criteria or any normative which rules the application and use of this promising material.

It has been observed that for flexural strengthening of structural members it is necessary to prestress the CFRP laminates in order to obtain a greater benefit from their properties. The non-prestressed application of CFRP laminates might improve, in the best case about 15% of the load carrying capacity of a structure.

When prestressing has been applied, it has been discovered that the shear stresses at the end of the laminates are higher which might leads to peeling of the laminates and failure of the strengthening system.

It can be seen from the properties of the laminate and the adhesive that by heating the adhesive, the stiffness is decreased which helps to transfer the prestressing force from the laminate to the structure with the decrease of the shear stress enabling to strengthen the structure. There is still a long way to go, because most of the strengthening systems are not viable and the long-term performance is still unknown.

The existing prestressing system used for concrete structures give us a starting point to come up with a new improved system for steel structures. Different models of anchorage devices used for concrete are also key elements for further application in steel structures, which should be more reliable due to its properties.

Concerning the adhesive, the experience of shaping it at the ends and tapering the laminates are important knowledge to try in order to lower the stress concentration at the ends of the laminate. The concept of curing the adhesive by heating has been recently implemented in the system of strengthening structural members with prestressed CFRP, in order to reduce the level of prestressing at the ends of the laminate. The shear stress at the ends of the laminate is also reduced without using mechanical anchorage system.

4 Principle of Controlling Interfacial Stresses

Interfacial stresses are developed in the bond line of a composite structure when the structure is loaded with the external load or due to prestressing. The interfacial stresses which develop are very high in magnitude and can even cause failure and lost the composite action of the structure. It is therefore of greater importance to decrease the interfacial stresses in the composite structure. In this chapter, a new technique for controlling the interfacial stresses in beams strengthened with prestressed bonded CFRP laminates is introduced and discussed.

4.1 Principle

As described earlier in order to increase the strength of the composite beam the laminates are to be prestressed and this can be done by various methods. The laminate is prestressed and bonded to the steel beam with adhesive. When the prestressing force is released, the force is transferred to the steel beam through the adhesive which makes the steel beam to camber upwards and induces the compressive force. During prestressing the laminate is elongated and tries to come back to its original state when the prestressing force is released. It is however prevented by the adhesive which has a considerable stiffness resulting in the development of shear stress in the bond line. The axial force from the CFRP which is to be transferred to the steel through the adhesive is increased from zero at the end of the laminate to the prestressing force (P_s) over a small length which causes higher shear and peeling stress at the end of the laminate. A part of the prestressing force (P_s) that is to be transferred from the CFRP laminate through the adhesive is depended on the stiffness of the adhesive. The stiffer the adhesive, the more force is transferred from the CFRP laminate to the steel, so that the total forces in steel and CFRP laminate are equal to the prestressed force. With the increase of stiffness more force to be transferred is linked resulting in the increase of the shear stress, the adhesive can transfer the force to the steel beam until it reaches the ultimate shear strength.

The principle of decreasing the shear stress at the end of a prestressed laminate can be described as a gradual transformation of prestressing force from the laminate to the steel beam. The transformation length is dependent on the stiffness of the adhesive. Test done by DMTA, reveals that the stiffness of the adhesive is decreased with the increasing temperature. The temperature of the adhesive can be increased by heating the adhesive over a certain distance from the end. With the decrease of temperature along the longitudinal direction, the stiffness is increased accordingly. As the stiffness of adhesive is less at the ends, a small amount of force is transferred to the laminate which is increased gradually with the increase of stiffness thus increasing the transfer length.

As the force to be transferred is increased gradually, the shear force in the adhesive starts from zero and reaches the maximum value gradually making the distribution of shear over a larger area along the length with the reduced peak value. In order to understand more about the behaviour of composite beam with the heating techniques one can study a simple steel plate with a thickness of 20mm and a width of 80mm strengthened with a CFRP laminate of thickness 4mm at the bottom, the laminate is bonded to the steel plate with an adhesive having a thickness of 1.5mm as shown in Figure 4.1.

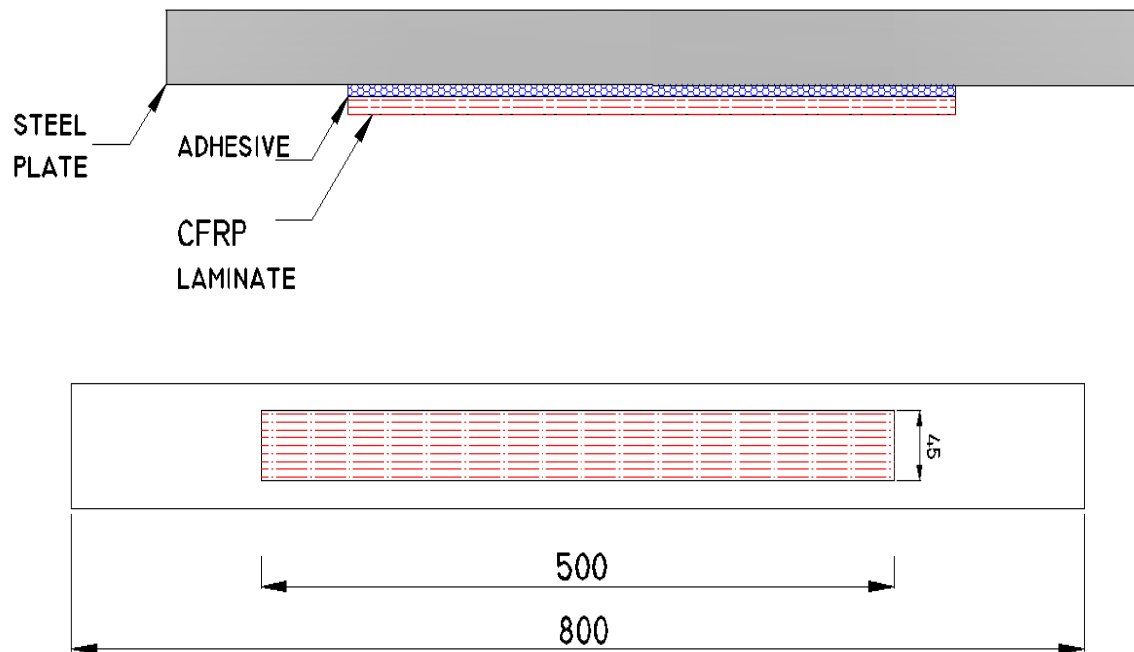


Figure 4.1 Cross-section and the plan of composite plate

When the steel plate is loaded in tension with a force (P) a part of the load (P_1) is transmitted to the CFRP laminates through the adhesive. The portion of the load carried by the laminate depends on its axial stiffness in relation to that of the steel plate. The axial force in the laminate is increased from zero at the ends to (P_1) over a smaller distance causing the higher shear and peeling stresses at the end of the laminate. Figure 4.2 shows how the force is transferred to the laminate and also the development of shear stress along the length of the adhesive.

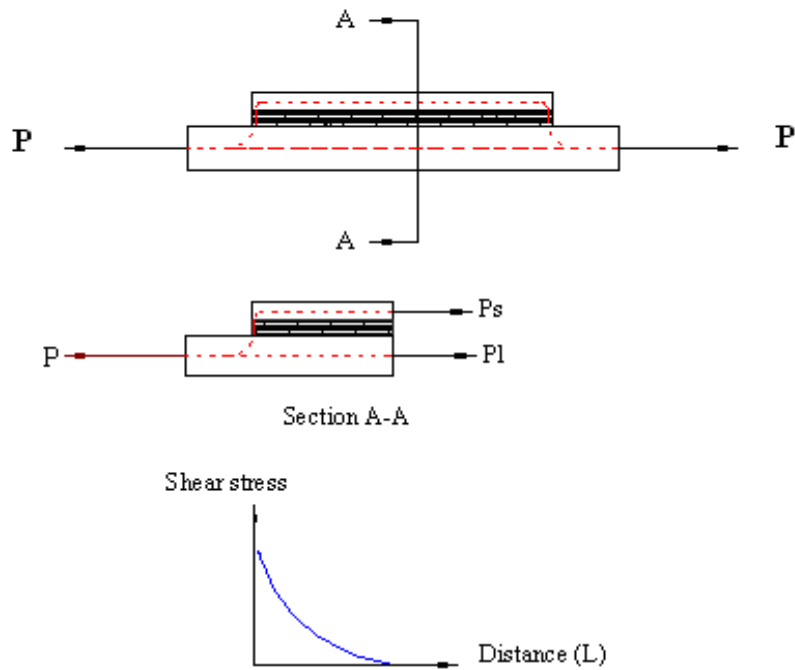


Figure 4.2 Transformation of the prestressed force in the composite plate

As explained earlier the shear stress can be decreased by heating the adhesive to a certain temperature. According to the results of DMTA tests, the stiffness of the adhesive is decreased with increasing temperature. The force to be transferred through the adhesive is linked from almost zero to the value P_1 gradually depending on the stiffness of the adhesive. As the stiffness is increased with the decreasing temperature through the length, the force to be transmitted is linked depending on the stiffness and increases accordingly, thus increasing the transfer length. With the increase of transfer length the shear stress is distributed over a larger region decreasing the peak value and increasing the tensile load to cause failure as shown in Figure 4.3.

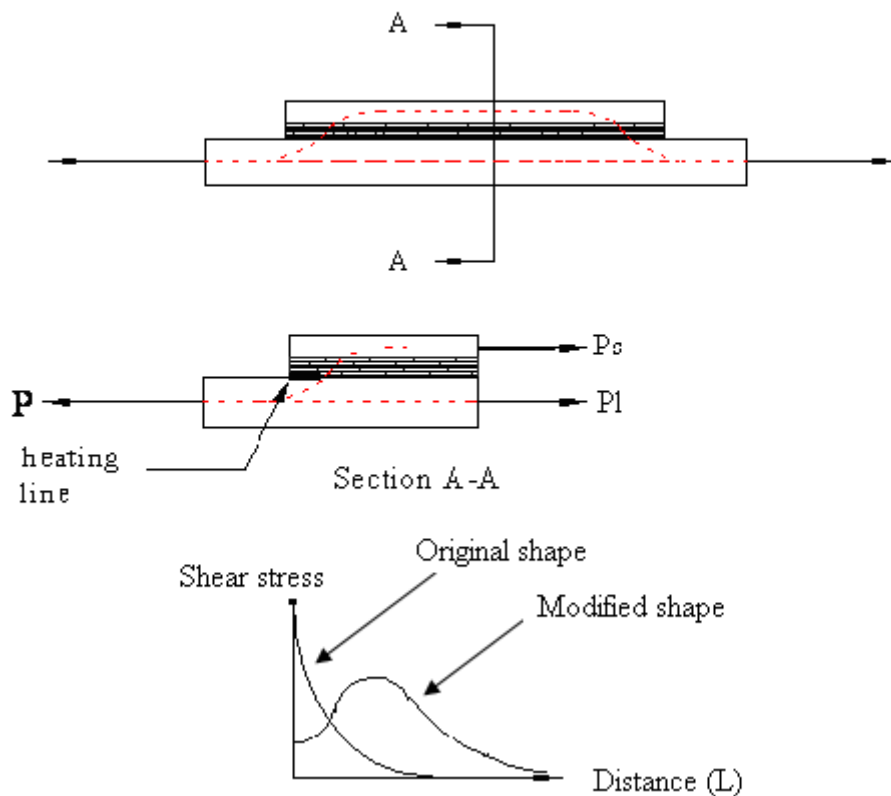


Figure 4.3 Transformation of the prestressing force in the composite plate in case of applying heat

The above model is simple and helps to understand the behaviour of the heat treated composite plate, the change in the stiffness of the adhesive with the temperature and its effect on the shear and peeling stresses at the end of the laminate. Figure 4.4 show that the stiffness of the adhesive is reduced with temperature drastically. The E-modulus Vs temperature curve is obtained from a DMTA test. DMTA is a powerful thermo-mechanic analysis for polymers and fibre materials. With DMTA the mechanical properties of a material over a wide range of temperature can be examined. The method is based on loading the tested element with dynamic or static load in a preferable temperature and / or frequency. The received results from the analysis are saved and drawn, where the modulus of elasticity of the tested elements and damping as a function of temperature or frequency can be seen. When the adhesive is at a temperature of 80°C the stiffness is reduced from 7 GPa to 0.05 GPa for the specific adhesive studied here.

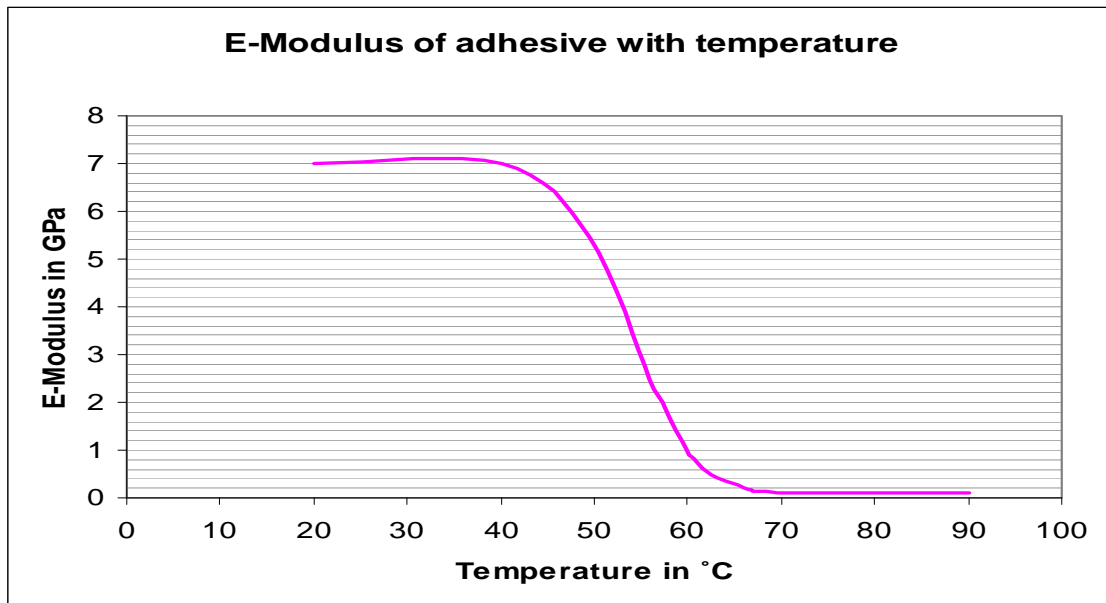


Figure 4.4 The E-modulus of adhesive with the temperature

The principle to reduce the shear stress at the end of the CFRP laminate is by heating the adhesive to a temperature of 80°C and reduce the stiffness gradually from 7 GPa to 0.05 GPa so that the force to be transferred is linked gradually with the increasing stiffness of the adhesive. When the force is linked gradually, the transfer length is increased, the shear stress is increased gradually causing a more uniformly distributed shear stress in the adhesive instead of a peak shear stress pattern at the end of the laminates as shown in Figure 4.3.

4.2 Consequences due to heating

Heating is a complicated technique with three different materials having different properties and forming a composite element. Steel is highly conductive while the adhesive and CFRP laminate are less conductive. The coefficient of expansion due to heating is higher for the adhesive compared to steel and CFRP laminate which has negligible expansion. Due to heating, the different materials can expand at different rates affecting the development of shear stresses in the composite member. The other factor affecting the shear stress is the distribution of the temperature in the three materials and most importantly in adhesive. The stiffness of the adhesive changes drastically from almost 5GPa to 0.9 GPa when the temperature is increased from 50 to 60 °C. In order to have a more uniform distribution of the temperature it is important to find a good location for the heat source. The distribution of temperature is affected by the conductivity of the materials as well as the duration of heating and the length along which the heat can be applied. If the heat is applied for a longer time the steel plate expands more as the temperature in the steel is higher and will be distributed over a larger area due to higher conductivity. The portion of adhesive which is near

the steel expands more due to higher temperature and higher co-efficient of expansion while the part of adhesive attached to the CFRP laminate expands less as the temperature in the CFRP laminate is less and also the co-efficient of expansion is negligible. This situation causes higher shear stresses. The force to be transferred is linked according to the stiffness. In order to obtain the distributed shear across the length of the adhesive the increase of the stiffness should be gradual which in turn depends on the temperature distribution. In order to obtain a good profile of temperature it is important to determine how to apply the heat, fix the position of heat source, the duration of heating and the length of heating.

5 Heat Transfer Essentials

As mentioned in the previous chapters, the end effect i.e. stress concentration around the adhesive free ends can be treated in several ways. The concept of heating has recently been utilized in the process of curing the adhesive to decrease the high shear stress produced at the ends due to prestressing of the CFRP laminates. Since heating is used in this thesis as a method to reduce shear and peeling stress concentration in the adhesive, it is essential to know the principle of heat transfers and the parameters that governing the flowing of heat as well as the effect of different material properties on the flow in different materials.

5.1 Definition of heat parameters

5.1.1 Heat transfers

Heat flows normally from a high temperature object to a lower temperature object. Heat transfer changes the internal energy of both systems involved according to the First law of Thermodynamics. The first law of thermodynamics is the application of the conservation of energy principle to heat and thermodynamic processes:

The change in internal energy of a system is equal to the heat added to the system minus the work done by the system

$$\Delta U = Q - W \quad (5.1)$$

The first law makes use of the key concepts of internal energy, heat, and system work. It is used extensively in the discussion of heat engines.

The heat transfer may occur by two mechanisms conduction and radiation. In engineering applications, the term *convective heat transfer* is used to describe the combined effects of conduction and fluid flow and is regarded as a third mechanism of heat transfer.

5.1.2 Conduction Heat Transfer

Heat energy will flow from the region of high temperature to the region of low temperature, when there is a temperature gradient within a body. This phenomenon is known as conduction heat transfer, and is described by **Fourier's Law** (named after the French physicist Joseph Fourier, $Q = -k \, dt/dx$),

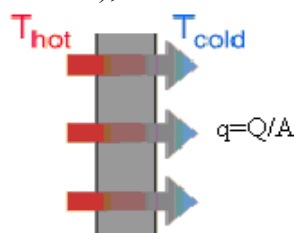


Figure 5.1 Conduction through body [32]

Heat Flux: The amount of heat, transferred in a liquid, in particular in the atmosphere, per unit of time through a unit area.

The rate at which heat is transferred is represented by the symbol Q . Common units for heat transfer rate is J/hr. Sometimes it is important to determine the heat transfer rate per unit area, or heat flux, which has the symbol q . Units for heat flux are J/hr-m. The heat flux can be determined by dividing the heat transfer rate Q by the area through which the heat is being transferred. [31]

$$q = \frac{Q}{A} \quad (5.2)$$

$$\frac{Q}{t} = \frac{kA(T_{hot} - T_{cold})}{d} \quad (5.3)$$

Where :

q = heat flux (J/hr-m);

Q = heat transfer rate (J/hr);

k = thermal conductivity of the barrier;

A = area (m^2);

d = thickness of barrier;

t =time

Thermal Conductivity: The heat transfer characteristics of a solid material are measured by a property called the *thermal conductivity* (k) measured in J/hr-m-K. It is a measure of a substance's ability to transfer heat through a solid by conduction.

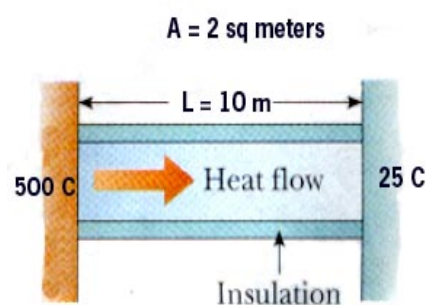
Conduction example[]:

The energy conduction per time through a Steel pipe with $K=14 \text{ J/s-m-C}$ in 40 Second can be calculated as follow:

$$\frac{Q}{t} = \frac{kA(T_2 - T_1)}{d}$$

$$\frac{Q}{t} = \frac{14 * 2 * (500 - 25)}{10} = 1330 \text{ J / S}$$

$$Q = 40 * 1330 = 5.32 * 10^4 \text{ J}$$



5.1.3 Convection Heat Transfer

Convection is heat flux by mass motion of a fluid such as air or water when the heated fluid is caused to move away from the source of heat, carrying energy with it. Convection above a hot surface occurs because hot air expands, becomes less dense, and rises. Hot water is likewise less dense than cold water and rises, causing convection currents which transport energy. The basic relationship for heat transfer by convection has the same form as that for heat transfer by conduction:

$$Q = h A \Delta T \quad (5.4)$$

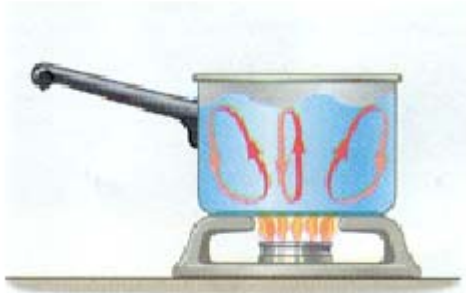
Where :

Q = rate of heat transfer (J/hr);

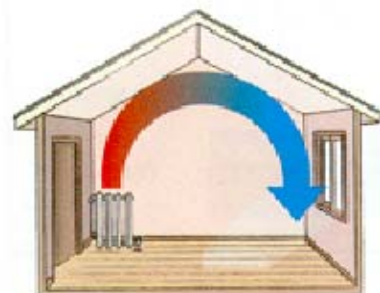
h = convective heat transfer coefficient (J/hr- m-°K);

A = surface area for heat transfer (m²);

ΔT = temperature difference (°K).



Hot water rises, cools and then falls



Heated air rises, cools and then falls. Air near heater is replaced by cooler air, and the cycle repeats

Figure 5.2 Type of convection [33]

The typical combined heat transfer situation can be illustrated by a flow in pipe at different situations as in Figure 5.3. Heat transfer by convection occurs between temperatures T_1 and T_2 ; heat transfer by conduction occurs between temperatures T_2 and T_3 ; and heat transfer occurs by convection between temperatures T_3 and T_4 .

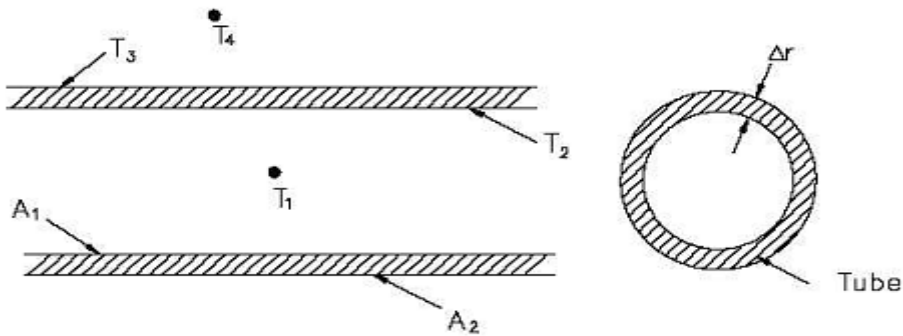


Figure 5.3 Conduction & Convection principle [30]

5.1.4 Radiation Heat Transfer

Radiation heat transfer is concerned with the exchange of thermal radiation energy between two or more bodies. Thermal radiation arises as a result of a temperature difference between 2 bodies. The heat transferred into or out of an object by thermal radiation is a function of several components. These include its surface reflectivity, emissivity, surface area, temperature, and geometric orientation with respect to other thermally participating objects. In turn, an object's surface reflectivity and emissivity is a function of its surface conditions (roughness, finish, etc.) and composition. The relationship governing radiation from hot objects is called the Stefan-Boltzmann [29].

$$P = e\sigma A(T^4 - T_c^4) \quad (5.5)$$

Where :

P= net radiated power;

e=emissivity (equal to 1 for ideal radiator);

A= radiating area;

T= temperature of radiator;

σ = Stefan's constant;

T_c = temperature of surroundings;

$\sigma=5.6703 \cdot 10^{-8}$ watt/m² K².

Example: How much does the human body radiate?

*Body temperature = 37 C = 37 + 273 = 310 K,
Estimate surface area A = 1.5 m² e = 0.70*

$$\begin{aligned} H &= esAT^4 \\ &= (0.70) \cdot (5.67 \times 10^{-8}) (1.5 \text{ m}^2) (310)^4 \\ &= 550 \text{ watts (5 light bulbs)} \end{aligned}$$

**The sun provides about 1000 watts per square meter at the Earth's surface. 30 % is reflected by human skin. 700 watts is absorbed per square meter.*



Radiant heat transfer does not need a medium, such as air or metal, to take place. Any material that has a temperature above absolute zero gives off some radiant energy. When a cloud covers the sun, both its heat and light diminish. This is one of the most familiar examples of heat transfer by thermal radiation

Black Body Radiation: A body that emits the maximum amount of heat for its absolute temperature is called a black body. Radiant heat transfer rate from a black body to its surroundings can be expressed by the following equation.

$$Q = \sigma AT^4 \quad (5.6)$$

Where :

Q= heat transfer rate (J/hr);

σ = Stefan-Boltzman constant ($5.6703 \times 10^{-8} \text{ W/m}^2 \cdot \text{K}^4$);

A= surface area (m²);

T = temperature (K).

Emissivity: Real objects do not radiate as much heat as a perfect black body. They radiate less heat than and are called gray bodies. To take into account the fact that real objects are gray bodies, previous Equation is modified to be of the following form.

$$Q = \epsilon \sigma AT^4 \quad (5.7)$$

Where :

ϵ = emissivity of the gray body (dimensionless).

Emissivity is simply a factor by which we multiply the black body heat transfer to take into account that the black body is the ideal case. Emissivity is a dimensionless number and has a maximum value of 1. [29]

5.1.5 Heat Capacity

The specific heat capacity of a solid or liquid is defined as the heat required to raise unit mass of substance by one degree of temperature. This can be stated by the following equation:

$$Q = c m \Delta T \quad (5.8)$$

Where :

Q= Heat supplied to the substance (J);

m= Mass of the substance (g);

c= Specific heat capacity $J^{\circ}C^{-1}g^{-1}$;

ΔT = Temperature rise ($^{\circ}C$).

5.1.6 Steady state analysis

Steady state analysis is related to the circumstance when the temperatures at all points in the conduction region are independent of time. The energy input to the region is conducted and is lost to the neighbouring environment and no storage of energy in the region occurs. This state is of interest in long rang steady operation of system.

5.1.7 Transient Analysis

This is related to the situation when energy storage does occur and the temperature distribution in the region of interest varies with time. The governing equation which is used to determine temperature distribution is:

$$\nabla (K \Delta T) + \bar{Q} = \rho c \frac{\partial T}{\partial t} \quad (5.9)$$

5.1.8 Coupled Thermal Analysis

A coupled temperature-displacement analysis is used to solve stress/displacement and temperature distribution at the same time. It is used when the thermal and mechanical solutions affect each other efficiently i.e. it is needed when the stress analysis is dependent on thermal distribution and the temperature distribution depend on the stress solution. For example, metalworking problem may include significant heating due to inelastic deformation of the material, which in turn changes the material properties.[32]

5.1.9 Uncoupled Thermal Analysis

Uncoupled heat transfer analysis is performed to calculate temperature distribution in the elements without considering the stresses and deformations in the body. This type of analysis is used to model solid body heat conduction with general temperature dependent conductivity, internal energy and general convection and radiation boundary conditions. Heat transfer problem can be linear or nonlinear, the nonlinearity occurs since the material properties are temperature dependent or because the boundary conditions are nonlinear.

5.1.10 Thermal Boundary Condition

Boundary conditions represent the flow of heat or temperature at the boundaries of a region. There are several common types of boundary condition that are simply expressed in mathematical form as in table 5.1. The first one is called *Dirichlet condition* or initial boundary condition, which corresponds to the situation for which the surface is maintained at a fixed temperature or as function of time $T(x, y, t)$. The second type is *Neumann condition* or natural boundary condition, which corresponds to the existence of a fixed or constant heat flux at the surface. The third one is a special case of the condition and corresponds to the perfectly insulated or adiabatic surface for which $(\frac{\partial T}{\partial x})_{x=0} = 0$. This case relates to the existence of convection heating (or cooling) at the surface.

Table 5.1 Different Types of Boundary Conditions

1. Constant surface temperature	$T(0,t)=T_s$
2. Constant surface heat flux	$-k\left(\frac{\partial T}{\partial x}\right)_{x=0} = q_s$
3. Convection surface condition	$-k\left(\frac{\partial T}{\partial x}\right)_{x=0} = h[T_\infty - T(0,t)]$

5.2 Mathematical Modelling

5.2.1 Solid mechanics

5.2.1.1 Stresses

The body is assumed to be continuous and there are two kinds of forces: body forces (i.e. force per unit volume), and surface forces (i.e. force per unit area). The surface of the body in the Figure 5.4 below which are obtained from a section of this body, can be considered as an external surface or an internal surface, the vector \bar{n} is a unit vector normal to the surface and directed out of the surface. The incremental force \bar{dP} acts on the infinitesimal surface area dA . When dA approaches zero, it is assumed that the ratio \bar{dP}/dA approach a value given by:

$$\bar{t} = \frac{\bar{dP}}{dA} \quad (5.10)$$

Where :

\bar{t} is the traction vector.

$$\bar{t} = [t_x t_y t_z]^T \quad (5.11)$$

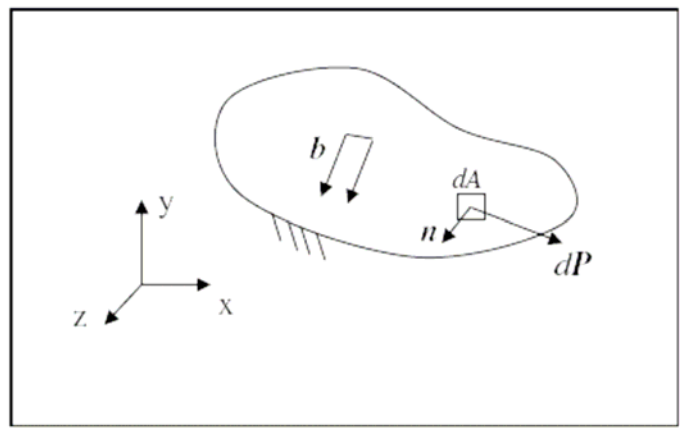


Figure 5.4 Force \bar{dP} on area dA with outer unit normal vector \bar{n}

The traction \bar{t} is related to the surface with the outer unit normal vector \bar{n} . If other sections through the same point are considered, the \bar{t} turns out to be different. Considering the traction vectors obtained with sections perpendicular to the coordinate axes, a new matrix can be defined as

$$\bar{S} = \begin{bmatrix} \bar{S}_x^T \\ \bar{S}_y^T \\ \bar{S}_z^T \end{bmatrix} = \begin{bmatrix} \sigma_{xx} & \sigma_{xy} & \sigma_{xz} \\ \sigma_{yx} & \sigma_{yy} & \sigma_{yz} \\ \sigma_{zx} & \sigma_{zy} & \sigma_{zz} \end{bmatrix}, \bar{\sigma} = [\sigma_{xx} \sigma_{yy} \sigma_{zz} \sigma_{xy} \sigma_{xz} \sigma_{yz}]^T \quad (5.12)$$

Where \bar{S} is the stress tensor and $\bar{\sigma}$ is the stress vector, see Figure 5.5. We can conclude that

$$\bar{t} = \bar{S} \bar{n} \quad (5.13)$$

This verifies that the stress tensor provides all the information to the traction vector to be derived for any direction \bar{n} .

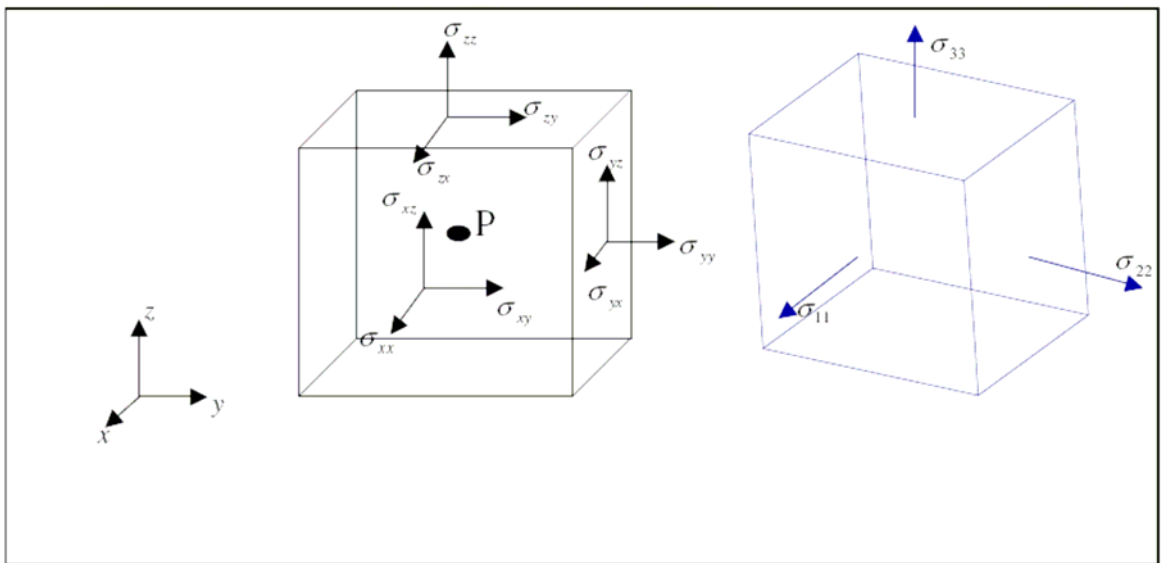


Figure 5.5 Stress vector at an arbitrary point P and principal stresses [11]

It is assumed there are only two kinds of forces acting on the body, \bar{t} along the boundary S and \bar{b} in the region V, so the equilibrium equation for an arbitrary part of the body is

$$\int_s \bar{t} dS + \int_s \bar{b} dv = 0 \quad (5.14)$$

For three-dimension bodies, the different equilibrium equations are as follows

$$\int_s \bar{t}_x dS + \int_s \bar{b}_x dv = 0, \quad \int_s \bar{t}_y dS + \int_s \bar{b}_y dv = 0, \quad \int_s \bar{t}_z dS + \int_s \bar{b}_z dv = 0, \quad (5.15)$$

As it is known that

$$\bar{t}_x = \bar{S}_x \cdot \bar{n} \quad \bar{t}_y = \bar{S}_y \cdot \bar{n} \quad \bar{t}_z = \bar{S}_z \cdot \bar{n} \quad (5.16)$$

For simplicity, take traction vector in x-direction as an example.

$$\begin{aligned} \int_s \bar{t}_x dS + \int_s \bar{b}_x dv &= 0 \Rightarrow \\ \int_s \bar{S}_x \cdot \bar{n} dS + \int_s \bar{b}_x dv &= 0 \end{aligned} \quad (5.17)$$

The first term can be reformulated using Gauss' divergence theorem

$$\int_s \bar{S}_x \cdot \bar{n} dS = \int_v \text{div} \bar{S}_x dV \Rightarrow \int_v (\text{div} \bar{S}_x + \bar{b}_x) dV = 0 \quad (5.18)$$

By using the definition of the divergence of a vector the previous equation can be written as

$$\frac{\partial \sigma_{xx}}{\partial x} + \frac{\partial \sigma_{xy}}{\partial y} + \frac{\partial \sigma_{xz}}{\partial z} + b_x = 0 \quad (5.19)$$

The same procedure can be used to derive equations in the two other directions; we obtain the following differential equations:

$$\begin{aligned} \frac{\partial \sigma_{xx}}{\partial x} + \frac{\partial \sigma_{xy}}{\partial y} + \frac{\partial \sigma_{xz}}{\partial z} + b_x &= 0 \\ \frac{\partial \sigma_{yx}}{\partial x} + \frac{\partial \sigma_{yy}}{\partial y} + \frac{\partial \sigma_{yz}}{\partial z} + b_y &= 0 \\ \frac{\partial \sigma_{zx}}{\partial x} + \frac{\partial \sigma_{zy}}{\partial y} + \frac{\partial \sigma_{zz}}{\partial z} + b_z &= 0 \end{aligned} \quad (5.20)$$

A new matrix differential operator is defined in order to compact the expression (5.19) for all directions.

$$\tilde{\nabla}^T = \begin{bmatrix} \frac{\partial}{\partial x} & 0 & 0 & \frac{\partial}{\partial y} & \frac{\partial}{\partial z} & 0 \\ 0 & \frac{\partial}{\partial y} & 0 & \frac{\partial}{\partial x} & 0 & \frac{\partial}{\partial z} \\ 0 & 0 & \frac{\partial}{\partial z} & 0 & \frac{\partial}{\partial x} & \frac{\partial}{\partial y} \end{bmatrix} \quad \sigma = \begin{bmatrix} \sigma_{xx} \\ \sigma_{yy} \\ \sigma_{xy} \\ \sigma_{xz} \\ \sigma_{yz} \end{bmatrix} \quad (5.21)$$

$$\tilde{\nabla}^T \sigma + b = 0 \quad (5.22)$$

Finally, the Plane Stress is defined as a stress state where the only nonzero stresses are σ_{xx} , σ_{yy} and σ_{xy} . Further derivations will be done under the assumption of plane stress where the stress vector can be written as [11]:

$$\sigma = \begin{bmatrix} \sigma_{xx} & \sigma_{yy} & \sigma_{xy} \end{bmatrix}^T \quad (5.23)$$

5.2.1.2 Strains

Strain is the geometrical expression of deformation caused by the action of stress on a physical body. Strain therefore expresses itself as a change of distance between two neighbouring material points as well as a change of angle between two intersecting lines. Before deformation we can describe the point by its coordinates (x, y, z) while after deformation the new point position is $(x + u_x, y + u_y, z + u_z)$ see Figure 5.6,

Where :

$$\mathbf{u} = \begin{bmatrix} u_x \\ u_y \\ u_z \end{bmatrix} \quad (5.24)$$

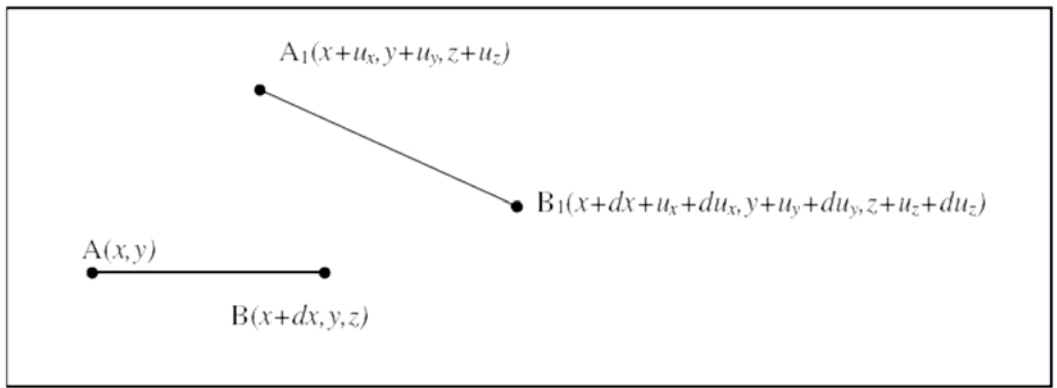


Figure 5.6 Deformation of a differential element parallel to x-direction [11]

The line between the points A and B that can be observed in the Figure 5.6 has a length of dx and it is assumed to be parallel to the x-axis, and after deformation the line moves to the line between the points A1 and B1. In order to compute the length of the deformed line we need the following expressions: [31]

$$\begin{aligned} du_x &= \frac{\partial u_x}{\partial x} dx + \frac{\partial u_x}{\partial y} dy + \frac{\partial u_x}{\partial z} dz \\ du_y &= \frac{\partial u_y}{\partial x} dx + \frac{\partial u_y}{\partial y} dy + \frac{\partial u_y}{\partial z} dz \\ du_z &= \frac{\partial u_z}{\partial x} dx + \frac{\partial u_z}{\partial y} dy + \frac{\partial u_z}{\partial z} dz \end{aligned} \quad (5.25)$$

It is obvious that the length of the line $|AB| = dx$. Likewise the length of the deformation can be obtained as

$$\begin{aligned} |A_1B_1| &= [(x + dx + u_x + du_x - x - u_x)^2 + (y + dy + u_y + du_y - y - u_y)^2 + \\ & (z + dz + u_z + du_z - z - u_z)^2]^{1/2} \Rightarrow \end{aligned} \quad (5.26)$$

i.e.

$$|A_1B_1| = [(dx + du_x)^2 + (dy + du_y)^2 + (dz + du_z)^2]^{1/2}$$

As the line AB is parallel to the x-axis, we have $dy=0$, $dz=0$ and this give

$$du_x = \frac{\partial u_x}{\partial x} dx, du_y = \frac{\partial u_y}{\partial x} dx, du_z = \frac{\partial u_z}{\partial x} dx \quad (5.27)$$

The equation (5.26) can be written as follow

$$|A_1B_1| = dx \left[\left(1 + \frac{\partial u_x}{\partial x}\right)^2 + \left(\frac{\partial u_y}{\partial x}\right)^2 + \left(\frac{\partial u_z}{\partial x}\right)^2 \right]^{1/2} \quad (5.28)$$

Assuming that the displacement gradients are very small

$$\left| \frac{\partial u_z}{\partial x} \right| \ll 1, \left| \frac{\partial u_x}{\partial x} \right| \ll 1, \left| \frac{\partial u_y}{\partial x} \right| \ll 1 \quad (5.29)$$

From the assumption (5.29) we can conclude that

$$\left(\frac{\partial u_y}{\partial x}\right)^2 + \left(\frac{\partial u_z}{\partial x}\right)^2 \ll \left(1 + \frac{\partial u_x}{\partial x}\right)^2 \quad (5.30)$$

The relative elongation of the infinitesimal line is:

$$\left(\frac{\partial u_y}{\partial x}\right)^2 + \left(\frac{\partial u_z}{\partial x}\right)^2 \ll \left(1 + \frac{\partial u_x}{\partial x}\right)^2 \quad \text{This expression can be simplified to}$$

$$|A_1B_1| = dx \left(1 + \frac{\partial u_x}{\partial x}\right) \quad (5.31)$$

The relative elongation of the infinitesimal line AB can be calculated from the (5.28) and (5.31)

$$\frac{|A_1B_1| - |AB|}{|A B|} = \frac{\partial u_x}{\partial x} \quad (5.32)$$

This is the relative elongation for a parallel line to the x-axis and it is the so-called normal strain ε_{xx} . Repeating the same development for a line parallel to the y-axes and z-axes we obtain all three normal strains as

$$\varepsilon_{xx} = \frac{\partial u_x}{\partial x}, \varepsilon_{yy} = \frac{\partial u_y}{\partial y}, \varepsilon_{zz} = \frac{\partial u_z}{\partial z} \quad (5.33)$$

Evaluating the changes of the angles between two orthogonal lines parallel to the coordinate axes in a similar way as in Figure, we get the shear strains

$$\gamma_{xy} = \frac{\partial u_x}{\partial y} + \frac{\partial u_y}{\partial x}, \gamma_{xz} = \frac{\partial u_x}{\partial z} + \frac{\partial u_z}{\partial x}, \gamma_{yz} = \frac{\partial u_y}{\partial z} + \frac{\partial u_z}{\partial y} \quad (5.34)$$

It appears that the shear strain is symmetric. The information above can be group in a compact form; a strain vector can be defined.

$$\bar{\varepsilon} = [\varepsilon_{xx} \varepsilon_{yy} \varepsilon_{zz} \varepsilon_{xy} \varepsilon_{xz} \varepsilon_{yz}]^T \quad (5.35)$$

As the strains are obtained as derivative of the displacements, so the equation (5.35) can be rewritten as

$$\varepsilon = \tilde{\nabla} u \quad (5.36)$$

A plane strain state can be defined as the deformation state where the only non-zero strains are ε_{xx} , ε_{yy} and γ_{xy} and furthermore there is nothing depending on the z-coordinate. This is equivalent to the following:

$$u_x = u_x(x, y), u_y = u_y(x, y), u_z = 0 \quad (5.37)$$

Further derivations will be done under the assumption of plane strain where the strain vector will be defined as:

$$\bar{\varepsilon} = [\varepsilon_{xx} \varepsilon_{yy} \varepsilon_{xy}]^T \quad (5.38)$$

5.2.2 Linear Elasticity

The relation between stresses and strains is called constitutive relation and there are many different kinds of such relations, e.g. elasticity, plasticity, viscoelasticity, viscoplasticity and creep is considered which is called *linear elasticity*. For one dimension linear elasticity the relation between strains and stresses is given by the Hooke's law

$$\sigma = D\varepsilon \quad (5.39)$$

D is constant for a given position and the matrix consists of 36 coefficients. If it is assumed that the strain energy of one point only depends on the final state and not in the manner it was reached, we will conclude that the 36 elasticity coefficients of D reduce to 21 independent coefficients. Studying the concept of strain energy W per unit volume of the body we can conclude that

$$W = \frac{1}{2} \varepsilon^T D \varepsilon \Rightarrow \varepsilon^T D \varepsilon > 0 \quad \forall \varepsilon \neq 0 \Rightarrow \det D \neq 0 \quad (5.40)$$

This means that (5.39) can be inverted to yield

$$\varepsilon = C\sigma; C = D^{-1} \quad (5.41)$$

Where C is a compliance or flexibility matrix

Further, the D matrix changes if another coordinate system is chosen. If every plane is a symmetry plane the D-matrix takes the same form irrespective of the coordinate system, it is equivalent to say the material is isotropic and it means it has the same properties in all directions. In this case the D-matrix is completely defined with only two independent *coefficients* E: *Young's Modulus*, and *v*: *Poisson's ratio*, for the 3-D case

$$D = \frac{E}{(1+\nu)(1-2\nu)} \begin{bmatrix} 1-\nu & \nu & \nu & 0 & 0 & 0 \\ \nu & 1-\nu & \nu & 0 & 0 & 0 \\ \nu & \nu & 1-\nu & 0 & 0 & 0 \\ 0 & 0 & 0 & \frac{1}{2}(1-2\nu) & 0 & 0 \\ 0 & 0 & 0 & 0 & \frac{1}{2}(1-2\nu) & 0 \\ 0 & 0 & 0 & 0 & 0 & \frac{1}{2}(1-2\nu) \end{bmatrix} \quad (5.42)$$

In addition, the materials is considered as inhomogeneous if D is depended on point position $D=D(x,y,z)$ otherwise it is called homogenous. From (5.39) and (5.42), we can conclude that the shear stress and shear strain are independent of the normal stress and normal strain

5.2.3 Initial strain

Initial strain is related to the case where there exist non-zero strains for a zero stresses. Considering the case of initial thermal strain ε_0 of an isotropic material which is free to expand as a result of a change of the temperature the generalized Hooke's law can be written as

$$\varepsilon = C\sigma + \varepsilon_0 \Rightarrow \sigma = D(\varepsilon - \varepsilon_0) \quad (5.43)$$

Where ε_0 is called initial strain, which is a strain for zero stress.

$$\varepsilon_0 = \alpha \Delta T \begin{bmatrix} 1 \\ 1 \\ 1 \\ 0 \\ 0 \\ 0 \end{bmatrix}, \text{ and } \alpha \text{ is the thermal expansion coefficient, } T \text{ is the temperature change.}$$

5.3 Thermal Analysis

5.3.1 Heat Transfer

5.3.2 One-dimensional heat flow

In this case the heat is assumed to be transferred only in one direction. For this purpose, an infinitely small part dx is considered, as illustrated in Figure 5.7.

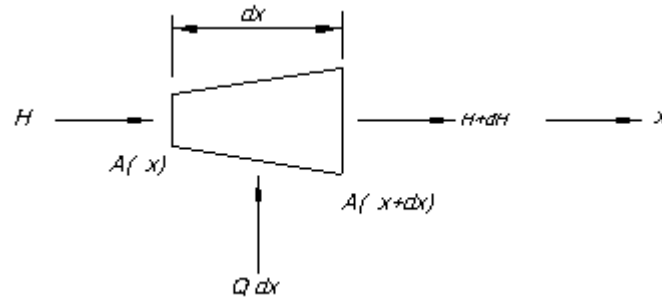


Figure 5.7 Infinitely small part [19]

In the above Figure, H represent the heat flow per unit time at position x , $H+dH$ denotes the heat outflow per unit time at position $x+dx$, and $Q dx$ is heat supply per unit time. For simplicity, the stationary condition is considered. The total inflow per unit time equals the total outflow per unit time. The equilibrium equation can be expressed as

$$H + Q dx = H + dH \quad (5.44)$$

and it can be further simplified

$$\frac{dH}{dx} = Q \quad \text{and by definition} \quad (5.45)$$

$$H(x) = A(x)q(x) \quad (5.46)$$

Where q is heat flux and it is positive when heat flows in x -direction. From (5.44) and (5.45)

$$\frac{d}{dx}(Aq) = Q \quad (5.47)$$

The relation, which describes how the heat flows within the material, is called the *constitutive relation*. With T being the temperature and k the thermal conductivity, Fourier's law of heat conduction states that the flux q is given by

$$q = -k \frac{dT}{dx} \quad (5.48)$$

The equations (5.47) and (5.48) can be expressed as the differential equation with h as the thickness of the one-dimensional element.

$$\frac{d}{dx} \left(Ak \frac{dT}{dx} \right) + Q = 0 \quad \text{with} \quad \frac{-h}{2} \leq x \leq \frac{h}{2} \quad (5.49)$$

5.3.2.1 Two-dimensional heat flow

Heat flows in various directions and this flow can be described by heat flux vector q . This flux has the direction of the heat flow and its length expresses the heat per unit time that passes through unit surface area perpendicular to the direction of heat flow. It is also important to define the amount of heat that passes through a unit area of the boundary per unit time q_n . According with these definitions the vectors are defined as

$$q = [q_x \ q_y]^T, \quad n = [n_x \ n_y]^T, \quad q_n = q^T n \quad (5.50)$$

Where n is a unit vector normal to the boundary and directed outwards. The heat flux vector q is directly related to the temperature gradient ∇T and this relation is expressed by the constitutive equation.

$$q = -K \nabla T \quad (5.51)$$

Where ∇T and K for two dimension is

$$\nabla T = \begin{bmatrix} \frac{\partial T}{\partial x} \\ \frac{\partial T}{\partial y} \end{bmatrix}, \quad K = \begin{bmatrix} k_{xx} & k_{xy} \\ k_{yx} & k_{yy} \end{bmatrix} \quad (5.52)$$

The components in the constitutive matrix K describe the thermal conductivity in two directions for a material. In general form K may be non-symmetric, but when dealing with primarily metals such as steel K can be symmetric, which means that

$$K = K^T \quad (5.53)$$

The heat flow differential equation can be derived using Gauss divergence theorem. For stationary (i.e. time independent) problem, the balance or conservation principle state that the amount of heat supplied to the body per unite time equals the amount of heat leaving the body per unit time.

$$\int_A QtdA = \oint_{\ell} q_n t d\ell \quad (5.54)$$

Where Q is the amount of heat supplied to the body per unit volume and per unit time and t is the thickness in the z-direction. Using the Gauss's divergence theorem yields:

$$\begin{aligned} \int_A QtdA &= \oint_{\ell} q_n t d\ell = \oint_{\ell} t \bar{q}^T \bar{n} d\ell = \oint_{\ell} (t \bar{q})^T \bar{n} d\ell = \int_A \text{div}(t \bar{q}) dA \Rightarrow \\ \int_A [tQ - \text{div}(t \bar{q})] dA &= 0 \end{aligned} \quad (5.55)$$

The region \mathbf{A} might be taken as any arbitrary part of the region for the entire body. So the strong form of two dimensional heat flow can be formulate as below,

$$\begin{aligned} \text{div}(t \bar{q}) &= tQ \\ \text{div}(tK\nabla T) &= tQ \Rightarrow \end{aligned} \quad (5.56)$$

And differential equation for isotropic material can be expressed as

$$\begin{aligned} \frac{\partial}{\partial x} \left(k_{xx} \frac{\partial T}{\partial x} \right) + \frac{\partial}{\partial y} \left(k_{yy} \frac{\partial T}{\partial y} \right) + Q &= 0 \Rightarrow \\ \nabla^T K \nabla T + Q &= 0 \end{aligned} \quad (5.57)$$

5.3.2.2 Transient heat conduction

Transient condition refers to the sort of problem in which the temperature in the conduction region varies with time. In most cases the body experiences an initial transient and eventually reaches the case of steady state. In the modelling of heat transfer presented in this thesis the time dimension has to be considered. The governing equations for the analysis of heat transfer under a transient state can be summarized as

$$\frac{\partial e}{\partial t} = -\text{div}(\bar{q}) + Q \quad (5.58)$$

Where, e is the heat content per unit volume. This is a general balance equation, or conservation principle. It is noted that the left-side hand is the rate of increase of the heat content. The heat input causes a raise in the temperature and the range of the change depends on the material properties, (i.e. on the heat capacity c). The relation between change in temperature and change in heat content is thus given by

$$\Delta e = \rho \cdot c \cdot \Delta T \Rightarrow$$

hence

$$\rho \cdot c \cdot \frac{\partial T}{\partial t} = \nabla^T (D \nabla T) + Q \quad (5.59)$$

The boundary condition, which may be time dependent, must be specified for this equation, along with an initial temperature distribution. The numerical study then determines how this distribution varies with time.

5.3.3 Solid Mechanics + Thermal analysis

Thermal- stress analysis is needed in the case when the mechanical and thermal solutions affect each other strongly, or when the model requires time dependent material response. In ABAQUS those kinds of analysis are treated using two analysis types, coupled thermal-stress analysis and uncoupled thermal-stress analysis.

In the Table 5.2 the different equations that have to be solved to achieve the solution of a thermal-stress problem. The unknowns are σ , ε , u , q , T .

Table 5.2 different constitutive equations

Equation System	Description	
$\tilde{\nabla}^T \sigma + b = 0$	<i>Force equilibrium</i>	5.60
$\varepsilon = \tilde{\nabla} u$	<i>Kinematics' relation</i>	5.61
$\varepsilon = C \sigma + \alpha \nabla T$	<i>Linear elasticity constitutive relation</i>	5.62
$q = -K \nabla T$	<i>Thermal constitutive relation</i>	5.63
$\nabla^T K \nabla T + Q = 0$	<i>Thermal conservation principle</i>	5.64

Constitutive equation in both thermal as well as stress analysis is time dependent, and both analyses can be coupled by the temperature change and displacement as primary unknown. The elimination of the stress and strain equations yields

$$\tilde{\nabla}^T \bar{D} (\tilde{\nabla} u - \alpha T m) + b = 0 \quad (5.65)$$

Thermal-stress relation can be rewrite in a more compact form

$$\begin{bmatrix} \tilde{\nabla}^T \bar{D} \tilde{\nabla} & -\alpha m \\ 0 & \nabla^T \mathbf{K} \nabla \end{bmatrix} \begin{bmatrix} u \\ T \end{bmatrix} = - \begin{bmatrix} b \\ Q \end{bmatrix} \quad (5.67)$$

The equation system can be solved sequentially i.e. we can get temperature from the equation (5.64) and then use that result to calculate displacement or strain from the equation (5.65). Once we have T and u, the flux and stresses can be solved from the equations (5.60), (5.61), (5.62) and (5.63).

6 Finite Element Modelling

6.1 Problem Description

Strengthening of steel member with prestressed CFRP laminate crates high shear stress at the laminate ends which might cause premature failure of the system. This problem has been studied, modelled and analysed using heating system as the means of reducing high shear stress and shifting their position from the ends. The model which is used in this study consists of Steel plate with a length of 800mm, width of 80mm and thickness of 20mm. this plate is to be reinforced with CFRP laminate underneath the bottom side in order to increase the total stiffness and/or the ultimate load carrying capacity as much as possible. The CFRP laminate used in this study has a dimension of (500x45x4 mm) and attached to the steel plate with the adhesive layer having the dimensions (500x45x1.5mm) as in Figure 6.1.

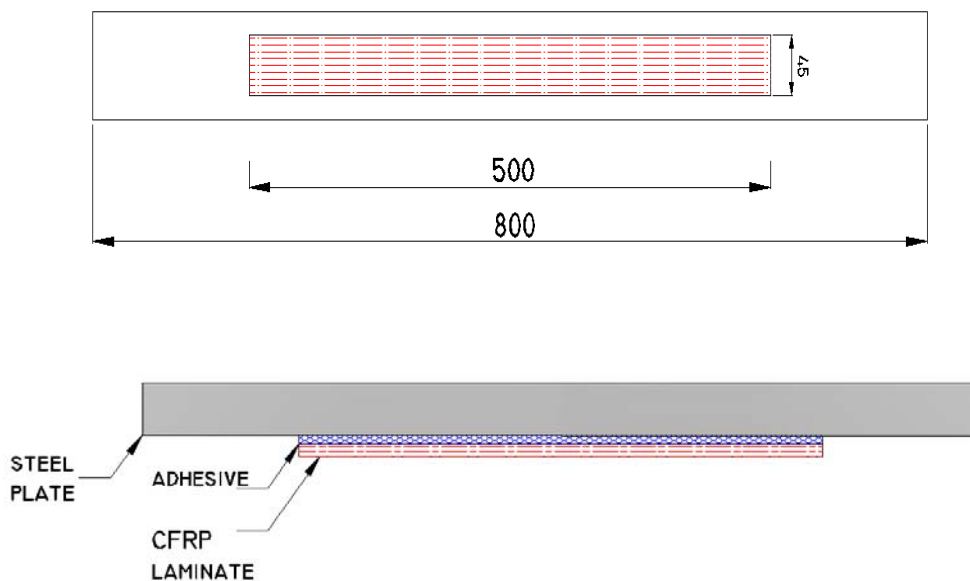


Figure 6.1 Plan and cross-section of the composite plate

Since the stresses which are induced in the member include the combined effect of temperature and external tension load, then all material properties which are associated with the temperature distribution as well as applied load should be defined in order to enable to perform uncoupled temperature-displacement analysis. The material properties which are used in the analysis are as given in table 6.1 below:

Table 6.1 Material properties for elements

Materials	Conductivity $\frac{w}{mm \cdot K}$	Density $\frac{kg}{mm^3}$	Modulus of elasticity $\frac{N}{mm^2}$	Poisson ratio	Expansion Coefficient $\frac{1}{K}$	Specific heat $\frac{j}{kg \cdot K}$
Steel	$46 * 10^{-3}$	$7.82 * 10^{-6}$	210000	0.29	$12 * 10^{-6}$	460
Adhesive	$0.1 * 10^{-3}$	$1.97 * 10^{-6}$	Temperature dependent	0.34	$60 * 10^{-6}$	900
CFRP	$0.4 * 10^{-3}$	$1.5 * 10^{-6}$	450000	0.3	$5 * 10^{-6}$	1200

It should be noted that the stiffness of the adhesive (epoxy) is strongly temperature dependent, i.e. adhesive become softer by increasing the temperature as mentioned in chapter 4. The values which have been used in the thermal modelling process is illustrated in the table 6.2.

Table 6.2 Modulus of elasticity for Adhesive (temperature dependent)

Temp. (°C)	20	30	40	50	60	70	80	90	100
Modulus of Elasticity (GPa)	7	7	6.22	5.44	0.933	0.0933	0.0505	0.042	0.042

Thermal-stress analysis is performed using finite element method. The problem is modelled and analyzed using finite element software. Analytical calculation of the temperature distribution in a model can be quite difficult and time consuming. Transient analysis and temperature dependent material properties make the heat transfer problem highly non-linear. Non-linear differential equations are very difficult to be solved and sometimes even impossible. For this reasons, numerical techniques are often performed in order to solve complicated mathematical problems (e.g. nonlinear thermal problems). These techniques are implemented in the *ABAQUS* software program in this thesis. *ABAQUS* software is a collection of applications for finite element analysis. It provides complete and powerful solutions for routine and sophisticated linear and nonlinear engineering problems, using the finite element method. [34].

Two types of analysis are performed by *ABAQUS*, thermal analysis and stress analysis (i.e. uncoupled temperature- displacement analysis). One of the most important features when working with finite element analysis tool is the element type provided by the program. In this model two different types of element have been chosen for both analyses. The table 6.3 shows the element that has been used in the thesis.

Table 6.3 ABAQUS element types used in the analysis.

Analysis Type	Element type	ABAQUS type	Element
Solid mechanic	2D plane stress	CPS8	
Heat conduction	2D heat transfer	DC2D8	

The way of modelling and analysing the strengthened plate is described more in details later on in this chapter.

6.2 Finite Element Modelling

The three different components in the composite member are modelled using two-dimensional shell element. They are assembled together and then merged so that the parts don't act independently. Essential partitions for heat application and meshing are also made and they are explained in more details later on in this chapter.

In order to make the model time efficient the geometric symmetry in vertical direction is considered, i.e. only half of the composite plate in the longitudinal direction is modelled and the boundary conditions on the symmetry line is applied in such a way so as to simulate the effect of the whole plate.

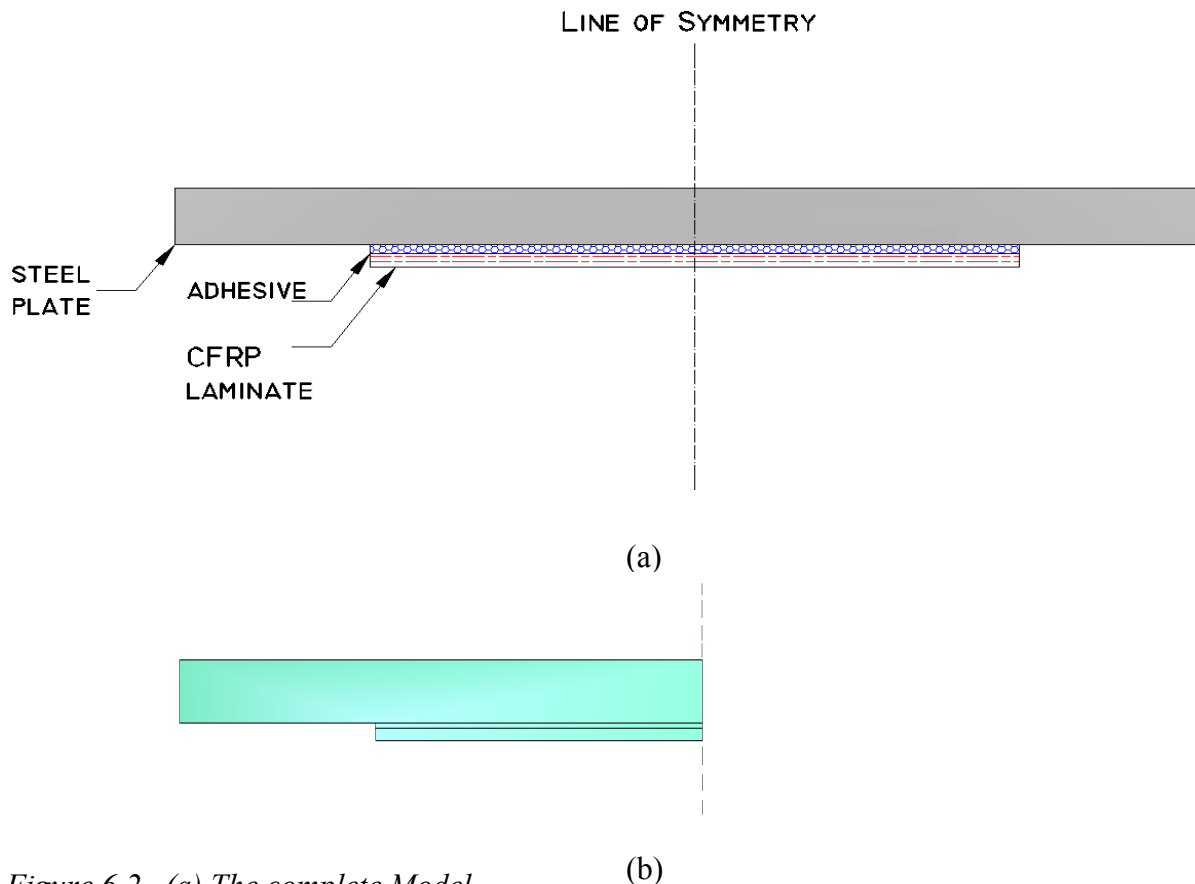


Figure 6.2 (a) The complete Model

(b) The model used in ABAQUS with Symmetry line

6.3 Thermal analysis

In *ABAQUS*, uncoupled heat transfer analysis is used to model the composite plate with temperature dependent properties, convection and radiation boundary conditions. Uncoupled heat transfer problems are those in which the temperature field is calculated without considering the stress-deformation in the model which is studied and then implementing the temperature distribution results in mechanical analysis to study and determine the stress distribution due to heating effect in the model.

There are several kinds of non linearity which can be identified in the transient heat transfer problem these can be classified into:

- 1) **Material nonlinearities:** like
 - Adhesive materials properties.
- 2) **Boundary nonlinearity**
 - Convection and radiation boundary conditions, where the convection coefficient is a function of temperature.

6.3.1 Material Properties

The composite plate studies in this thesis experience thermal load as well as mechanical load (tension of the plate). Since the composite plate consists of components with different mechanical and thermal properties, thermal strains may cause considerably high stresses along the adhesive- adherent interface and in the three components. Therefore it is essential to take thermal properties for different components in consideration. Thermal properties for adhesive and CFRP used in this thesis have been collected from different reference in the literature, and then reasonable values have been chosen which are more realistic and match the material properties which are available in market.

For thermal analysis, properties which effect the temperature distribution like (conductivity, specific heat, and thermal expansion) in addition to the mechanical properties need to be defined. The conductivity of materials is one of the most important properties in thermal analysis. It is defined as the measure of temperature distribution in different direction (i.e. the higher the conductivity the faster temperature will transfers through the thickness). From table 6.1 it is apparent that the steel plate has higher conductivity which means that the temperature distribution through the steel is higher than other components.

The coefficient of expansion is the fractional change in length of each component in the composite member per degree of temperature change, and it is the measure of displacement due to thermal effect (i.e. the higher the coefficient of expansion for the component the larger the displacement of that component when heating load is applied). The effects of these properties are discussed more in details later on in this thesis.

The steel and CFRP are modeled as linearly elastic. The reason why the CFRP is modeled as a linear elastic material can be understood from the brittle behavior of CFRP observed in the tension test. As mentioned in the previous chapters, CFRP

laminates can be of different grades, a high-strength or high-modulus or ultra-high-modulus. Laminate with high stiffness and low strength is more brittle, but by increasing the strength of the laminate and decreasing the stiffness, the opportunity of getting more flexible laminate will increase (i.e. the ultimate strain will increase). Therefore in our analysis we tried to use laminate which is more flexible and has high strength. Figure 6.3 explain how the stiffness which is represented by angle between (σ - ϵ) is reduced by increasing the strength and strain.

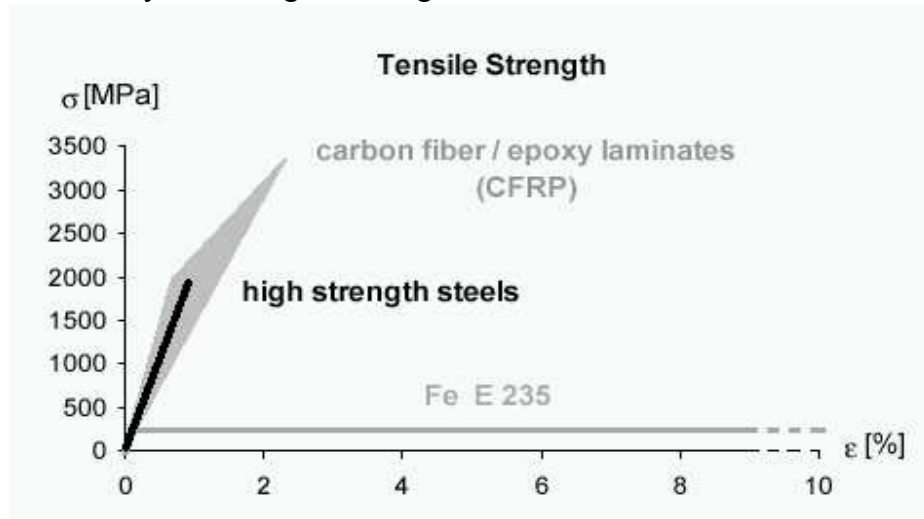


Figure 6.3 Tensile strength of CFRP [37]

The adhesive has non-linear behaviour and it is temperature dependent, From the material properties table 6.2 it is apparent that there is a significant change in the stiffness of the adhesive by increasing the temperature especially between (40°C-60°C). This drastic change in stiffness has considerable effect on the stresses distribution in the member. Figure 6.4 below shows an example of how flexible the adhesive will be with increasing temperature from -20°C to 40°C.

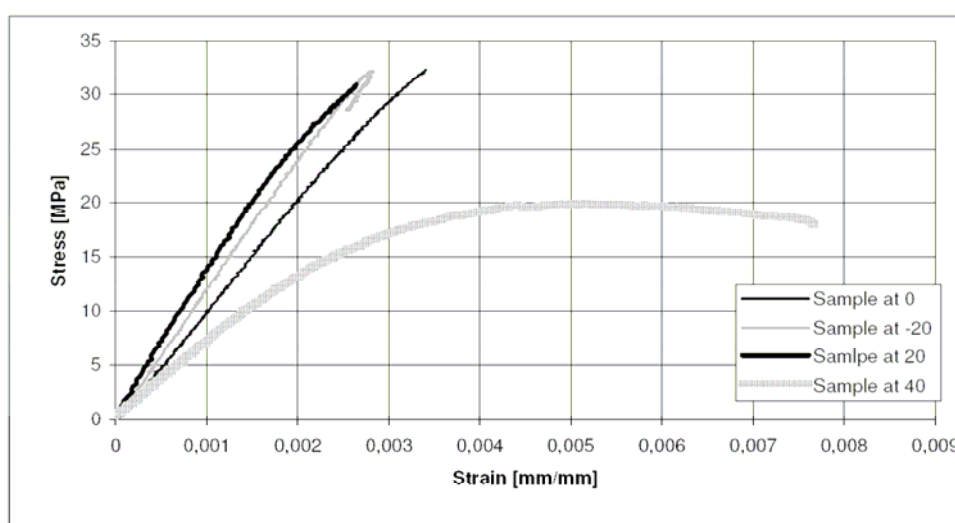


Figure 6.4 Behaviour of adhesive at different temperature.

Below is an example how the material properties have been defined in ABQUS and how the adhesive stiffness changes with temperature.

```
** MATERIALS
**
*Material, name=Adhesive
*Conductivity
0.0004,
*Density
1.97e-06,
*Elastic
7000., 0.34, 293.
7000., 0.34, 303.
6222., 0.34, 313.
5440., 0.34, 323.
933., 0.34, 333.
93., 0.34, 343.
50.56, 0.34, 353.
42., 0.34, 363.
42., 0.34, 373.
*Expansion
6e-05,
*Specific Heat
900.,



---


*Material, name=CFRP
*Conductivity
0.05,
*Density
1.5e-06,
*Elastic
450000., 0.3
*Expansion
1.2e-06,
*Specific Heat
1200.,



---


*Material, name=Steel
*Conductivity
0.046,
*Density
7.82e-06,
*Elastic
210000., 0.29
*Expansion
0.,
*Specific Heat
460.,
**
```

6.3.2 Thermal Boundary Conditions and load application

Boundary condition is the decisive part in all types of analysis, and care should be taken in choosing boundary condition, because any incorrect definition of boundary conditions leads to results which are unfeasible. Thermal boundary conditions which are represented by temperature boundary defines the way of transferring temperature from the surface of the heated member to the surroundings, and it is modelled by natural heat convection and radiation from the surface. Convection follows Newton's law, the rate of loss of heat per unite area due to convection is:

$$q = h_c(T_i - T_\infty)$$

Where :

T_i = initial temperature (temperature of the member before applying heat load);
 T_∞ = temperature of the member after a certain time of heating in transient analysis;
 h_c = convection coefficient;
 $(T_i - T_\infty) = \Delta T$ = temperature difference.

Initial condition is one of the most important factors which influence the final result, it means for any surface where T is not prescribed and no external flux is applied, the default condition in program is $q=0$ across the surface. That is, there is no heat flow through the surface (i.e. the surface is perfectly insulated).

The option for application of a convection and radiation surface boundary condition in ABAQUS is *surface film condition (Sfilm)* in interaction module, which is applied to the element edges in a two dimensions model. It is noted that the convection boundary conditions depend strongly on the convection heat transfer coefficient (h_c) which in turn depends on the temperature difference between the surface and the surrounding. In thermal analysis calculation, it is necessary to define *initial temperature field* in the analysis, which represent the elements temperature (i.e. initial temperature condition for the element as mentioned above) before applying thermal load. In case when initial temperature field is not defined, the default condition in the software gives initial temperature (T_i) =0 across the surface, this result in unexpected heat flux on the surface due to convection and radiation heat transfer from the heated member to the surrounding.

The surface film condition which is used in ABAQUS is calculated by implementing the following equations [7].

$$h_c = \frac{2.175}{D^{0.076}} (\Delta T)^{0.308}$$

$$D = \frac{2 \cdot Area}{perimeter}$$

$$\alpha_r = 4 * 0.9 * 5.67 * 10^{-8} T_s^3 \Rightarrow (Kilven)$$

$$\text{surface film coefficient} = h_c + \alpha_r$$

where

Area is the surface area of the member

perimeter is the perimeter of the surface

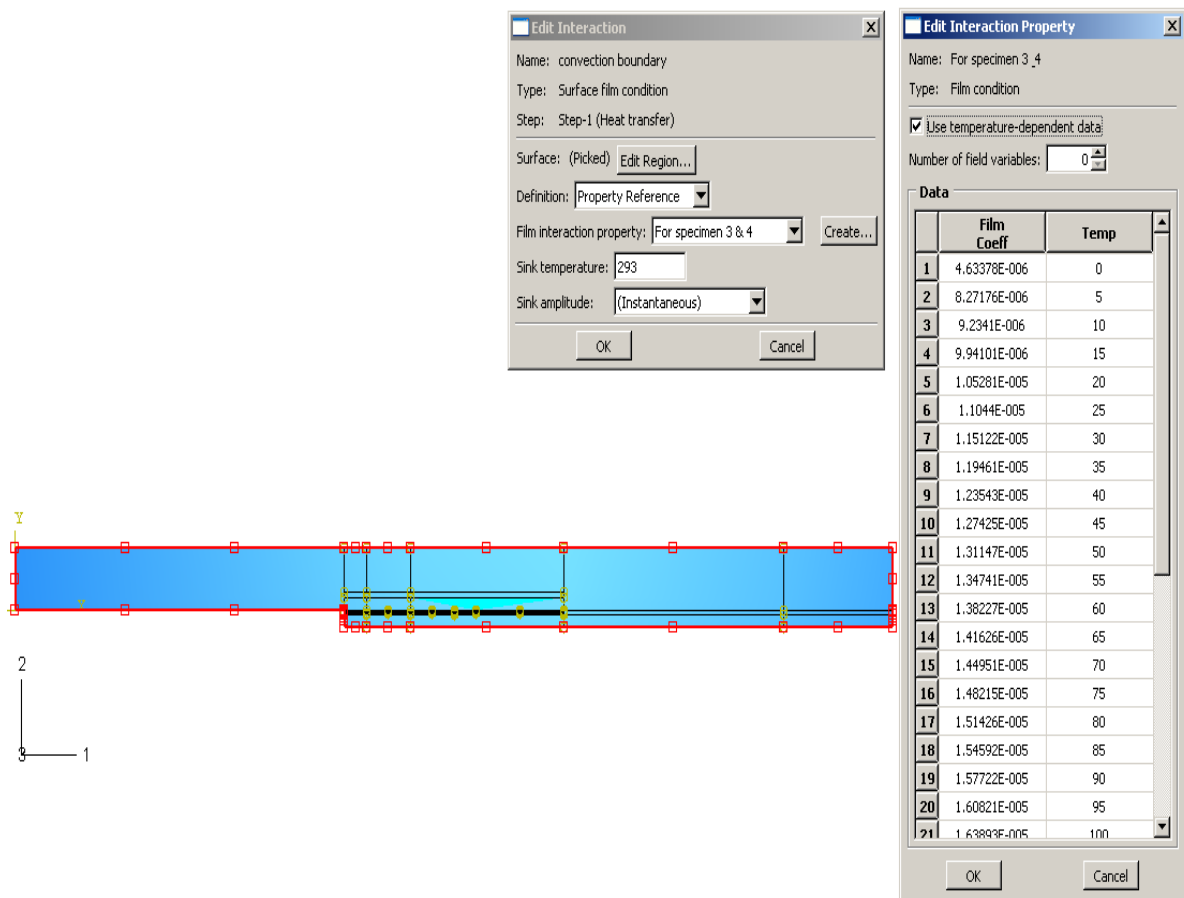


Figure 6.5 The surface film condition defined in ABAQUS

Appendix B contains the way of calculating convection and radiation coefficient for different temperature condition.

The procedure of implementing the above surface film coefficient in the program to calculate temperature in the boundaries is explained in more details in the following part of the input file.

```

** INTERACTION PROPERTIES
**
*Film Property, name="For specimen 3 & 4"
4.63378e-06, 0.
8.27176e-06, 5.
9.2341e-06, 10.
9.94101e-06, 15.
1.05281e-05, 20.
1.1044e-05, 25.
1.15122e-05, 30.
1.19461e-05, 35.
1.23543e-05, 40.
1.27425e-05, 45.
1.31147e-05, 50.
1.34741e-05, 55.
1.38227e-05, 60.
1.41626e-05, 65.
1.44951e-05, 70.
1.48215e-05, 75.
1.51426e-05, 80.
1.54592e-05, 85.
1.57722e-05, 90.
1.60821e-05, 95.
1.63893e-05, 100.
1.66943e-05, 105.
1.69976e-05, 110.
1.72995e-05, 115.
1.76002e-05, 120.
1.79002e-05, 125.
1.81995e-05, 130.
1.84985e-05, 135.
1.87973e-05, 140.
1.90961e-05, 145.
1.93952e-05, 150.
1.96946e-05, 155.
1.99946e-05, 160.
2.02952e-05, 165.
2.05965e-05, 170.
2.12021e-05, 180.
**
** FIELDS
**
** Name: Field-1 Type: Temperature
*Initial Conditions, type=TEMPERATURE
_PickedSet95, 293.
** -----
**
** STEP: Step-1
**
*Step, name=Step-1, inc=1250
*Heat Transfer, end=PERIOD, deltmx=500., mxdem=0.75
1., 1800., 1e-05, 1.,
**
** BOUNDARY CONDITIONS
**
** Name: BC-1 Type: Temperature
*Boundary, amplitude=Amp-1
_PickedSet154, 11, 11, 353.
**
** INTERACTIONS
**
** Interaction: convection boundary
*Sfilm
_PickedSurf96, F, 293., "For specimen 3 & 4"

```

The composite plate is heated up by applying a heat of 80°C for a certain time and along a certain distance. The heating load is applied as a temperature boundary in three different positions. These are the interface between steel plate-adhesive, in the middle of adhesive and in the interface between adhesive-CFRP. This procedure is done in order to find out the optimum position of heating. It should be noted that the heat is not applied instantaneously, but along a certain time using the amplitude option in ABAQUS. The purpose of using the amplitude option is to decrease the rapid change of temperature in the heated member which in turn influences the material properties and then the stress distribution especially in adhesive.

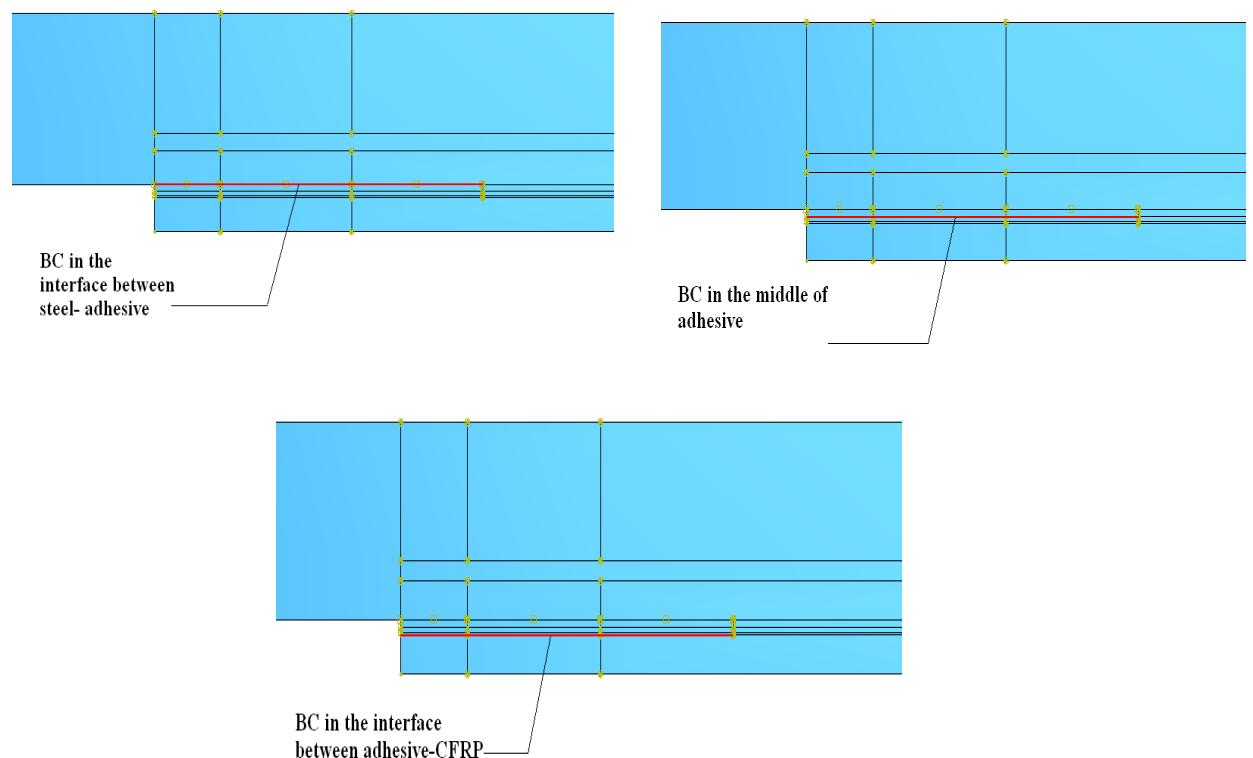


Figure 6.6 Application of heat at different positions

6.3.3 Transient thermal analysis

As mentioned before uncoupled heat transfer analysis is used to model member heat conduction with general conductivity, convection and radiation boundary conditions. Heat transfer problems can be nonlinear because the material properties are temperature dependent or because the boundary conditions are nonlinear. Boundary conditions are very often nonlinear; for example, film coefficients can be functions of surface temperature.

ABAQUS uses an iterative scheme to solve nonlinear heat transfer problems in steady state or in transient analysis, and it usually uses automatic time increment schemes for the solution of transient problems. Newton's method is used to solve the nonlinear equations in *ABAQUS*, and the iteration is continued until the automatic convergence checking scheme in *ABAQUS* determines that the solution is accurate i.e. it is close to the exact solution of the nonlinear system.

The time increments which are selected automatically based on the user-prescribed maximum allowable nodal temperature change in an increment $\Delta\theta_{\max}$, and in this case *ABAQUS* will restrict the time increments to ensure that this value is not exceeded at any node (except nodes with boundary conditions) during any increment of the analysis.

One advantage of using transient analysis is that the temperature can be calculated at any time increment and heat distribution can be visualized during that time. *ABAQUS/Standard* provides tolerance parameters to indicate the level of accuracy required in the approximate time integration of transient effects that have a physical time scale, and parameters that control the increase and reduction of the time increment like initial, maximum, minimum time increment and maximum allowable nodal temperature change in an increment $\Delta\theta_{\max}$.

Table 6.4 Important parameters for the stability of the analysis

Time period (Sec)	Increment size (Sec)	Initial increment (Sec)	Min. increment (Sec)	Max. increment (Sec)	Max. allowable Temp. °K
1800	1850	1	$1 \cdot 10^{-6}$	1	500

Choosing an initial time increment is an important problem in the discretized approximation of transient process like heat transfer. The spatial element size and the time step are related to the fact that extent time steps should be smaller than a certain size. A simple formula provides the minimum usable increment:

$$\Delta t \geq \frac{\rho c}{6K} \Delta l^2$$

Where:

Δt is the time increment;

ρ is the density;

c is the specific heat;

K is the thermal conductivity;

Δl is the distance between nodes for element near surface with highest temperature gradient.

If time increments are smaller than this value, spurious oscillations can appear in the solution, in particular in the vicinity of boundaries with rapid temperature changes. These oscillations are non physical and may cause problems if temperature dependent material properties are present. For example, the radiation flux for each surface is calculated based on the average of the nodal temperatures on that surface. This value of radiation flux is then distributed to each node in proportion to its area. Consequently, the mesh must be sufficiently fine that temperature differences across elements are small. Otherwise, computed fluxes at nodes with temperatures above the surface average will be excessively low, and the fluxes at nodes with below-average temperatures will be too high. This tends to bring a spatially oscillatory solution and some 'bumps' are present in the temperature profile. [34]

For this reason a solution of this problem could be to reduce element size in the vicinity of high temperature gradients. This means refining the mesh size and consequently increasing the number of elements.

Since the composite plate consist of three different materials and equation above is applicable just for temperature distribution through one material. Therefore time increment which used to solve thermal analysis is chosen larger than the greatest value using equation above and for three materials.

6.3.4 Meshing

All components in the composite plate are modelled using the same technique. An eight –node quadratic quadrilateral heat transfer element with four integration points (DC2D8) is used in modelling of the composite plate. Since the stress concentrations occur around the adhesive free ends, mesh areas in these locations are refined in order to obtain the reasonable accuracy in the computations.

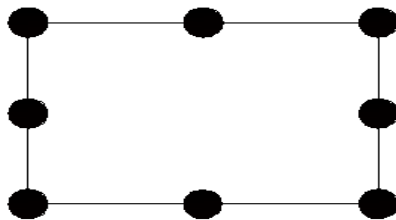


Figure 6.7 Explanatory view of an 8-node heat transfer element used for analysis

Convergence study is made using two models with different mesh sizes. The first model has the mesh with uniform element size along the composite plate through the thickness, while different element sizes are used through the thickness depending on the thickness of each part of the composite (i.e. steel plate, adhesive and CFRP laminate).

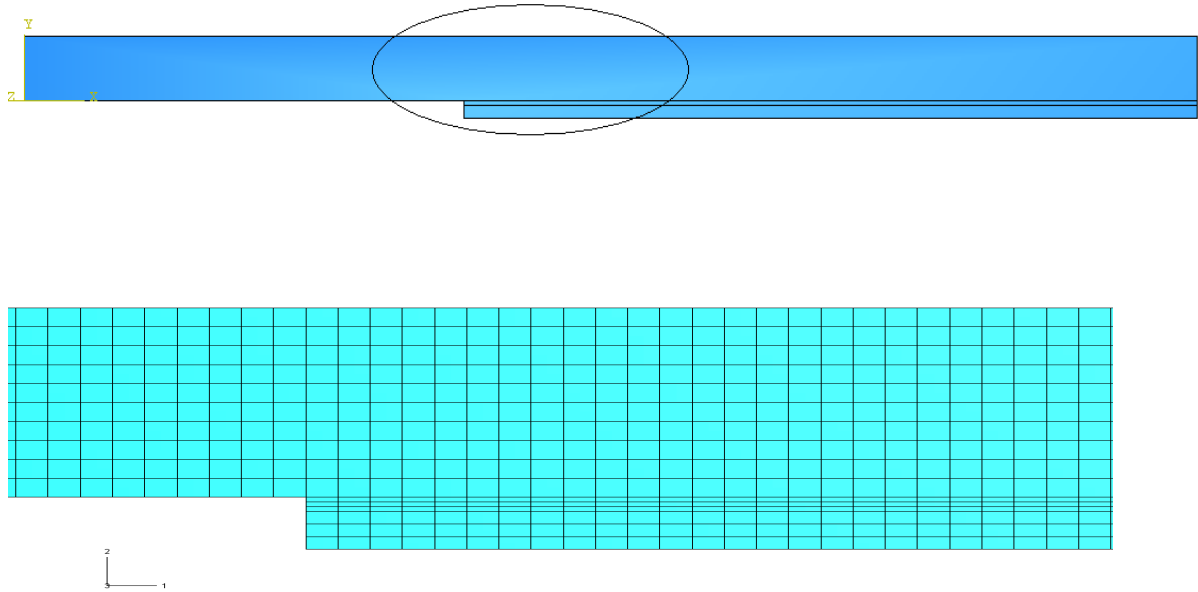


Figure 6.8 Mesh dimensions illustrated for the first model

The dimension for different composite plate components for the first model with coarser mesh are illustrated in table below

Table 6.5 Number of Elements used in each layer in the mesh system

Composite plate component	Steel plate	Adhesive layer	CFRP laminate
Numbers of elements	200*10	200*3	200*3

In order to capture high shear stress at the ends of the joint between steel plate and the laminate, finer mesh size is used. Therefore in the second model, the composite plate is partitioned into five regions with different sizes in longitudinal direction and meshed with five different mesh sizes as well as in Figure 6.9. Since the adhesive layer is much interesting, very dens mesh have been used to capture temperature distribution and stresses more accurately. The parts of steel plate and CFRP laminate which are close to adhesive are meshed with very fine mesh, the parts which are far away from the adhesive meshed with coarser mesh size and both different mesh sizes are connected to each other by creating a tetrahedral mesh region in between as in Figure 6.9. The first (20 mm) of the adhesive is meshed with very fine mesh especially in the longitudinal direction to monitor the temperature distribution from the heat source and through the thickness of different elements, and coarser mesh is used in the following regions and so on. The reason for creating many sections is to get a good results and on the same time to save computational effort. Figure 6.10 below shows the partitioned regions as well as the mesh dimensions for the half of the composite plate.

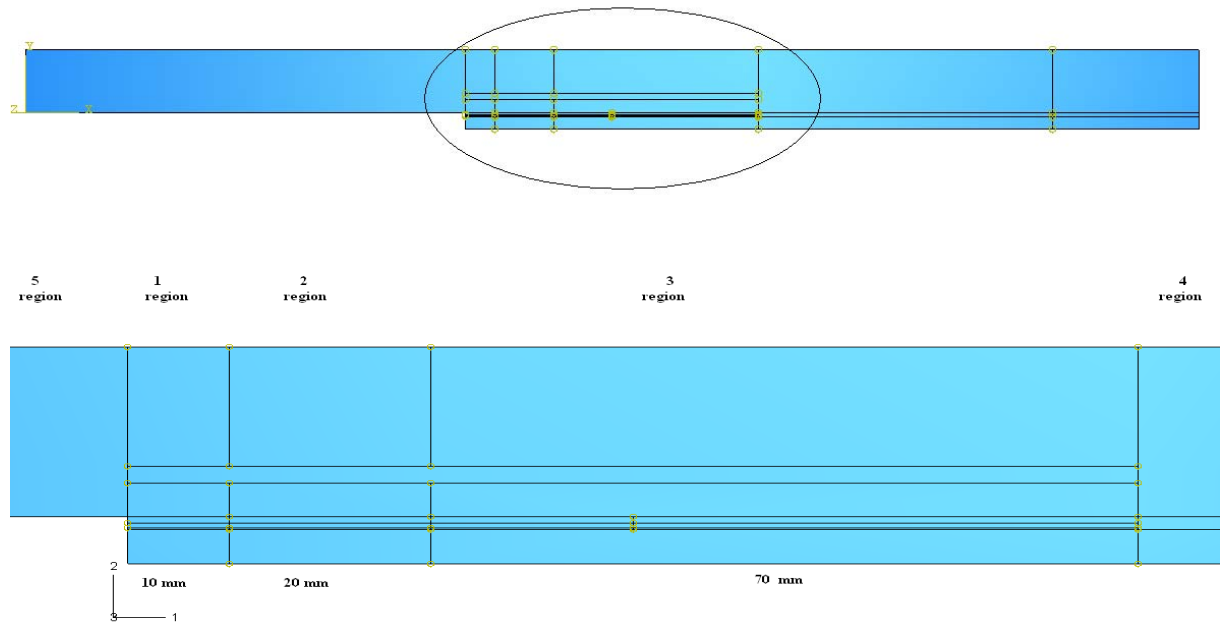


Figure 6.9 Partitioning of the composite plate

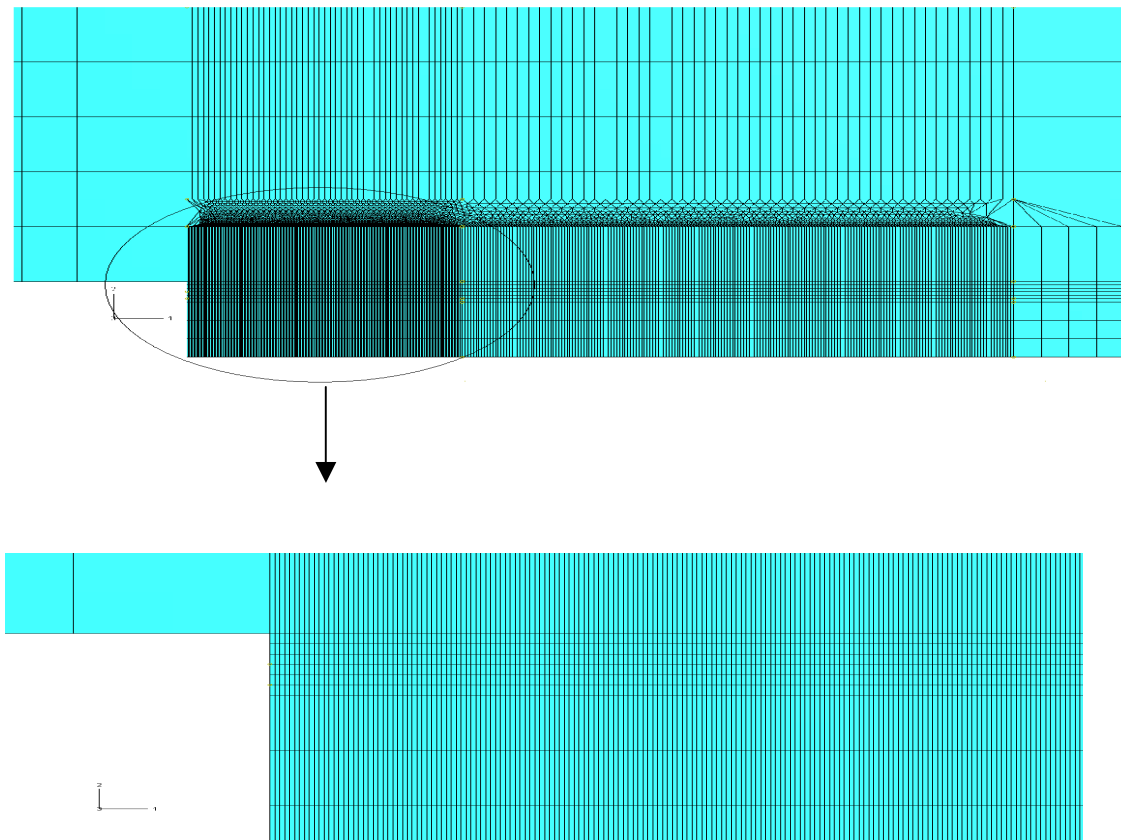


Figure 6.10 Mesh dimensions illustrated in different components

The meshes have different sizes in different regions as mentioned before. The Table 6.6 illustrate mesh dimension in every region, the first dimension is along the bond line and the second one is through the thickness.

Table 6.6 Number of elements in the different layers and for different regions in the second model with finer mesh.

Regions	Adhesive	Steel plate close to adhesive	Steel plate far away from adhesive	CFRP
1	200*6	200*2	50*14	200*3
2	200*6	200*2	50*14	200*3
3	70*6	70*2	10*14	70*3
4	25*6	25*2	35*20	25*3
5	-	75*20		-

6.4 Stress analysis (Mechanical analysis)

Stress analysis of adhesively CFRP bonded to the bottom of steel plate is carried out using linear finite element method in *ABAQUS* program. In the analysis, the temperature distribution effect due to heating of the adhesive in the previous thermal analysis is attributed, in addition to the influence of the tension force which is applied on the ends of the steel plate. The analysis is performed in two steps,

- Step one: Include thermal stresses which are introduced due to adding of necessary constraints to eliminate rigid body movement (i.e. defining of mechanical boundary conditions). Temperature distribution affects are considered by writing or/and defining the results from the thermal analysis in the input file of the stress analysis.
- Step two: general static analysis is defined in this step, which include the introduction of stresses after applied tension force due to restricting the movement of the member by defining mechanical boundary conditions. This step includes the total effect of thermal load as well as the mechanical load.

In this analysis the same material properties which are used in the thermal analysis are defined.

6.4.1 Mechanical Boundary Conditions and load application

Boundary conditions of the model are applied on the surfaces. In the modelling of this member, boundary conditions are defined just on three surfaces. The first one is the BC that controls the movement in the y-direction along the upper surface of the steel plate (i.e. the displacement of the plate in the y-direction is locked to zero value) see Figure 6.11. The symmetry line in the vertical direction in the Figure 6.11 is said to be fixed in the x-z direction (i.e. the displacement of the composite plate in the x-z direction will be equal to zero) and also the rotation about z-axis is locked along that line, but the translation in y-direction is allowed. The rotation about z-axis is locked along the face where load is applied as in Figure 6.11.

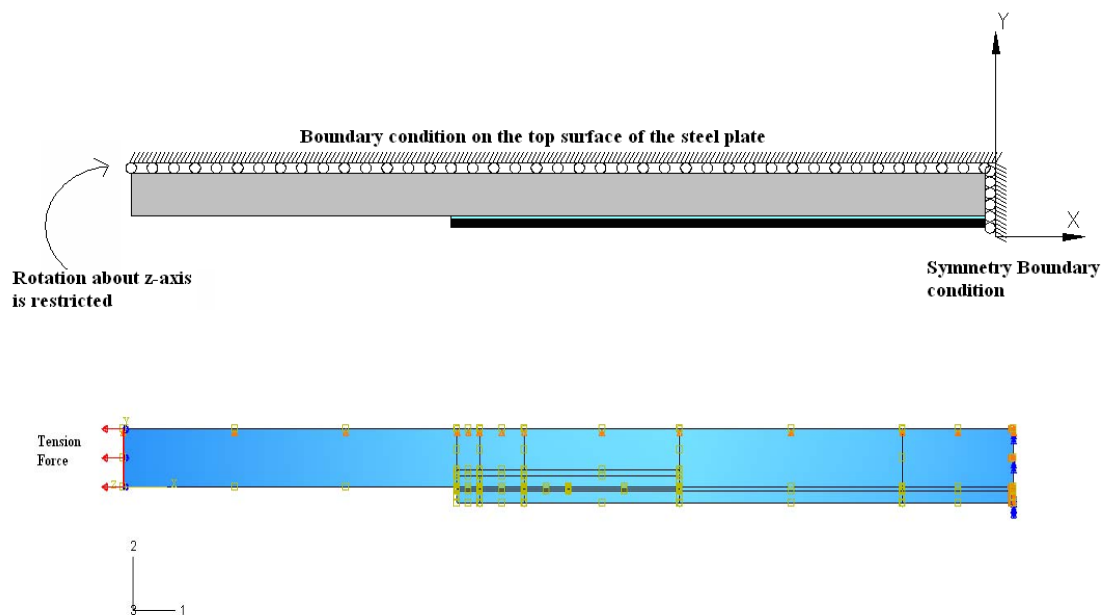


Figure 6.11 Descriptions of Boundary Conditions and load application

The application of the tension force is made by giving a certain pressure on the steel plate face at the ends. A load of 450 Mpa is applied which is equivalent to yield stress of the steel.

6.4.2 Meshing

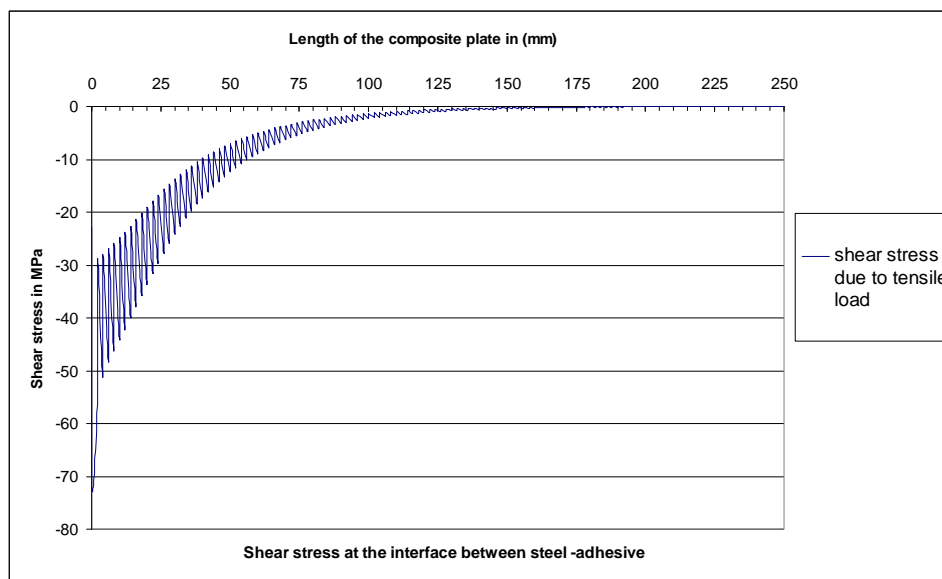
Same mesh pattern and configuration which is used in the thermal analysis is applied in this analysis. Only thing which is changed in this case is the element type and an eight –node quadratic quadrilateral plane stress element with four integration points (CPS8) is used in modelling of the composite plate see Figure 6.8.

7 Results & Discussion

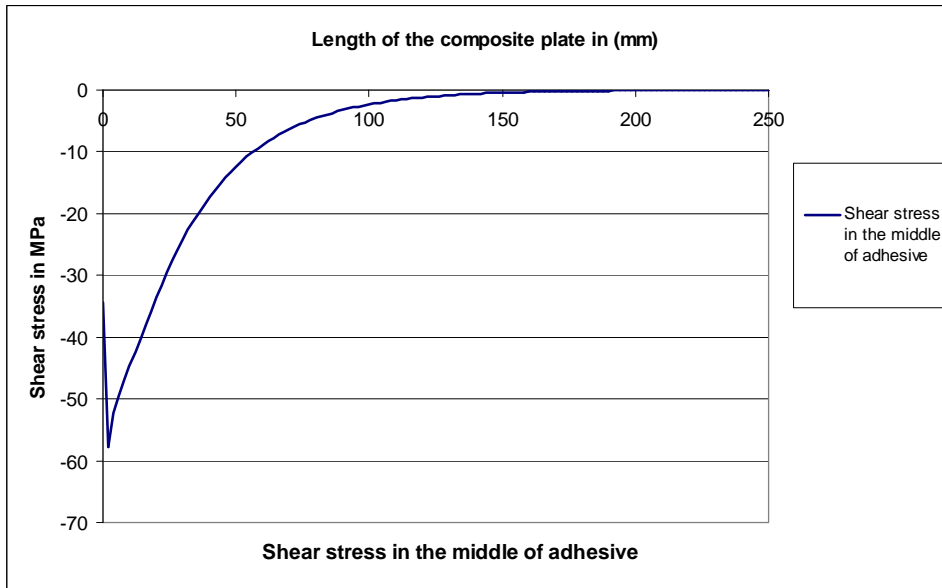
The problems that are studied in this thesis are the shear stresses, the peeling stresses at the interfaces between steel, adhesive, CFRP laminate and the normal stresses in the CFRP laminate. Previous chapters explain the development of stresses in the composite plate and the ways to reduce it. The model is analysed in the Finite Element programme *ABAQUS*. Several different analyses are done for the model in order to study the effect of different parameters on the behaviour of the strengthened composite plate. The position of the heating source, duration of heating and the length of the heat source were changed in order to see the effect on the shear and peeling stresses developed in the composite plate. The parametric study for the material properties was also performed to distinguish the affect on the shear and peeling stresses in the composite plate.

7.1 Mechanical Analysis/ Development of shear and peeling stresses

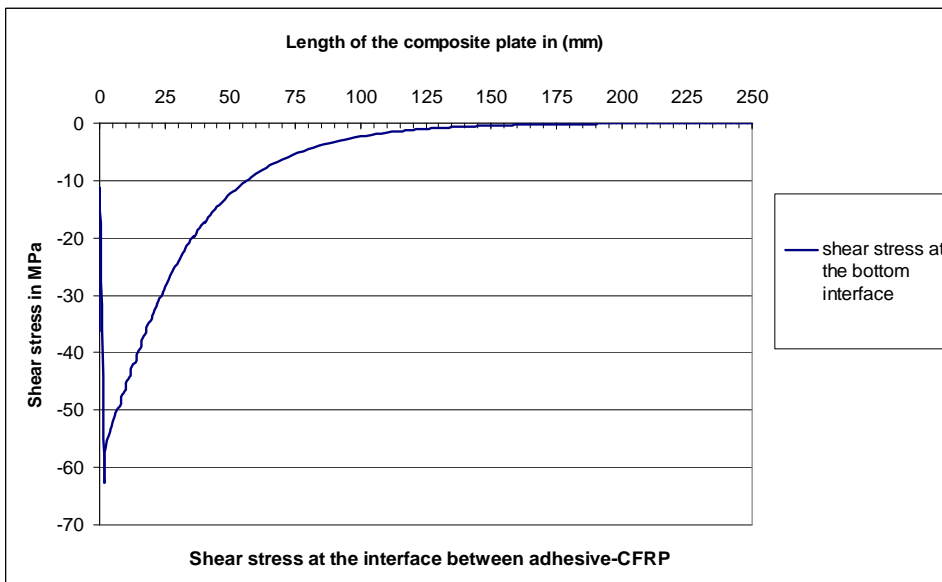
The mechanical analysis begins with the composite plate loaded in tension with a load of 440kN applied as pressure. The behaviour of the composite plate under the load and the development of shear and peeling stresses at the interfaces between steel, adhesive, CFRP laminate and in the middle of adhesive layer are studied.



(a)



(b)



(c)

Figure 7.1 Shear stress at different positions in adhesive layer

The Figure 7.1 explain that the tensioning of the composite plate result in high shear stress at the connection point between steel plate and CFRP laminate and then it reduces gradually along the length until zero value at the symmetry line. The development of high shear stress along the bond line is due to the difference in deformation between steel plate and CFRP. The shear stress developed is dependent on the stiffness of the steel, adhesive and CFRP. The upper part of adhesive attached to the steel plate is displaced through a larger distance compared to the part attached to the CFRP laminate resulting in the development of shear stress as in Figure 7.2. Stiffness of the adhesive has an effect on the transferring of load from steel to CFRP

laminate. Higher the stiffness of adhesive, greater amount of force is linked instantaneously over a smaller distance which is to be transferred to the CFRP laminate resulting in higher shear stress at the end of the laminate. This high shear stress may cause failure in adhesive layer, since the ultimate shear strength of the adhesive type considered in this study is around (25-35MPa) which is lower than the shear stress produced due to tension force.

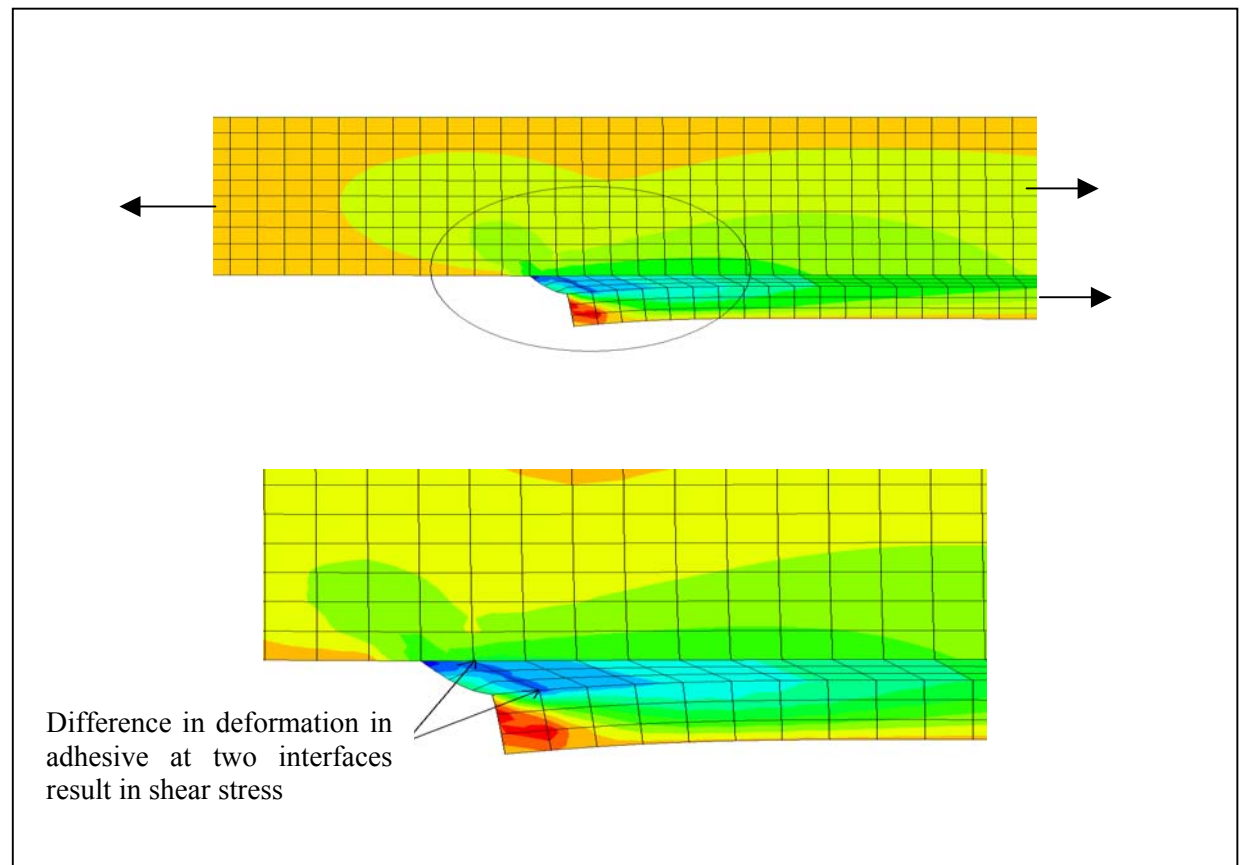


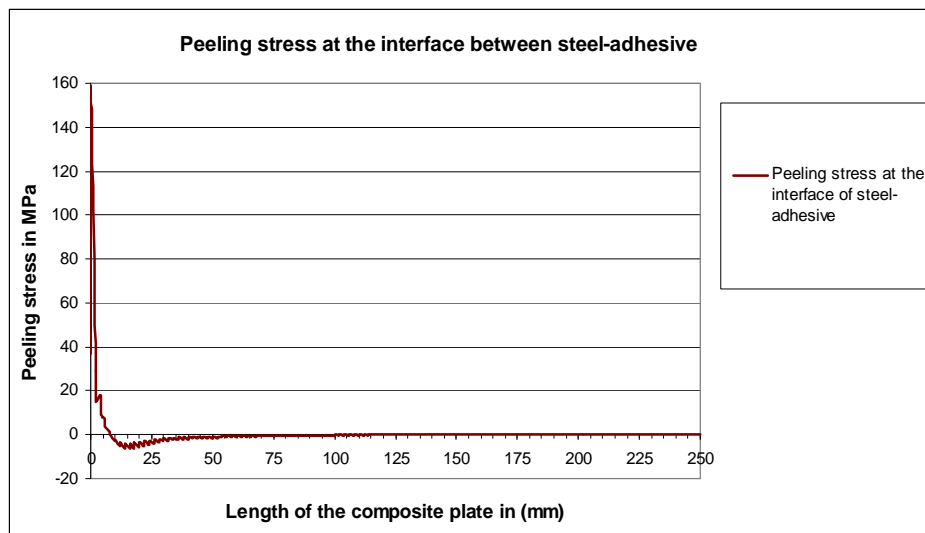
Figure 7.2 Development of shear stress in adhesive layer

The peak values of the shear stress in Figures 7.1 (a) and (c) are due to singularity and incompatibility problem. At the interface between steel plate and adhesive the high peak value in one of the nodes (singularity problem) is due to the change of geometry. The fluctuating values of shear stress along the interface are due to incompatibility between two different materials (i.e. steel plate and adhesive have different material properties like stiffness). The same incompatibility problem can be seen at the interface between adhesive and CFRP laminate.

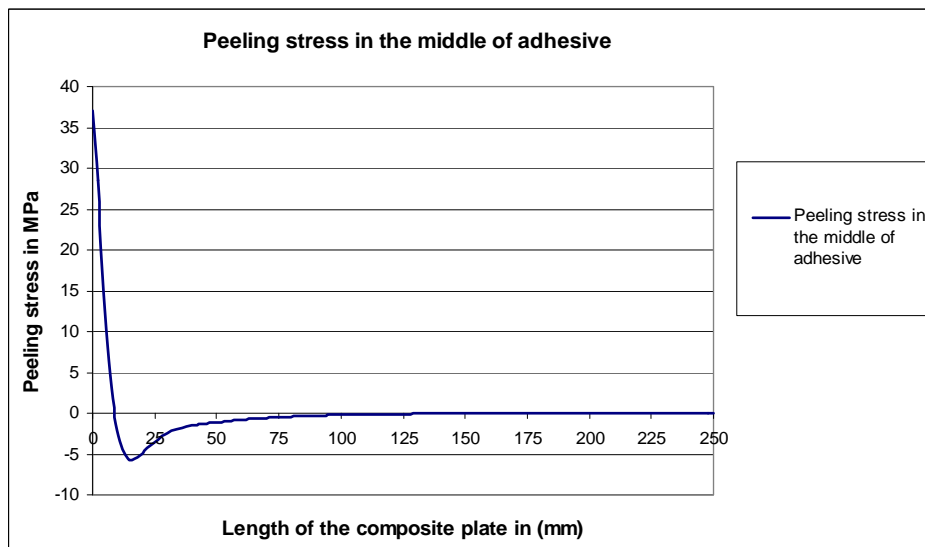
The heating of the composite plate develops the peeling stress. Due to heating at the interface of steel-adhesive, the steel plate expands. The movement of the steel is restricted by the adhesive attached to it which induces the compression force in the steel plate. The CFRP cannot expand due to heating as the coefficient of expansion for

the CFRP laminate is almost zero. The expansion of the steel and the adhesive causes the tension force in the CFRP. The eccentricity of the forces in the composite plate causes the bending moment. As a result of bending moment the peeling stresses are developed at the interfaces as shown in Figure 7.15.

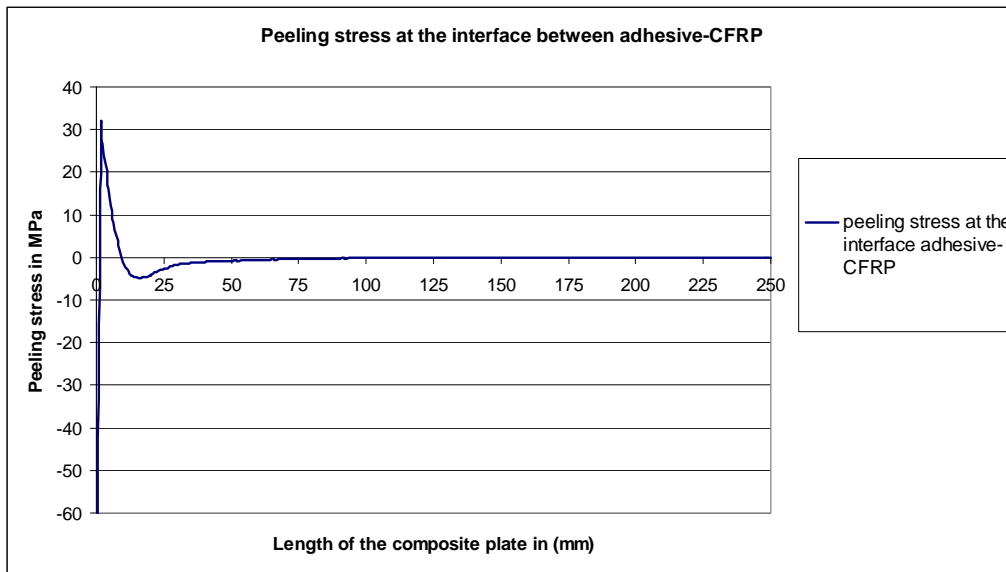
Analysis results show that high peeling stresses are obtained in the adhesive due to bending of the CFRP laminate at the joint corners. The bending in CFRP laminate is due to the tension force applied at the end of steel plate. Due to loading the steel plate displaces in the horizontal direction. The movement of the steel is resisted by the adhesive attached to it resulting in the development of compression force in steel. The CFRP laminate is not displaced by the load as the stiffness is much higher. Hence the tension force is developed in the CFRP laminate. The eccentricity of the two forces results in the bending moment of the composite plate, developing the peeling stresses at the interface as shown in Figure 7.4. The very high peak value of peeling stress in Figure 7.3 (a) and (c) is due to singularity and compatibility problem at the interfaces.



(a)



(b)



(c)

Figure 7.3 Peeling stress at different positions in adhesive layer

The Figure below illustrates how tensioning of composite plate affects the CFRP laminate which is bended downwards resulting in peeling stress in adhesive layer.

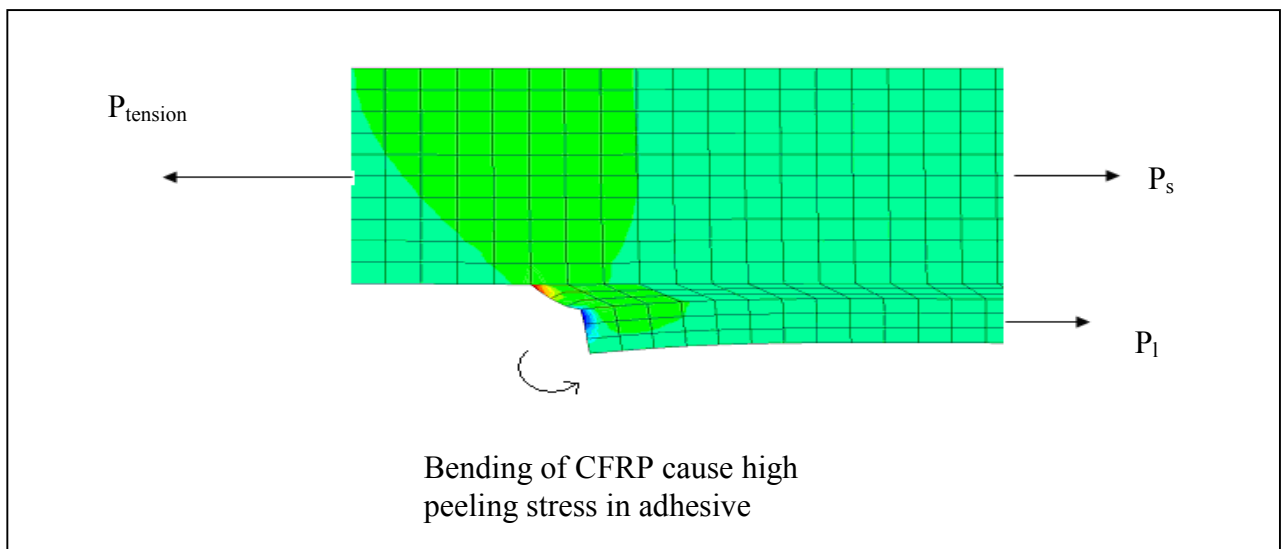


Figure 7.4 The effect of tensile load on the CFRP laminate

For the current mesh density, the values of maximum shear and peeling stresses at different positions are as follow.

Table 7.1 Maximum values of shear and peeling stress at different positions

<i>Stresses</i> <i>MPa</i>	<i>Interface between</i> <i>Steel-adhesive</i>	<i>Middle of the</i> <i>adhesive</i>	<i>Interface between</i> <i>adhesive-CFRP</i>
Shear stress	-71.8	-57.82	-62.25
Peeling stress	159.08	37.12	-79.27

7.2 Convergence Study

Before finalising the model, a convergence study is performed under the application of 440 kN of tension load to determine the most appropriate mesh size to use. Based on the results from the convergence study, the thermal and mechanical analyses are then performed to find the resulting stress and strain distributions. As mentioned in the previous chapter the convergence study is done to refine the mesh in the region where shear and peeling stresses are very sensitive. It is also helpful to capture the smallest change occurred in the regions where the interfacial stresses are susceptible to change with the applied load. By refining the mesh the results obtained will be more reliable. During the convergence study the mesh is refined where the stresses have peak values. The mesh size is refined through the thickness and along the length in the adhesive, CFRP and steel. For the adhesive layer the element thickness is decreased from 0.5mm through the thickness to 0.25mm which is more than sufficient to capture the shear stress in the adhesive as in Figure 7.5, while it is kept constant in steel plate and CFRP.

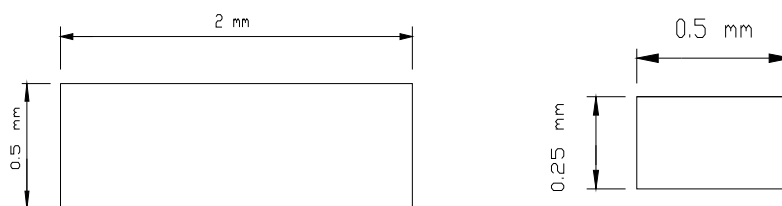


Figure 7.5 Different element dimensions in adhesive layer

The composite plate is divided into several regions in the longitudinal direction. For a distance of 20 mm from the connection point between steel and adhesive-CFRP the element length is reduced from 2 mm to 0.5 mm which helps to capture the changes in interfacial stresses (especially peeling stress). The regions where the interfacial stresses are not sensitive with the load are made coarser in order to save the memory of the system and time for each analysis. The details of the different mesh density are shown in Figure 7.6.

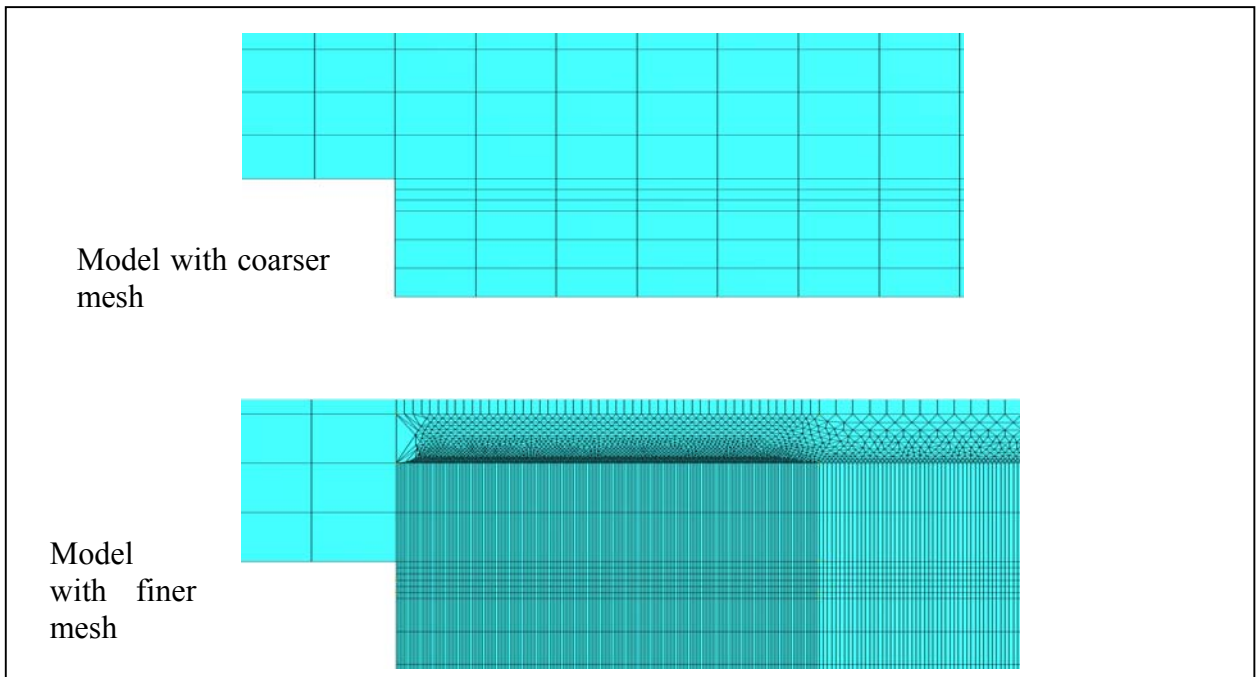
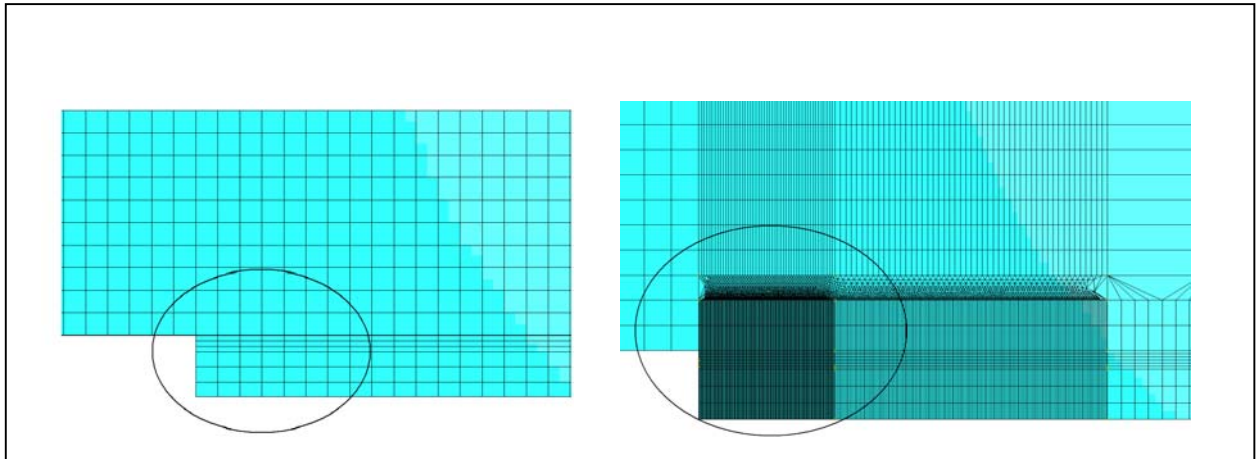
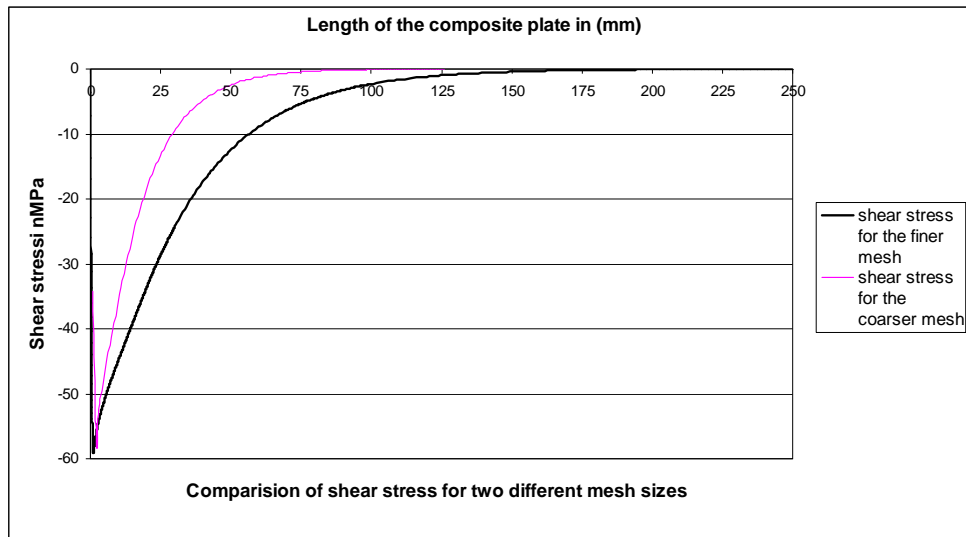
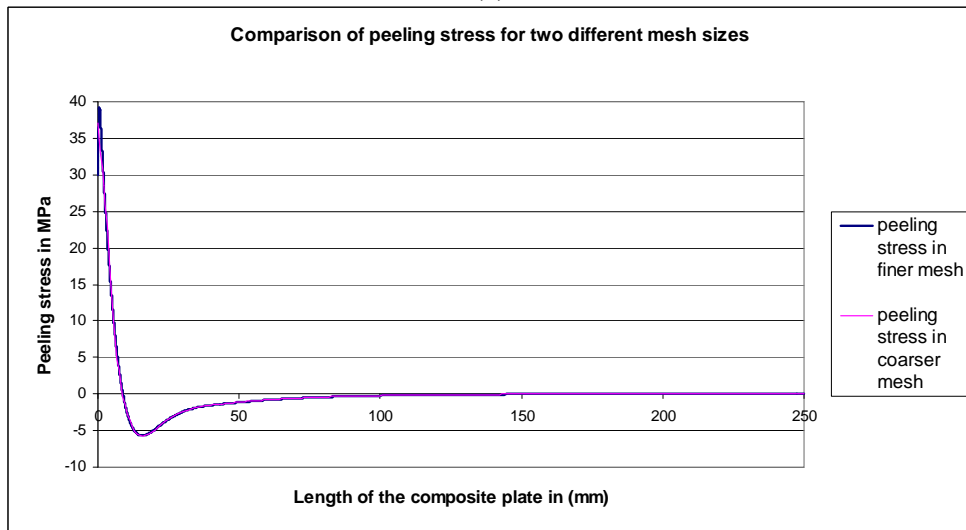


Figure 7.6 Convergence study for two different mesh sizes

The Figure below shows the comparison between the shear and peeling stresses for two different mesh sizes plotted in the middle of the adhesive, the Figure 7.7 (a) is for the coarse mesh and Figure 7.7 (b) is for the finer mesh.



(a)



(b)

Figure 7.7 Comparison of interfacial stresses plotted in the middle of adhesive with different mesh sizes.

Table 7.2 Comparison of shear stress values in MPa at different positions for different mesh density

<i>Position</i>			<i>Coarser Mesh</i>	<i>Finer Mesh</i>
Interface	between	Steel-	-71.8	-98.46
adhesive				
In the middle of adhesive			-57.82	-59.16
Interface	between	adhesive-	-62.25	-56.76
CFRP				

Table 7.3 Comparison of peeling stress values in MPa at different positions for different mesh density

<i>Position</i>	<i>Coarser Mesh</i>	<i>Finer Mesh</i>
Interface between Steel-adhesive	159.08	348.51
In the middle of adhesive	37.12	39.15
Interface between adhesive-CFRP	-79.27	-153.59

From Figures 7.7 and the Tables 7.2 and 7.3 it can be concluded that the model with fine mesh size especially in the adhesive layer is much better to use in the further analysis like thermal and mechanical analysis. In case of finer mesh, more nodes have been created and included in the calculation of the stress distribution. These nodes help to capture the variation of stresses over a smaller distance with respect to load and get more accurate results. The use of finer mesh will help to monitor the temperature distribution in a better way which is much sensitive and has to be seized more accurately. It is worthy to have more nodes so that the distance between the nodes is decreased and the change in the temperature through the composite plate can be obtained more precisely.

7.3 Validation of the Model

In order to verify the model the results obtained from the *ABAQUS* are compared with the analytical solution attached as a Math Cad file in *Appendix C*. Higher shear stress is obtained in the analytical solution at the position where the CFRP laminate is attached to the steel plate in comparison with the finite element model. Figure 7.8 shows the shear stress distribution in the middle of the adhesive for both cases.

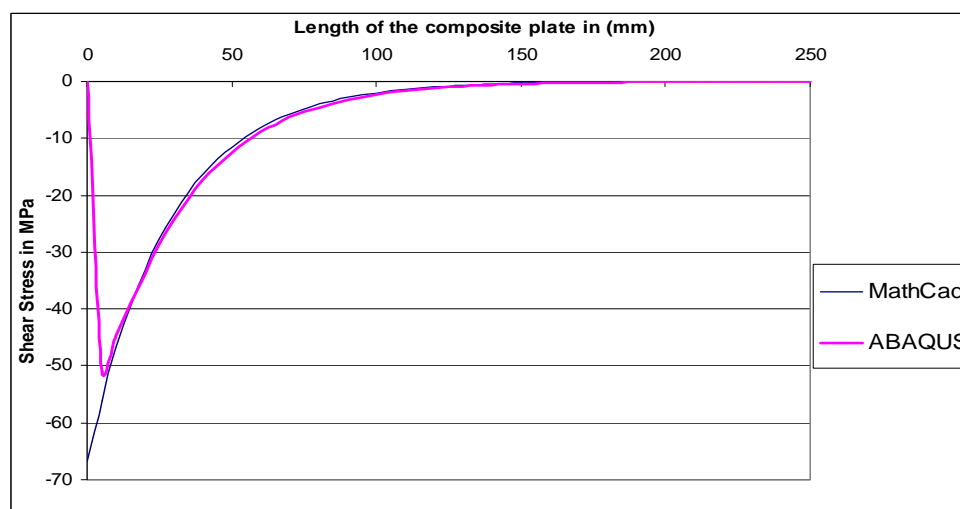


Figure 7.8 Comparison between numerical and analytical solution for the shear stress distribution

As it is seen from the above results the two graphs are in great agreement except the peak value. The analytical solution includes some simplifications like stress distribution through the adhesive thickness is constant. The other simplification is the shear stress starts from the maximum value at the position where the CFRP laminate is glued to the steel plate with the aid of adhesive (i.e. at distance equal to zero at the beginning) when loaded in tension. Due to which the gradual increase of the shear stress cannot be seen. Whereas in the finite element analysis the shear stress start from zero value at the connection point between steel plate and CFRP laminate. It reaches the peak value over a very short distance as the normal stresses increases to maximum value depending on the stiffness. The zero value of the shear stress cannot be captured in the analytical solution because first order differential equations are used, whereas ABAQUS can capture the zero shear stress. Hence from the above results it is confirmed that the model used in ABAQUS is correct.

7.4 Thermal Analysis

The aim of the thermal analysis is to investigate the distribution of temperature in different layers of the composite plate when the heat is applied. Heating the composite plate for a certain temperature has significant effects on the material properties of adhesive layer used to bond the CFRP laminate to the steel plate. The modification of the stiffness of adhesive is beneficial to decrease the high shear stress developed at the ends of the CFRP laminate under the tensile load application.

Adhesive layer will soften at the position where heat is applied and a very small amount of force can be linked to the CFRP laminate from the steel plate at that position. The forces are linked gradually depending on the stiffness of adhesive which makes the shear stress to distribute over a larger distance. This process of heating and changing the properties of the adhesive layer helps to redistribute the interfacial stresses over the larger area along the bond line. Different parameters are studied to choose the optimal case where temperature distribution is more uniform and gradual. The parameters which are of interest are as follows:

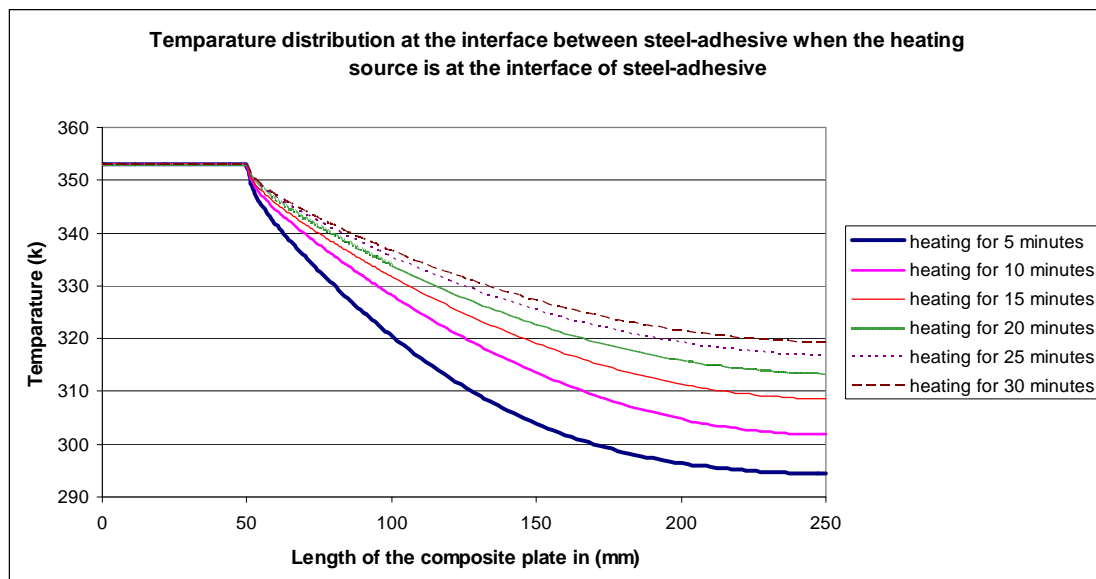
- Location of the heat source, the heat is applied at positions which are more beneficial to have good distribution of temperature, e.g. at the interface between steel plate-adhesive, in the middle of adhesive and at the interface between adhesive-CFRP laminate.
- Time of heating, since the composite plate consists of components with different thermal material properties like conductivity it is very difficult to have an optimal time for heating. In this analysis several heating times are tested (5, 10, 15, 20, 25, 30 minutes).
- Length of heat source application, the source with two different lengths is used to explain the effect of length on temperature distribution in the composite plate. In this case the source with length of *50 mm* and *100 mm* are applied.

The above parameters have interactive effect on temperature distribution and later on stress distribution. The parameters above are compared and explained in details to choose the most favourable solution.

Temperature Distribution

The gradual distribution of the temperature along the composite plate as well as through the adhesive layer result in more uniform change in the adhesive stiffness, which in turn affect the shear stress distribution along the member. The study of the heat locations gives more understanding of the temperature distribution depending on the thermal properties for different components.

- For the case when the heating was applied for a length of 50mm at the interface of steel and adhesive for five different time of heating 5, 10, 15, 20, 25 and 30 minutes. The temperature distributions for different time of heating in the adhesive obtained are shown in Figure 7.9.



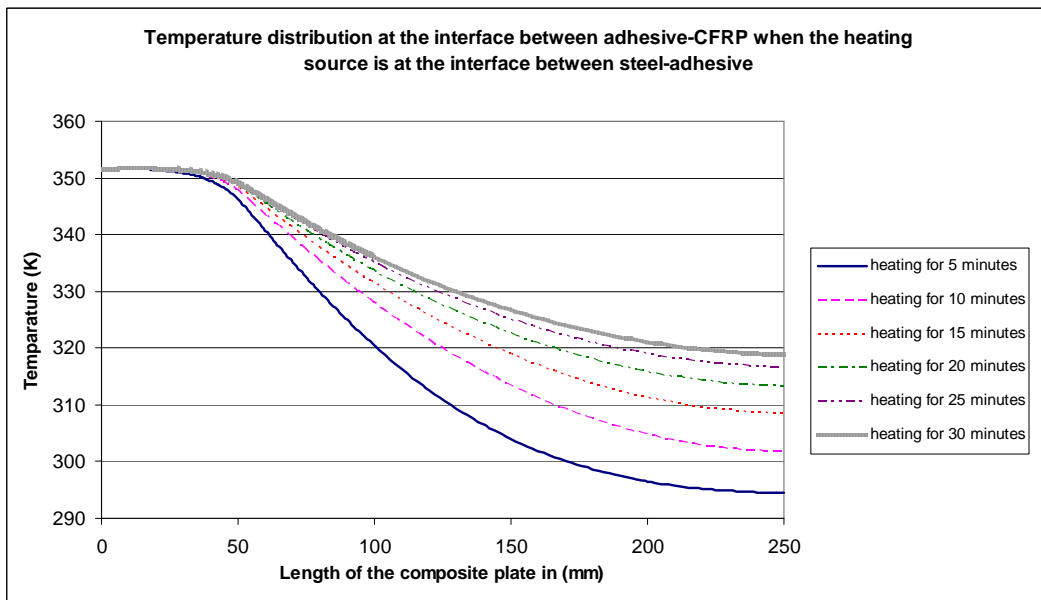
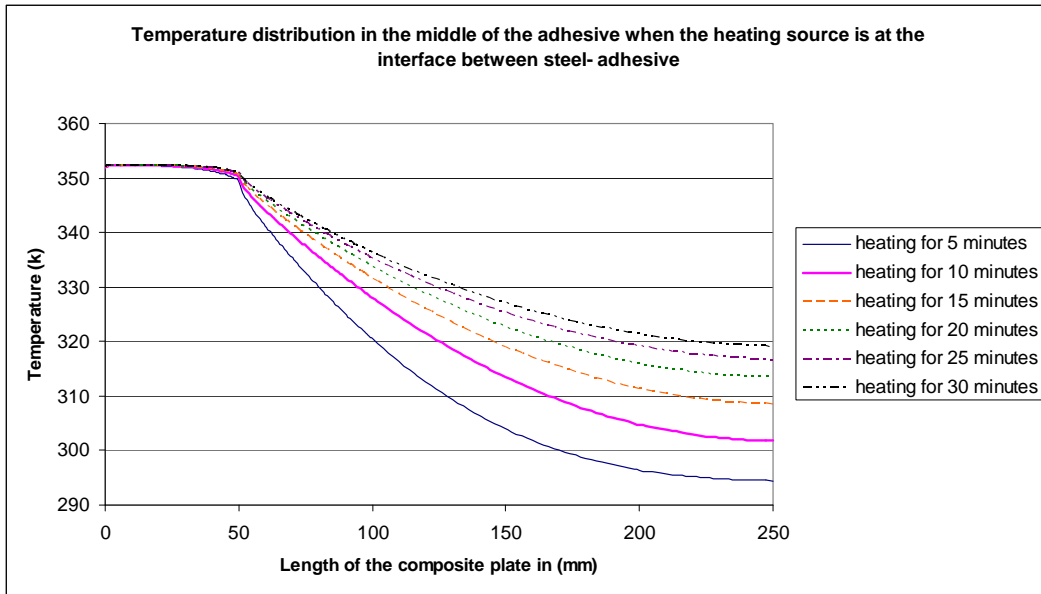


Figure 7.9 Temperature distribution for different heating time when heated at the interface of steel-adhesive plotted at different positions.

- For the case where the heat source is applied in the middle of the adhesive for a length of 50mm and for five different time of heating 5, 10, 15, 20, 25 and 30 minutes, the following temperature distributions were obtained as shown in Figure 7.10.

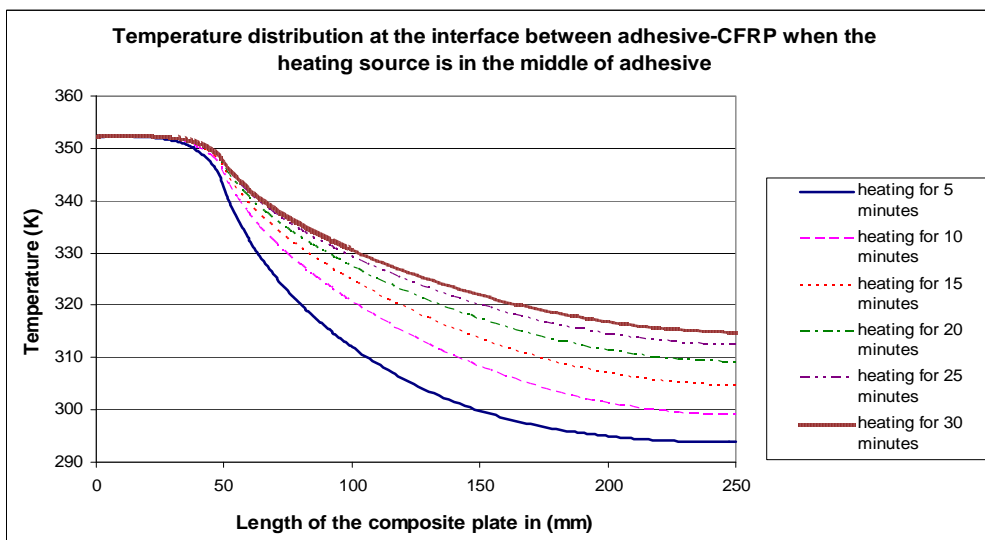
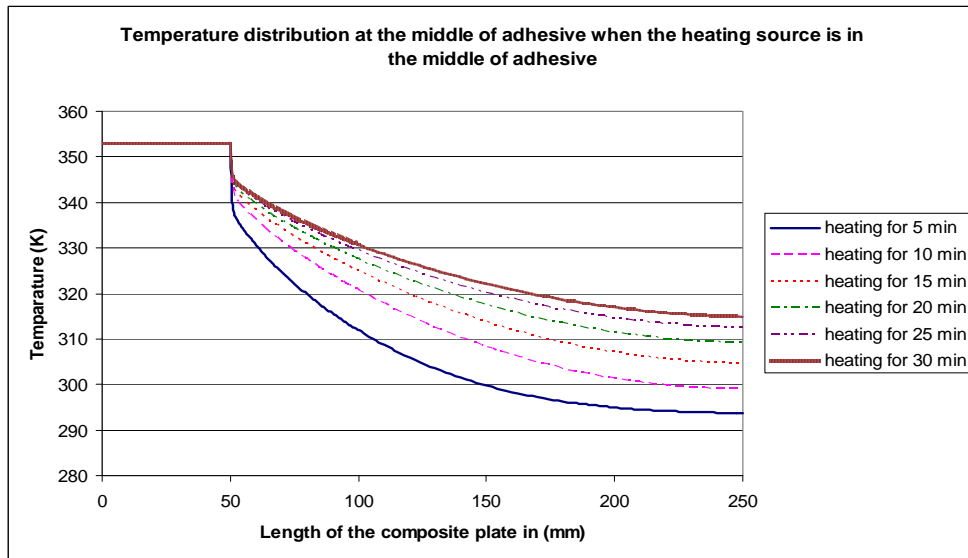
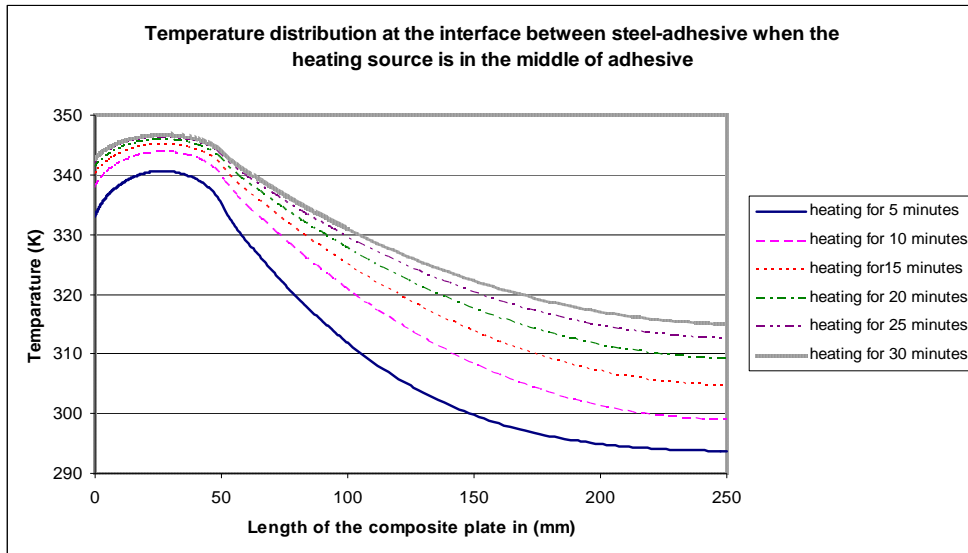
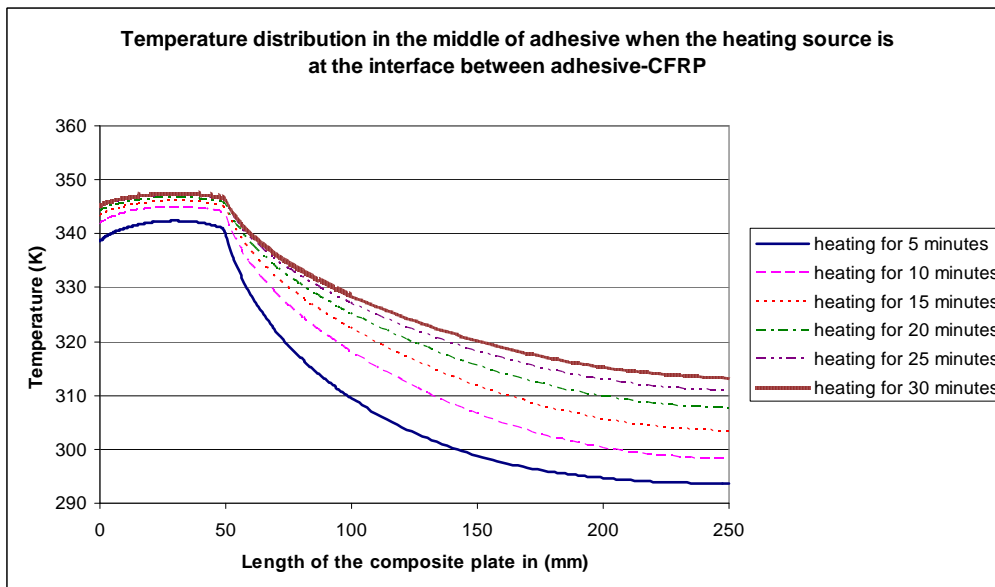
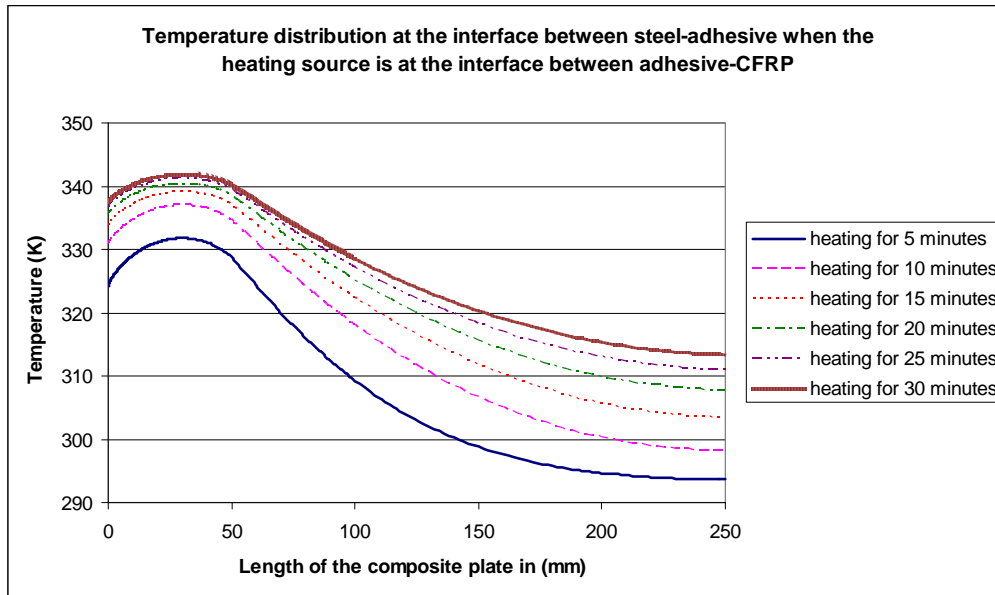


Figure 7.10 Temperature distribution for different heating time when heated in the middle of adhesive plotted at different positions.

- For the case where the heating source is applied at the interface of the adhesive-CFRP over a length of 50mm and for five different time of heating 5, 10, 15, 20, 25 and 30 minutes, the distribution of temperature as shown in Figure 7.11 was obtained.



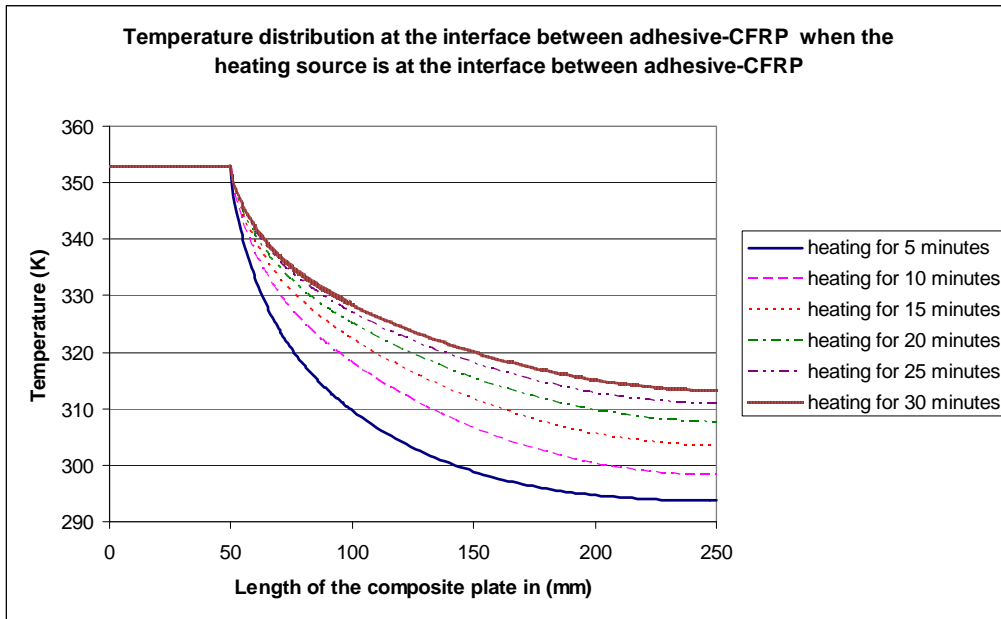


Figure 7.11 Temperature distributions for different heating time in the interface adhesive-CFRP laminate

Table 7.4.a The temperature distribution at different locations and for different time of heating.

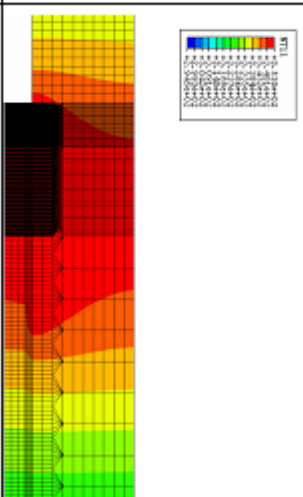
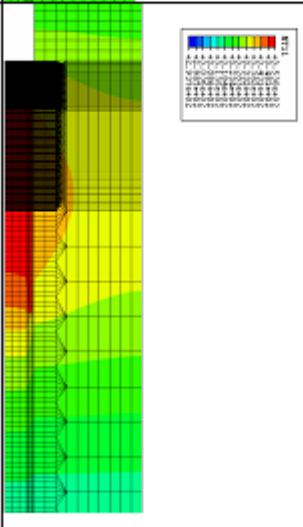
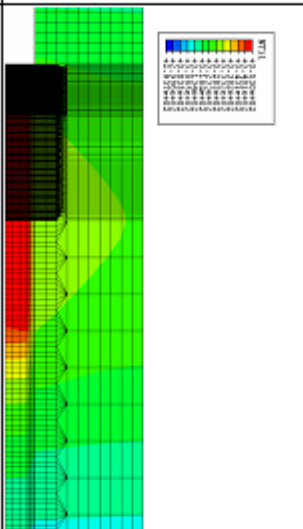
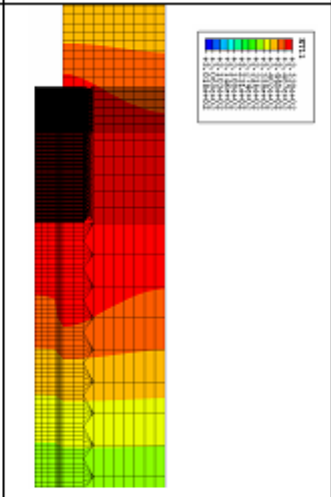
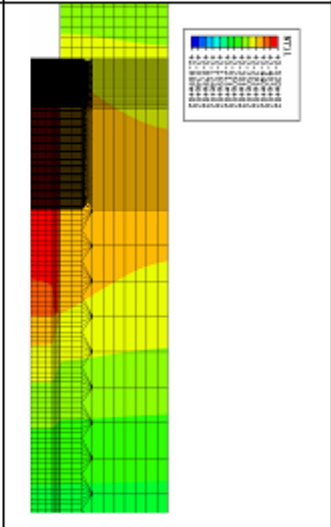
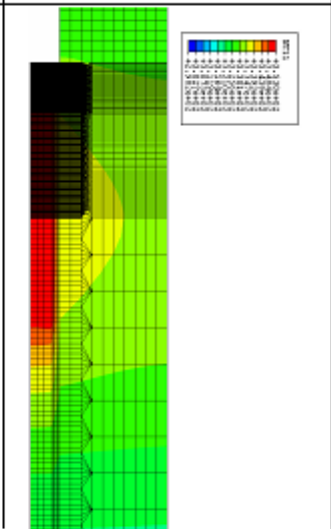
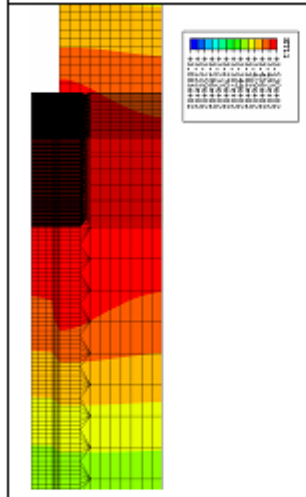
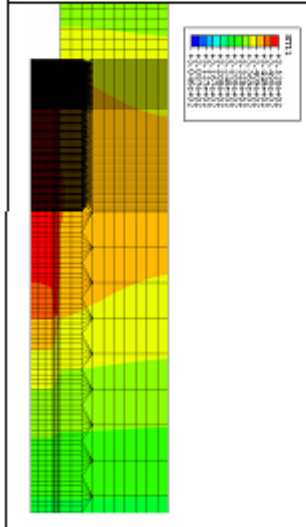
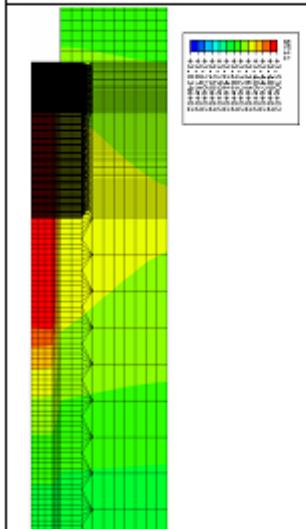
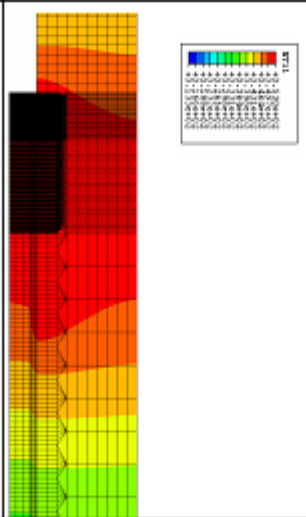
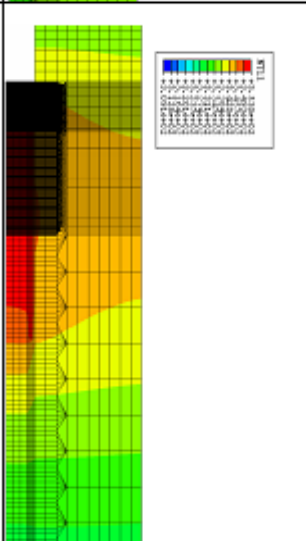
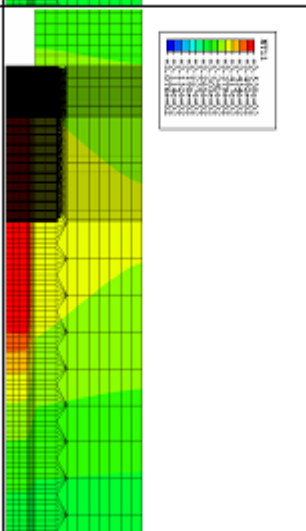
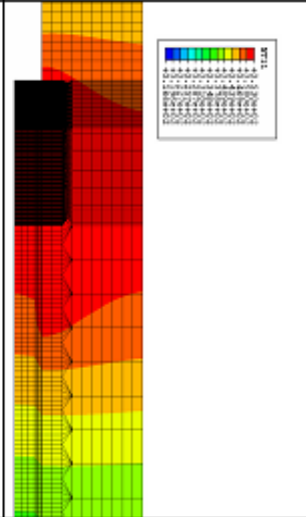
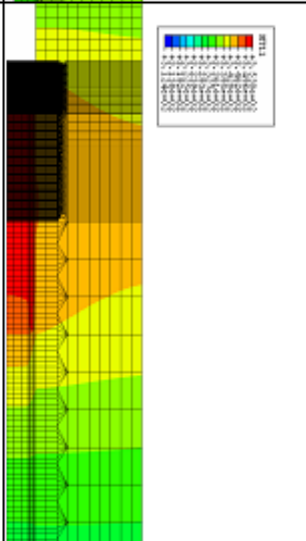
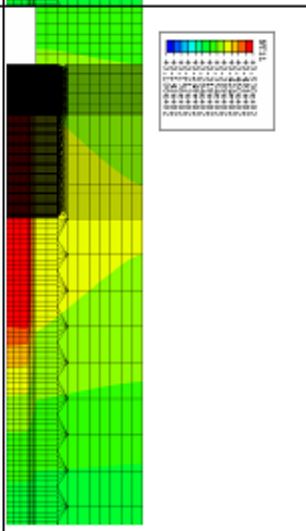
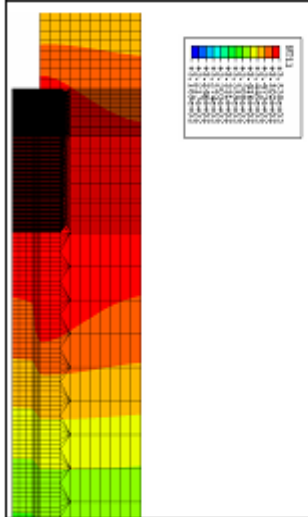
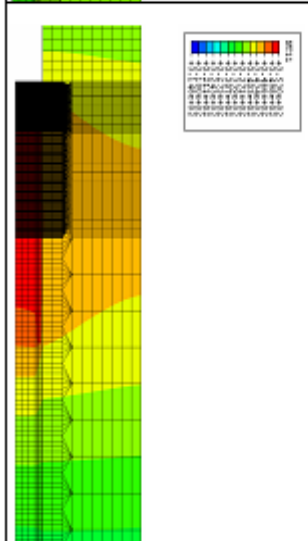
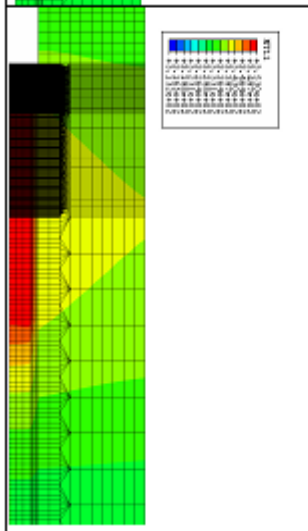
Time (Minute)	Distribution of temperature at the interface between steel-adhesive	Distribution of temperature in the middle of adhesive	Distribution of temperature at the interface between adhesive-CFRP
5	 <p>Heatmap showing temperature distribution at the steel-adhesive interface at 5 minutes. The color scale ranges from 20°C (blue) to 100°C (red). High temperatures are concentrated at the top surface of the adhesive.</p>	 <p>Heatmap showing temperature distribution in the middle of the adhesive at 5 minutes. The color scale ranges from 20°C (blue) to 100°C (red). High temperatures are concentrated at the top surface, with some penetration into the middle.</p>	 <p>Heatmap showing temperature distribution at the adhesive-CFRP interface at 5 minutes. The color scale ranges from 20°C (blue) to 100°C (red). High temperatures are concentrated at the top surface, with some penetration into the adhesive.</p>
10	 <p>Heatmap showing temperature distribution at the steel-adhesive interface at 10 minutes. The color scale ranges from 20°C (blue) to 100°C (red). High temperatures are concentrated at the top surface.</p>	 <p>Heatmap showing temperature distribution in the middle of the adhesive at 10 minutes. The color scale ranges from 20°C (blue) to 100°C (red). High temperatures are concentrated at the top surface.</p>	 <p>Heatmap showing temperature distribution at the adhesive-CFRP interface at 10 minutes. The color scale ranges from 20°C (blue) to 100°C (red). High temperatures are concentrated at the top surface.</p>
15	 <p>Heatmap showing temperature distribution at the steel-adhesive interface at 15 minutes. The color scale ranges from 20°C (blue) to 100°C (red). High temperatures are concentrated at the top surface.</p>	 <p>Heatmap showing temperature distribution in the middle of the adhesive at 15 minutes. The color scale ranges from 20°C (blue) to 100°C (red). High temperatures are concentrated at the top surface.</p>	 <p>Heatmap showing temperature distribution at the adhesive-CFRP interface at 15 minutes. The color scale ranges from 20°C (blue) to 100°C (red). High temperatures are concentrated at the top surface.</p>

Table 7.4.b The temperature distribution at different locations and for different time of heating

Time (Minute)	Distribution of temperature at the interface between steel-lathesive	Distribution of temperature in the middle of adhesive	Distribution of temperature at the interface between adhesive-CFRP
20	 <p>Temperature distribution at the interface between steel-lathesive at 20 minutes. The plot shows a high-temperature region (red) near the steel-lathesive interface, which tapers off towards the middle of the adhesive. A color scale legend is provided.</p>	 <p>Temperature distribution in the middle of adhesive at 20 minutes. The plot shows a moderate temperature region (yellow) in the middle of the adhesive, with a color scale legend.</p>	 <p>Temperature distribution at the interface between adhesive-CFRP at 20 minutes. The plot shows a low-temperature region (green) at the interface, with a color scale legend.</p>
25	 <p>Temperature distribution at the interface between steel-lathesive at 25 minutes. The high-temperature region (red) has expanded further into the adhesive. A color scale legend is provided.</p>	 <p>Temperature distribution in the middle of adhesive at 25 minutes. The moderate temperature region (yellow) has expanded. A color scale legend is provided.</p>	 <p>Temperature distribution at the interface between adhesive-CFRP at 25 minutes. The low-temperature region (green) remains relatively stable. A color scale legend is provided.</p>
30	 <p>Temperature distribution at the interface between steel-lathesive at 30 minutes. The high-temperature region (red) is at its maximum extent. A color scale legend is provided.</p>	 <p>Temperature distribution in the middle of adhesive at 30 minutes. The moderate temperature region (yellow) is at its maximum extent. A color scale legend is provided.</p>	 <p>Temperature distribution at the interface between adhesive-CFRP at 30 minutes. The low-temperature region (green) remains stable. A color scale legend is provided.</p>

It should be noted that the graphs in the Figure 7.9, 7.10 and 7.11 are plotted at different positions and it is wise to consider the results in the middle of adhesive to avoid the singularity and incompatibility problems at the interfaces.

The temperature distribution when the heat source is at the interface of steel-adhesive as in the Figure 7.9 shows that the temperature is decreasing more gradually with increasing of heating time. The best profile of temperature distribution can be seen at the end of the 30 minutes of heating. Heating at the interface between steel and adhesive causes the steel plate to heat up more and has higher temperature due to the high conductivity than any other materials in the composite plate. Due to which the adhesive layer is heated up helping to obtain more uniform temperature distribution in adhesive. Longer the heat is applied, hotter the steel plate becomes and helps in heating the adhesive in an indirect way causing the gradual decrease of temperature distribution along the longitudinal direction. It is found that the temperature in the middle of the adhesive is 80°C (equivalent to 353 K) for a distance of 35 mm from the connection point even though the heating source is located at the top interface, then it is decreased gradually in the longitudinal direction. The decrease of the temperature in the adhesive is due to the low conductivity of the adhesive material. The difference in temperature at the point of heating and at the symmetric line is reduced by time and after 30 minutes of heating the temperature is found to be around 47°C (320K).

The Figure 7.10 shows that the temperature is almost constant along the heating source, and severe change in temperature is seen just at the end of the heating source. The variation of temperature is found through the adhesive thickness even though it has very small thickness. The reason is that the adhesive has very low conductivity and due to the convection boundary conditions the heat tries to escape from the shortest possible way i.e. in the downward direction which makes it difficult to heat up the upper part of the adhesive compared to the lower part as shown in the Table 7.4 a & b.

The effect of thermal material properties on temperature distribution is more evident in the Figure 7.11 where the heating source is located at the interface between adhesive-CFRP laminate. The desired temperature distribution in the middle of the adhesive is not obtained even after heating the interface of adhesive-CFRP laminate for 30 minutes. The most of the temperature is dissipated to the surrounding through the CFRP laminate instead of heating up the adhesive. The main cause for the dissipation of heat is that the conductivity of the adhesive layer is very low and the heat take the shortest way to colder regions in the surrounding instead of following through the adhesive and then steel plate to dissipate to the colder regions as shown in table 7.4 a & b.

- The length of heat source to be applied is also investigated to choose the more beneficial length of heating resulting in gradual temperature distribution along the length of composite plate and through the thickness of different layers. The comparison between temperature distributions obtained due to the heat source of lengths 50 mm and 100 mm has been monitored.

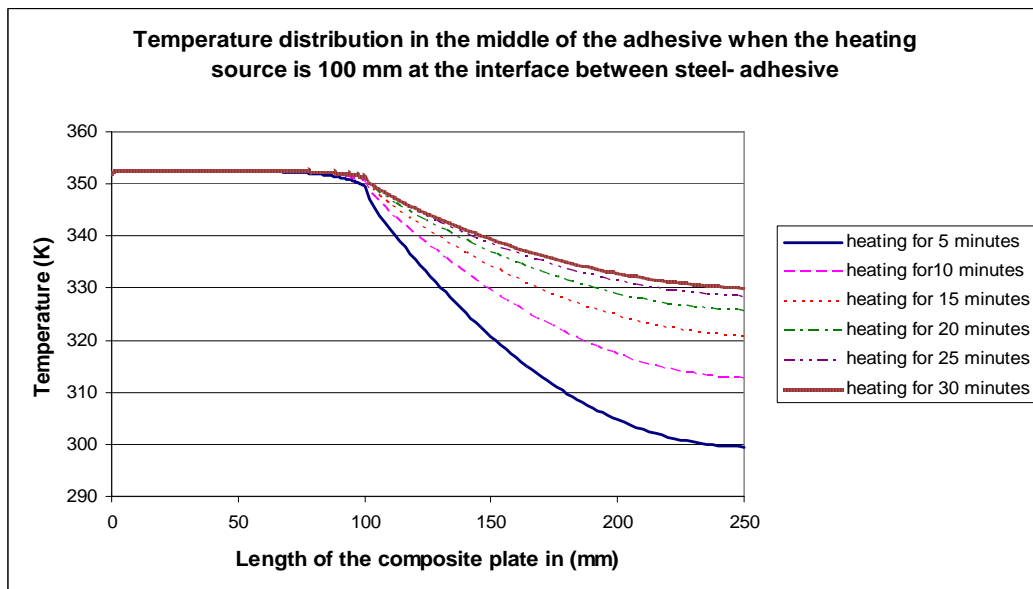
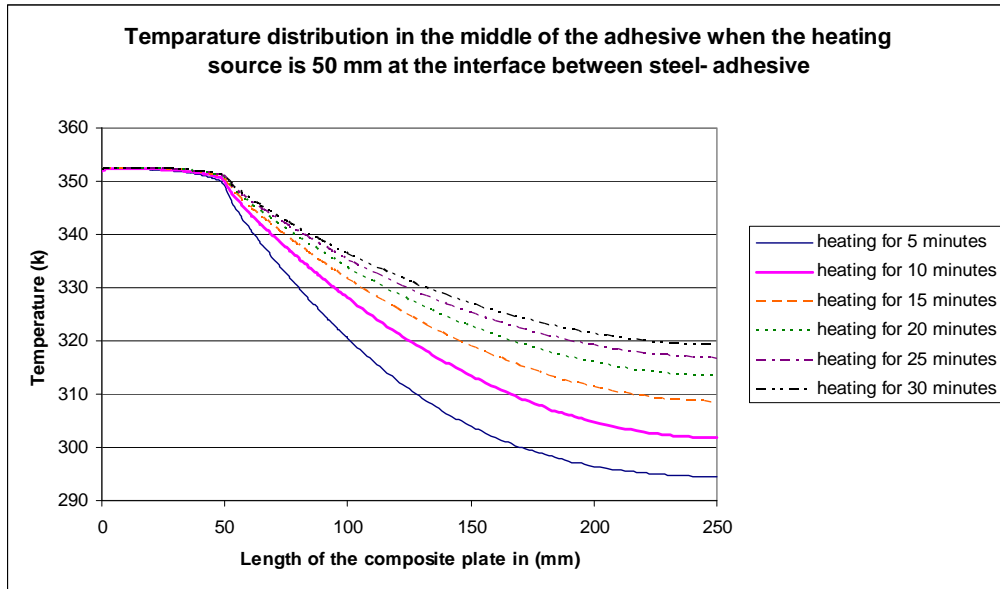


Figure 7.12 Comparisons of heating source with two different lengths at different time of heating

From the Figure 7.12, it can be concluded that the temperature has the same distribution for different heating lengths, the only thing which changes is the position of that distribution. With the larger length of heating the temperature distribution is shifted towards the symmetry line. The distribution of isothermal lines in both cases is shown in Figure 7.13 which helps to understanding the temperature distribution look like.

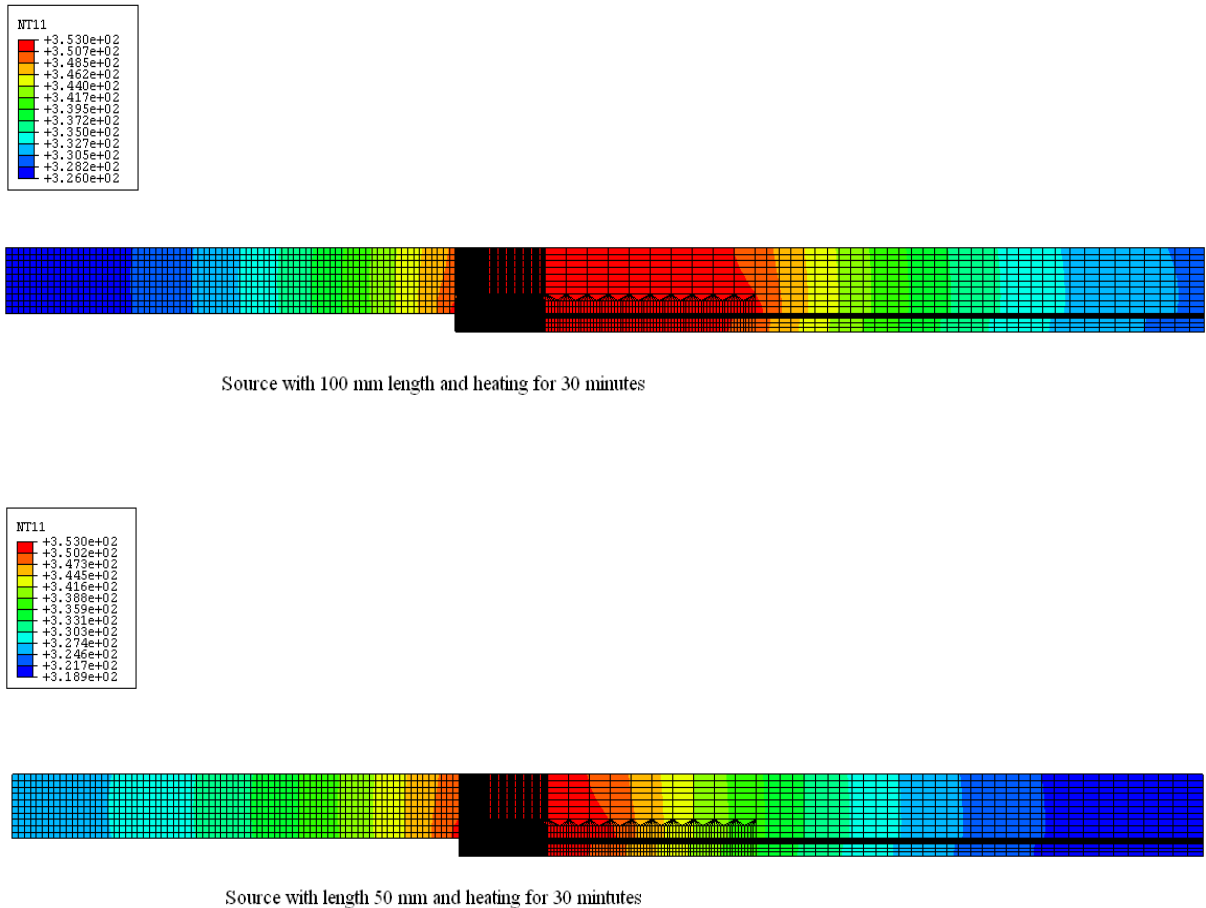


Figure 7.13 Distribution of isothermal lines for the source of heating with different lengths applied at the interface of steel-adhesive.

7.5 Thermal stress analysis

Heating of the composite plate result in movement of the components to a certain distance depending on the expansion coefficient of each component. Restraining of this movement causes the interfacial stresses in the composite plate. Due to diversity of mechanical and thermal properties of materials used in the composite structure different stresses are developed.

When heat was applied the heat transfer occurs through all the components depending on the conductivity, consequently the temperatures at different part of the adhesive layer can have similar or different distributions depending on the type of the thermal situation (i.e. location of heating source, time of heating and length of the heat source). The thermal and mechanical properties of the adhesive and adherents mismatches with each other such as thermal conductivities, expansion coefficients and Modulus of Elasticity causing thermal stress along the interfaces and in their neighbourhood. When the interface of steel plate-adhesive layer is heated, for the given mechanical and thermal boundary conditions the following shear stresses are obtained.

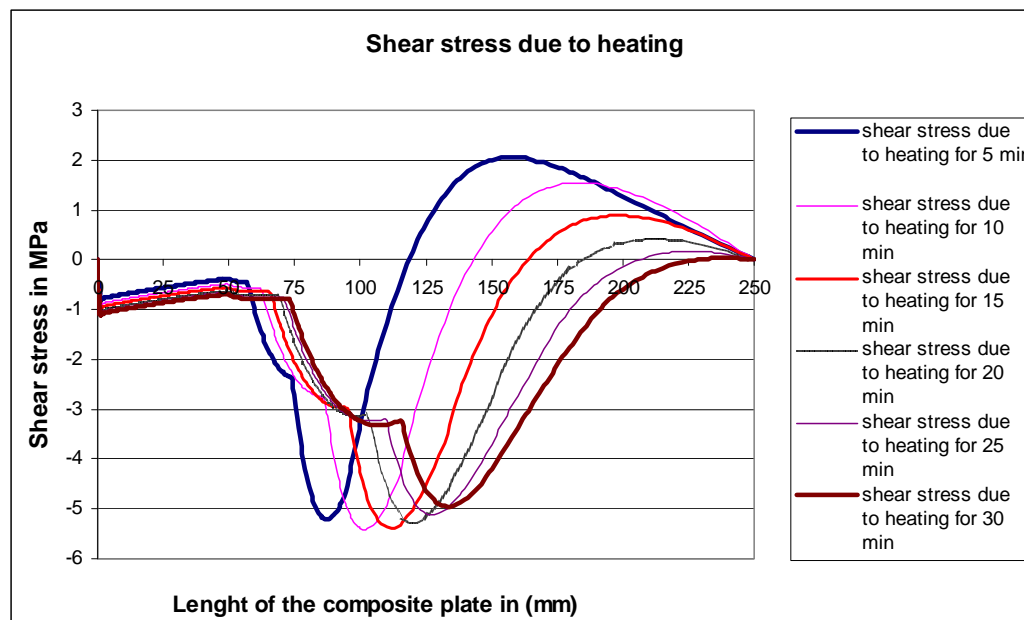


Figure 7.14 Shear stress distributions due to heating at the interface of steel-adhesive for different time plotted in the middle of adhesive

The Figure 7.14 above corresponds to the shear stress developed in the middle of the adhesive layer in order to avoid the problem of incompatibilities at the interfaces. Heating of the steel-adhesive interface for 50 mm length and for certain time develops the stresses in the composite plate due to difference in thermal expansion. The difference in expansion of steel plate and adhesive layer develop shear stress in the adhesive layer. The shear stress distribution is very low at the position where temperature boundary condition is applied (i.e. at the 50 mm from the connection point of steel-adhesive where the temperature is 353 K or 80 °C). It is because the adhesive is soft and has very low stiffness due to which it follows freely with the movement of steel due to thermal expansion. The shear stress in the adhesive layer increases after 50 mm from the end of the CFRP laminate (i.e. after the heating source) as the temperature is decreasing from 80 °C to about 30 °C at the symmetry line. The change in temperature along the composite plate causes the increase of modulus of elasticity for adhesive. As the stiffness of adhesive is increased the adhesive restricts the movement of the steel resulting in development of the shear stress.

When the heat was applied for 5 minutes the steel plate is heated more locally and expands in both directions without having much influence of the symmetry boundary conditions. As a result the angle of shear stress is changed and the value of shear stress changes from negative to positive. When the time of heating is increased, the heating effect will be global causing the steel plate to expand in only one direction due to the symmetry boundary conditions. The angle of shear stress will decrease in the longitudinal direction as the stiffness of the adhesive is increased.

The heating of the composite plate also develops the peeling stress. Due to heating at the interface of steel-adhesive, the steel plate expands. The movement of the steel is restricted by the adhesive attached to it which induces the compression force in the steel plate. The CFRP cannot expand due to heating as the coefficient of expansion for the CFRP laminate is almost zero. The expansion of the steel and the adhesive causes the tension force in the CFRP. The eccentricity of the forces in the composite plate causes the bending moment. As a result of bending moment the peeling stresses are developed at the interfaces as shown in Figure 7.15.

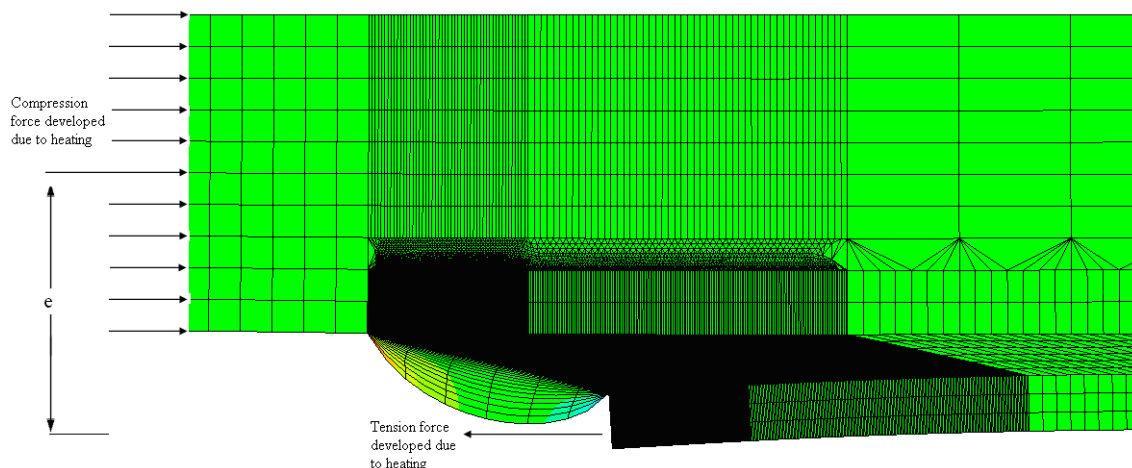


Figure 7.15 Development of peeling stress in the CFRP layer due to eccentricity of force in the steel plate

In order to avoid the incompatibility at the interfaces the peeling stress distribution is plotted in the middle of the adhesive.

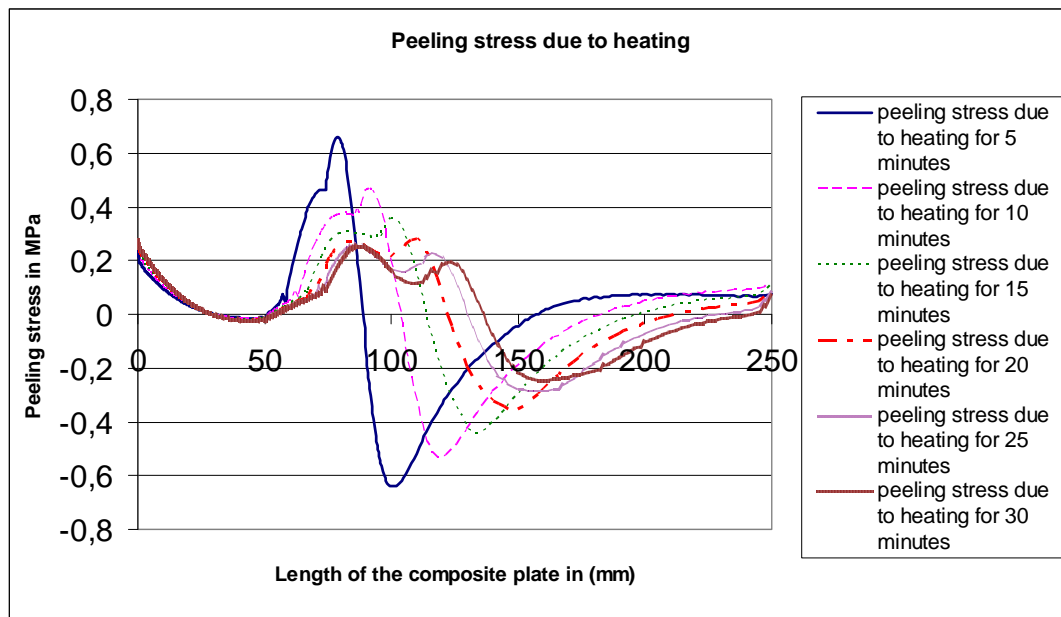


Figure 7.16 Peeling stress due to heating at the interface between steel-adhesive plotted in the middle of the adhesive

The peeling stress developed due to heating are small in magnitude as shown in Figure 7.16. The variable distribution of the peeling stress between (50 mm-150 mm) along the member is due to the change of temperature in the longitudinal direction affecting the expansion of the three materials in the composite plate.

7.6 Stress analysis due to combined effect of heating and tensioning

The composite plate is heated to 80°C (353 K) at the interface of steel-adhesive for 5 minutes and then a tensile load of 275 MPa (equivalent to yield strength of the steel) is applied as a pressure over an area of 80x20mm. The Figure 7.17 shows the shear stress distribution at different locations of the composite plate.

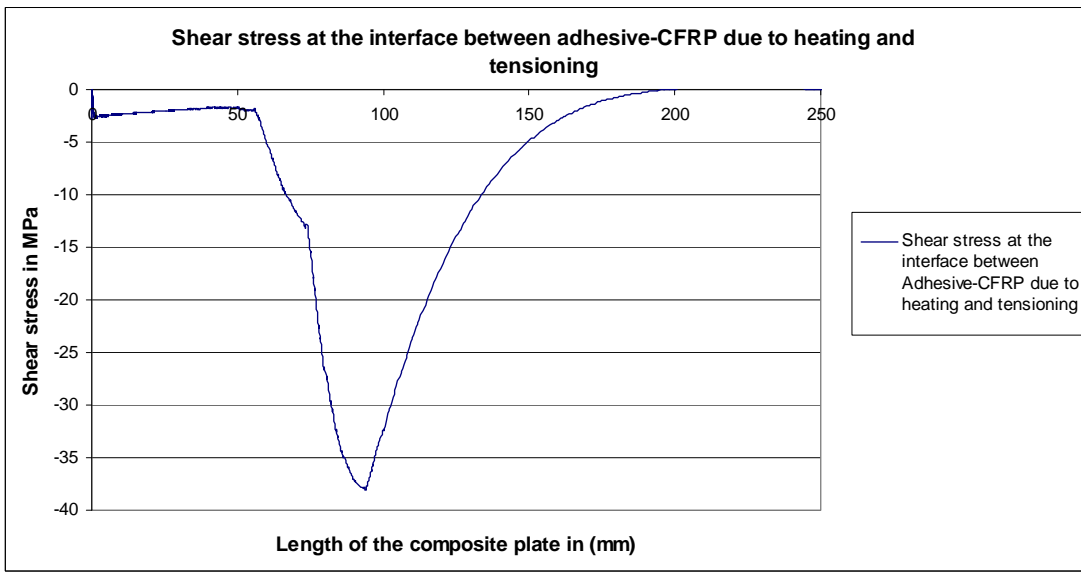
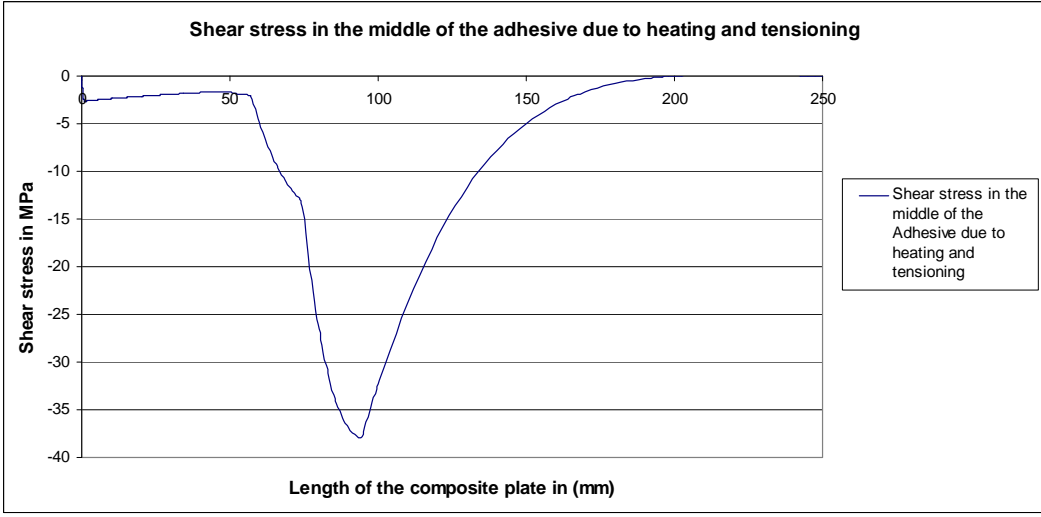
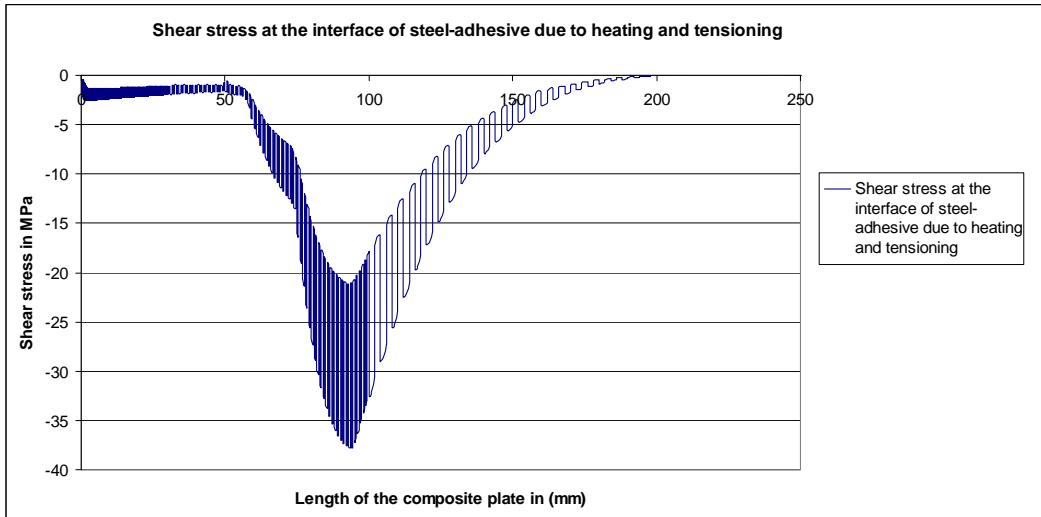


Figure 7.17 Distribution of shear stress due to combined effect of heating and tensioning plotted at different positions of the composite plate

From the Figure 7.17 it can be seen that the shear stress is about -37.9 MPa which is less in comparison with the original case (when only tensioning load is applied) as shown in Figure 7.1.

The shear stress increases after the length of heat source, because the temperature is decreasing from (353 K or 80°C) to about (323 K or 50°C) through a distance of 50 mm from the end of the heat source as shown in Figure 7.18. The decrease of temperature causes the increase in the stiffness of the adhesive. With the gradual increase of stiffness the shear stress is also increased gradually from -1.65 MPa at 50 mm to -37.3 MPa at 94.5mm from the end of the CFRP laminate. The same principle is also applicable in case of heating for more time.

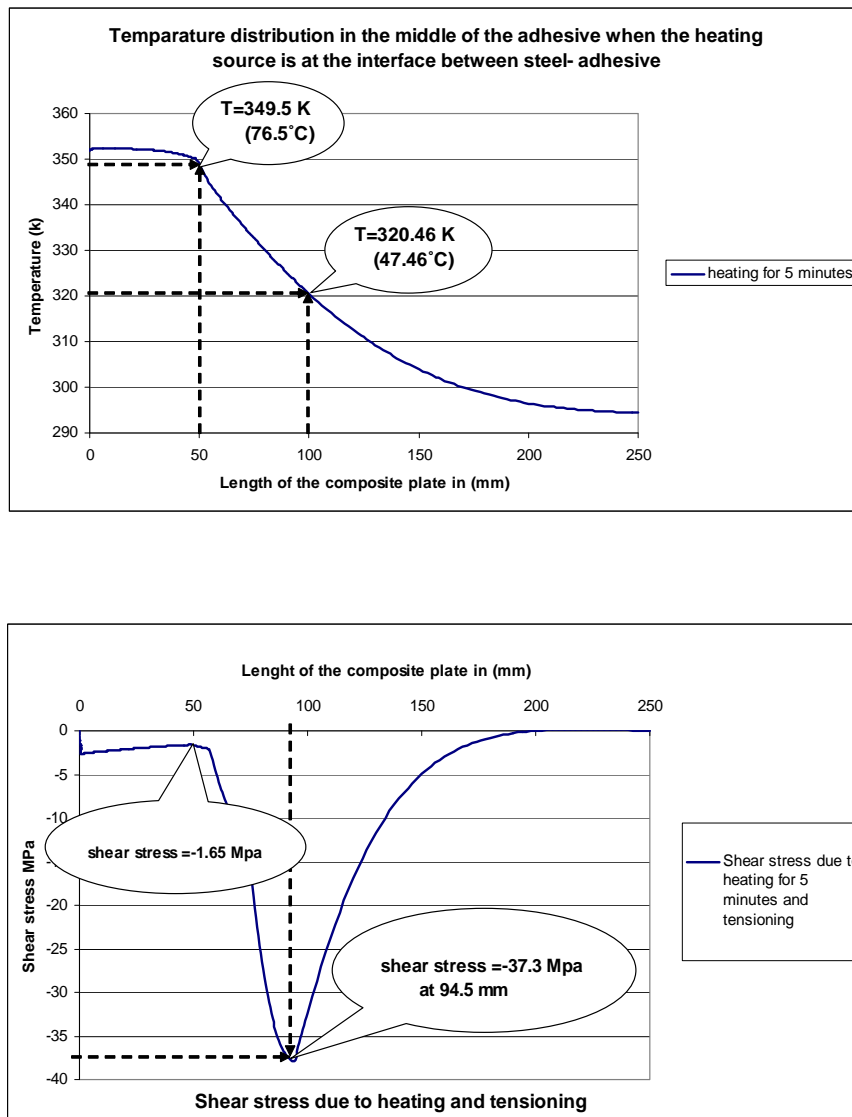


Figure 7.18 Development of shear stress peak value after heating for 5 minutes and tensioning of the steel plate

The shear stress can be further explained as a function of Shear modulus, deformation, thickness of the adhesive layer and can be written as

$$\tau = G \cdot \frac{\delta}{t}$$

Where :

G= Shear modulus;

δ = Deformation;

t = Thickness of the adhesive layer.

From the Figure 7.19 it can be seen that the adhesive is displaced through a larger distance when the heat and load is applied. Even though the displacement of adhesive is greater the shear stress is very low. The reason is the stiffness (G) of the adhesive is negligible and does not resist the movement of the steel. Whereas the region where the stiffness (G) of adhesive is higher a smaller displacement causes higher shear stress.

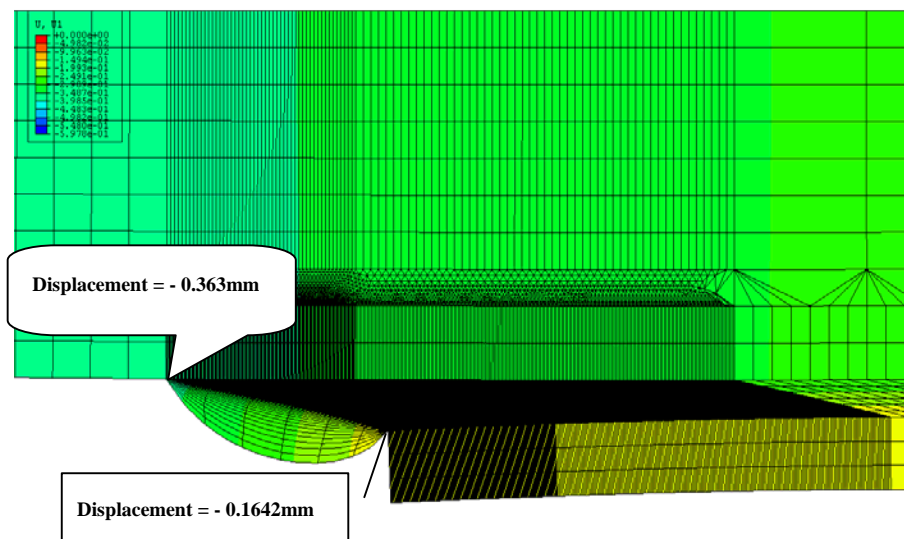


Figure 7.19 Displacement in different layers when heated for 5 minutes and tensioning with the load.

The combined effect of heating time and the application of tensile load on the shear stress distribution is further studied. The shear stress distribution in the middle of the adhesive for different heating time and after loading is shown in Figure 7.20.

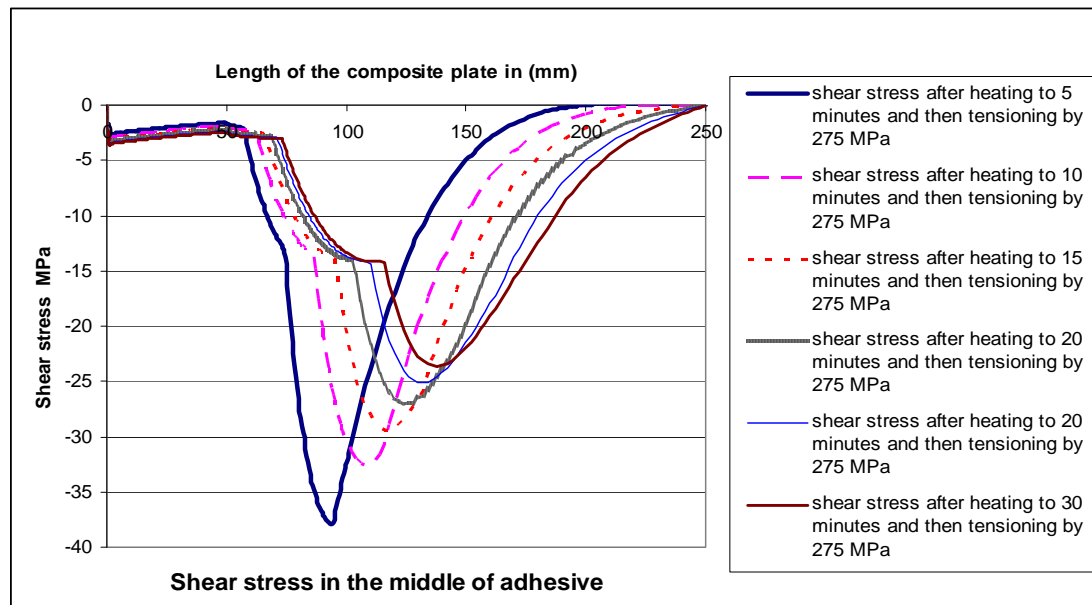


Figure 7.20 Shear stress distributions in the middle of adhesive due to combined effect of heating and loading

It can be noted that the shear stress is decreasing with the increase time of heating and tensioning. The forces to be transferred to the CFRP laminate are linked gradually with the increasing stiffness of the adhesive. Consequently the shear stress along the bond line increase where more force is transferred resulting in redistribution of the shear stress in the adhesive layer. As the shear stress is distributed over the area the peak value is reduced and moved from the end of the bond line.

The tensioning of the steel plate by applying an external tension load creates reaction stresses (normal stress) in the composite plate. The amount of normal stress in the CFRP laminate depends on how much the stresses are linked up or transferred from steel plate to the CFRP through the adhesive. The stiffer the adhesive more force is transferred to the CFRP laminate. The stiffness of the adhesive is increased with the heating. The force to be transferred is linked slowly depending on the stiffness of adhesive causing the normal stress to increase gradually and reaches the maximum value.

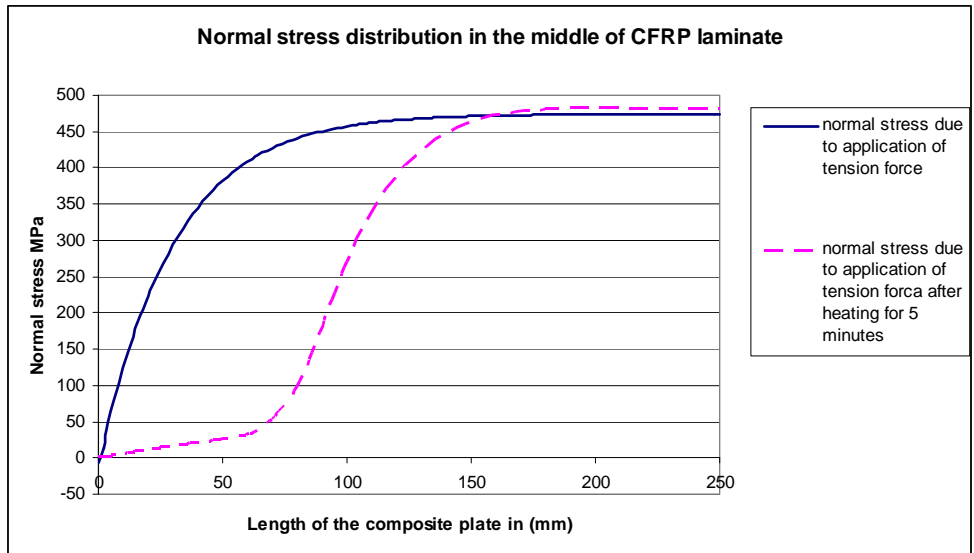


Figure 7.21 Normal stress distributions in CFRP laminate.

For the original case, When the tensile load is applied the normal stress in the adhesive and CFRP increases from zero to the maximum value over a smaller length. The sudden increase of normal stress causes peak shear stresses. While in the case, when the adhesive layer is heated for a certain time the stress transformation from steel to CFRP laminate become more gradual. Hence the normal stress is increased more gradually as in Figure 7.21 and 7.22.

The distribution of the normal stress becomes more gradual by increasing the heating time i.e. to 30 minutes as shown in Figure 7.22. Heating of the adhesive for more time leads to more gradual distribution of the temperature in the adhesive layer. This results in increase of the modulus of elasticity gradually. With the increasing stiffness the forces are linked up slowly. Hence the normal stress also increases gradually and reaches the maximum value after a larger distance. Due to which the shear stress peak value is lower compared to peak value of shear stress for the case of 5 minutes of heating and tensioning (See Figure 7.20).

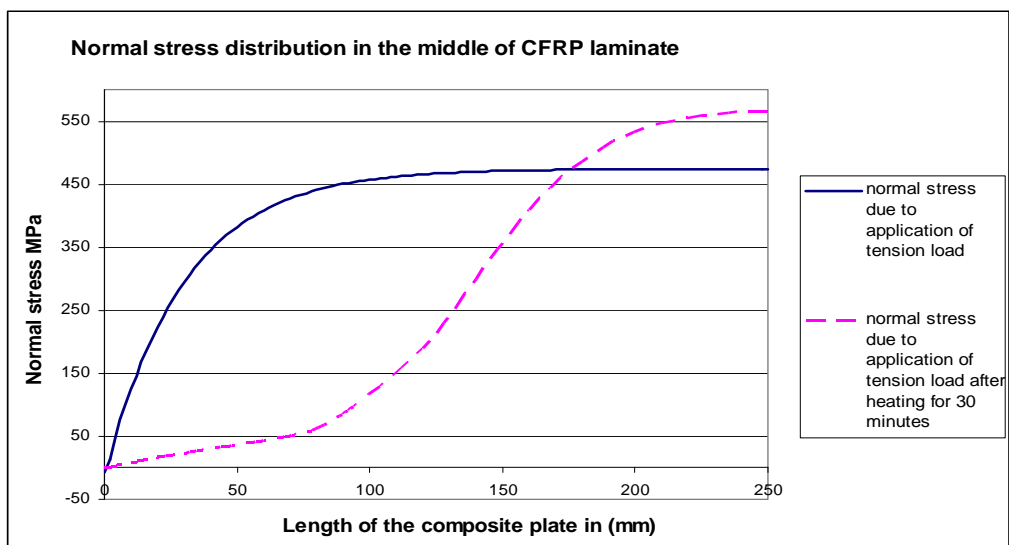


Figure 7.22 Normal stress distributions in CFRP laminate

The peeling stress developed due to heating and tensioning in the middle of the adhesive is shown in Figure 7.23. The magnitude of the peeling stress is very less compared to the original case.

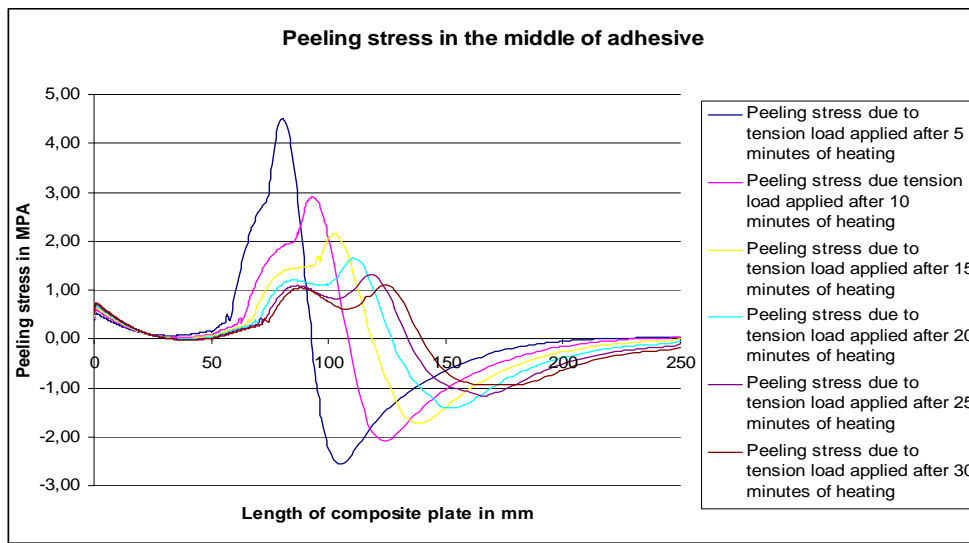


Figure 7.23 Peeling stress distribution in the middle of Adhesive due to tension load and for different time of heating

It is seen that with the increase in time of heating and then loading the peeling stresses are decreased. The principle behind the development of peeling stresses is the same which is explained in section 7.15. Due to the eccentricity between the compression force in steel plate and tensile force in CFRP laminate develops the bending moment. This bending moment causes the peeling of the adhesive as shown in Figure 7.24.

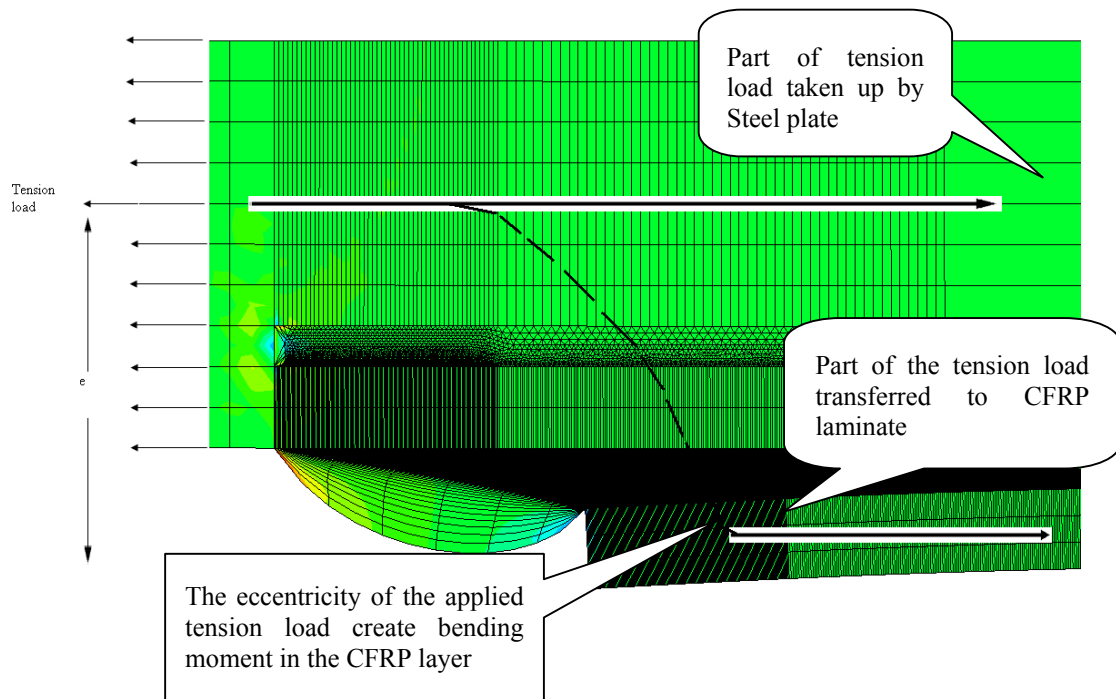
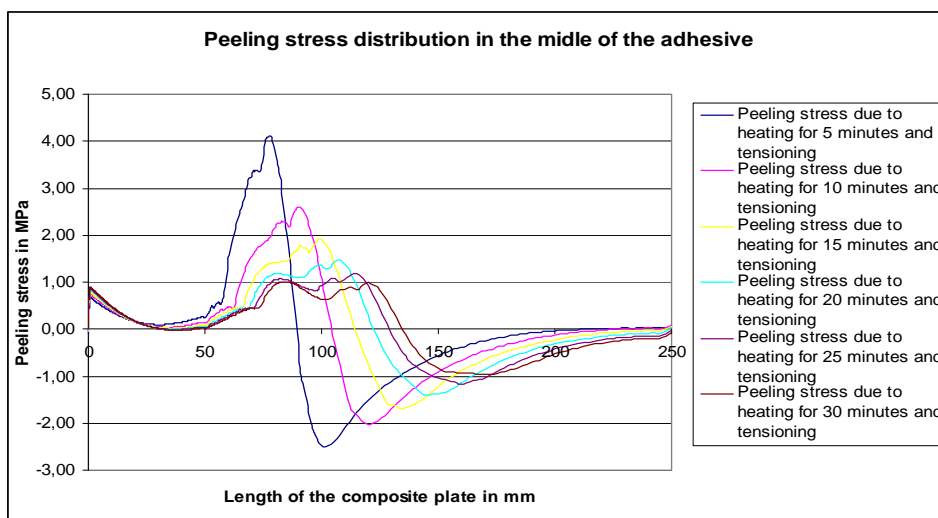
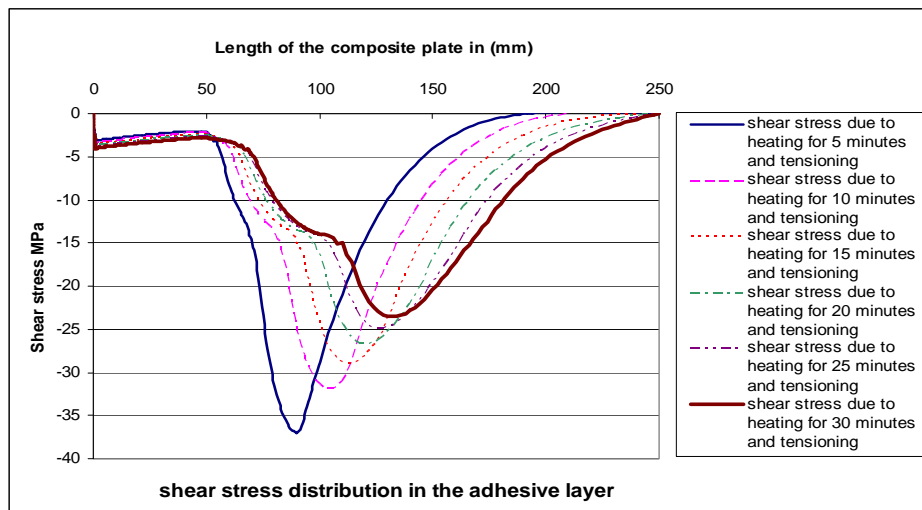


Figure 7.24 Peeling stress development and the way of transforming tension load in the composite plate

7.7 Parametric Study

Materials with different properties can be manufactured depending on the purpose for which they are used. Many kinds of adhesives and CFRP laminates with different material properties like stiffness, strength, conductivity, expansion coefficient and so on are available in the market. The most interesting properties which are related to the thermal stress analysis in this thesis are conductivity and expansion coefficient. As mentioned before the conductivity is the factor which affects temperature distribution through the thickness in the specific layer. Therefore it is valuable to study adhesive layer with different conductivity to see the consequence on the shear and peeling stresses. The adhesive with conductivity equal to $0.4 \times 10^{-3} \text{ w/mmK}$ is used. The effect of the above factor on the shear stress, peeling stress distribution in the middle of adhesive and normal stress in the CFRP laminate is shown in Figure 7.25.



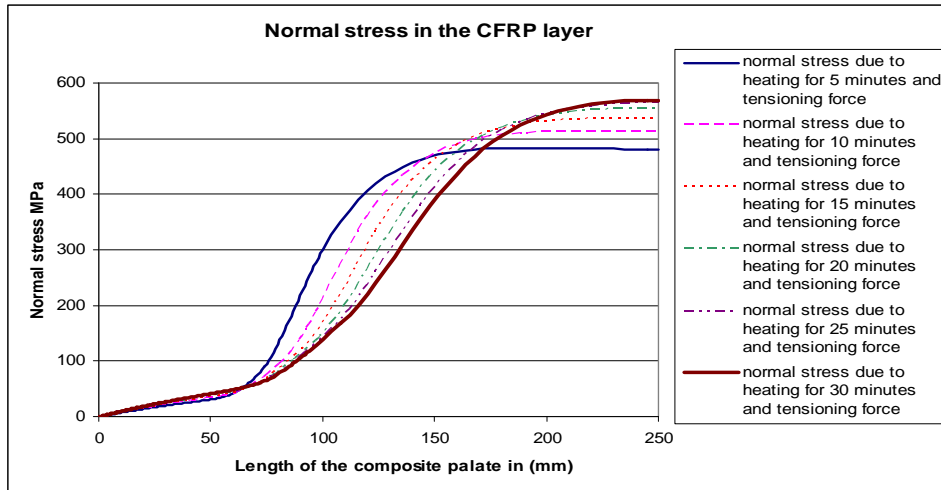
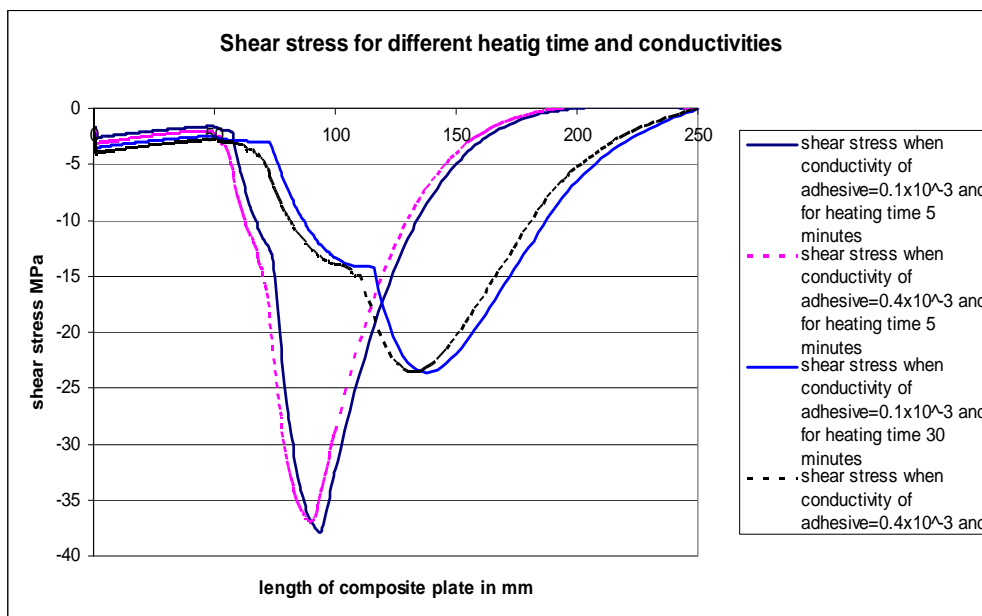


Figure 7.25 Shear, peeling and normal stress distribution for adhesive with higher conductivity

The shear and peeling stresses are decreased with the increase time of heating and then loading. It is evident from Figure 7.25 (c) that the most gradual increase of normal stress is with the case of heating for 30 minutes and applying the load. Hence the shear stress is distributed over a larger area with the increasing normal stress reducing the peak value.

The comparison of shear and normal stress for the adhesive with higher and original conductivity values (K) is shown in Figure 7.26.



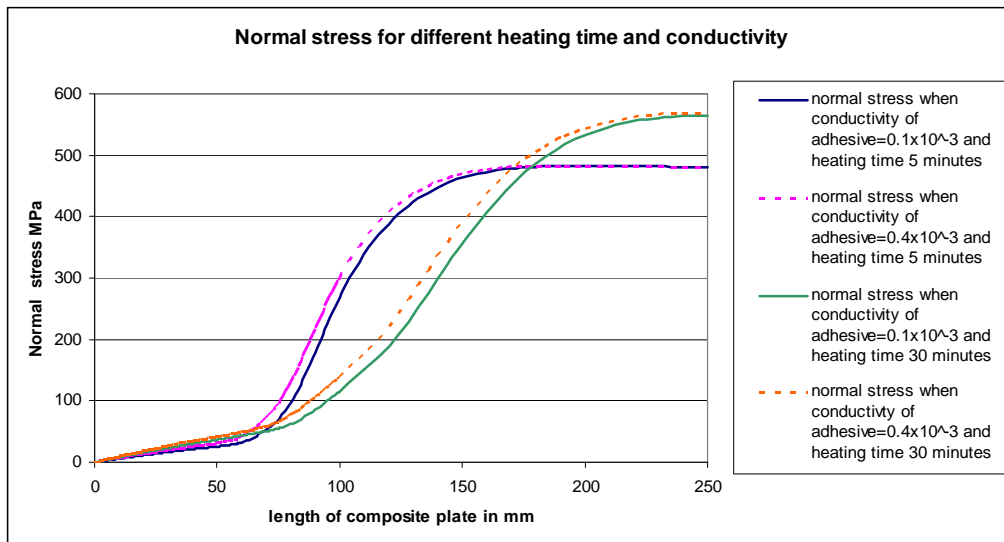


Figure 7.26 Comparison of shear and normal stress distribution for different conductivity

The shear stress and normal stress distribution for 5 and 30 minutes of heating is shown in the Figure 7.26. The results show that the shear stress due to the adhesive with higher conductivity is more or less same as the original case. The shear stress and the normal stress have almost the identical pattern and values for both the cases. As the heating time is increased the steel gets hotter and supplies the heat to the adhesive. The conductivity of adhesive is very low, the time of heating for the transmission of heat through the adhesive is insufficient. Hence the conductivity of adhesive has a very little effect on the shear distribution with in the range of heating.

The other important parameter studied is the co-efficient of expansion for CFRP laminate. The co-efficient of expansion for CFRP laminate is changed from 5×10^{-6} to 0 K^{-1} . The shear stress and the normal stress distribution are shown in Figure 7.27.

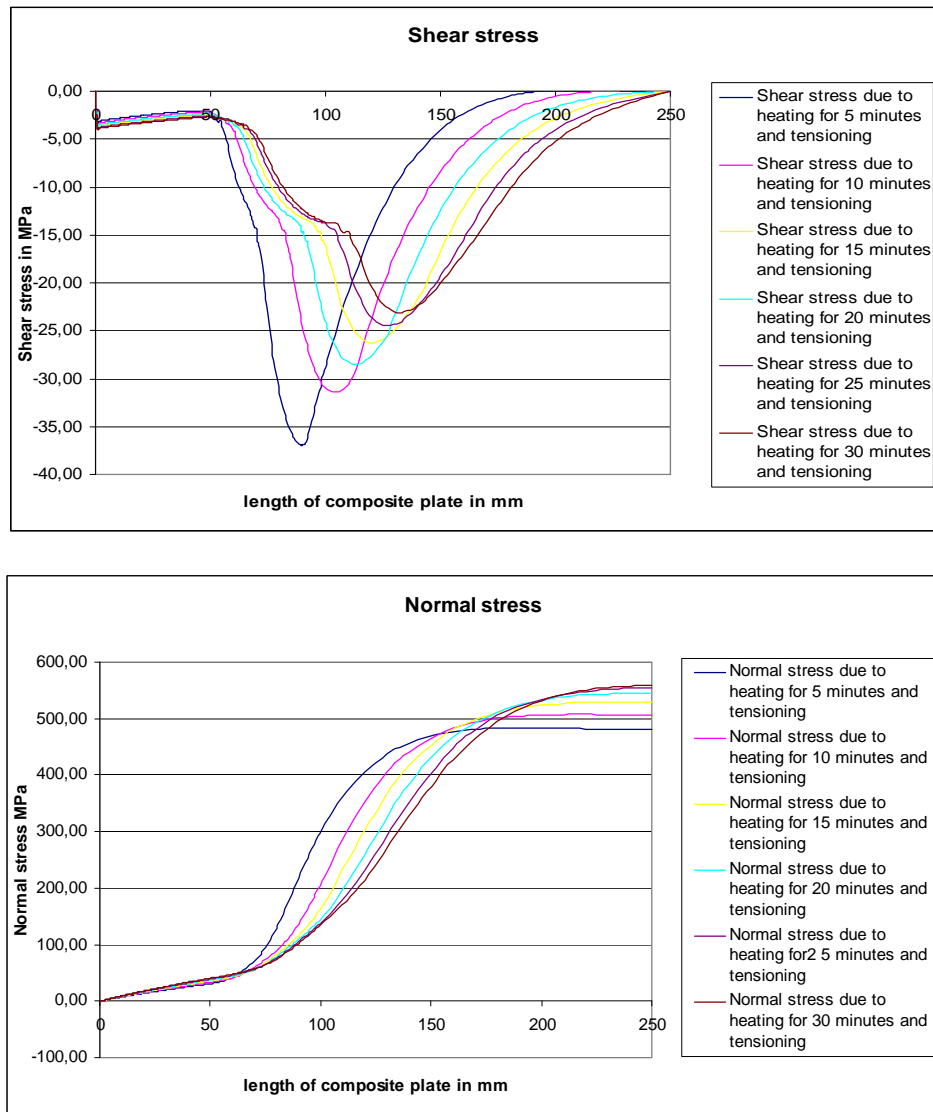


Figure 7.27 Shear and normal stress distribution with the expansion coefficient of CFRP laminate equal to zero

The distribution of shear and normal stresses with the expansion coefficient equal to zero has the same pattern as the original case. The shear stress is decreased with the increase time of heating and then loading. It is marked from Figure 7.27 that the most gradual increase of normal stress is with the case of heating for 30 minutes and applying the load. Hence the shear stress is distributed over a larger area with the increasing normal stress reducing the peak value as explained earlier.

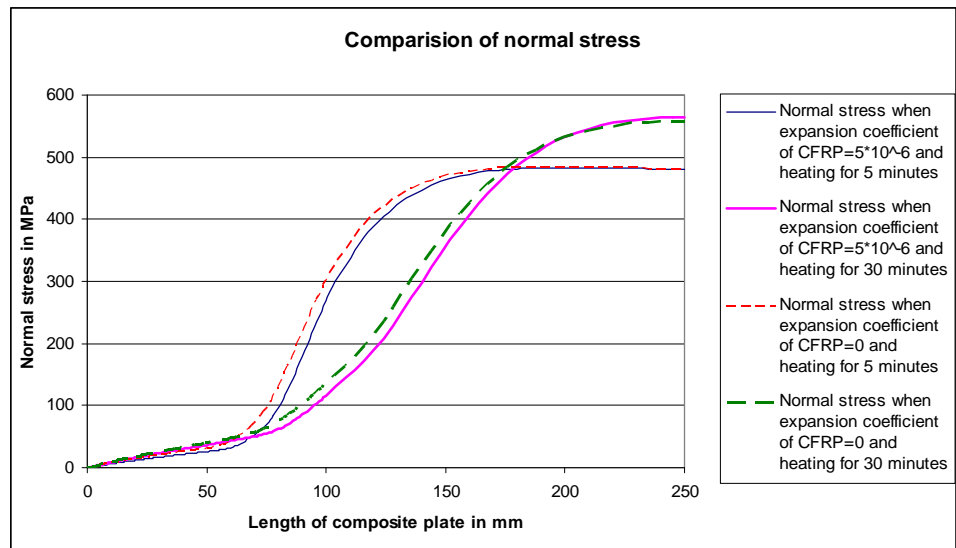
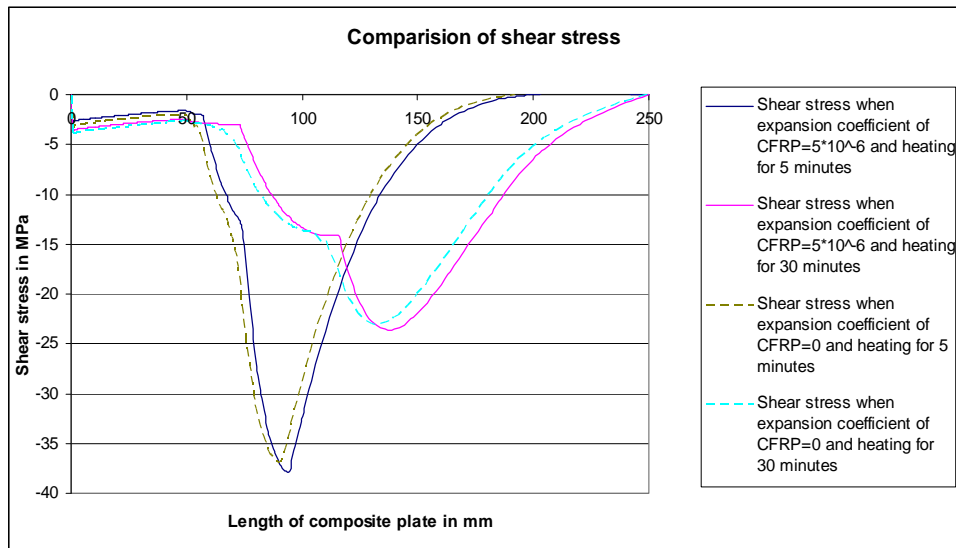


Figure 7.28 Comparison of shear and normal stress distribution

The shear stress and normal stress distribution are compared for 5 and 30 minutes of heating as shown in the Figure 7.28. The shear stress is decreased a little when the expansion coefficient is changed to zero. The expansion coefficient has little effect for this range of heating.

8 Summary and Conclusions

Discussions and conclusions of each part are made in the respective chapters throughout the text. However for the sake of completeness these are again outlined here. Conclusions from the analyses of thermal and mechanical models are also found in this chapter.

The result from the mechanical finite element model is compared with the analytical solution in MathCad model for the validation of the FE model. The results show that the two models are in good agreement, confirming that the finite element model is correct. A tensile load of 160 kN was applied to the composite plate. The shear stress developed in the adhesive was 25.46 MPa, which is equal to the ultimate shear strength of the adhesive. When the heat was applied, the tensile load was increased to 440 kN. The maximum shear stress developed in the adhesive was 23.6 MPa. With heating the shear stress is distributed over a larger area decreasing the peak value. Hence the heating technique increased the load carrying capacity of composite plate by 275% without any failure in adhesive.

8.1 Temperature distribution and interfacial stresses

The results from the thermal analysis of the model regarding the interfacial stresses in the adhesive show that all the parameters studied affect the stresses to some extent. The location of heat, time of heating and the length of heat source have an influence on the temperature distribution which in turn affect the interfacial stresses. The results show that the best possible temperature distribution in adhesive is obtained when the heat was applied at the interface between steel and adhesive. The decrease of temperature in the adhesive layer is more gradual when heated at this location.

The composite plate has different material properties influencing the temperature distribution. It is of great concern to know the time of heating required for the gradual temperature distribution. The results show that the temperature distribution is affected by the heating time. The best possible temperature distribution in the adhesive layer is obtained after 30 minutes of heating at the interface of steel-adhesive.

The length of heat source has a little effect on the temperature distribution in the adhesive layer. When the different heat source lengths were chosen it was observed that only the position of temperature distribution was shifted when the heating length was changed.

When the heat is applied at the interface of steel-adhesive for 30 minutes the shear and peeling stresses developed in the adhesive were very low 5 and 0.2 MPa respectively.

The interfacial stresses developed due to the combined effect of heating and loading are studied for the composite plate and the results were very satisfying. It is seen that interfacial stresses decrease with the increased time of heating. The tensile load is applied to the composite plate after 30 minutes of heating at the interface of steel-adhesive. The shear stress developed in the middle of adhesive is 23.6 MPa. Hence it can be concluded that the interfacial stresses decreases with the increase of heating time.

The peeling stress is developed when the composite plate is heated and loaded in tension. The bending moment is produced in the CFRP laminate resulting in the development of peeling stress. The magnitude of the peeling stress is low and is of less concern.

The normal stress in the CFRP laminate is the result of the tension load transferred through the adhesive. The normal stress is increased slowly and reaches the maximum value when the heat is applied and loaded. It can be concluded that with the increase of heating time the maximum value of normal stress is reached over a longer distance. However the peak value of the normal stress is the same for the different heat time irrespective of the length required to reach it.

This conclusion is only valid for the model analysed by finite element analysis since it is the only model analysed for both interfacial stresses.

8.2 Further studies

- In the finite element models, the boundary conditions are of greater importance. The thermal boundary used in this project was the convection boundary. Even though it was good enough to use the film co-efficient to define it, still a more detail study is required.
- The composite plate is associated with different material having different properties. In order to perform the thermal and mechanical analysis the material properties play an important role. Hence a deeper knowledge of temperature dependent material properties is required.
- It is seen that the time of heating has the affect on the interfacial stresses. The stress distributions due to heating up to about 30 minutes were studied. More detailed study on the effect of heating time is required.
- Parametric studies were not intended to be a part of this study. For this reason, a limited number of parametric studies were performed. For the range of study done with the conductivity of adhesive it is difficult to conclude the effect of it on the interfacial stresses. A complete study for the conductivity of adhesive is needed.

- The effect of expansion coefficient of CFRP laminate on the interfacial stresses was performed. For the extent of study done for the expansion coefficient was not sufficient enough to conclude the effect on interfacial stresses. A comprehensive study for the expansion coefficient is required.
- Analysis of a real beam with prestressing of CFRP laminate should be performed.
- Tests should be performed in the reality to confirm the results of FE model.

9 References

- [1] Abu-Hawash, A., Klaiber, F.W., Lee, Y., Brent M. Phares and Terry J. Wipf (2003): Strengthening of Steel Girder Bridges Using FRP. *Proceedings of the 2003 Mid-Continent Transportation Research Symposium, Ames, Iowa, August 2003*. Iowa State University.
- [2] Al-Emrani, M., Kliger, R. (2006): Analysis of Interfacial Shear Stress in Beams Strengthened with Bonded Prestressed Laminates. *Department of Structural Engineering, Chalmers University of Technology, Sweden, 2006*.
- [3] Almakt, M.M., Balazs, G.L., Pilkoutas, K. (1998): Strengthening of RC Element by CFRP Plates Local Failure. *PhD Symposium in Civil Engineering 1998 Budapest, Department of Reinforced Concrete Structure, university of Budapest, H1521 Budapest, 1998*.
- [4] Altenbach, H., Altenbach, J., Kissing, W. (2004): Mechanics of Composite Structural Elements
- [5] Andrä, H.P., Maier, M., Poorbiazar, M. (2004): Carbon Fibre Composites for a new Generation of Tendons. *Conference on Application of FRP Composites in Construction and Rehabilitation of Structures, May 4, 2004, Tehran, Iran*
- [6] Andrä, H.P., Maier, M., Peter, H., Gusia, P.J. (2005): A new Approach of Bonded Anchorages for CFRP Prestressing Tendons and Cables. *Proceedings of International Symposium on Bond Behaviour of FRP in Structures (BBFS2005)*.
- [7] Awbi, H.B., Hatton, A., (1999): Natural Convection from heated Room Surface. *Department of Construction Management and Engineering, The University of Reading, Reading, UK. PII:s0378-7788(99)00004-3*
- [8] Butros, F., Miranda, F.R., (2004): Prestressed advanced Composite for Strengthening Steel Structures, Development and design of prestressing and anchorage system. *Master's Thesis, Department of Structural Engineering, Chalmers University of Technology, Publication No. 04:13, Göteborg Sweden, 2004*
- [9] Cadei, J.M.C., Stratford, T.J., Hollaway, L.C., Duckett, W.G., (2004): Strengthening metallic Structures Using Externally Bonded Fibre-Reinforced Polymers
- [10] Garden, H.N., Hollaway, L.C. (1998). An Experimental Study of the Influence of Plate End Anchorage Carbon Fibre Composite Plates Used to Strengthen Reinforced Concrete Beams. *Composite structures*. Vol. 42, 1998, pp.175-188.
- [11] Gonzalez, H.D. (2005): Consolidation and thermal- stress analysis by FEM- Application to road mechanic. *Master's Thesis, Department of Applied Mechanics, Chalmers University of Technology, Publication No. 2005:34, Göteborg Sweden*

- [12] El-Hacha, R., Wight, R.G., Green, M.F. (2001): Prestressed Fibre- Reinforced Polymer Laminates for Strengthening Structures. *Prog. Struct Engng mater*, Vol. 3 1998, pp.111-121
- [13] El-Hacha, R., Wight, R.G., Green, M.F. (2003): Innovative System For Prestressing Fiber-Reinforced Polymer Sheets. *ACI Structural Journal*, Vol. 100 No. 3, 2003, pp.305-312
- [14] Hollaway, L.C., Cadie, j. (2002): Progress in the technique of upgrading metallic structures with advanced polymer composites. *Prog. Struct. Engng Mater*, 2002; 4: 131–148 (DOI: 10.1002/pse.112)
- [15] Ingles, N., Mendoza, C., (2004): Experimental Study of Steel-CFRP Composite Elements. . *Mater's Thesis. Department of Structural Engineering. Chalmers University of Technology*, Publication No. 04:9, Goteborg Sweden, 2004
- [16] Kiviloo, C., Westerdahl, J. (2003): Utmatningsförstärkning av stålbro med förspända Kolfiberlaminat. *Mater's Thesis. Department of Structural Engineering. Chalmers University of Technology*, Publication No. 03:02, Goteborg Sweden, 2003
- [17] Meier, U. (2001): Polyfunctional use of Advanced Composite Materials with Concrete. *Swiss Federal Laboratories Materials Testing and Research EMPA*, Switzerland. (2001)
- [18] Menashi, L., Jiji. (1998): Heat Transfer Essential, printed in USA. ISBN 1-56700-114-9
- [19] Nilsson,J., Samuelsson,R.(2002): -TAPS-Thermal Analysis for Pipe Systems, Development of software for analysis of transient heat transfer in pipe. *Mater's Thesis. Department of Structural Mechanic. Chalmers University of Technology*, Publication No. 02:13, Goteborg Sweden, 2002
- [20] Ottosen, N., Peterson, H, (1992): Finite Element Method, printed and pound in Great Britain. ISBN 0-13-473877-2
- [21] Piyong, Y., Silva, P.F., Nanni, A.: Flexural Strengthening of Concrete Slabs by a Three-stage Prestressing FRP System Enhanced with the Presence of GFRP Anchor Spikes. *University of Missouri-Rolla, Rolla, MO 65401, USA*
- [22] Piyong Y., Silva, P.F., Nanni, A. (2004): Flexural Performance of RC Beams Strengthened With Prestressed CFRP Sheets. *Proceedings of Society for the Advancement of Material and Process Engineering 2004 Symposium*, Long Beach, USA, 2004, 9pp.

- [23] Rosenboom, O., Hassan, T. and Rizkalla, S. (2006): "Flexural Behavior of Aged Prestressed Concrete Girders Strengthened with Various FRP Systems", *Technical paper*. Dept. of Civil Engineering, North Carolina State University, 2006.
- [24] Schnerch, D., Dawood, M., Rizkalla, S., and Sumner, E.(2006): "Proposed Design Guidelines for Strengthening of Steel Bridges with FRP Materials". *Technical rapport*, No. IS-06-02, January 2006, pp.1-37.
- [25] Schnerch, D., Dawood, M., Sumner, E.M., Rizkalla, S. (2005) : STRENGTHENING STEEL-CONCRETE COMPOSITE BRIDGES WITH HIGH MODULUS CARBON FIBER REINFORCED POLYMER (CFRP) LAMINATES. *Composites in Construction 2005 – Third International Conference, Hamelin et al (eds)*, France, July 11 – 13, 2005
- [26] Shaat, A., Schnerch, D., Fam, A., Rizkalla, S. (2003): Retrofit of Steel Structures Using Fiber Reinforced Polymers (FRP): State-of-the-Art. *Research paper*, 2003.
- [27] Ye 1, L.P., Lu 1, X. Z., Chen, J. F., (2005): DESIGN PROPOSALS FOR THE DEBONDING STRENGTHS OF FRP STRENGTHENED RC BEAMS IN THE CHINESE DESIGN CODE. *Proceedings of International Symposium on Bond Behaviour of FRP in Structures (BBFS 2005)*, Dec, 7-9, Hong Kong, China, pp 45-54 Chen and Teng (eds).

Internet Source

- [28] [http:// www.sika-construction.com](http://www.sika-construction.com)
- [29] <http://www.stresscrete.co.nz/educ/fprestress.html>

Fundamental of prestressing.

- [30] <http://www4.ncsu.edu/~srizkal/Publications/techreports.html>

Technical journal and rapport on FRP

- [31] http://www.efunda.com/formulae/heat_transfer/conduction/overview_cond.cfm
http://www.tpub.com/content/doe/h1012v2/css/h1012v2_25.htm
<http://hyperphysics.phy-astr.gsu.edu/Hbase/thermo/heatra.html>

Heat Transfers Formulations

- [32] <http://hyperphysics.phy-astr.gsu.edu/hbase/thermo/heatra.html>
- [33] <http://sol.sci.uop.edu/~jfalward/heattransfer/heattransfer.html>
- [34] ABAQUS Manual

[35] http://www.mdacomposites.org/mda/PSGbridge_concreterepair_intro.html

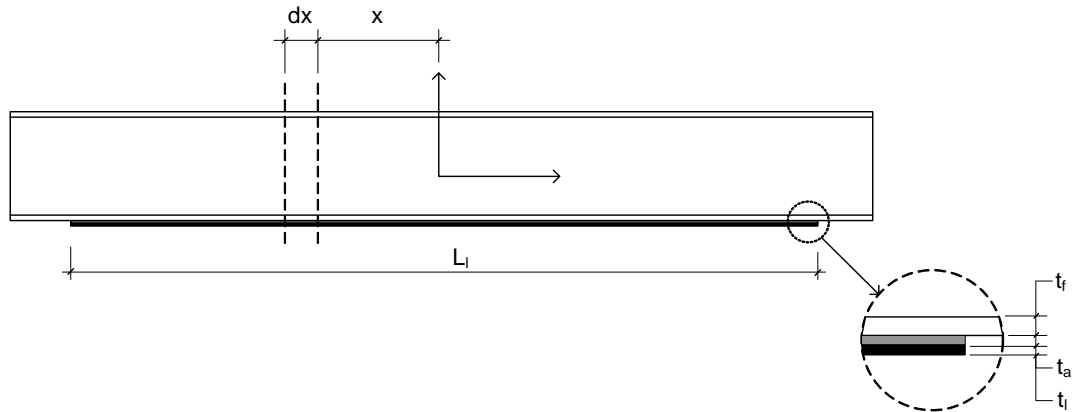
[36] <http://www.studionunziata.com/download/ISEC-02-339%20en.pdf>

[37] lecture notes from the supervisor

10 Appendix

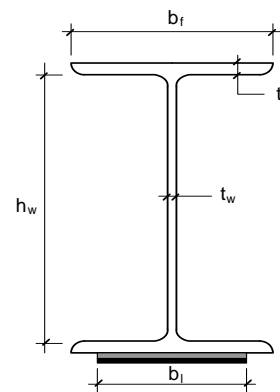
Appendix A

DERIVATION OF BENDING AND SHEAR STRESSES IN STEEL BEAM STRENGTHENED WITH PRESTRESSED CFR-LAMINATE



Assumptions :

1. Linear elastic materials
2. Isotropic adhesive
3. Adhesive is only subjected to shear
4. CFRL is only subjected to tension

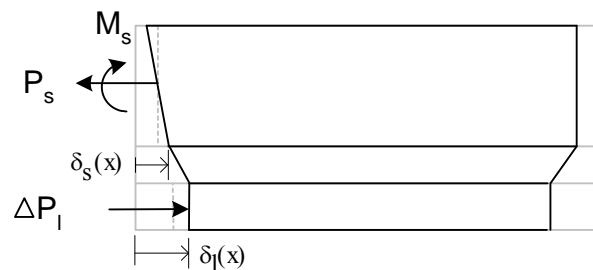


Deformation compatibility

$$\gamma(x) = \frac{\delta_I(x) - \delta_S(x)}{t_a}$$

But

$$\gamma(x) = \frac{\tau(x)}{G}$$



➔
$$\tau(x) = \frac{G_a}{t_a} \cdot (\delta_I(x) - \delta_S(x)) \dots\dots\dots (1)$$

$$\frac{d}{dx} \delta_s(x) = \varepsilon_s(x) = \frac{-P_s(x)}{A_s \cdot E_s} + \frac{-M_s(x)}{I_s \cdot E_s} \cdot \frac{h}{2} \quad \dots\dots\dots (2)$$

$$\frac{d}{dx} \delta_I(x) = \Delta \varepsilon_I(x) = \frac{\Delta P_I(x)}{A_I \cdot E_I} = \frac{P_0 - P_I(x)}{A_I \cdot E_I} \quad \dots\dots\dots (3)$$

Deriving equation (1) with respect to x

$$\frac{d}{dx} \tau(x) = \frac{G_a}{t_a} \cdot \left(\frac{d}{dx} \delta_I(x) - \frac{d}{dx} \delta_s(x) \right)$$

$$\Rightarrow \frac{d}{dx} \tau(x) = \frac{G_a}{t_a} \cdot \left(\frac{P_0}{A_I \cdot E_I} - \frac{P_I(x)}{A_I \cdot E_I} + \frac{P_s(x)}{A_s \cdot E_s} + \frac{M_s(x)}{I_s \cdot E_s} \cdot \frac{h}{2} \right) \quad \dots\dots\dots (4)$$

Equilibrium

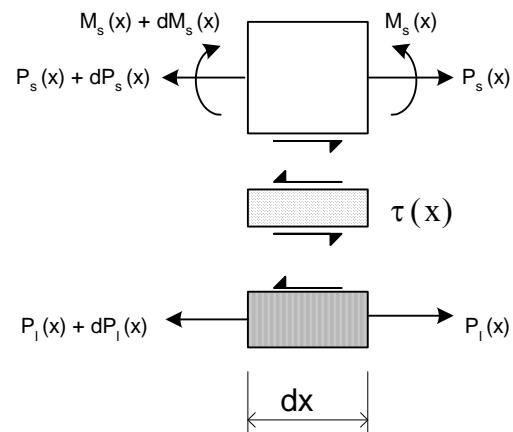
H:

$$\frac{d}{dx} P_s(x) = b_I \cdot \tau(x) \quad \dots\dots\dots (5)$$

$$\frac{d}{dx} P_I(x) = -b_I \cdot \tau(x) \quad \dots\dots\dots (6)$$

M:

$$\frac{d}{dx} M_s(x) = b_I \cdot \frac{h}{2} \cdot \tau(x) \quad \dots\dots\dots (7)$$



Deriving eq (4) yields:

$$\frac{d^2}{dx^2}\tau(x) = \frac{G_a}{t_a} \cdot \left(\frac{-1}{A_1 \cdot E_1} \cdot \frac{d}{dx} P_1(x) + \frac{1}{A_s \cdot E_s} \cdot \frac{d}{dx} P_s(x) + \frac{h}{2I_s \cdot E_s} \cdot \frac{d}{dx} M_s(x) \right) \dots\dots\dots (8)$$

Inserting the equilibrium conditions (5) - (7) in (4) results:

$$\frac{d^2}{dx^2}\tau(x) = \frac{G_a}{t_a} \cdot \left(\frac{b_1}{A_1 \cdot E_1} + \frac{b_1}{A_s \cdot E_s} + \frac{b \cdot h^2}{4I_s \cdot E_s} \right) \cdot \tau(x) \dots\dots\dots (9)$$

$$\frac{d^2}{dx^2}(\tau(x)) = \omega^2 \cdot \tau(x) \dots\dots\dots (10)$$

In which
$$\omega^2 = \frac{G_a}{t_a} \cdot \left(\frac{b_1}{A_1 \cdot E_1} + \frac{b_1}{A_s \cdot E_s} + \frac{b \cdot h^2}{4I_s \cdot E_s} \right)$$

Equation (5) has the solution:

$$\tau(x) = C_1 \cdot e^{\omega x} + C_2 \cdot e^{-\omega x} \dots\dots\dots (11)$$

Boundary conditions

1) $\delta_1(x=0) = \delta_s(x=0) = 0$

Together with equation (1), this gives:

$$\tau(x=0) = 0 \quad \Rightarrow \quad C_1 = -C_2$$

$$P_1\left(x = \frac{L}{2}\right) = P_s\left(x = \frac{L}{2}\right) = M_s\left(x = \frac{L}{2}\right) = 0 \quad M(x=0) = P_0 \cdot \frac{h}{2}$$

Inserting in (4) gives:

$$\frac{d}{dx} \tau(x) = \frac{G \cdot P_0}{t_0 \cdot A_1 \cdot E_1} = \omega \cdot C_1 \cdot e^{\frac{\omega L}{2}} - \omega \cdot C_2 \cdot e^{-\frac{\omega L}{2}}$$

$$\Rightarrow C_1 = -C_2 = \frac{G_a \cdot P_0}{t_a \cdot A_1 \cdot E_1} \cdot \frac{1}{2 \cdot \omega \cdot \cosh\left(\frac{\omega \cdot L}{2}\right)}$$

Substituting in (11) gives:

$$\tau(x) = \frac{G_a \cdot P_0}{t_a \cdot A_1 \cdot E_1} \cdot \frac{\sinh(\omega \cdot x)}{\omega \cdot \cosh\left(\frac{\omega \cdot L}{2}\right)} \quad \dots\dots\dots (12)$$

Deriving (12) and equating with (4) after substituting:

$$M_s(x) = -P_1(x) \cdot \frac{h}{2} \quad \left(\frac{h}{2} > t_a, t_l\right)$$

$$P_1(x) = -P_s(x)$$

$$\frac{d}{dx} \tau(x) = \frac{G}{t_0} \cdot \left(\frac{P_0}{A_1 \cdot E_1} - \frac{P_1(x)}{A_1 \cdot E_1} - \frac{P_1(x)}{A_s \cdot E_s} - \frac{P_1(x)}{I_s \cdot E_s} \cdot \frac{h^2}{4} \right) = \frac{G \cdot P_0}{t_0 \cdot A_1 \cdot E_1} \cdot \frac{\cosh(\omega \cdot x)}{\cosh\left(\omega \cdot \frac{L}{2}\right)}$$

$$P_1(x) = \frac{P_0}{A_1 \cdot E_1} \cdot \left(1 - \frac{\cosh(\omega \cdot x)}{\cosh\left(\omega \cdot \frac{L}{2}\right)} \right) \cdot \frac{1}{\frac{1}{A_1 \cdot E_1} + \frac{1}{A_s \cdot E_s} + \frac{h^2}{4 \cdot E_s \cdot I_s}} \quad \dots\dots\dots (13)$$

$$P_S(x) = -P_1(x) \dots\dots\dots (14)$$

$$M_S(x) = -P_0 \cdot \frac{h}{2} \cdot \frac{1 - \frac{\cosh(\omega \cdot x)}{\cosh\left(\omega \cdot \frac{L}{2}\right)}}{1 + \frac{A_1 \cdot E_1}{A_S \cdot E_S} + \frac{A_1 \cdot E_1 \cdot h^2}{4 \cdot E_S \cdot I_S}} \dots\dots\dots (15)$$

Example

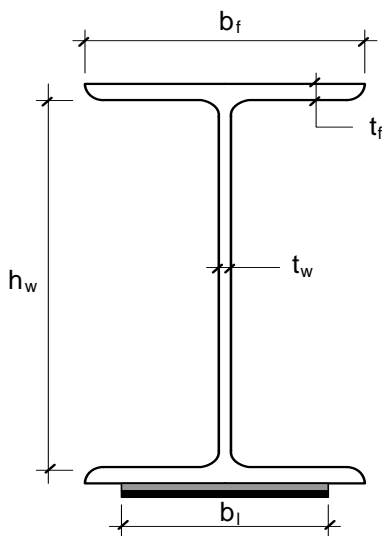
$$P_0 = 142.8 \text{ kN}$$

<u>Adhesive</u>	<u>Laminate</u>	<u>Steel beam</u>
$E_{adh} := 14 \text{ GPa}$	$E_1 := 200 \cdot 10^3 \text{ MPa}$	$E_S := 210 \cdot 10^3 \text{ MPa}$
$\nu_{adh} := 0.3$	$b_1 := 100 \text{ mm}$	$b := 300 \text{ mm} \quad h := 290 \text{ mm}$
$\underline{G} := \frac{E_{adh}}{2 \cdot (1 + \nu_{adh})}$	$t_1 := 1.4 \text{ mm}$	$t_f := 14 \text{ mm} \quad t_w := 10 \text{ mm}$
$t_0 := 2 \text{ mm}$	$A_1 := b_1 \cdot t_1$	$A_S := 2 \cdot (b \cdot t_f) + h \cdot t_w$

$$I_S := \frac{t_w \cdot h^3}{12} + b \cdot t_f \cdot \left(\frac{h}{2}\right)^2$$

$$W_S := \frac{I_S}{\frac{h}{2}}$$

$$\underline{L} := 6.5 \text{ m}$$



Prestressing

$$\sigma_0 := 1020 \text{ MPa}$$

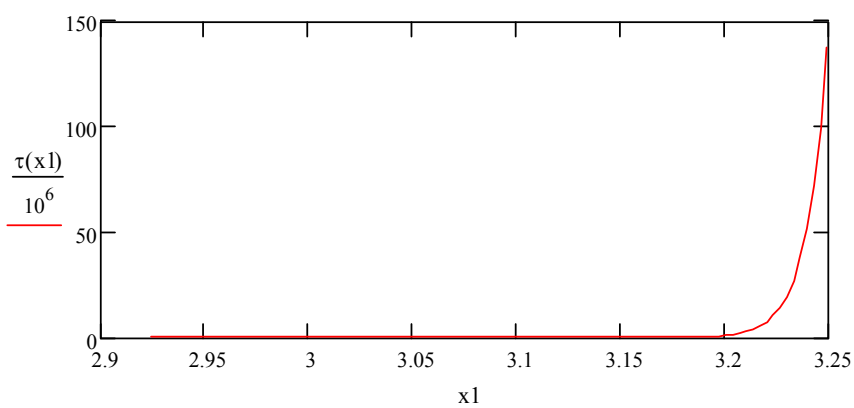
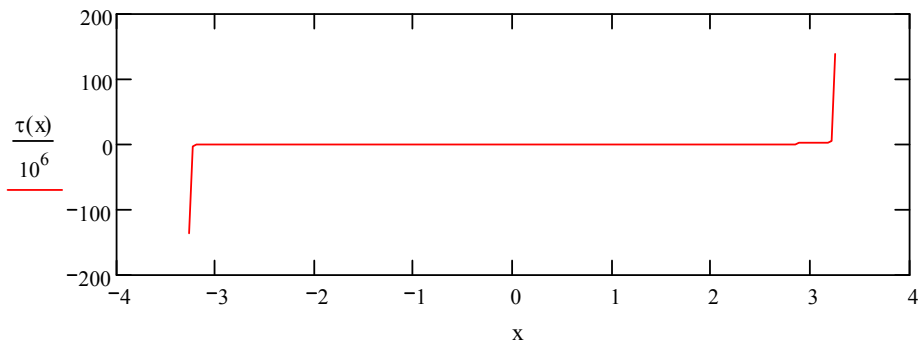
$$P_0 := \sigma_0 \cdot t_1 \cdot b_1$$

$$x := \frac{-10L}{20}, \frac{-9.9L}{20} \dots \frac{10L}{20}$$

$$\omega := \sqrt{\frac{G}{t_0} \cdot \left(\frac{b_l}{A_l \cdot E_l} + \frac{b_l}{A_s \cdot E_s} + \frac{b_l \cdot h^2}{4I_s \cdot E_s} \right)}$$

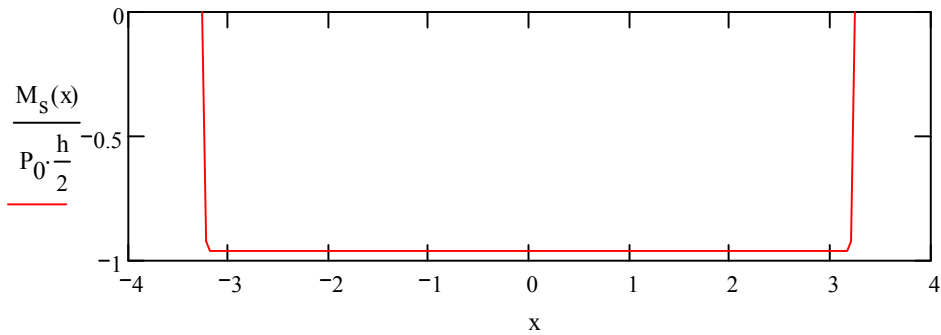
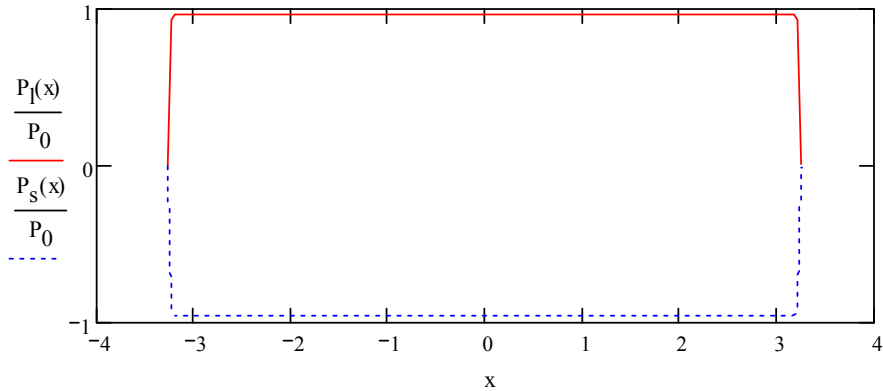
$$\tau(x) := \frac{G \cdot P_0}{t_0 \cdot A_l \cdot E_l} \cdot \frac{\sinh(\omega \cdot x)}{\omega \cdot \cosh\left(\frac{\omega \cdot L}{2}\right)}$$

$$\tau\left(\frac{L}{2}\right) = 137.466 \text{MPa}$$

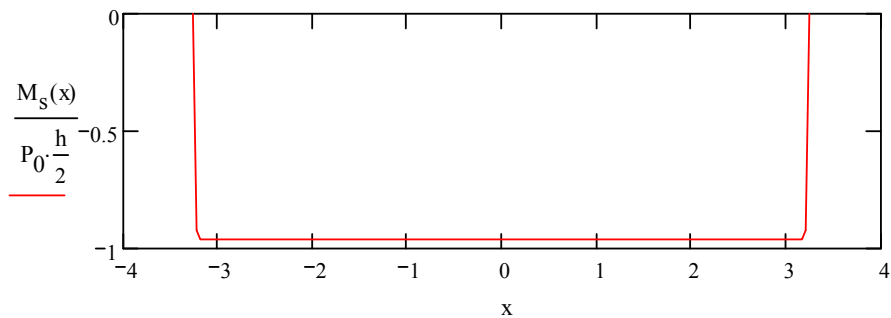


$$P_I(x) := \frac{P_0}{A_I \cdot E_I} \cdot \left(1 - \frac{\cosh(\omega \cdot x)}{\cosh\left(\omega \cdot \frac{L}{2}\right)} \right) \cdot \frac{1}{\frac{1}{A_I \cdot E_I} + \frac{1}{A_S \cdot E_S} + \frac{h^2}{4 \cdot E_S \cdot I_S}}$$

$$P_S(x) := -P_I(x)$$



$$M_S(x) := -P_0 \cdot \frac{h}{2} \cdot \frac{1 - \frac{\cosh(\omega \cdot x)}{\cosh\left(\omega \cdot \frac{L}{2}\right)}}{1 + \frac{A_I \cdot E_I}{A_S \cdot E_S} + \frac{A_I \cdot E_I \cdot h^2}{4 \cdot E_S \cdot I_S}}$$



Appendix B

Convection and radiation coefficient calculation

$$h_c = \frac{2.175}{D^{0.076}} (\Delta T)^{0.308}$$

$$D = \frac{2 \cdot Area}{parimeter}$$

$$\alpha_r = 4 * 0.9 * 5.67 * 10^{-8} T_s^3 \Rightarrow (Kilven)$$

area of steel = (0.4 + 0.04 + 0.15) * 0.08 = 0.0472m²

area of adhesive and CFRP = (0.0055 * 2 + 0.25) * 0.045 = 0.011745m²

total areas = 0.058945m²

parimeter = (0.4 + 0.02 + 0.15 + 0.0055 + 0.25 + 0.0055 + 0.02)0.851m

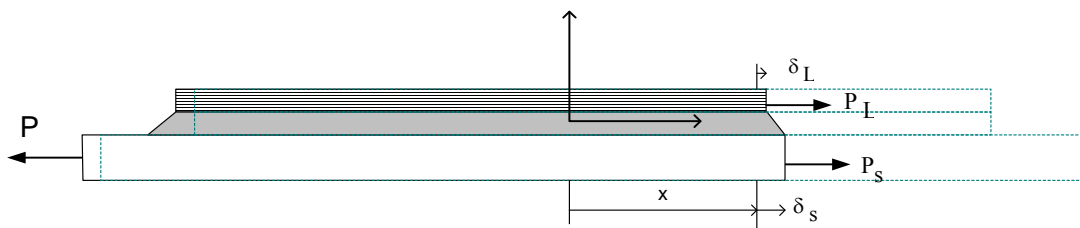
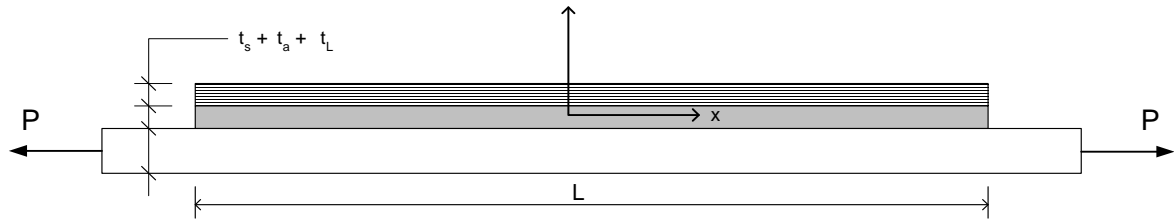
$$D = \frac{2 * Area}{parimeter} = 0.86$$

Delta T	alpha	hc*10 ⁻⁶	radiation+convection	Values used in ABAQUS
0	4,63E-06	0	4,6301E-06	4.63009719282969E-06
5	4,75E-06	3,65425E-06	8,40811E-06	8.40810539398917E-06
10	4,88E-06	4,52392E-06	9,40373E-06	9.40372679320303E-06
15	5,01E-06	5,12568E-06	1,01336E-05	0.0000101336326719612
20	5,14E-06	5,60057E-06	1,07389E-05	0.0000107389026628962
25	5,27E-06	5,99903E-06	1,127E-05	0.0000112699741497328
30	5,41E-06	6,34554E-06	1,17514E-05	0.0000117513688131314
35	5,54E-06	6,65408E-06	1,21971E-05	0.0000121970740843685
40	5,68E-06	6,93346E-06	1,26159E-05	0.0000126159098588511
45	5,82E-06	7,1896E-06	1,30138E-05	0.0000130138371862059
50	5,97E-06	7,42674E-06	1,33951E-05	0.0000133950961909099
55	6,11E-06	7,64798E-06	1,37628E-05	0.0000137628238729553
60	6,26E-06	7,85572E-06	1,41194E-05	0.0000141194148113888
65	6,41E-06	8,05179E-06	1,44667E-05	0.0000144667440747317
70	6,57E-06	8,23769E-06	1,48063E-05	0.0000148063114239101

75	6,72E-06	8,41461E-06	1,51393E-05	0.0000151393381785516
80	6,88E-06	8,58355E-06	1,54668E-05	0.0000154668343728621
85	7,04E-06	8,74533E-06	1,57896E-05	0.0000157896465818105
90	7,21E-06	8,90066E-06	1,61085E-05	0.0000161084927793144
95	7,37E-06	9,05012E-06	1,6424E-05	0.0000164239882623552
100	7,54E-06	9,19423E-06	1,67367E-05	0.0000167366652757095
105	7,71E-06	9,33344E-06	1,7047E-05	0.0000170469881032731
110	7,89E-06	9,46813E-06	1,73554E-05	0.0000173553648370885
115	8,06E-06	9,59865E-06	1,76622E-05	0.0000176621566717671
120	8,24E-06	9,7253E-06	1,79677E-05	0.0000179676853285702
125	8,42E-06	9,84835E-06	1,82722E-05	0.0000182722390470401
130	8,61E-06	9,96804E-06	1,85761E-05	0.0000185760774662867
135	8,79E-06	1,00846E-05	1,88794E-05	0.0000188794356361
140	8,98E-06	1,01982E-05	1,91825E-05	0.0000191825273392117
145	9,18E-06	1,0309E-05	1,94855E-05	0.000019485547863172
150	9,37E-06	1,04172E-05	1,97887E-05	0.0000197886763286944
155	9,57E-06	1,05229E-05	2,00921E-05	0.0000200920776577356
160	9,77E-06	1,06264E-05	2,03959E-05	0.0000203959042467833
165	9,97E-06	1,07275E-05	2,07003E-05	0.0000207002973972669
170	1,02E-05	1,08266E-05	2,10054E-05	0.0000210053885445786
180	1,06E-05	1,10189E-05	2,16181E-05	0.0000216181474663279

Appendix C

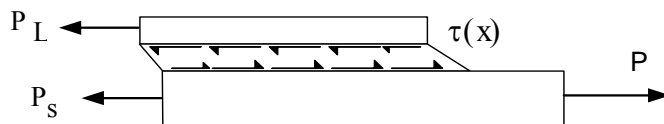
Derivation of shear and normal stresses in axially loaded composite steel-FRP member



$$\gamma(x) = \frac{\tau(x)}{G_a} = \frac{\delta_s(x) - \delta_L(x)}{t_a} \quad \dots\dots\dots(1)$$

$$\tau(x) = \frac{G_a}{t_a} \cdot (\delta_s(x) - \delta_L(x)) \quad \dots\dots\dots(2)$$

Equilibrium requires:



$$P_L(x) = \int_{\frac{L}{2}}^x -\tau(x) \cdot b_L dx \quad \varepsilon_L(x) = \frac{-b_L}{E_L \cdot A_L} \cdot \int_{\frac{L}{2}}^x \tau(x) dx \quad \dots\dots\dots(3)$$

$$P_S(x) = P + \int_{\frac{L}{2}}^x \tau(x) \cdot b_L dx \quad \varepsilon_S(x) = \frac{b_L}{E_S \cdot A_S} \cdot \left(P + \int_{\frac{L}{2}}^x \tau(x) dx \right) \dots\dots\dots(4)$$

$$\delta_L(x) = \int_{\frac{L}{2}}^x \varepsilon_L(x) dx = \frac{-b_L}{E_L \cdot A_L} \cdot \int_{\frac{L}{2}}^{\frac{L}{2}} \int_{\frac{L}{2}}^x \tau(x) dx dx \quad \dots\dots\dots(5)$$

$$\delta_S(x) = \int_{\frac{L}{2}}^x \varepsilon_S(x) dx = \frac{b_L}{E_S \cdot A_S} \cdot \left(\int_{\frac{L}{2}}^x P dx + \int_{\frac{L}{2}}^x \int_{\frac{L}{2}}^x \tau(x) dx dx \right) \dots\dots\dots(6)$$

Substituting (5) and (6) in (2) gives

$$\tau(x) = \frac{G_a}{t_a} \cdot \left[\frac{b_L}{E_S \cdot A_S} \cdot \left(\int_{\frac{L}{2}}^x P dx + \int_{\frac{L}{2}}^x \int_{\frac{L}{2}}^x \tau(x) dx dx \right) + \frac{b_L}{E_L \cdot A_L} \cdot \int_{\frac{L}{2}}^{\frac{L}{2}} \int_{\frac{L}{2}}^x \tau(x) dx dx \right] \dots\dots\dots(7)$$

$$\frac{d}{dx} \tau(x) = \frac{G_a \cdot b_L}{t_a} \cdot \left[\frac{1}{E_S \cdot A_S} \cdot \left(P + \int_{\frac{L}{2}}^x \tau(x) dx \right) + \frac{1}{E_L \cdot A_L} \cdot \int_{\frac{L}{2}}^x \tau(x) dx \right] \dots\dots\dots(8)$$

Which, considering (3) and (4) can be written as:

$$\frac{d}{dx} \tau(x) = \frac{G_a \cdot b_L}{t_a} \cdot \left(\frac{P_S(x)}{E_S \cdot A_S} - \frac{P_L(x)}{E_L \cdot A_L} \right) \quad \dots\dots\dots(9)$$

From (8) returns:

$$\frac{d^2}{dx^2}\tau(x) = \frac{G_a \cdot b_L}{t_a} \cdot \left(\frac{1}{E_S \cdot A_S} + \frac{1}{E_L \cdot A_L} \right) \cdot \tau(x) \quad \dots\dots\dots(10)$$

Or

$$\frac{d^2}{dx^2}\tau(x) = \omega^2 \cdot \tau(x)$$

Which has the solution in the form: $\tau(x) = A \cdot e^{\omega \cdot x} + B \cdot e^{-\omega \cdot x} \quad \dots\dots\dots(11)$

Where
$$\omega = \sqrt{\frac{G_a \cdot b_L}{t_a} \cdot \left(\frac{1}{E_S \cdot A_S} + \frac{1}{E_L \cdot A_L} \right)}$$

Boundary Conditions

Symmetry gives $\delta_S(x=0) = \delta_L(x=0) = 0$

Substituting in (2) results:

$$\tau(x=0) = 0 \quad \text{which putting i (11) gives} \quad A = -B$$

At $x = L/2$

$$P_S \left(x = \frac{L}{2} \right) = P$$

$$P_L \left(x = \frac{L}{2} \right) = 0$$

Substituting in (9) results:

$$\frac{d}{dx}\tau(x) = \frac{G_a}{t_a} \cdot \left(\frac{P}{A_S \cdot E_S} \right) = A \cdot \omega \cdot e^{\frac{\omega \cdot L}{2}} - B \cdot \omega \cdot e^{\frac{-\omega \cdot L}{2}}$$

$$\frac{G_a}{t_a} \cdot \frac{P}{A_s \cdot E_s} = A \cdot \omega \cdot \left(e^{\frac{\omega \cdot L}{2}} + e^{-\frac{\omega \cdot L}{2}} \right)$$

$$A = -B = \frac{G_a}{t_a} \cdot \frac{P}{A_s \cdot E_s} \cdot \frac{1}{2 \cdot \omega \cdot \cosh\left(\frac{\omega \cdot L}{2}\right)} \dots\dots\dots(12)$$

Putting in 11 Gives:

$$\tau(x) = \frac{G_a}{t_a} \cdot \frac{P}{A_s \cdot E_s} \cdot \frac{\sinh(\omega \cdot x)}{\omega \cdot \cosh\left(\frac{\omega \cdot L}{2}\right)} \dots\dots\dots(13)$$

From the equilibrium condition in (3) we have:

$$P_L(x) = \int_{\frac{L}{2}}^x -\tau(x) \cdot b_L \, dx$$

$$P_L(x) = -P \cdot \frac{G_a \cdot b_L}{t_a \cdot A_s \cdot E_s} \cdot \frac{\cosh(\omega \cdot x) - \cosh\left(\frac{\omega \cdot L}{2}\right)}{\omega^2 \cdot \cosh\left(\frac{1}{2} \cdot \omega \cdot L\right)} \dots\dots\dots(14)$$

$$P_S(x) = P \left(1 + \frac{G_a \cdot b_L}{t_a \cdot A_s \cdot E_s} \cdot \frac{\cosh(\omega \cdot x) - \cosh\left(\frac{\omega \cdot L}{2}\right)}{\omega^2 \cdot \cosh\left(\frac{1}{2} \cdot \omega \cdot L\right)} \right) \dots\dots\dots(15)$$

Example 1.

<u>Steel</u>	<u>Laminate</u>	<u>Epoxy</u>
$b_S := 75\text{mm}$	$b_L := 50\text{mm}$	
$t_S := 20\text{mm}$	$t_L := 4\text{mm}$	$t_a := 1.5\text{mm}$
$E_S := 210\text{GPa}$	$E_L := 450\text{GPa}$	$E_a := 7\text{GPa}$
		$G_a := \frac{E_a}{2 \cdot (1 + 0.3)}$

$$f_{ys} := 275\text{MPa}$$

$$\tau_{ua} := 25\text{MPa}$$

Load

$$A_s := b_s \cdot t_s$$

$$f_{uL} := 1000\text{MPa}$$

$$P := 160\text{kN}$$

$$A_L := b_L \cdot t_L$$

$$P_s := f_{ys} \cdot b_s \cdot t_s$$

$$L := 500\text{mm}$$

$$P_s = 412.5\text{kN}$$

$$\omega := \sqrt{\frac{G_a \cdot b_L}{t_a} \cdot \left(\frac{1}{E_L \cdot A_L} + \frac{1}{E_s \cdot A_s} \right)} \quad \omega = 35.806 \frac{1}{\text{m}}$$

$$\tau(x) := \frac{G_a \cdot P}{\omega \cdot t_a \cdot E_s \cdot A_s} \cdot \frac{\sinh(\omega \cdot x)}{\cosh\left(\frac{\omega \cdot L}{2}\right)}$$

$$x := -250\text{mm}, -245\text{mm}, 250\text{mm}$$

$$P_L(x) := -P \cdot \frac{G_a \cdot b_L}{t_a \cdot A_s \cdot E_s} \cdot \frac{\cosh(\omega \cdot x) - \cosh\left(\frac{\omega \cdot L}{2}\right)}{\omega^2 \cdot \cosh\left(\frac{1}{2} \cdot \omega \cdot L\right)}$$

$$\sigma_L(x) := \frac{P_L(x)}{A_L}$$

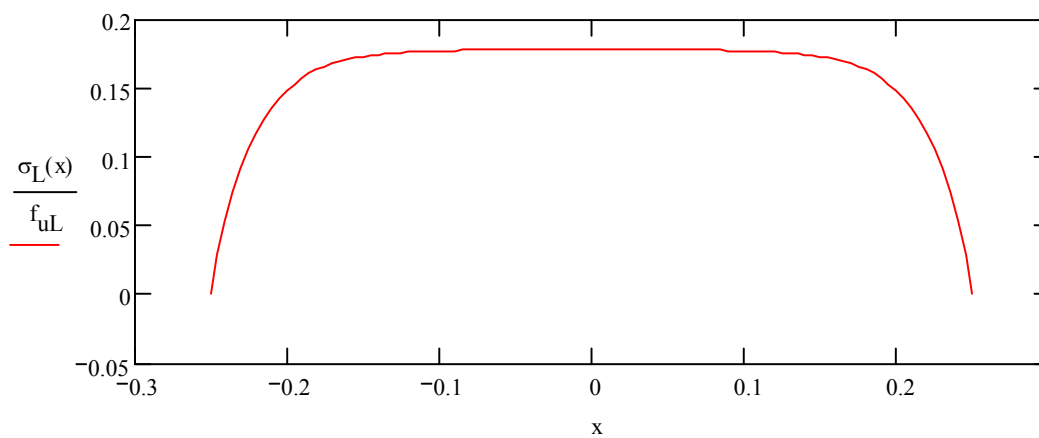
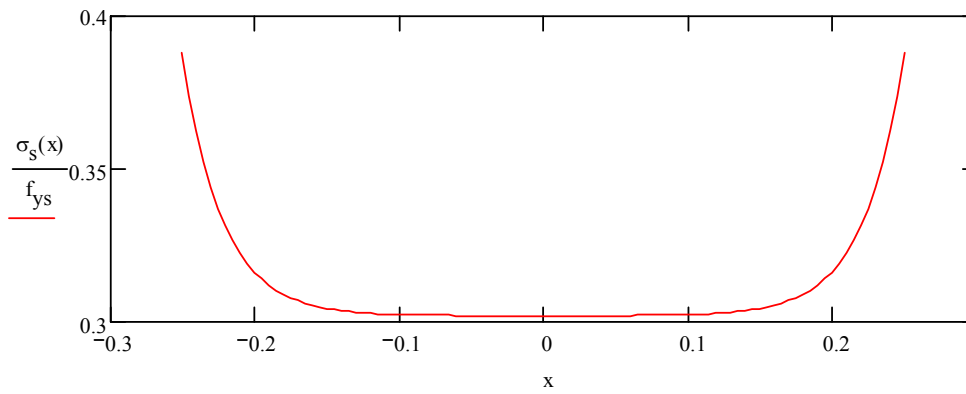
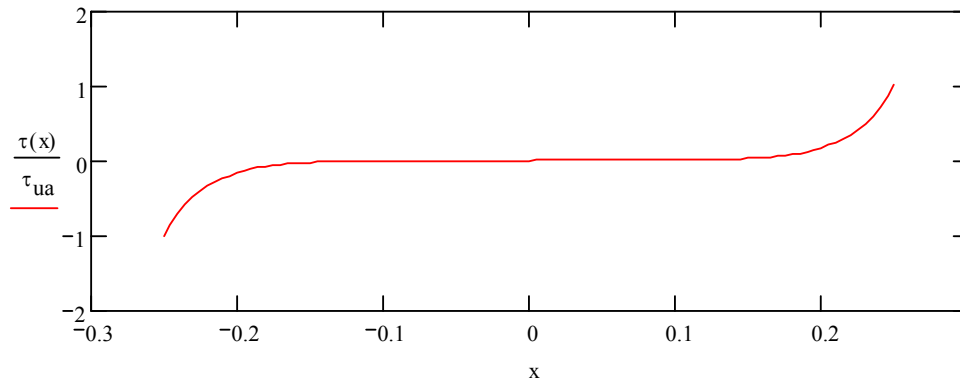
$$\sigma_L(0\text{m}) = 177.732\text{MPa}$$

$$P_s(x) := P \cdot \left(1 + \frac{G_a \cdot b_L}{t_a \cdot A_s \cdot E_s} \cdot \frac{\cosh(\omega \cdot x) - \cosh\left(\frac{\omega \cdot L}{2}\right)}{\omega^2 \cdot \cosh\left(\frac{1}{2} \cdot \omega \cdot L\right)} \right)$$

$$\sigma_s(x) := \frac{P_s(x)}{A_s}$$

$$\sigma_s(0\text{m}) = 82.969\text{MPa}$$

$$\tau\left(\frac{L}{2}\right) = 25.462\text{MPa}$$



Appendix D

A truncated input file from thermal analysis in composite plate final.cae; results are shown and discussed in chapter 7.4.

```
*Heading
** Job name: Job-thermalanalysis Model name: Thermal Economical Model
*Preprint, echo=NO, model=NO, history=NO, contact=NO
**
** PARTS
**
*Part, name="Composite Plate"
*End Part
**
**
** ASSEMBLY
**
*Assembly, name=Assembly
**
*Instance, name="Composite Plate-1", part="Composite Plate"
*Node
    1,          250.,          -1.25
    2,          200.,          -1.25
    3,          200.,          -1.5
.....
    36285,     150.024994,          -5.5
    36286,     150.024994,     -2.83333325
    36287,          150.,          -3.5
    36288,          150.,     -2.16666651
*Element, type=DC2D8
    1,    1,    47,    144,    4, 25676, 25677, 25678, 25679
    2,    47,    48,    143,    144, 25680, 25681, 25682, 25677
    3,    48,    49,    142,    143, 25683, 25684, 25685, 25681
    4,    49,    50,    141,    142, 25686, 25687, 25688, 25684
.....
    14044, 25589, 25592, 4349, 4350, 25594, 25673, 4424, 25672
    14045, 25592, 25595, 4348, 4349, 25597, 25674, 4423, 25673
    14046, 25595, 25598, 4347, 4348, 25600, 25675, 4422, 25674
    14047, 25598, 4336,    46, 4347, 25601, 4346, 4421, 25675
*Element, type=DC2D6
    5321, 7415,    21, 2126, 7416, 2326, 7417
    5322, 7415, 2126, 2125, 7417, 2325, 7418
    5323, 7419, 3577, 3578, 7420, 3627, 7421
    5324,    32,    19, 2401, 7422, 2471, 7423
.....
    12008, 15074, 7432, 16546, 20170, 20212, 18622
    12009, 20203, 19951, 19845, 20205, 20201, 20209
    12010, 20203, 9470, 13175, 20210, 20217, 20204
    12011, 15074, 16545, 19477, 18623, 20198, 20216
    12012, 15074, 15076, 13175, 15079, 20167, 20169
*Nset, nset=_PickedSet2, internal
    7,    8,    16,    17,    18,    19,    20,    21,    22,    26,
    31,    32,    33,    34,    35,    36
        37,    38,    42,    43,    44,    45,    46,    196,    197,
    198,    199,    200,    201,    202,    203,    204
.....
    32191, 32192, 32193, 32194, 32195, 32196, 32197, 32198, 32199, 32200,
    32201, 32202, 32203, 32204, 32205, 32206
```



```

32207, 32208, 32209, 32210, 32211, 32212, 32213, 32214, 32215,
32216, 32217, 32218, 32219, 32220, 32221, 32222
32223, 32224, 32225, 32226, 32227, 32228, 32229, 32230, 32231,
32232, 32233, 32234, 32235, 32236, 32237, 32238
32239, 32240, 32241, 32242, 32243, 32244, 32245, 32246, 32247,
32248, 32249
*Elset, elset=_PickedSet2, internal
 2321, 2322, 2323, 2324, 2325, 2326, 2327, 2328, 2329,
2330, 2331, 2332, 2333, 2334, 2335, 2336
 2337, 2338, 2339, 2340, 2341, 2342, 2343, 2344, 2345,
2346, 2347, 2348, 2349, 2350, 2351, 2352
.....
14002, 14003, 14004, 14005, 14006, 14007, 14008, 14009, 14010, 14011,
14012, 14013, 14014, 14015, 14016, 14017
 14018, 14019, 14020, 14021, 14022, 14023, 14024, 14025, 14026,
14027, 14028, 14029, 14030, 14031, 14032, 14033
 14034, 14035, 14036, 14037, 14038, 14039, 14040, 14041, 14042,
14043, 14044, 14045, 14046, 14047
*Nset, nset=_PickedSet4, internal
 3, 4, 10, 23, 24, 25, 27, 28, 29,
30, 39, 40, 41, 96, 97, 98
 99, 100, 101, 102, 103, 104, 105, 106, 107,
108, 109, 110, 111, 112, 113, 114
 115, 116, 117, 118, 119, 120, 121, 122, 123,
124, 125, 126, 127, 128, 129, 130
.....
36247, 36248, 36249, 36250, 36251, 36252, 36253, 36254, 36255, 36256,
36257, 36258, 36259, 36260, 36261, 36262
 36263, 36264, 36265, 36266, 36267, 36268, 36269, 36270, 36271,
36272, 36273, 36274, 36275, 36276, 36277, 36278
 36279, 36280, 36281, 36282, 36283, 36284, 36285, 36286, 36287, 36288
*Elset, elset=_PickedSet4, internal
 3911, 3912, 3913, 3914, 3915, 3916, 3917, 3918, 3919,
3920, 3921, 3922, 3923, 3924, 3925, 3926
 3927, 3928, 3929, 3930, 3931, 3932, 3933, 3934, 3935,
3936, 3937, 3938, 3939, 3940, 3941, 3942
 3943, 3944, 3945, 3946, 3947, 3948, 3949, 3950, 3951,
3952, 3953, 3954, 3955, 3956, 3957, 3958
.....
13255, 13256, 13257, 13258, 13259, 13260, 13261, 13262, 13263, 13264,
13265, 13266, 13267, 13268, 13269, 13270
 13271, 13272, 13273, 13274, 13275, 13276, 13277, 13278, 13279,
13280, 13281, 13282, 13283, 13284, 13285, 13286
 13287, 13288, 13289, 13290, 13291, 13292, 13293, 13294, 13295,
13296, 13297
*Nset, nset=_PickedSet5, internal
 1, 2, 3, 4, 5, 6, 7, 8, 9,
10, 11, 12, 13, 14, 15, 16
 17, 18, 23, 24, 25, 26, 41, 42, 47,
48, 49, 50, 51, 52, 53, 54
 55, 56, 57, 58, 59, 60, 61, 62, 63,
64, 65, 66, 67, 68, 69, 70
 71, 72, 73, 74, 75, 76, 77, 78, 79,
80, 81, 82, 83, 84, 85, 86
.....
33436, 33437, 33438, 33439, 33440, 33441, 33442, 33443, 33444, 33445,
33446, 33447, 33448, 33449, 33450, 33451
 33452, 33453, 33454, 33455, 33456, 33457, 33458, 33459, 33460,
33461, 33462, 33463, 33464, 33465, 33466, 33467
 33468,
*Elset, elset=_PickedSet5, internal

```

```

    1,      2,      3,      4,      5,      6,      7,      8,      9,
10,     11,     12,     13,     14,     15,     16
    17,     18,     19,     20,     21,     22,     23,     24,     25,
26,     27,     28,     29,     30,     31,     32
    33,     34,     35,     36,     37,     38,     39,     40,     41,
42,     43,     44,     45,     46,     47,     48
    49,     50,     51,     52,     53,     54,     55,     56,     57,
58,     59,     60,     61,     62,     63,     64

```

```

.....
12835, 12836, 12837, 12838, 12839, 12840, 12841, 12842, 12843, 12844,
12845, 12846, 12847, 12848, 12849, 12850
 12851, 12852, 12853, 12854, 12855, 12856, 12857, 12858, 12859,
12860, 12861, 12862, 12863, 12864, 12865, 12866
 12867, 12868, 12869, 12870, 12871, 12872

```

```

** Region: (Adhesive:Picked)
*Elset, elset=_PickedSet5, internal
    1,      2,      3,      4,      5,      6,      7,      8,      9,
10,     11,     12,     13,     14,     15,     16
    17,     18,     19,     20,     21,     22,     23,     24,     25,
26,     27,     28,     29,     30,     31,     32
    33,     34,     35,     36,     37,     38,     39,     40,     41,
42,     43,     44,     45,     46,     47,     48
    49,     50,     51,     52,     53,     54,     55,     56,     57,
58,     59,     60,     61,     62,     63,     64

```

```

.....
12835, 12836, 12837, 12838, 12839, 12840, 12841, 12842, 12843, 12844,
12845, 12846, 12847, 12848, 12849, 12850
 12851, 12852, 12853, 12854, 12855, 12856, 12857, 12858, 12859,
12860, 12861, 12862, 12863, 12864, 12865, 12866
 12867, 12868, 12869, 12870, 12871, 12872

```

```

** Section: Adhesive
*Solid Section, elset=_PickedSet5, material=Adhesive
45.,
** Region: (Steel:Picked)
*Elset, elset=_PickedSet2, internal
 2321, 2322, 2323, 2324, 2325, 2326, 2327, 2328, 2329,
2330, 2331, 2332, 2333, 2334, 2335, 2336
 2337, 2338, 2339, 2340, 2341, 2342, 2343, 2344, 2345,
2346, 2347, 2348, 2349, 2350, 2351, 2352
 2353, 2354, 2355, 2356, 2357, 2358, 2359, 2360, 2361,
2362, 2363, 2364, 2365, 2366, 2367, 2368
 2369, 2370, 2371, 2372, 2373, 2374, 2375, 2376, 2377,
2378, 2379, 2380, 2381, 2382, 2383, 2384

```

```

.....
14002, 14003, 14004, 14005, 14006, 14007, 14008, 14009, 14010, 14011,
14012, 14013, 14014, 14015, 14016, 14017
 14018, 14019, 14020, 14021, 14022, 14023, 14024, 14025, 14026,
14027, 14028, 14029, 14030, 14031, 14032, 14033
 14034, 14035, 14036, 14037, 14038, 14039, 14040, 14041, 14042,
14043, 14044, 14045, 14046, 14047

```

```

** Section: Steel
*Solid Section, elset=_PickedSet2, material=Steel
80.,
** Region: (CFRP:Picked)
*Elset, elset=_PickedSet4, internal
 3911, 3912, 3913, 3914, 3915, 3916, 3917, 3918, 3919,
3920, 3921, 3922, 3923, 3924, 3925, 3926
 3927, 3928, 3929, 3930, 3931, 3932, 3933, 3934, 3935,
3936, 3937, 3938, 3939, 3940, 3941, 3942
 3943, 3944, 3945, 3946, 3947, 3948, 3949, 3950, 3951,
3952, 3953, 3954, 3955, 3956, 3957, 3958

```

```

.....
13255, 13256, 13257, 13258, 13259, 13260, 13261, 13262, 13263, 13264,
13265, 13266, 13267, 13268, 13269, 13270
 13271, 13272, 13273, 13274, 13275, 13276, 13277, 13278, 13279,
13280, 13281, 13282, 13283, 13284, 13285, 13286
 13287, 13288, 13289, 13290, 13291, 13292, 13293, 13294, 13295,
13296, 13297
** Section: CFRP
*Solid Section, elset=_PickedSet4, material=CFRP
45.,
*End Instance
**
*Nset, nset=_PickedSet95, internal, instance="Composite Plate-1",
generate
 1, 36288, 1
*Elset, elset=_PickedSet95, internal, instance="Composite Plate-1",
generate
 1, 14047, 1
*Nset, nset=_PickedSet150, internal, instance="Composite Plate-1"
 8, 16, 17, 18, 1104, 1105, 1106, 1107, 1108,
1109, 1110, 1111, 1112, 1113, 1114, 1115
 1116, 1117, 1118, 1119, 1120, 1121, 1122, 1125, 1126,
1127, 1128, 1129, 1130, 1131, 1132, 1133
 1134, 1135, 1136, 1137, 1138, 1139, 1140, 1141, 1142,
1143, 1144, 1145, 1146, 1147, 1148, 1149
.....
30762, 30764, 30766, 30768, 30770, 30772, 30774, 30776, 30778, 30780,
30782, 30784, 30786, 30788, 30790, 30792
 30794, 30796, 30798, 30800, 30802, 30804, 30806, 30808, 30810,
30812, 30814, 30816, 30818, 30820, 30822, 30824
 30826, 30828, 30830, 30832, 30834, 30836, 30838, 30840, 30841
*Elset, elset=_PickedSet150, internal, instance="Composite Plate-1"
 1063, 1066, 1069, 1072, 1075, 1078, 1081, 1084, 1087, 1090, 1093,
1096, 1099, 1102, 1105, 1108
 1111, 1114, 1117, 1120, 1521, 1522, 1523, 1524, 1525, 1526, 1527,
1528, 1529, 1530, 1531, 1532
 1533, 1534, 1535, 1536, 1537, 1538, 1539, 1540, 1541, 1542, 1543,
1544, 1545, 1546, 1547, 1548
 1549, 1550, 1551, 1552, 1553, 1554, 1555, 1556, 1557, 1558, 1559,
1560, 1561, 1562, 1563, 1564
.....
2269, 2270, 2271, 2272, 2273, 2274, 2275, 2276, 2277, 2278, 2279,
2280, 2281, 2282, 2283, 2284
 2285, 2286, 2287, 2288, 2289, 2290, 2291, 2292, 2293, 2294, 2295,
2296, 2297, 2298, 2299, 2300
 2301, 2302, 2303, 2304, 2305, 2306, 2307, 2308, 2309, 2310, 2311,
2312, 2313, 2314, 2315, 2316
 2317, 2318, 2319, 2320
*Elset, elset=__PickedSurf91_S2, internal, instance="Composite Plate-
1", generate
 13372, 14047, 75
*Surface, type=ELEMENT, name=_PickedSurf91, internal
__PickedSurf91_S2, S2
*Elset, elset=__PickedSurf96_S4, internal, instance="Composite Plate-
1"
 661, 861, 1721, 1921, 2121, 3911, 3914, 3917, 3920,
3923, 3926, 3929, 3932, 3935, 3938, 3941
 3944, 3947, 3950, 3953, 3956, 3959, 3962, 3965, 3968,
3971, 3974, 3977, 3980, 3983, 3986, 3989
 3992, 3995, 3998, 4001, 4004, 4007, 4010, 4013, 4016,
4019, 4022, 4025, 4028, 4031, 4034, 4037

```

```

.....
12943, 12953, 12963, 12973, 12983, 12993, 13003, 13013, 13023, 13033,
13043, 13053, 13063, 13073, 13083, 13093
 13103, 13113, 13123, 13133, 13143, 13153, 13163, 13173, 13183,
13193, 13203, 13213, 13223, 13226, 13229, 13232
 13235, 13238, 13241, 13244, 13247, 13250, 13253, 13256, 13259,
13262, 13265, 13268, 13271, 13274, 13277, 13280
 13283, 13286, 13289, 13292, 13295
*Elset, elset=__PickedSurf96_S1, internal, instance="Composite Plate-
1", generate
 13298, 13372,      1
*Elset, elset=__PickedSurf96_S2, internal, instance="Composite Plate-
1"
 3460, 12785, 12788, 12791, 12794, 12797, 12800, 12803, 12806,
12809, 12812, 13372, 13447, 13522, 13597, 13672
 13747, 13822, 13897, 13972, 14047
*Elset, elset=__PickedSurf96_S3, internal, instance="Composite Plate-
1"
 5318, 5319, 5320, 12810, 12811, 12812, 12867, 12868, 12869,
12870, 12871, 12872, 12963, 12964, 12965, 12966
 12967, 12968, 12969, 12970, 12971, 12972, 13973, 13974, 13975,
13976, 13977, 13978, 13979, 13980, 13981, 13982
 13983, 13984, 13985, 13986, 13987, 13988, 13989, 13990, 13991,
13992, 13993, 13994, 13995, 13996, 13997, 13998
 13999, 14000, 14001, 14002, 14003, 14004, 14005, 14006, 14007,
14008, 14009, 14010, 14011, 14012, 14013, 14014
 14015, 14016, 14017, 14018, 14019, 14020, 14021, 14022, 14023,
14024, 14025, 14026, 14027, 14028, 14029, 14030
 14031, 14032, 14033, 14034, 14035, 14036, 14037, 14038, 14039,
14040, 14041, 14042, 14043, 14044, 14045, 14046
 14047,
*Surface, type=ELEMENT, name=_PickedSurf96, internal
__PickedSurf96_S4, S4
__PickedSurf96_S1, S1
__PickedSurf96_S2, S2
__PickedSurf96_S3, S3
*End Assembly
*Amplitude, name=Amp-1
10., 0.858, 20., 0.886, 30., 0.915, 40., 0.943
50., 0.9716, 60., 1.
**
** MATERIALS
**
*Material, name=Adhesive
*Conductivity
 0.001,
*Density
 1.97e-06,
*Elastic
 7000., 0.34, 293.
 7000., 0.34, 303.
 6222., 0.34, 313.
 5440., 0.34, 323.
 933., 0.34, 333.
 93., 0.34, 343.
 50.56, 0.34, 353.
 42., 0.34, 363.
 42., 0.34, 373.
*Expansion
 6e-05,
*Specific Heat

```

```

900.,
*Material, name=CFRP
*Conductivity
  0.05,
*Density
  1.5e-06,
*Elastic
450000., 0.3
*Expansion
  5e-06,
*Specific Heat
1200.,
*Material, name=Steel
*Conductivity
  0.046,
*Density
  7.82e-06,
*Elastic
210000., 0.29
*Expansion
  1.2e-05,
*Specific Heat
460.,
**
** INTERACTION PROPERTIES
**
*Film Property, name="For specimen 3 & 4"
4.63378e-06, 0.
8.27176e-06, 5.
9.2341e-06, 10.
9.94101e-06, 15.
1.05281e-05, 20.
1.1044e-05, 25.
1.15122e-05, 30.
1.19461e-05, 35.
1.23543e-05, 40.
1.27425e-05, 45.
1.31147e-05, 50.
1.34741e-05, 55.
1.38227e-05, 60.
1.41626e-05, 65.
1.44951e-05, 70.
1.48215e-05, 75.
1.51426e-05, 80.
1.54592e-05, 85.
1.57722e-05, 90.
1.60821e-05, 95.
1.63893e-05, 100.
1.66943e-05, 105.
1.69976e-05, 110.
1.72995e-05, 115.
1.76002e-05, 120.
1.79002e-05, 125.
1.81995e-05, 130.
1.84985e-05, 135.
1.87973e-05, 140.
1.90961e-05, 145.
1.93952e-05, 150.
1.96946e-05, 155.
1.99946e-05, 160.
2.02952e-05, 165.

```

```

2.05965e-05, 170.
2.12021e-05, 180.
**
** FIELDS
**
** Name: Field-1   Type: Temperature
*Initial Conditions, type=TEMPERATURE
_PickedSet95, 293.
** -----
**
** STEP: Step-1
**
*Step, name=Step-1, inc=1900
*Heat Transfer, end=PERIOD, deltmx=500., mxdem=0.75
1., 1800., 1e-05, 1.,
**
** BOUNDARY CONDITIONS
**
** Name: BC-1 Type: Temperature
*Boundary, amplitude=Amp-1
_PickedSet150, 11, 11, 353.
**
** INTERACTIONS
**
** Interaction: convection boundary
*Sfilm
_PickedSurf96, F, 293., "For specimen 3 & 4"
**
** OUTPUT REQUESTS
**
*Restart, write, frequency=0
**
** FIELD OUTPUT: F-Output-1
**
*Output, field, variable=PRESELECT
**
** HISTORY OUTPUT: H-Output-1
**
*Output, history, variable=PRESELECT
*End Step

```

Appendix E

A truncated input file from mechanical analysis in composite plate final.cae; results are shown and discussed in section 7.6.

```
*Heading
** Job name: Job-mechanicalanalysis Model name: Thermal Mechanical
Model
*Preprint,      echo=NO,      model=NO,      history=NO,      contact=NO
**
** PARTS
**
*Part, name="Composite Plate"
*End Part
**
**
** ASSEMBLY
**
*Assembly, name=Assembly
**
**
*Instance, name="Composite Plate-1", part="Composite Plate"
*Node
    1,          250.,          -1.25
    2,          200.,          -1.25
    3,          200.,          -1.5
    .....
    36284,      150.,      -4.83333302
    36285,      150.024994,      -5.5
    36286,      150.024994,      -2.83333325
    36287,      150.,      -3.5
    36288,      150.,      -2.16666651
*Element, type=CPS8
    1,    1,    47,    144,    4, 25676, 25677, 25678, 25679
    2,    47,    48,    143,    144, 25680, 25681, 25682, 25677
    3,    48,    49,    142,    143, 25683, 25684, 25685, 25681
    4,    49,    50,    141,    142, 25686, 25687, 25688, 25684
    .....
    14045, 25592, 25595, 4348, 4349, 25597, 25674, 4423, 25673
    14046, 25595, 25598, 4347, 4348, 25600, 25675, 4422, 25674
    14047, 25598, 4336, 46, 4347, 25601, 4346, 4421, 25675
*Element, type=CPS6M
    5321, 7415, 21, 2126, 7416, 2326, 7417
    5322, 7415, 2126, 2125, 7417, 2325, 7418
    5323, 7419, 3577, 3578, 7420, 3627, 7421
    5324, 32, 19, 2401, 7422, 2471, 7423
    .....
    12010, 20203, 9470, 13175, 20210, 20217, 20204
    12011, 15074, 16545, 19477, 18623, 20198, 20216
    12012, 15074, 15076, 13175, 15079, 20167, 20169
*Nset, nset=_PickedSet2, internal
    7,    8,    16,    17,    18,    19,    20,    21,    22,
    26,    31,    32,    33,    34,    35,    36
    37,    38,    42,    43,    44,    45,    46,    196,    197,
    198,    199,    200,    201,    202,    203,    204
    205,    206,    207,    208,    209,    210,    211,    212,    213,
    214,    215,    216,    217,    218,    219,    220
    221,    222,    223,    224,    225,    226,    227,    228,    229,
    230,    231,    232,    233,    234,    235,    236
    .....
```

32207, 32208, 32209, 32210, 32211, 32212, 32213, 32214, 32215, 32216,
 32217, 32218, 32219, 32220, 32221, 32222
 32223, 32224, 32225, 32226, 32227, 32228, 32229, 32230, 32231,
 32232, 32233, 32234, 32235, 32236, 32237, 32238
 32239, 32240, 32241, 32242, 32243, 32244, 32245, 32246, 32247,
 32248, 32249
 *Elset, elset=_PickedSet2, internal
 2321, 2322, 2323, 2324, 2325, 2326, 2327, 2328, 2329,
 2330, 2331, 2332, 2333, 2334, 2335, 2336
 2337, 2338, 2339, 2340, 2341, 2342, 2343, 2344, 2345,
 2346, 2347, 2348, 2349, 2350, 2351, 2352
 2353, 2354, 2355, 2356, 2357, 2358, 2359, 2360, 2361,
 2362, 2363, 2364, 2365, 2366, 2367, 2368

 14002, 14003, 14004, 14005, 14006, 14007, 14008, 14009, 14010, 14011,
 14012, 14013, 14014, 14015, 14016, 14017
 14018, 14019, 14020, 14021, 14022, 14023, 14024, 14025, 14026,
 14027, 14028, 14029, 14030, 14031, 14032, 14033
 14034, 14035, 14036, 14037, 14038, 14039, 14040, 14041, 14042,
 14043, 14044, 14045, 14046, 14047
 *Nset, nset=_PickedSet4, internal
 3, 4, 10, 23, 24, 25, 27, 28, 29,
 30, 39, 40, 41, 96, 97, 98
 99, 100, 101, 102, 103, 104, 105, 106, 107,
 108, 109, 110, 111, 112, 113, 114
 115, 116, 117, 118, 119, 120, 121, 122, 123,
 124, 125, 126, 127, 128, 129, 130

 36247, 36248, 36249, 36250, 36251, 36252, 36253, 36254, 36255, 36256,
 36257, 36258, 36259, 36260, 36261, 36262
 36263, 36264, 36265, 36266, 36267, 36268, 36269, 36270, 36271,
 36272, 36273, 36274, 36275, 36276, 36277, 36278
 36279, 36280, 36281, 36282, 36283, 36284, 36285, 36286, 36287, 36288
 *Elset, elset=_PickedSet4, internal
 3911, 3912, 3913, 3914, 3915, 3916, 3917, 3918, 3919,
 3920, 3921, 3922, 3923, 3924, 3925, 3926
 3927, 3928, 3929, 3930, 3931, 3932, 3933, 3934, 3935,
 3936, 3937, 3938, 3939, 3940, 3941, 3942
 3943, 3944, 3945, 3946, 3947, 3948, 3949, 3950, 3951,
 3952, 3953, 3954, 3955, 3956, 3957, 3958

 13255, 13256, 13257, 13258, 13259, 13260, 13261, 13262, 13263, 13264,
 13265, 13266, 13267, 13268, 13269, 13270
 13271, 13272, 13273, 13274, 13275, 13276, 13277, 13278, 13279,
 13280, 13281, 13282, 13283, 13284, 13285, 13286
 13287, 13288, 13289, 13290, 13291, 13292, 13293, 13294, 13295,
 13296, 13297
 *Nset, nset=_PickedSet5, internal
 1, 2, 3, 4, 5, 6, 7, 8, 9,
 10, 11, 12, 13, 14, 15, 16
 17, 18, 23, 24, 25, 26, 41, 42, 47,
 48, 49, 50, 51, 52, 53, 54
 55, 56, 57, 58, 59, 60, 61, 62, 63,
 64, 65, 66, 67, 68, 69, 70
 71, 72, 73, 74, 75, 76, 77, 78, 79,
 80, 81, 82, 83, 84, 85, 86

 33420, 33421, 33422, 33423, 33424, 33425, 33426, 33427, 33428, 33429,
 33430, 33431, 33432, 33433, 33434, 33435
 33436, 33437, 33438, 33439, 33440, 33441, 33442, 33443, 33444,
 33445, 33446, 33447, 33448, 33449, 33450, 33451


```

33452, 33453, 33454, 33455, 33456, 33457, 33458, 33459, 33460,
33461, 33462, 33463, 33464, 33465, 33466, 33467
33468,
*Elset, elset=_PickedSet5, internal
  1,    2,    3,    4,    5,    6,    7,    8,    9,
10,   11,   12,   13,   14,   15,   16
17,   18,   19,   20,   21,   22,   23,   24,   25,
26,   27,   28,   29,   30,   31,   32
33,   34,   35,   36,   37,   38,   39,   40,   41,
42,   43,   44,   45,   46,   47,   48
49,   50,   51,   52,   53,   54,   55,   56,   57,
58,   59,   60,   61,   62,   63,   64
65,   66,   67,   68,   69,   70,   71,   72,   73,
74,   75,   76,   77,   78,   79,   80
.....
12835, 12836, 12837, 12838, 12839, 12840, 12841, 12842, 12843, 12844,
12845, 12846, 12847, 12848, 12849, 12850
12851, 12852, 12853, 12854, 12855, 12856, 12857, 12858, 12859,
12860, 12861, 12862, 12863, 12864, 12865, 12866
12867, 12868, 12869, 12870, 12871, 12872
** Region: (Adhesive:Picked)
*Elset, elset=_PickedSet5, internal
  1,    2,    3,    4,    5,    6,    7,    8,    9,
10,   11,   12,   13,   14,   15,   16
17,   18,   19,   20,   21,   22,   23,   24,   25,
26,   27,   28,   29,   30,   31,   32
33,   34,   35,   36,   37,   38,   39,   40,   41,
42,   43,   44,   45,   46,   47,   48
49,   50,   51,   52,   53,   54,   55,   56,   57,
58,   59,   60,   61,   62,   63,   64
.....
3901, 3902, 3903, 3904, 3905, 3906, 3907, 3908, 3909, 3910,
12813, 12814, 12815, 12816, 12817, 12818
12819, 12820, 12821, 12822, 12823, 12824, 12825, 12826, 12827,
12828, 12829, 12830, 12831, 12832, 12833, 12834
12835, 12836, 12837, 12838, 12839, 12840, 12841, 12842, 12843,
12844, 12845, 12846, 12847, 12848, 12849, 12850
12851, 12852, 12853, 12854, 12855, 12856, 12857, 12858, 12859,
12860, 12861, 12862, 12863, 12864, 12865, 12866
12867, 12868, 12869, 12870, 12871, 12872
** Section: Adhesive
*Solid Section, elset=_PickedSet5, material=Adhesive
45.,
** Region: (Steel:Picked)
*Elset, elset=_PickedSet2, internal
 2321, 2322, 2323, 2324, 2325, 2326, 2327, 2328, 2329,
2330, 2331, 2332, 2333, 2334, 2335, 2336
2337, 2338, 2339, 2340, 2341, 2342, 2343, 2344, 2345,
2346, 2347, 2348, 2349, 2350, 2351, 2352
2353, 2354, 2355, 2356, 2357, 2358, 2359, 2360, 2361,
2362, 2363, 2364, 2365, 2366, 2367, 2368
2369, 2370, 2371, 2372, 2373, 2374, 2375, 2376, 2377,
2378, 2379, 2380, 2381, 2382, 2383, 2384
.....
13986, 13987, 13988, 13989, 13990, 13991, 13992, 13993, 13994, 13995,
13996, 13997, 13998, 13999, 14000, 14001
14002, 14003, 14004, 14005, 14006, 14007, 14008, 14009, 14010,
14011, 14012, 14013, 14014, 14015, 14016, 14017
14018, 14019, 14020, 14021, 14022, 14023, 14024, 14025, 14026,
14027, 14028, 14029, 14030, 14031, 14032, 14033

```

```

14034, 14035, 14036, 14037, 14038, 14039, 14040, 14041, 14042,
14043, 14044, 14045, 14046, 14047
** Section: Steel
*Solid Section, elset=_PickedSet2, material=Steel
80.,
** Region: (CFRP:Picked)
*Elset, elset=_PickedSet4, internal
3911, 3912, 3913, 3914, 3915, 3916, 3917, 3918, 3919,
3920, 3921, 3922, 3923, 3924, 3925, 3926
3927, 3928, 3929, 3930, 3931, 3932, 3933, 3934, 3935,
3936, 3937, 3938, 3939, 3940, 3941, 3942
3943, 3944, 3945, 3946, 3947, 3948, 3949, 3950, 3951,
3952, 3953, 3954, 3955, 3956, 3957, 3958
3959, 3960, 3961, 3962, 3963, 3964, 3965, 3966, 3967,
3968, 3969, 3970, 3971, 3972, 3973, 3974
.....
13223, 13224, 13225, 13226, 13227, 13228, 13229, 13230, 13231,
13232, 13233, 13234, 13235, 13236, 13237, 13238
13239, 13240, 13241, 13242, 13243, 13244, 13245, 13246, 13247,
13248, 13249, 13250, 13251, 13252, 13253, 13254
13255, 13256, 13257, 13258, 13259, 13260, 13261, 13262, 13263,
13264, 13265, 13266, 13267, 13268, 13269, 13270
13271, 13272, 13273, 13274, 13275, 13276, 13277, 13278, 13279,
13280, 13281, 13282, 13283, 13284, 13285, 13286
13287, 13288, 13289, 13290, 13291, 13292, 13293, 13294, 13295,
13296, 13297
** Section: CFRP
*Solid Section, elset=_PickedSet4, material=CFRP
45.,
*End Instance
**
*Nset, nset=_PickedSet95, internal, instance="Composite Plate-1",
generate
1, 36288, 1
*Elset, elset=_PickedSet95, internal, instance="Composite Plate-1",
generate
1, 14047, 1
*Nset, nset=_PickedSet134, internal, instance="Composite Plate-1"
8, 16, 17, 18, 1104, 1105, 1106, 1107, 1108,
1109, 1110, 1111, 1112, 1113, 1114, 1115
1116, 1117, 1118, 1119, 1120, 1121, 1122, 1125, 1126,
1127, 1128, 1129, 1130, 1131, 1132, 1133
1134, 1135, 1136, 1137, 1138, 1139, 1140, 1141, 1142,
1143, 1144, 1145, 1146, 1147, 1148, 1149
1150, 1151, 1152, 1153, 1154, 1155, 1156, 1157, 1158,
1159, 1160, 1161, 1162, 1163, 1164, 1165
.....
30730, 30732, 30734, 30736, 30738, 30740, 30742, 30744, 30746, 30748,
30750, 30752, 30754, 30756, 30758, 30760
30762, 30764, 30766, 30768, 30770, 30772, 30774, 30776, 30778,
30780, 30782, 30784, 30786, 30788, 30790, 30792
30794, 30796, 30798, 30800, 30802, 30804, 30806, 30808, 30810,
30812, 30814, 30816, 30818, 30820, 30822, 30824
30826, 30828, 30830, 30832, 30834, 30836, 30838, 30840, 30841
*Elset, elset=_PickedSet134, internal, instance="Composite Plate-1"
1063, 1066, 1069, 1072, 1075, 1078, 1081, 1084, 1087, 1090, 1093,
1096, 1099, 1102, 1105, 1108
1111, 1114, 1117, 1120, 1521, 1522, 1523, 1524, 1525, 1526, 1527,
1528, 1529, 1530, 1531, 1532
1533, 1534, 1535, 1536, 1537, 1538, 1539, 1540, 1541, 1542, 1543,
1544, 1545, 1546, 1547, 1548

```

```

1549, 1550, 1551, 1552, 1553, 1554, 1555, 1556, 1557, 1558, 1559,
1560, 1561, 1562, 1563, 1564
.....
2285, 2286, 2287, 2288, 2289, 2290, 2291, 2292, 2293, 2294, 2295,
2296, 2297, 2298, 2299, 2300
2301, 2302, 2303, 2304, 2305, 2306, 2307, 2308, 2309, 2310, 2311,
2312, 2313, 2314, 2315, 2316
2317, 2318, 2319, 2320
*Nset, nset=_PickedSet136, internal, instance="Composite Plate-1"
  40, 41, 42, 44, 3970, 3971, 3972, 3973, 3974, 3994, 3995,
3996, 3997, 3998, 3999, 4000
  4001, 4002, 4003, 4004, 4043, 4044, 4045, 4046, 4047, 4048, 4049,
4050, 4051, 4052, 4053, 4054
  4055, 4056, 4057, 4058, 4059, 4060, 4061
*Elset, elset=_PickedSet136, internal, instance="Composite Plate-1"
  12810, 12811, 12812, 12867, 12868, 12869, 12870, 12871, 12872,
12963, 12964, 12965, 12966, 12967, 12968, 12969
  12970, 12971, 12972
*Nset, nset=_PickedSet137, internal, instance="Composite Plate-1"
  35, 36, 37, 38, 43, 44, 45, 3703, 3704, 3705, 3706,
3707, 3708, 3709, 3710, 3711
  3712, 3713, 3714, 3715, 3716, 3717, 3718, 3719, 3720, 3721, 3722,
3723, 3724, 3725, 3726, 3727
  3728, 3729, 3730, 3731, 3732, 3733, 3734, 3735, 3736, 3737, 3738,
3739, 3740, 3741, 3742, 3743
.....
4287, 4288, 4289, 4290, 4291, 4292, 4293, 4294, 4295, 4296, 4297,
4298, 4299, 4300, 4301, 4302
  4303, 4304, 4305, 4306, 4307, 4308, 4309, 4310, 4311, 4312, 4313,
4314, 4315, 4316, 4317, 4318
  4319, 4320, 4321, 4322, 4323, 4324, 4325, 4326, 4327
*Elset, elset=_PickedSet137, internal, instance="Composite Plate-1"
  12013, 12020, 12027, 12034, 12041, 12048, 12055, 12062, 12069,
12076, 12083, 12090, 12097, 12104, 12111, 12118
  12125, 12132, 12139, 12146, 12153, 12160, 12167, 12174, 12181,
12188, 12195, 12202, 12209, 12216, 12223, 12230
.....
13329, 13330, 13331, 13332, 13333, 13334, 13335, 13336, 13337,
13338, 13339, 13340, 13341, 13342, 13343, 13344
  13345, 13346, 13347, 13348, 13349, 13350, 13351, 13352, 13353,
13354, 13355, 13356, 13357, 13358, 13359, 13360
  13361, 13362, 13363, 13364, 13365, 13366, 13367, 13368, 13369,
13370, 13371, 13372
*Nset, nset=_PickedSet138, internal, instance="Composite Plate-1"
  45, 46, 4328, 4329, 4330, 4331, 4332, 4333, 4334, 4335, 4336,
4337, 4338, 4339, 4340, 4341
  4342, 4343, 4344, 4345, 4346
*Elset, elset=_PickedSet138, internal, instance="Composite Plate-1",
generate
  13372, 14047, 75
*Elset, elset=__PickedSurf91_S2, internal, instance="Composite Plate-
1", generate
  13372, 14047, 75
*Surface, type=ELEMENT, name=_PickedSurf91, internal
__PickedSurf91_S2, S2
*Elset, elset=__PickedSurf96_S4, internal, instance="Composite Plate-
1"
  661, 861, 1721, 1921, 2121, 3911, 3914, 3917, 3920,
3923, 3926, 3929, 3932, 3935, 3938, 3941
  3944, 3947, 3950, 3953, 3956, 3959, 3962, 3965, 3968,
3971, 3974, 3977, 3980, 3983, 3986, 3989

```

```

3992, 3995, 3998, 4001, 4004, 4007, 4010, 4013, 4016,
4019, 4022, 4025, 4028, 4031, 4034, 4037
4040, 4043, 4046, 4049, 4052, 4055, 4058, 4061, 4064,
4067, 4070, 4073, 4076, 4079, 4082, 4085
.....
13103, 13113, 13123, 13133, 13143, 13153, 13163, 13173, 13183, 13193,
13203, 13213, 13223, 13226, 13229, 13232
13235, 13238, 13241, 13244, 13247, 13250, 13253, 13256, 13259,
13262, 13265, 13268, 13271, 13274, 13277, 13280
13283, 13286, 13289, 13292, 13295
*Elset, elset=__PickedSurf96_S1, internal, instance="Composite Plate-
1", generate
13298, 13372, 1
*Elset, elset=__PickedSurf96_S2, internal, instance="Composite Plate-
1"
3460, 12785, 12788, 12791, 12794, 12797, 12800, 12803, 12806,
12809, 12812, 13372, 13447, 13522, 13597, 13672
13747, 13822, 13897, 13972, 14047
*Elset, elset=__PickedSurf96_S3, internal, instance="Composite Plate-
1"
5318, 5319, 5320, 12810, 12811, 12812, 12867, 12868, 12869,
12870, 12871, 12872, 12963, 12964, 12965, 12966
12967, 12968, 12969, 12970, 12971, 12972, 13973, 13974, 13975,
13976, 13977, 13978, 13979, 13980, 13981, 13982
13983, 13984, 13985, 13986, 13987, 13988, 13989, 13990, 13991,
13992, 13993, 13994, 13995, 13996, 13997, 13998
13999, 14000, 14001, 14002, 14003, 14004, 14005, 14006, 14007,
14008, 14009, 14010, 14011, 14012, 14013, 14014
14015, 14016, 14017, 14018, 14019, 14020, 14021, 14022, 14023,
14024, 14025, 14026, 14027, 14028, 14029, 14030
14031, 14032, 14033, 14034, 14035, 14036, 14037, 14038, 14039,
14040, 14041, 14042, 14043, 14044, 14045, 14046
14047,
*Surface, type=ELEMENT, name=_PickedSurf96, internal
__PickedSurf96_S4, S4
__PickedSurf96_S1, S1
__PickedSurf96_S2, S2
__PickedSurf96_S3, S3
*Elset, elset=__PickedSurf143_S2, internal, instance="Composite
Plate-1", generate
13372, 14047, 75
*Surface, type=ELEMENT, name=_PickedSurf143, internal
__PickedSurf143_S2, S2
*End Assembly
*Amplitude, name=Amp-1
12., 0.8284, 24., 0.8713, 36., 0.9142, 48., 0.9571
60., 1.
**
** MATERIALS
**
*Material, name=Adhesive
*Conductivity
0.001,
*Density
1.97e-06,
*Elastic
7000., 0.34, 293.
7000., 0.34, 303.
6222., 0.34, 313.
5440., 0.34, 323.
933., 0.34, 333.

```

```

    93., 0.34, 343.
    50.56, 0.34, 353.
*Expansion
    6e-05,
*Specific Heat
    900.,
*Material, name=CFRP
*Conductivity
    0.05,
*Density
    1.5e-06,
*Elastic
    450000., 0.3
*Expansion
    5e-06,
*Specific Heat
    1200.,
*Material, name=Steel
*Conductivity
    0.046,
*Density
    7.82e-06,
*Elastic
    210000., 0.29
*Expansion
    1.2e-05,
*Specific Heat
    460.,
**
** INTERACTION PROPERTIES
**
*Film Property, name="For specimen 3 & 4"
    4.63378e-06, 0.
    8.27176e-06, 5.
    9.2341e-06, 10.
    9.94101e-06, 15.
    1.05281e-05, 20.
    1.1044e-05, 25.
    1.15122e-05, 30.
    1.19461e-05, 35.
    1.23543e-05, 40.
    1.27425e-05, 45.
    1.31147e-05, 50.
    1.34741e-05, 55.
    1.38227e-05, 60.
    1.41626e-05, 65.
    1.44951e-05, 70.
    1.48215e-05, 75.
    1.51426e-05, 80.
    1.54592e-05, 85.
    1.57722e-05, 90.
    1.60821e-05, 95.
    1.63893e-05, 100.
    1.66943e-05, 105.
    1.69976e-05, 110.
    1.72995e-05, 115.
    1.76002e-05, 120.
    1.79002e-05, 125.
    1.81995e-05, 130.
    1.84985e-05, 135.
    1.87973e-05, 140.

```

```

1.90961e-05, 145.
1.93952e-05, 150.
1.96946e-05, 155.
1.99946e-05, 160.
2.02952e-05, 165.
2.05965e-05, 170.
2.12021e-05, 180.
**
** FIELDS
**
** Name: Field-1   Type: Temperature
*Initial Conditions, type=TEMPERATURE
_PickedSet95, 293.
** -----
**
** STEP: Step-1
**
*Step, name=Step-1, inc=1900
*Static
1., 1800., 1e-05, 1.
*TEMPERATURE,File=Job-thermalanalysis.odb

**
** BOUNDARY CONDITIONS
**
** Name: BC-2 Type: Symmetry/Antisymmetry/Encastre
*Boundary
_PickedSet136, YASYMM
** Name: BC-3 Type: Displacement/Rotation
*Boundary
_PickedSet137, 2, 2
** Name: BC-4 Type: Displacement/Rotation
*Boundary
_PickedSet138, 6, 6
**
** OUTPUT REQUESTS
**
*Restart, write, frequency=0
**
** FIELD OUTPUT: F-Output-1
**
*Output, field, variable=PRESELECT
**
** HISTORY OUTPUT: H-Output-1
**
*Output, history, variable=PRESELECT
*End Step
** -----
**
** STEP: Step-2
**
*Step, name=Step-2, inc=5
*Static
1., 1., 1e-05, 1.
**
** LOADS
**
** Name: tensile load   Type: Pressure
*Dslload
_PickedSurf143, P, -275.
**

```

```
** OUTPUT REQUESTS
**
*Restart, write, frequency=0
**
** FIELD OUTPUT: F-Output-1
**
*Output, field, variable=PRESELECT
**
** HISTORY OUTPUT: H-Output-1
**
*Output, history, variable=PRESELECT
*End Step
```